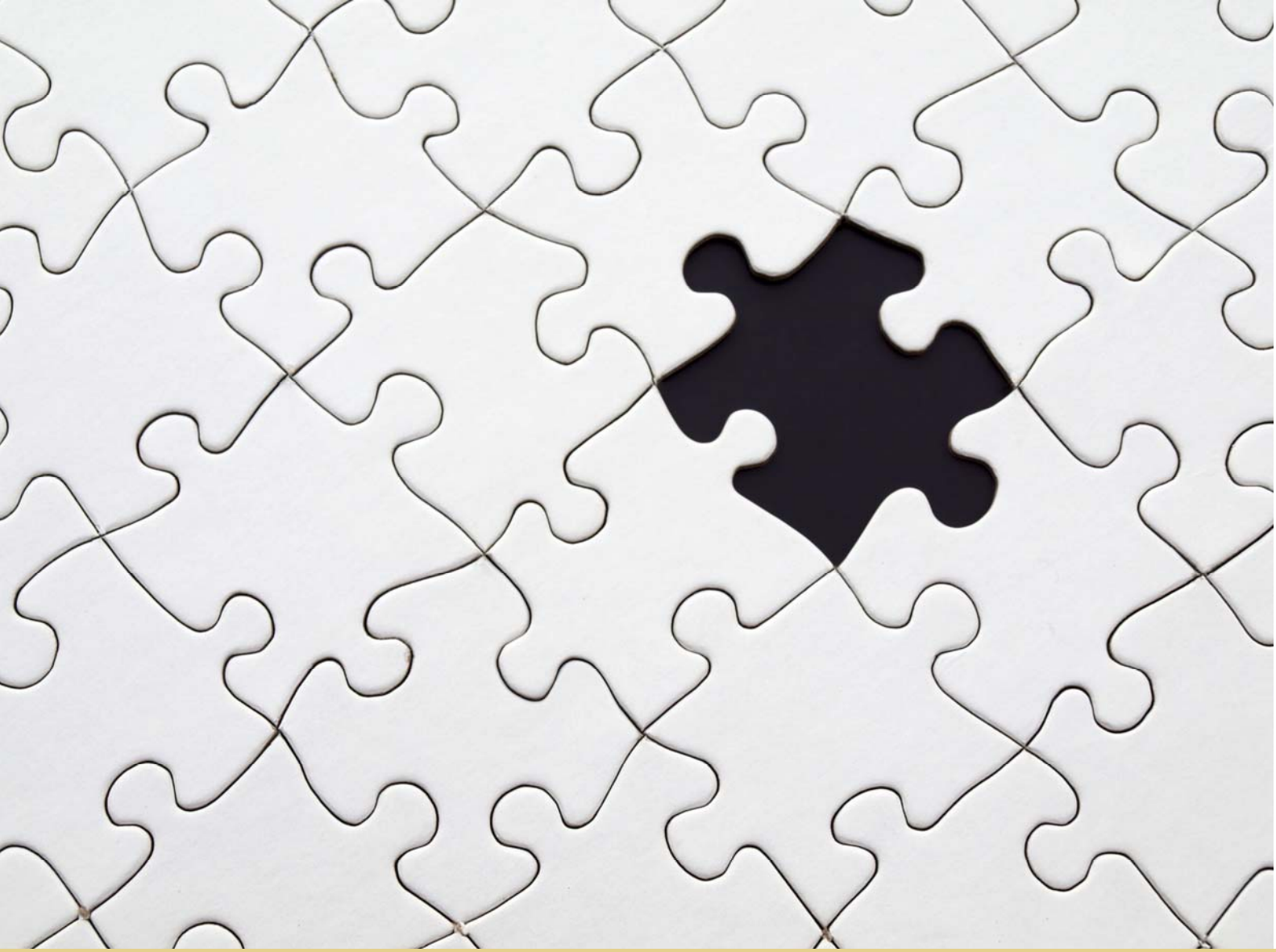

André Carlos Silva Ferreira de Carvalho

Ghrelin administration as a novel strategy to delay aging in Hutchinson-Gilford Progeria Syndrome

Master Dissertation in Cellular and Molecular Biology, supervised by Célia Aveleira, PhD and Professor Carlos Duarte
To be presented to the Life Sciences department of the Faculty of Sciences and Technology of the University of Coimbra

Agosto 2017

· U C ·

UNIVERSIDADE DE COIMBRA

· U C ·

UNIVERSIDADE DE COIMBRA

Ghrelin administration as a novel strategy to delay aging in Hutchinson-Gilford Progeria Syndrome

Student:
André Carlos Silva Ferreira de Carvalho

Supervisors:
Célia Aveleira, PhD
Carlos Duarte, PhD

Thesis submitted in fulfillment of the requirements for the Master degree in Cellular and Molecular Biology

Neuroendocrinology and Aging Group at the
Center for Neuroscience and Cell Biology of the
University of Coimbra

August, 2017

Cover note:
Finding the missing piece?
Image obtained from https://www.foodtalk.org/content/putting-pieces-together.

Thesis Project in fulfilment of the requirements for a Master degree in Molecular and Cellular Biology, under the supervision of Doctor Célia Alexandra Aveleira, Center for Neuroscience and Cell Biology of the University of Coimbra and Institute for Innovation and Health Research of the University of Oporto, and co-supervision of Professor Carlos Jorge Alves Miranda Bandeira Duarte, Faculty of Sciences and Technology and Center for Neuroscience and Cell Biology of the University of Coimbra.

This work was performed in the Neuroendocrinology and Aging group, of the Center for Neuroscience and Cell Biology of the University of Coimbra, Portugal.
This study is supported by Progeria Research Foundation (USA; PRF2014-53 and PRF2015-60); FEDER through Programa Operacional Factores de Competitividade COMPETE2020; and National funds via FCT – Fundação para a Ciência e Tecnologia under strategic project POCI-01-0145-FEDER-007440 and FCT Investigator Programme (IF/00825/2015).

Acknowledgments

In first place, I would like to thank Professor Cláudia Cavadas for giving me the opportunity to develop my master's thesis in the Neuroendicronology and Aging Group, and for all the useful comments during this time.

I would like to also express my most sincere gratefulness to Célia, for sharing with me this work and without whom all this process would have been impossible. Thank you for all the interesting discussions, the support and encouragement, and all the hours devoted to make this possible.

I take the opportunity to acknowledge Professor Carlos Duarte, not only due to the fact that was my internal supervisor, but also because it was one of the persons who had an impact on my academic evolution.

I could not finish without expressing my gratitude to all the members of the Neuroendocrinology an Aging Group for receiving me in such a warm way. In particularly, I thank Marisa and Mariana, who helped me in every task and with whom I learned a lot.

I must express my profound thankfulness to my family and friends for providing me all the support I needed through all these years.

Finally, I acknowledge the funding entities that supported this work.

Table of Contents

List of abbreviations

ACTH – Adrenocorticotropic Hormone

ADP – Adenosine Diphosphate

AgRP – Agouti Related Protein

AH – Anterior Hypothalamic Area

AMPK – Adenosine monophosphate (AMP)-activated protein kinase

ARC – Arcuate Nucleus

ATM – Ataxia Telangiectasia Mutated

ATP – Adenosine Triphosphate

AWS – Atypical Werner Syndrome

BAT – Brown Adipose Tissue

BCA – Bicinchoninic Acid

BDNF – Brain-Derived Neurotrophic Factor

BSA – Bovine Serum Albumin

cAMP – cyclic Adenosine Monophosphate

CAPS – N-Cyclohexyl-3-Aminopropanesulfonic Acid

CART – Cocaine-and-Amphetamine-Regulated-Transcript

CD11b – Cluster of Differentiation 11b

CHIP - C terminus of HSC70-Interacting Protein

CMA – Chaperone-mediated Autophagy

CNS – Central Nervous System

CRH – Corticotropin Releasing Hormone

DAG – Diacylglicerol

DMH – Dorsomedial Hypothalamic Nucleus

DNA – Deoxyribonucleic Acid

DTT – Dithiothreitol

ECM – Extracellular Matrix

ERK – Extracellular signal–regulated Kinase

FOXO1 – Forkhead box protein O1

GABA – Gamma-aminobutyric Acid

GDP – Guanosine Diphosphate

GFAP – Glial Fibrillary Acidic Protein

GH – Growth Hormone

GHRH – Growth Hormone-releasing Hormone

GHRL – Ghrelin Gene

GHS-R – Growth Hormone Secretagogue Receptor

GnRH – Gonadotropin Releasing Hormone

GOAT – Ghrelin O-acyl-transferase

GPCR – G-protein Coupled Receptors

GR – Glucocorticoid Receptor

GTP – Guanosine Triphosphate

H3K27me3 – trimethylation in the lysine 27 of the histone 3

HGPS – Hutchinson-Gilford progeria syndrome

HGPS-iPSCs – HGPS-induced-Pluripotent Stem Cells

HMG-CoA – 3-hydroxy-3-methylglutaryl-coenzyme A

hMSC – human Mesenchymal Stem Cells

HP1α – Heterochromatin Protein 1 alfa

HPA – Hypothalamic-Pituitary-Adrenal

HSC70 – Heat Shock Cognate Protein 70

HSP – Heat Shock Proteins

HUVECs – Human Umbilical Vein Endothelial Cells

Iba-1 – Ionized calcium binding adaptor molecule 1

IGF-1 – Insulin-like Growth Factor 1

IIS – Insulin and IGF-1 Signaling pathway

IKK-β – Inhibitor of nuclear factor kappa-B kinase subunit beta

IL-10 – Interleukin 10

IL-1β – Interleukin 1-Beta

INK4a –

IP_3 – Inositol 1,4,5-phosphate

IRS-1 – Insulin Receptor Substrate-1

Ki67 – Antigen Ki67

LAP2α – Lamin associated polypeptide 2 alfa

LC3B – Microtubule-Associated Protein Light Chain-3B

LHA – Lateral Hipothalamic Area

LMNA – Lamin A

MAPK – Mitogen Activated Protein Kinase

MC2 – Melanocortin 2

MC3 – Melanocortin-3

miR9 – microRNA 9

MMP – Metalloproteinase

MPO – Medial Preoptic Area

MR – Mineralocorticoid Receptor

mRNA – Messenger Ribonucleic Acid

MTOR – Mechanistic Target of Rapamycin

MTORC2 – MTOR complex 2

Na_3VO_4 – Sodium Orthovanadate

NAD – Nicotinamide Adenine Dinucleotide

NaF – Sodium Fluoride

NeuN – RNA binding protein, fox-1 homolog 3

Nf-kB – Nuclear factor kappa B

NPY – Neuropeptide Y

Nrf2 – Nuclear factor (erythroid-derived 2)-like 2

OCT – Optimum Cutting Temperature compound

p16 – Cyclin-Dependent Kinase Inhibitor 2A

p16 – Cyclin-dependent kinase inhibitor 2A

p21 – Cyclin-Dependent Kinase Inhibitor 1

p38 – Mitogen-activated Protein Kinase 14

p53 – Tumor Suppressor p53

PARP1 – Poly (ADP-ribose) Polymerase 1

PBS – Phosphate-Buffered Saline

PCNA – Proliferating Cell Nuclear Antigen

PHA – Posterior Hypothalamic Area

PI3Kβ – Phosphatidylinositol-4,5-bisphosphate 3-kinase beta

PIP_2 – Phosphatidylinositol 4,5-biphosphate

PKA – Protein Kinase A

PKB/Akt – RAC-alpha serine/threonine-protein Kinase

PKC – Protein Kinase C

PLC – Phospholipase C

PMSF – Phenylmethylsulfonyl Fluoride

POMC – Pro-opio Melanocortin

PPARγ – Peroxisome Proliferator-activated Receptor gamma

pRb – Tumor supressor Retinoblastoma

PVDF – Polyvinylidene Difluoride

PVN – Paraventricular Nucleus

qPCR – quantitative teal-time Polymerase Chain Reaction

RD – Restrictive Dermopathy

RIPA – Radio-immunoprecipitation Assay

ROS – Reactive Oxygen Species

S6K1 – Ribosomal protein S6 kinase beta-1

SASP – Senescence Associated Secretory Phenotype

SCN – Suprachiasmatic Nucleus

SDS – Sodium Dodecyl Sulfate

SGZ – Subgranular Zone

sHSP – small HSP

siRNA – silencing RNA

SIRT1 – NAD-dependent deacetylase sirtuin-1

SIRT6 – NAD-dependent deacetylase sirtuin-6

SKIP – Ski-interacting Protein

SOX2 – (Sex determining region Y)-box 2

SQSTM1 – Sequestosome-1

SR – Serine-arginine family of proteins

SREBP1 – Sterol Regulatory Element-Binding transcription factor 1

SRSF5 – Serine/arginine-rich Splicing Factor 5

SVZ – Subventricular Zone

TBS-T – Tris-buffered saline and Tween 20

TERT – Telomerase Reverse Transcriptase

TGF-β – Transforming Growth Factor beta

TK – Tyrosine Kinase

TNF-α – Tumor Necrosis Factor-Alpha

TRH – Thyrotropin-releasing Hormone

UCP1 – Uncoupling Protein 1

UCP2 –Uncoupling Protein 2

UPS – Ubiquitin-proteasome System

VEGF – Vascular Endothelial Growth Factor

VMH – Ventromedial Nucleus

VSMC – Vascular Smooth Muscle Cell

WAT – White Adipose Tissue

ZMPSTE24 – Zincmetalloproteinase STE24

Abstract

Hutchinson-Gilford progeria syndrome (HGPS), a lethal genetic disorder, is characterized by premature aging. HGPS is most commonly caused by a de novo point mutation (C608G) within the LMNA gene, producing an abnormal lamin A protein termed progerin, whose accumulation leads to premature cellular senescence. HGPS children have short stature, low body weight, lipodystrophy and skin and bone abnormalities. The cardiovascular system is severely affected and, in most of the cases, children succumb to myocardial infarction or stroke at an average age of 14.6 years.

Intriguingly, patients show an apparent absence of neurological symptoms, which has been attributed to the regulation of progerin expression in neural cells by microRNA 9. However, no further studies addressed this issue, and therefore, the actual impact of the disease on the brain remains elusive. In line with this, and given the role of hypothalamic dysfunction on whole-body aging, the first aim of this study was to investigate the effect of premature aging on the hypothalamus of a HGPS mouse model, the *Lmna*$^{G609G/G609G}$ mice.

The results obtained suggest that the protein levels of neuropeptide Y (NPY) and agouti-related protein (AgRP) increased, while the protein levels of pro-opiomelanocortin (POMC), decreased, in the hypothalamus of *Lmna*$^{G609G/G609G}$ mice along time. Interestingly, opposite trends in the gene expression of these neuropeptides were observed in these mice. The neuronal nuclei marker NeuN levels were also decreased suggesting that hypothalamic neuronal structure may be affected, however, no changes in the expression of sex determining region Y)-box 2 (SOX2), a marker of neurogenesis, and brain-derived neurotrophic factor (BDNF), a neurotrophic factor, were found. Our results also suggest impairments in the immunity of *Lmna*$^{G609G/G609G}$ mice given the decline in the expression and/or protein levels of inflammatory markers, namely Glial fibrillary acidic protein (GFAP),an astrocyte marker, ionized calcium binding adaptor molecule 1 (Iba-1), a microglia marker, and interleukin-10 (IL-10), an anti-inflammatory cytokine. These are the first evidences pointing to hypothalamic dysfunction in this HGPS mouse model, with putative relevance for HGPS premature aging progression.

Ghrelin is a 28 aminoacid acylated peptide that constitutes the endogenous ligand for growth hormone secretagogue receptor (GHS-R). Ghrelin and its receptor are widely expressed in the body and have been shown to have beneficial effects on several body functions and organs known to be affected in HGPS: stimulation of food intake and adiposity, cardiovascular protection, bone remodeling and cellular proliferation. Moreover, recent data from our group showed that ghrelin stimulates autophagy and promotes progerin clearance, rescues nuclear abnormalities, decreases DNA damage and enhances cell proliferative capacity, delaying cellular senescence in HGPS cells. Taking this into account, the second aim of this study was to investigate

whether ghrelin administration delays premature aging phenotype of *Lmna*$^{G609G/G609G}$ mice.

Ghrelin-treated *Lmna*$^{G609G/G609G}$ mice showed an overall healthier appearance. Ghrelin induced an increase, although modest, in the body weight of *Lmna*$^{G609G/G609G}$ mice, preventing the progressive loss of weight at later stages of the disease. It also increased blood glucose levels in *Lmna*$^{G609G/G609G}$ mice. Ghrelin-treated mice showed some alterations in locomotor activity and behavior, with decreased distanced travelled, mean velocity and time spent within arena center, suggesting that ghrelin may be potentiating anxiogenic behaviors. The size of most organs did not change with ghrelin treatment. However, we observed that the weight of gonadal white adipose tissue was higher in ghrelin-treated *Lmna*$^{G609G/G609G}$ mice, and this increase was concomitant with an increase in white adipocyte size. We also observed that ghrelin increased the thickness of subcutaneous fat layer in the skin, which may be related with adipocyte proliferation and differentiation. Ghrelin-treated *Lmna*$^{G609G/G609G}$ mice showed an increase in the thickness of the epidermis, enhanced hepatocyte proliferation and an increase in the splenic lymphatic tissue area, suggesting an effect on cell proliferation in these organs. An increase in muscle fibers size was also observed in *Lmna*$^{G609G/G609G}$ mice upon ghrelin treatment. Ghrelin modulated autophagy and cell proliferation, two mechanisms known to be compromised with aging. However, these effects were organ dependent. Surprisingly, we found that ghrelin decreased NPY and AgRP expression in the hypothalamus of *Lmna*$^{G609G/G609G}$ mice, but had the opposite effect on *Lmna*$^{+/+}$ mice. It also attenuated the decrease in GFAP expression observed in these mice, and increased IL-10 expression. Altogether, these results show ghrelin beneficial effects on *Lmna*$^{G609G/G609G}$ body weight, hypoglycemia, and lipodystrophy and in the histological structure of several organs, ameliorating the premature aging phenotype of *Lmna*$^{G609G/G609G}$ mice.

In summary, this study was the first to suggest hypothalamic alterations in a HGPS mouse model. Nevertheless, more studies are needed to better understand the role of hypothalamus on HGPS progression. In addition, this study supports ghrelin administration as a promising therapeutic strategy to thwart HGPS progression.

Resumo

A síndrome de Hutchinson-Gilford (HGPS) é uma doença genética rara caracterizada por um envelhecimento prematuro. É causada por uma mutação pontual (C608G) no gene LMNA, que leva à síntese de uma proteina lamina A anormal, denominada progerina, e cuja acumulação provoca senescência celular. Crianças com HGPS apresentam baixa estatura e peso corporal, lipodistrofia e problemas ao nível da pele e ossos. O sistema cardiovascular é gravemente afectado, sendo as principais causas de morte, numa idade média de 14,6 anos, enfarte do miocárdio e acidente vascular cerebral.

Os doentes não demonstram sintomas ao nível neurológico, o que tem sido associado à regulação da expressão de progerina pelo microRNA 9, em células neurais. No entanto, pouco mais se conhece acerca do impacto da doença ao nível do cérebro. Neste sentido, e atendendo ao papel da disfunção hipotalâmica no processo sistémico de envelhecimento, o primeiro objectivo deste estudo foi compreender o efeito do envelhecimento prematuro no hipotálamo de um modelo animal de HGPS, o murganho *Lmna*$^{G609G/G609G}$.

Os resultados obtidos sugerem que os níveis proteícos do NPY e AgRP aumentaram, enquanto que os de POMC diminuíram, ao longo do tempo, no hipotálamo de murganhos *Lmna*$^{G609G/G609G}$. Curiosamente, observaram-se tendências opostas na expressão génica destes neuropéptidos. Os níveis do marcador neuronal NeuN também se encontraram diminuídos, sugerindo que a estrutura neuronal do hipotálamo possa estar afetada. Porém, não foram observadas alterações na expressão de SOX2, marcador de neurogénese, nem de BDNF, um factor neurotrófico. Os resultados também apontam para fragilidades no sistema imunitário destes murganhos dado o declínio d a expressão génica ou dos níveis proteícos de proteínas envolvidas no processo inflamatório, como GFAP, um marcador de astrócios, Iba-1, um marcador de microglia IL-10, uma citocina anti-inflamatória. Estas são as primeiras evidências que sugerem uma disfunção hipotalâmica neste modelo, com relevo na progressão do envelhecimento prematuro em HGPS.

A grelina é o ligando endógeno do receptor do secretoma da hormona do crescimento (GHS-R). Tanto ela como o seu receptor são amplamente expressos no organismo, sendo descritos diversos efeitos benéficos em órgãos afectados pela HGPS: estimulação do apetite e adiposidade, protecção ao nível cardiovascular, remodelação dos ossos e proliferação celular. Recentemente, resultados obtidos pelo nosso grupo mostram que a grelina estimula a autofagia e promove a degradação da progerina, resgata anomalias nucleares, diminui danos no DNA, e induz a proliferação celular, retardando a senescência em células de doentes com HGPS. Atendendo a estes efeitos, o segundo objectivo deste estudo foi perceber se a administração de grelina retarda a progressão do envelhecimento prematuro em murganhos *Lmna*$^{G609G/G609G}$.

Murganhos *Lmna*$^{G609G/G609G}$ tratados com grelina demonstraram uma aparência mais saudável, sem sinais de cifose na coluna. O tratamento com grelina

induziu um aumento ligeiro no peso corporal dos mesmos, prevenindo a perda de peso em fases avançadas da doença. Os níveis de glucose no sangue também aumentaram com o tratamento. Observámos alterações na actividade locomotora e comportamento destes murganhos após administração de grelina, nomeadamente, houve uma diminuição da distância percorrida, velocidade média e do tempo despendido no centro da arena, sugerindo que o tratamento pode induzir ansiedade. O tamanho da maior parte dos órgãos não sofreu alterações significativas após tratamento com grelina. No entanto, observámos que o peso do tecido adiposo branco aumentou em muganhos *Lmna*$^{G609G/G609G}$ tratados com grelina, o que foi suportado pelo aumento do tamanho dos adipócitos. Também observámos que a grelina aumentou a espessura da camada de gordura subcutânea na pele, o que pode estar relacionado com a proliferação e diferenciação de adipócitos. Adicionalmente, murganhos *Lmna*$^{G609G/G609G}$ tratados com grelina apresentram um aumento da espessura da epiderme na pele, um aumento da proliferação de hepatócitos no fígado e um aumento da área do tecido linfático no baço, o que sugere que a grelina tem um efeito na proliferação celular nestes órgãos. Também foi observado um aumento do tamanho das fibras musculares nos murganhos *Lmna*$^{G609G/G609G}$ tratados com grelina. A grelina também mostrou ter efeitos na regulação da autofagia e proliferação celular, dois mecanismos que se sabem estar comprometidos durante o envelhecimento. Porém, as alterações observadas dependenderam do órgão estudado. Inesperadamente, o tratamento com grelina diminuiu a expressão de NPY e AgRP no hipotálamo de murganhos *Lmna*$^{G609G/G609G}$, mas teve o efeito oposto em murganhos *Lmna*$^{+/+}$. Também atenuou a diminuição da expressão de GFAP observada na primeira parte do trabalho, e aumentou a expressão de IL-10. Estes resultados mostram que a grelina tem efeitos benéficos no peso corporal, hipoglicémia, lipodistrofia e na histopatologia de vários órgãos em murganhos *Lmna*$^{G609G/G609G}$, apontando para melhorias no fénotipo deste modelo.

Em suma, este estudo foi o primeiro a apontar para alterações hipotalâmicas num modelo de murganhos HGPS. No entanto, são necessários mais estudos com vista a compreender a função do hipotálamo na progressão de HGPS. Mais ainda, este estudo apresenta a grelina como uma uma estratégia promissora para atrasar ou bloquear o envelhecimento prematuro que caracteriza a HGPS.

Chapter 1

Introduction

1. Introduction

1.1. Aging

According to the World Population Ageing 2015 report of the United Nations, the world's population is aging, with almost every country showing an increase in the proportion of elderly, and this problem has a tendency to be exacerbated in the following years (Figure 1.1). Although this event is partly caused by an improvement of the health policies, it may also represent a burden due to its socioeconomic impact, with greater expenses in healthcare. Thus, a clearer understanding of the mechanisms underlying the aging process is, now more than ever, a necessity.

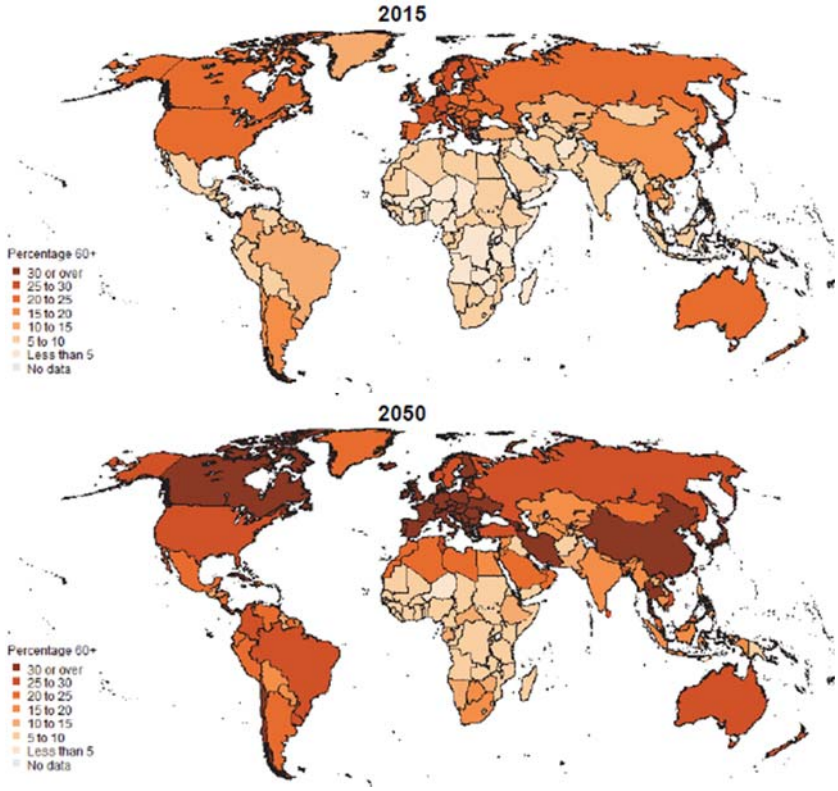

Figure 1.1. **Percentage of the population over 60 years old in 2015 and its expected evolution in 2050.** (Data source: United Nations, 2015).

Aging is associated with increased risk of developing several pathologies and chronic diseases (Kirkwood 2005), such as metabolic syndrome, cancer, cardiovascular and liver disease, and neurodegenerative disorders like Alzheimer's and Parkinson's disease, among others, which lead to a generalized discomfort and worse quality of life in older stages. It is linked to a progressive process of generalized loss of function that affects all tissues of our body, rendering a higher vulnerability and more pronounced difficulties to face environmental challenges and adapt to adverse situations (Kirkwood 2005).

The mechanisms classically thought to mediate the aging process include: increase of mutations and DNA damage; telomere reduction and loss of cell division capacity (Kim Sh *et al.* 2002); impaired mitochondria and consequent decrease in

adenosine triphosphate (ATP) production; and altered protein function and accumulation damaged proteins (Kirkwood 2005). Although each of these mechanisms is associated with aging, none of them could explain it alone, hence the construction of an integrated theory, considering many different events, was needed. This holistic point of view was achieved by Carlos López-Otín and colleagues who proposed the nine hallmarks of aging (Lopez-Otin *et al.* 2013) that represent common denominators mechanisms underlying the aging process, which co-occur during aging and are interconnected: genomic instability, telomere attrition, epigenetic alterations, loss of proteostasis, deregulated nutrient sensing, mitochondrial dysfunction, cellular senescence, stem cell exhaustion, and altered intercellular communication.

1.1.2. Hallmarks of aging

1.1.2.1. Genomic instability

Somatic mutations appear in cells and accumulate throughout life, leading to genetic damage which constitutes one of the most frequent events in aged cells (Moskalev *et al.* 2013). These mutations are caused by extrinsic insults, either physical, chemical or biological, or intrinsic insults, like replication errors, reactive oxygen species (ROS) or defects in the repair mechanisms of DNA (Hoeijmakers 2009). Mitochondrial DNA also harbors mutations that contribute to the aging phenotype. Actually, mitochondrial DNA is especially prone to acquire and build-up such mutations due to the oxidative environment and the decreased fidelity of the repair mechanisms (Linnane *et al.* 1989, Park and Larsson 2011).

All the modifications in the DNA have the potential to affect genes and pathways that are critical to the normal functioning of cells. To protect themselves against these insults, cells possess a complex system of DNA repair mechanisms capable of handling DNA damage (Garinis *et al.* 2008). These mechanisms are able to maintain genomic and mitochondrial DNA integrity, telomere functionality and structure (Blackburn *et al.* 2006, Kazak *et al.* 2012). DNA repair mechanisms activate specific proteins such as poly (ADP-ribose) polymerase 1 (PARP1) and ataxia telangiectasia mutated (ATM), that will in turn trigger the activation of multiple proteins involved in autophagy regulation, cell cycle, apoptosis and DNA repair. However, with time, DNA damage progressively accumulates reaching a critical threshold at which this highly complex and functional system cannot cope with leading to cellular senescence and ultimately cell death.

The impairment of the signaling pathways can constitute a harmful event that may lead to the deregulation of the cells, and consequently lead to the loss of function of tissues (Lopez-Otin *et al.* 2013). Supporting the notion that genomic instability and consequent mutations have an impact on aging is the finding that Werner syndrome, a type of progeria syndrome, is caused by the loss of function of a component of the DNA repair machinery (Lopez-Otin *et al.* 2013) and results in an accelerated aging phenotype.

1.1.2.2. Telomere attrition

Telomeres are specialized structures in the ends of chromosomes and are essential to protect and stabilize the integrity of the DNA. However, telomeres are particularly susceptible to deterioration, losing the capacity to replicate completely the terminal ends of linear DNA molecules with age (Blackburn *et al.* 2006). To maintain the telomeres the enzyme telomerase is of major importance because it is the only DNA polymerase known with the ability to replicate the terminal ends of linear DNA molecules (Blackburn *et al.* 2006). Most mammalian somatic cells do not express telomerase and these results in progressive telomere attrition which had been proposed to be the trigger of cellular senescence (Blasco 2007). This process is involved in the loss of proliferative capacity of cells cultured *in vitro* after some passages, even when nutrients and space are available, which is known as the Hayflick limit (Hayflick and Moorhead 1961). In fact, DNA damage in telomeres is not corrected in an efficient manner and it is effective in inducing senescence (Fumagalli *et al.* 2012).

Telomere shortening is thought to mediate aging since forced expression of telomerase, resulting in increased length of telomeres, is able to delay Hayflick limit in cultured cells for an undefined amount of time (Bodnar *et al.* 1998). One strong indication in this direction comes from animal models: wild-type mice with shorter telomeres, generated by the successive crossing of *m*TR$^{+/-}$ heterozygous mice (Armanios *et al.* 2009) showed decreased lifespan, while mice with lengthened telomeres, due to the constitutive expression of telomerase reverse transcriptase (TERT), were described to have increased lifespan (Tomas-Loba *et al.* 2008). In humans, the absence of telomerase is connected with the development of diseases in which there is a loss of tissue regenerative capacity (Armanios 2013) and accelerated aging.

1.1.2.3. Epigenetic alterations

In recent studies on aging it has been proposed that the number of alterations in the epigenetic patterns increases and these changes are fundamentally influenced by environmental factors (Talens *et al.* 2012). These variations in the epigenetic patterns are age-associated and include histone modifications, DNA methylation, chromatin remodeling and transcriptional alterations which affect multiple nuclear processes such as gene transcription and silencing, cell cycle progression, DNA replication/repair and telomere structure/function (Talens *et al.* 2012, Lopez-Otin *et al.* 2013). Consequently, it affects genomic stability and the maintenance of heterochromatic domains. It has been proposed that epigenetic alterations correlate with age-related diseases, particularly cancer, since some of the epigenetic modifications in cancer and in aging are similar. This suggests that accumulation of these defects with age may lead to higher susceptibility to cellular malignant transformation and to develop cancer. Epigenetic changes are both responsive to and effectors of the aging process (Gonzalo 2010).

Epigenetic changes are associated with alterations in the expression of genes that can lead to the disruption of the normal functioning of the cells. Molecules that act on the epigenetic modulation of the genome can also have an important role in the changes of the expression of some genes during aging. For instance, sirtuins, deacetylases dependent of NAD^+, have been identified as anti-aging factors due to their actions in the improvement of aging aspects in mice (Sebastian *et al.* 2012). Overexpression of several isoforms of sirtuins has been shown to improve aging associated features (Lopez-Otin *et al.* 2013) which supports the idea that epigenetic regulation can affect aging.

Aging is also associated with loss of global heterochromatin and related chromatin disorganization (Oberdoerffer and Sinclair 2007). Supporting this notion, it was shown that flies with mutated heterochromatin protein 1 alfa (HP1α), a protein involved in the formation and maintenance of heterochromatin, present shorter lifespan (Larson *et al.* 2012). Concordantly, in the same study, the authors observed that its overexpression led to the extension of the flies' lifespan.

Interestingly, cells and mice models of progeroid syndromes show patterns of DNA methylation and histone modifications resembling those found in normal aging (Shumaker *et al.* 2006).

1.1.2.4. Loss of proteostasis

Continuous turnover between the synthesis and degradation of proteins is an extremely dynamic cellular process that prevents the accumulation of harmful substrates or components that lose functionality in the intracellular environment. This process is indispensable to keep the cellular machinery free from damaged proteins that could be toxic and interfere with the normal cellular function (Kirschner 1999, Squier 2001). The mechanisms involved in the preservation of the protein homeostasis, also called proteostasis, comprise the translation machinery, chaperones and proteolytic systems, namely the ubiquitin-proteasome system (UPS) and autophagy, and are collectively termed the proteostasis network (Balch *et al.* 2008, Kim *et al.* 2013).

Molecular chaperones, or heat shock proteins (HSP), belong to the HSP70, HSP90, DNAJ/HSP40, chapeonin/HPS60 and small HSP (sHSP) families and are pivotal for the correct *de novo* folding of proteins, refolding of proteins after stress, protein trafficking and also to their degradation (Feldman and Frydman 2000, Kim *et al.* 2013). These molecules have an important contribution in the maintenance of proteostasis and its age-related decline can be caused by a decreased ability of the cells to upregulate chaperones synthesis upon accumulation of unfolded and misfolded proteins or the sequestration of chaperones in protein aggregates (Calderwood *et al.* 2009, Vanhooren *et al.* 2015).

The clearance of misfolded, small short-lived, proteins is performed by the UPS. The proteins are targeted to the proteasome, a 26S multicatalytic protease, comprising

2 19S regulatory particles and the 20S proteolytic core (Chondrogianni and Gonos 2012). In order to be delivered to the proteasome, proteins have to be first polyubiquitinated by the concerted activity of E1 ubiquitin-activating enzymes, E2 ubiquitin-conjugating enzymes, and E3 ubiquitin ligases (Finley 2009). Once in the proteasome, ubiquitin chains are removed from the substrates to allow their entrance in the proteolytic core and consequent degradation (Finley 2009). The UPS activity seems to be decreased with aging, thus contributing to the age-related loss of proteostasis (Tomaru *et al.* 2012).

Another mechanism that leads to the degradation of cellular components is autophagy. This process is responsible for the removal of larger protein aggregates, insoluble inclusions and even entire damaged organelles (Yang and Klionsky 2010, Choi *et al.* 2013). There are 3 types of autophagy described so far: macroautophagy, microautophagy and chaperone-mediated autophagy (CMA). The most studied is the macroautophagy, where regions of the cytosol, damaged proteins or organelles are engulfed by a double-membrane vesicle structure, the autophagossome, which fuses with the lysosome for the degradation of the cargo (Yang and Klionsky 2010).

Proteins are the main effectors of the cells and need to be properly folded in order to play their role. The alteration in protein dynamics and proteostasis has been linked to aging, with the presence of misfolded and aggregated proteins being shown to have direct actions on age-related diseases like Alzheimer's and Parkinson's (Powers *et al.* 2009, Koga *et al.* 2011). Accordingly, it was shown that the activity of both autophagy and UPS have an age-related decline (Rubinsztein *et al.* 2011, Tomaru *et al.* 2012), which leads to a decreased capacity of the cells to eliminate toxic proteins and replace them for healthy ones.

Studies have suggested a strong link between protein health and aging. The knock-out of the C terminus of heat shock cognate protein 70 (HSC70)-Interacting Protein (CHIP), a cochaperone of the heatshock family, in mice caused a reduced lifespan and an accelerated aging phenotype related with impaired protein quality control (Min *et al.* 2008). In concordance, it was observed that a long-lived strain of dwarf mice exhibits an upregulation of some heat-shock proteins (Swindell *et al.* 2009). Furthermore, rapamycin delays aging phenotype in mice (Wilkinson *et al.* 2012) by stimulating autophagy and enhancing the degradation and turnover of proteins.

1.1.2.5. Deregulated nutrient sensing

There are several pathways within our cells that can sense levels of energy and nutrient and subsequently trigger adequate adaptive responses to changes in their microenvironment. Among them there are: the insulin and IGF-1 signaling pathway (IIS), the mechanistic target of rapamycin (MTOR), the 5' adenosine monophosphate-activated protein kinase (AMPK) and sirtuins (Houtkooper *et al.* 2010, Lopez-Otin *et al.* 2013). These signaling pathways are interconnected and are responsible for the

orchestration of the metabolic regulation of the cells according to the extracellular conditions.

IGF-1 is a very conserved pathway that regulates aging, being activated when nutrients are in abundance and in response to growth hormone (GH) levels. This pathway targets the Forkhead box protein O1 (FOXO1) family of transcription factors and the MTOR complexes, known to be also important in the aging process. It has been described an age-related decline of the levels of GH and IGF-1, also observed in some progeroid mice models (Schumacher *et al.* 2008). However, the attenuation of IIS pathway leads to extension of lifespan in several models (Fontana *et al.* 2010). Constitutively decreased IIS signaling in experimental animals may have beneficial effects on survival due to lower rates of cell growth and metabolism, which can protect cells from excessive damage (Lopez-Otin *et al.* 2013).

MTOR kinase is the master regulator of anabolic metabolism (Laplante and Sabatini 2012) and downregulation of its activity seems to be essential in order to increase lifespan (Harrison *et al.* 2009, Lamming *et al.* 2012, Johnson *et al.* 2013). On the other hand, the anabolic activity of MTOR is associated with accelerated aging.

As previously described, the pathways mentioned are interconnected, which means that modulation of one of them impacts the others. AMPK and sirtuins have opposite effects to IIS and MTOR, since they signal low levels of energy and nutrients, leading to catabolism. Dietary restriction increases life and healthspan in most models studied, including non-human primates, by affecting all of these signaling pathways (Colman *et al.* 2009, Fontana *et al.* 2010, Mattison *et al.* 2012). The diminished intake of calories renders a negative energy status in the cells, which activates the cellular pathways related with catabolism, namely, the AMPK and sirtuins. Activation of AMPK is known to inhibit MTOR and consequently mediates lifespan increase in worms and mice whereas sirtuins activity enhances antioxidant defenses, improves fatty acid oxidation and promotes mitochondrial formation. Besides, low glucose levels due to reduced calorie intake will also inhibit the IGF1 pathway, and thus decrease even further MTOR activity, activating autophagy and other processes involved in the maintenance of homeostasis (Lopez-Otin *et al.* 2013).

1.1.2.6. Mitochondrial dysfunction

Mitochondria are the organelles responsible for the production of the majority of energy in the aerobic cells. However, the efficiency of the respiratory chain diminishes as the age of the organisms progresses, which results in less ATP production and leakage of electrons and ROS (Green *et al.* 2011).

Until recently, aging was thought to be mediated by a progressive mitochondrial dysfunction that would lead to increased production of ROS and further damage on the mitochondria and other cell's components (Harman 1965). But this view has been challenged by discoveries showing ROS signaling triggering proliferation and survival responses under stress condition (Sena and Chandel 2012). These findings suggest that

ROS primary outcome is the activation of survival responses but with aging, and associated increases in cellular stress and damage, its levels are upregulated beyond a certain threshold, which aggravate the age-associated damage. Basically, ROS in controlled amounts can trigger protective mechanisms, but once they are in excessive concentration become harmful to the cells (Hekimi *et al.* 2011). Excessive ROS and mitochondria deficiencies lead to decrease cellular homeostasis and accelerate aging and promote disease (Green *et al.* 2011).

1.1.2.7. Cellular senescence

Cellular senescence is triggered by several different mechanisms, including telomere shortening, accumulation of DNA damage, oxidative stress or hyperproliferative stimuli and represents a permanent arrest of the cell cycle (van Deursen 2014). All these events build-up as the cell, and the organism, ages resulting in the increase of the number of senescent cells (van Deursen 2014). The accumulation of senescent cells can be due to an increase in the number of cells entering senescence or to a decrease in their clearance by immune cells (Lopez-Otin *et al.* 2013).

Senescence arises as a compensatory mechanism with the purpose of avoiding the proliferation of damaged cells that have the potential to become oncogenic. However, other functions have been proposed due to their role in wound healing and development (van Deursen 2014).

Senescent cells lose their functionality and, therefore, do not contribute for the function of the tissue where are included, which makes their replacement essential. The process of replacement involves the clearance of the senescent cells by the immune system and the mobilization of stem cells to replace them (Lopez-Otin *et al.* 2013). With age, the turnover system becomes inefficient and the stem cells lose their regenerative capacity, resulting in accumulation of senescent cells that can compromise the tissues and contribute to the aging phenotype. In addition, this is aggravated by changes in the secreted molecules of senescent cells. These cells have a particular secretome, named senescence-associated secretory phenotype (SASP) that consists of proinflammatory cytokines, chemokines and metalloproteinases (MMP) which promote inflammation, influencing the surrounding cells and microenvironment. Stem and progenitor cells, in addition to somatic cells, are affected and consequently the regeneration of the tissues is impaired. The degradation of the extracellular matrix (ECM) leads to an abnormal tissue architecture, and all these events contribute to the aging process (Rodier and Campisi 2011, van Deursen 2014).

Findings supporting this notion come from different studies where it is shown that targeting specifically senescent cells, promoting their clearance, ameliorates the health and increases lifespan of different animal models (Merino *et al.* 2015, Baker *et al.* 2016).

1.1.2.8. Stem cell exhaustion

One of the features observed in aging is the decline in the regenerative potential of the tissues, and this is related to decreased capacity of cells to proliferate and replace the damaged ones. Also, it was observed that tissues age, in part, because of defective proliferation of stem cells, which do not replace the cleared senescent cells (Lopez-Otin *et al.* 2013). This loss of replicative potential of stem cells can be related with hallmarks described so far, for instance telomere attrition (Sharpless and DePinho 2007), DNA damage accumulation (Rossi *et al.* 2007) and overexpression of cell cycle inhibitors (Janzen *et al.* 2006). It is argued that the induction of INK4a and the decrease in the expression of IGF-1 during aging can be seen as mechanisms that try to maintain the quiescence of stem cells, in order to limit their exhaustion at earlier stages (Lopez-Otin *et al.* 2013). This exposes the intricate and complex connectivity between all the hallmarks.

Strategies involving stem cells rejuvenation have been proposed to reverse the aging phenotype (Rando and Chang 2012) suggesting a link between the genetic and molecular pathways of stem cell quiescence and self-renewal and longevity.

1.1.2.9. Altered intercellular communication

With aging, several changes occur at the cellular level that lead to compromised intercellular communication at neuronal, endocrine or even neuroendocrine level (Russell and Kahn 2007, Laplante and Sabatini 2012, Zhang *et al.* 2013).

The chronic proinflammatory phenotype observed in aging leads to the deregulation of the signaling of several hormones and is commonly called “inflammaging” (Salminen *et al.* 2012). The emergence of this inflammatory state can have its origin in several factors like the dysfunction of the immune system, the SASP of senescent cells, the enhanced expression of the nuclear factor kappa B (NF-kB) transcription factor that results in the activation of inflammatory pathways or the accumulation of tissue damage that trigger inflammatory responses (Salminen *et al.* 2012).

One strong evidence linking inflammation and aging came from Zhang and colleagues study, where they show increased expression of NF-kB in the hypothalamus due to inflammatory and stress responses. This increased NF-kB activity leads to the deregulation of the release of hormones by hypothalamus, including gonadotropin-releasing hormone (GnRH). They show that the inhibition of the inflammatory pathways triggered by NF-kB is sufficient to extend lifespan (Zhang *et al.* 2013). A positive and future point of interest is that the restoration of the cellular defective communication caused by aging through genetic, pharmacological and especially nutritional interventions can improve the intercellular gap that aging promotes (Freije and Lopez-Otin 2012). In fact, some studies have found that the administration of anti-inflammatory drugs increases longevity (Strong *et al.* 2008, Rothwell *et al.* 2011). Besides inflammation, it is possible to speculate that the altered gene expression can

have an impact on aging. It is possible that the activation or inhibition of some genes may contribute even further to the aging phenotype (Lopez-Otin *et al.* 2013).

1.2. Lamins

One major cause of genomic instability, one hallmark of aging, is the defects in nuclear lamina. Nuclear lamins constitute the main components of the nuclear lamina and participate in genome maintenance (Liu *et al.* 2005, Gonzalez-Suarez and Gonzalo 2010, Gruenbaum and Medalia 2015). Lamins, type V intermediate filament proteins, are structural components of the nuclear lamina, a protein network that lines the inner nuclear membrane and determines the shape, integrity and size of the nucleus (Burke and Stewart 2006, Swift *et al.* 2013).

Lamins can be classified into two types: the B-type lamins, including the major isoforms Lamins B1 and B2, necessary for replication and transcription, meaning it is not possible for cells to live without this type of lamin; and the A-type lamins, including the major isoforms, Lamins A and C (Burke and Stewart 2006). These types of nuclear laminas consist in a globular C-terminal tail domain, a α-helical rod domain important for dimerization and an N-terminal head domain (Hennekam 2006, Swift *et al.* 2013). These lamins are, primarily, synthesized in the cytoplasm and afterwards imported to the nucleus (Bridger *et al.* 1993, Hozak *et al.* 1995, Gruenbaum *et al.* 2005), constituting the inner nuclear membrane (Worman and Bonne 2007). Besides their structural and biochemical differences, B-type lamins differ from A-type lamins because they are expressed throughout development while the latter only start to be expressed in later stages (Eckersley-Maslin *et al.* 2013, Gruenbaum and Medalia 2015).

Due to their localization lamins play important roles related with DNA and nuclei functions. Indeed, it has been described their importance in a multitude of functions ranging from the structural arrangement of the nucleus to gene regulation, DNA repair and also mechanosignaling pathways (Gruenbaum and Medalia 2015, Vidak and Foisner 2016). Many of these diverse roles are achieved by the direct interaction with different proteins. One example is lamin associated polypeptide 2 alfa (Lap2α) that can form a complex with lamin A and is thought to regulate cell proliferation and differentiation mediated by the retinoblastoma protein (Markiewicz *et al.* 2002, Dorner *et al.* 2006, Naetar *et al.* 2008), and chromatin organization (Zhang *et al.* 2013, Bronshtein *et al.* 2015). Lamin A was also described to directly interact and activate SIRT6, thus promoting DNA repair. The authors further hypothesized that this activation occurred because lamin A binds SIRT6, stimulating its recruitment to the chromatin and enabling the interaction with the right partners in this task (Ghosh *et al.* 2015). The same group showed previously that lamin A also interacts with SIRT1 (Liu *et al.* 2012).

In vertebrates, lamins A and C are alternatively spliced transcripts of the LMNA gene which include 12 exons and are expressed mainly in differentiated cells (Furukawa *et al.* 1994, Machiels *et al.* 1996, Burke and Stewart 2006, Swift *et al.* 2013).

While LMNA exons 1-10 encode both lamins A and C, exons 11 and 12 encode the carboxy-terminal tail of lamin A. Lamin C is directly translated and directed to the nuclear envelope while lamin A is synthesized as prelamin A which contains in its C-terminus a CaaX box (cysteine, 2 aliphatic amino acids, any amino acid) and, as lamins B1 and B2, needs to undergo several posttranslational processing steps to become fully mature and functional (Young *et al.* 2005). The first three steps of the processing are common between type-B lamins and lamin A and start with the addition, by a farnesyl transferase, of a farnesyl group to the cysteine residue in the CaaX box. Then, zincmetalloproteinase STE24 (ZMPSTE24) cleaves the –aaX peptide and the farnesylated cysteine residue left is carboxymethylated. The processing of B-type lamins stops at this point; however, lamin A goes through an additional step: the removal of 15 amino acids from its C-terminal, including the carboxymethylated and farnesylated cysteine, accomplished by the action of ZMPSTE24 (Figure 1.3) (Weber *et al.* 1989, Beck *et al.* 1990, Sinensky *et al.* 1994, Pendas *et al.* 2002). The hydrophobic farnesyl group confers to the molecules the ability to strongly interact with the inner nuclear membrane, hence, lamins of the B-type, which remain with the farnesylated cysteine, are predominantly located at the nuclear periphery. On the other hand, lamin A, which is depleted of such group, can also be found in the interior of the nucleus (Dechat *et al.* 2010, Kolb *et al.* 2011).

Alterations in the structure, localization or function of lamins can result in significant alterations in the cell structure and function. Mutations in the LMNA gene can lead to severe phenotypes and are termed laminopathies (Vidak and Foisner 2016), including, lipodystrophies, muscular dystrophy disorders, peripheral neuropathies, and the study of these gained more attention by aging researchers when it was discovered that the mutations in these lamins also could originate premature aging syndromes, such as Hutchinson-Gilford Progeria Syndrome (HGPS), Atypical Werner Syndrome (AWS) and Restrictive Dermopathy (RD) (Gonzalo and Kreienkamp 2015, Gonzalo and Eissenberg 2016, Vidak and Foisner 2016).

1.3. Hutchinson-Gilford Progeria Syndrome (HGPS)

HGPS, commonly known as Progeria, is a rare genetic condition characterized by premature and accelerated aging (Hennekam 2006, Gordon *et al.* 2014). This disease was first described by Jonathan Hutchinson in 1886 (Hutchinson 1886) in a 3 years old boy. Later a second case was portrayed in 1895 by Hutchinson but Hastings Gilford was the one who described it in great detail. Later, Gilford crossed the information between the two patients and designated the disease as a premature aging syndrome based on the overall resemblance of patients to aged individuals (Gilford 1897, Gilford 1904). For more than a century, the characterization of this syndrome was extremely difficult due to the fact that it is one of the rarest diseases in the world, affecting scarcely 1 per 4-8 million newborns worldwide (Hennekam 2006). Currently, as of April 2017, there are 148 children living with progeria in 46 different countries

(www.progeriaresearch.org/patient_registry.0120 html). The onset of the symptoms occur within the first year of life (Ullrich and Gordon 2015). The progressive and degenerative process initiated at this point leads these children to have an average lifespan of 14.6 years old, succumbing predominantly due to myocardial infarction and stroke (Gordon *et al.* 2014).

1.3.1. Clinical features

The clinical characteristics of patients with HGPS are remarkably consistent and individuals appear very similar in phenotype, although some signs and symptoms vary in age depending on the onset and severity of the disease (Merideth *et al.* 2008)

HGPS patients have a normal early development which is reflected by a regular weight at birth, but within the first year of life they start to manifest typical features of premature aging (Figure 1.2) (Ullrich and Gordon 2015).

The most noticeable and characteristic traits derived from HGPS, besides the growth impairment (Gordon *et al.* 2007) and reduced body weight, are the craniofacial abnormalities and skin changes, accompanied by loss of hair (alopecia) and fat (lipodystrophy). As the disease progresses problems in bones and joints become evident, as well as the development of atherosclerosis (Merideth *et al.* 2008, Ullrich and Gordon 2015). Due to the loss of hair and subcutaneous fat the vasculature in these children is very pronounced, especially in the scalp (Figure 1.2). Additionally, the lipodystrophy leads also to insulin resistance (but not diabetes) and sensitivity to cold (Merideth *et al.* 2008, Gerhard-Herman *et al.* 2012).

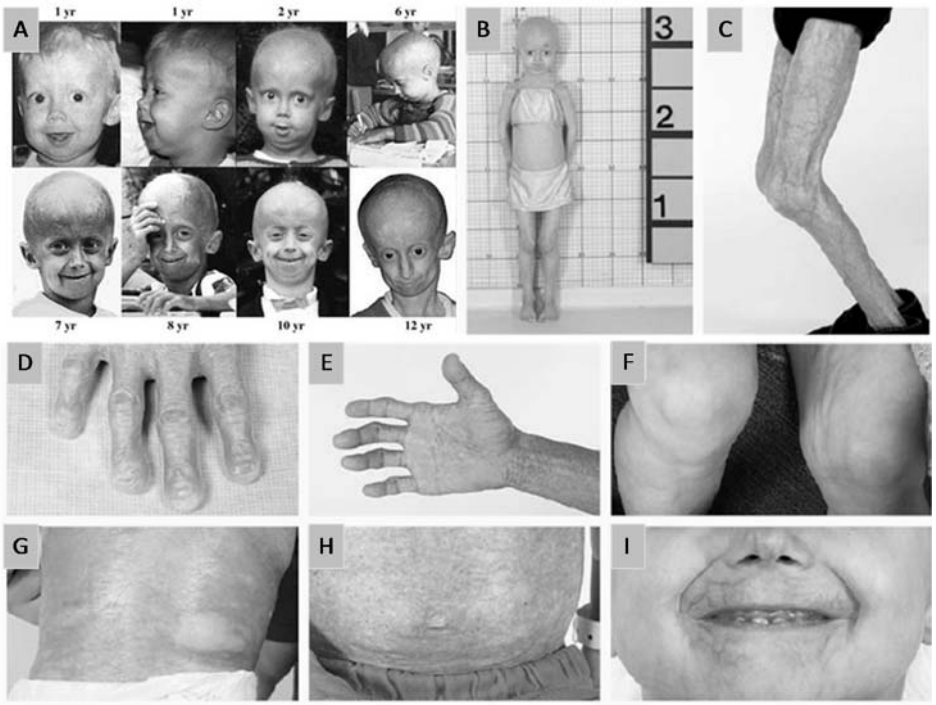

Figure 1.2. **HGPS clinical features.** (A) HGPS progression in one individual. HGPS patients seem healthy until the first year of age, when become to develop symptoms of the disease. (B) It is visible growth retardation, accompanied by alopecia and premature aging. (C) Knee joints and contractures and

prominent veins. (D, E) Tufting of the fingers and phalangeal joint contractures. (F) Cellulite. (G) Areas of hypopigmented skin. (H) Abdominal shrinkage. (I) Circumoral cyanosis. Adapted from (Hennekam 2006, Merideth *et al.* 2008).

Children with HGPS have a short and thin stature, with an average height of 110 cm and the mean weight of 14.5 kg (Hennekam 2006) and do not become sexually mature and therefore do not reproduce, but are considered intellectually normal and do not show signs of alterations in organs such as the liver, lungs, bone marrow and gastrointestinal and immune systems (Ullrich and Gordon 2015). However, these children present significant vascular changes including accelerated vascular stiffening, occlusive disease, atherosclerotic plaque formation and in later years valvular and cardiac insufficiency leading to angina, dyspnea and hypertension. The main cause of death are cardiovascular complications, including myocardial infarction or stroke due to the fast progress of atherosclerosis (Ullrich and Gordon 2015).

HGPS patients present multisystemic premature aging alterations similar, in many aspects, to the observed during natural aging; however, patients do not appear to develop cognitive deterioration nor dementia, although the occurrence of silent infarcts in a great percentage of the these children (Silvera *et al.* 2013) and the consequent accumulated damage, leads to permanent neurologic symptoms (Ullrich and Gordon 2015).

1.3.2. Etiology

HGPS can be classified as a classical HGPS, the most common variant which follows an autosomal dominant pattern of inheritance and is caused by a spontaneous point mutation within LMNA gene, and as non-classical HGPS, which follows an autosomal recessive pattern of inheritance (Hennekam 2006).

Classical HGPS is caused by a *de novo* heterozygous point mutation in LMNA gene exon 11 in which the cytosine in the position 1824 is altered to a thymine (1824C>T) (De Sandre-Giovannoli *et al.* 2003, Eriksson *et al.* 2003), that gives rise to a silent substitution in the codon 608 (G608G). Even though it does not alter the amino acid sequence, the mutation activates a cryptic donor site that results in the transcription of a prelamin A mRNA with a deletion of 150 nucleotides. When translated, it generates a mutant truncated lamin A named progerin, which lacks 50 amino acids near its C-terminus. Among these excluded amino acids lies the ZMPSTE24 recognition site, which was previously mentioned as an important mediator in the processing of prelamin A (Eriksson *et al.* 2003), that in these conditions is not able to identify the local of proteolytic cleavage (Figure 1.3). This deletion does not affect, however, the nuclear localization signal nor the ability of progerin to interact with normal lamin A (Sinensky *et al.* 1994). Consequently, progerin does not undergo through the farnesyl group excision but goes to the nucleus becoming strongly associated with the inner nuclear membrane and shifting its predominant localization to the nuclear periphery (Dechat *et al.* 2007). This leads to its abnormal association

with the nuclear membrane which induces numerous nuclear envelope abnormalities (Figure 1.4) (Goldman *et al.* 2004, Dechat *et al.* 2007).

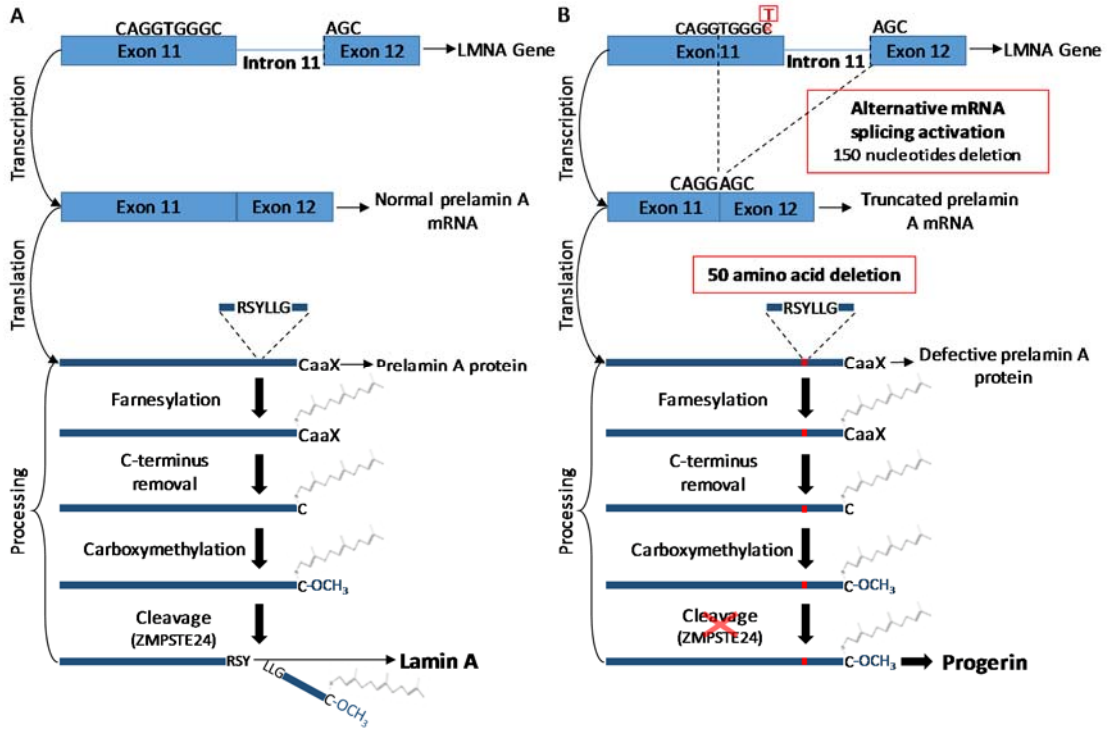

Figure 1.3. **Lamin A and progerin processing**. (A) Illustration of the normal events during lamin A synthesis, including transcription, translation and posttranslational processing. (B) Illustration of the defective processing of progerin, which remais permanently farnesylated. Adapted from: (Coutinho *et al.* 2009, Reunert *et al.* 2012)

In HGPS the unmutated LMNA allele guarantees the transcription of the normal amount of lamin A, whereas the mutated one produces both abnormal (85 %) and normal (15 %) transcripts (Reddel and Weiss 2004). The clinical features of the disease are caused precisely by the action of this aberrant lamin A in a dominant-negative manner (Ullrich and Gordon 2015). Recent studies show that progerin is more resistant to degradation than lamin A or B, which further aggravates the HGPS phenotype (Wu *et al.* 2016).

Individuals carrying the mutation seem normal at birth and only develop the symptoms later because progerin is not expressed during early fetal development when cells are not fully differentiated, similarly to lamin A (Liu *et al.* 2011).

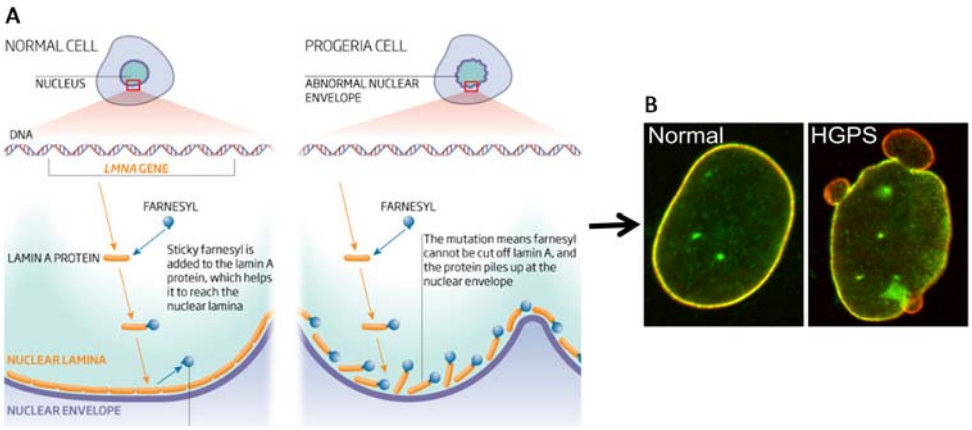

Figure 1.4. **Nuclear defects in HGPS cells**. (A) Lamin A and progerin inclusion in the nuclear envelope of normal and HGPS cells, respectively. Adapted from NewScientist. (B) Immunostaining of skin fibroblasts taken from a normal individual (left) and a HGPS patient (right) showing nuclear blebbing. Lamin A/C is labelled red and lamin B1 in green (Shimi *et al.* 2012).

1.3.3. Progerin and hallmarks of aging

In the past few years many different studies contributed to the association between HGPS and normal aging. Indeed, many of the cellular features occurring in HGPS are shared with normal aging (Burtner and Kennedy 2010) and, interestingly, it was found that the cells and tissues of healthy aged individuals also accumulate progerin. The LMNA gene, even when not mutated, can sporadically use the cryptic splice site typically associated with HGPS, producing progerin and accumulating it at a slow rate (Scaffidi and Misteli 2006, McClintock *et al.* 2007) as observed in vascular tissues, skin and even adipose tissue of healthy individuals (McClintock *et al.* 2007, Olive *et al.* 2010, Revechon *et al.* 2017).

1.3.3.1. Genomic instability and altered gene expression

The accumulation of progerin has consequences in the nuclear morphology and chromatin organization (Eriksson *et al.* 2003) as expected since lamins are important components of the nuclear envelope. The nuclei of the cells harboring high amounts of progerin become lobulated with a thicker lamina and there is a decrease in the expression of HP1α and Lap2α which can be related with loss of peripheral heterochromatin (Goldman *et al.* 2004, Vidak *et al.* 2015).

It was demonstrated that progerin binds lamin A and that this is deleterious for the cells since the disruption of such interaction was able to ameliorate the HGPS phenotype of HGPS cells (Lee *et al.* 2016). Progerin may interfere with the normal function of lamin A by sequestering it in the nuclear periphery and preventing its dynamic flow. Indeed, lamin A in healthy cells can move between the nuclear membrane and the nucleoplasm regulating the stiffness of the nucleus (Swift *et al.* 2013) but becomes immobilized in the periphery in HGPS cells (Goldman *et al.* 2004) leading to rigidity of this structure and impairing mechanosignaling pathways (Dahl *et al.* 2010). Supporting the importance of this toxic process, cardiovascular system,

bones and joints, structures that are submitted to a lot of mechanical stress, are among the most affected organs in the context of the disease. In addition to the described above, Ghosh and colleagues revealed that progerin binds SIRT6 and is able to sequester this deacetylase at the nuclear periphery, preventing its recruitment to the chromatin (Ghosh *et al.* 2015). In fact, they demonstrated that this interaction has higher affinity than the lamin A/SIRT6, revealing a dominant-negative role for progerin. Since SIRT6 is involved in the activation of DNA repair mechanisms, the impairment of its activity can constitute a means by which DNA instability occurs in HGPS (Ghosh *et al.* 2015).

All these effects can have a great impact on gene expression, and along with the impairment of DNA repair mechanisms, foster genomic instability and telomere attrition (Gonzalo and Kreienkamp 2015).

1.3.3.2. Telomere attrition

Benson and colleagues showed that progerin-induced DNA damage is also localized in the telomeres and that it can provoke chromosomal aberrations in HGPS cells (Benson *et al.* 2010). By infecting HGPS cells with viral vectors carrying telomerase they were able to rescue the characteristic premature senescence observed in these cells. This extension in the cellular lifespan was correlated with decreased protein levels of p53, p16 and p21 compared to controls (Benson *et al.* 2010). This way, progerin was associated with telomeric deformations and this is possibly caused by the disruption of the interaction between lamins and the ends of the chromosomes, leading to inefficient maintenance and repair in the telomeres. These findings point to the role of telomere dysfunction in the development of the cellular senescence in HGPS condition (Benson *et al.* 2010).

1.3.3.3. Epigenetic alterations

The epigenetic regulation of the genome is also destabilized in HGPS cells (Shumaker *et al.* 2006, McCord *et al.* 2013).

The patterns of methylation in CgP sites appear to be corrupted in HGPS cells when compared to normal ones (Heyn *et al.* 2013) and when looking for primary HGPS fibroblasts it was observed alterations in the patterns of methylation in the lysine 27 of the histone 3 (H3K27me3), an heterochromatin repressive mark (McCord *et al.* 2013). Moreover, in the latter study, it was shown that DNA-lamin A/C associations were compromised in the HGPS fibroblasts and this was related with loss of spatial compartmentalization of active and inactive chromatin domains (McCord *et al.* 2013).

1.3.3.4. Mitochondrial dysfunction and oxidative stress

Mitochondrial dysfunction appears to be a process that is triggered by accumulation of progerin, emphasizing the link between accelerated and normal aging processes. In fact, fibroblasts obtained from HGPS patients revealed a marked

downregulation of mitochondrial oxidative phosphorylation proteins, including cytochrome c, among others (Rivera-Torres *et al.* 2013). It was found that HGPS fibroblasts present a severely impaired mitochondrial function, which culminates with a lower ATP synthesis (Rivera-Torres *et al.* 2013). These findings are supported by a subsequent study where induced expression and accumulation of progerin through lentiviral infection in 3T3L1 preadipocytes led to diminished proliferative capacity and defects in adipogenic ability (Mateos *et al.* 2015). The authors assessed that the mitochondrial function of the cells expressing progerin was impaired, which was corroborated by a downregulation of the protein cytochrome c and an increase in the production of superoxide anion (Mateos *et al.* 2015). In progeroid mice, there is also an hyperactivation of NF-kB, an important transcription factor activated during stress and inflammation (Osorio *et al.* 2012) which can also be related with the chronic inflammation observed in HGPS models.

Taking into account the abovementioned, chronic oxidative stress emerges as an additional factor contributing for the harmful effects of progerin accumulation. Kubben and collaborators found that progerin can also block the antioxidant nuclear factor (erythroid-derived 2)-like 2 (Nrf2) pathway (Kubben *et al.* 2016), which can further aggravate the consequences of excessive ROS production. Nrf2 was shown to be sequestered by progerin, resulting in its subcellular mislocalization and hindered transcriptional activity (Kubben *et al.* 2016). Given that this transcription factor is involved in the activation of antioxidant genes, repression of this pathway may underlie the chronic oxidative stress observed in HGPS (Kubben *et al.* 2016).

1.3.3.5. Cellular senescence and stem cell exhaustion

The premature senescence of the cells has been considered one of the major mediators of the aging phenotype in HGPS. As a matter of fact, HGPS cells show hyperactivation of the p53 signaling pathway and consequent upregulation of its target genes (Varela *et al.* 2005, Kudlow *et al.* 2008).

Supporting evidences for the significance of senescence in progeroid syndromes, and possibly in HGPS, came from the work of Baker and colleagues (Baker *et al.* 2011). Using a very elegant strategy they were able to prevent the accumulation of senescent cells in a progeroid mouse model, and it increased health and mean lifespan of the animals, delaying the aging phenotype (Baker *et al.* 2011). Furthermore, using the same approach, they were able to have similar results in natural aging mice (Baker *et al.* 2016) highlighting cellular senescence as a central aging promoting mechanism.

In normal conditions, senescent cells are eliminated by immune cells and replaced through proliferation and differentiation of stem cells from the surrounding tissue. However, progerin accumulation was also shown to decrease the epidermal populations of adult stem cells in the skin of mice bearing the HGPS mutation, with a consequent impaired wound healing process (Rosengardten *et al.* 2011). Moreover, progerin seems to interfere with the function of human mesenchymal stem cells

(hMSC), leading changes in their identity and abnormalities within the differentiation process (Espada *et al.* 2008, Scaffidi and Misteli 2008, Rosengardten *et al.* 2011).

Altogether, the findings suggest that the different tissues are compromised because the fully mature cells become unhealthy, losing the capacity to proliferate and perfectly perform their roles, while the pools of stem cells become unable to compensate these defects. This culminates with the loss of function of the different tissues and the multisystem failure associated with aging and HGPS.

1.3.4. Altered signaling pathways

Gene expression is dependent on various factors in which are included lamina-chromatin interactions, microRNA regulation or the availability of transcription factors (Prokocimer *et al.* 2013), and consequently, it is possible to reason that in HGPS cells gene expression is altered.

One of the most important pathways affected in HGPS described so far is the tumor suppressor retinoblastoma (pRb) that is essential in determining cell fate and differentiation (Marji *et al.* 2010). Normally, lamin A/LAP2α complexes interact with this protein but this association is compromised in the context of the disease which leads to mislocalization, increased degradation and inactivation of pRb (Prokocimer *et al.* 2013).

Some lights have been shed on the molecular mechanisms underlying the characteristic defects on skin, vasculature, bone and adipose tissue of HGPS patients. Regarding the skin and vasculature problems, it has been documented that in normal conditions lamin A is responsible for the inhibition of fibroblast hyperproliferation promoted by transforming growth factor beta (TGF- β) signaling. However, in HGPS the interaction between these two players is deregulated which may represent an opportunity for the uncontrolled growth of fibroblasts and the consequent development of fibrosis (Van Berlo *et al.* 2005, Prokocimer *et al.* 2013). Using fibroblasts from a progeria mouse model it was unraveled that the Wnt/β-catenin signaling is decreased under HGPS conditions. This finding was associated with defective expression of genes related to extracellular matrix (ECM) (Hernandez *et al.* 2010). Moreover, progerin was shown to disrupt the interaction between lamin A and ski-interacting protein (SKIP), a co-activator of Notch. This interaction results in the sequestration of SKIP, however, in HGPS the loss of this link causes an excessive Notch signaling (Scaffidi and Misteli 2008). Interestingly, Wnt signaling is crucial for the correct development of bones and cartilages and Notch pathway regulates cell fate and stem cell differentiation during osteogenesis and adipogenesis (Vidak and Foisner 2016). The deregulation of these pathways may explain some of the problems observed in the bones in the context of the disease.

Progerin accumulation seems also to be related with the lipodistrophy observed in HGPS patients. The process of adipogenesis is controlled by the regulatory element-binding transcription factor 1 (SREBP1) and peroxisome proliferator-activated receptor

gamma (PPARγ). However, progerin can sequester SREBP1 at the nuclear envelope, and down-regulate PPARγ, leading to a decreased expression of their target genes and inhibition of adipocyte differentiation (Capanni *et al.* 2005, Maraldi *et al.* 2008).

Lastly, it was demonstrated that there is a detrimental deregulation of the somatotropic axis signaling in a HGPS mouse model, expressed by diminished levels of circulating IGF-1 along with increased GH levels (Marino *et al.* 2010), typical features of GH resistance. The authors suggest that this unbalance contributes to the characteristic muscle problems, decreased bone mineral density, alopecia, skin atrophy and hypoglycemia observed in the disease (Marino *et al.* 2010).

Nevertheless, a remarkable feature in the disease is that not all tissues are equally affected. For instance, in neurons, the activity of microRNA 9 (miR9) clears progerin preventing its accumulation, and thereby avoiding the direct damage in the nervous system of the patients. Moreover, overexpression of this microRNA in non-neural HGPS cells alleviated the nuclear blebbing, proving that miR9 action is sufficient to protect them from injuries induced by progerin accumulation (Nissan *et al.* 2012).

1.3.5. Models of progeria

The identification and unraveling of mechanisms underlying HGPS has been dependent on studies using different models of the disease. Among these it is possible to include *in vitro* and *in vivo* models that can recapitulate part of the features presented by HGPS patients and cells.

Primary cultures of cells obtained from HGPS patients, mostly dermal fibroblasts, are among the most used experimental models to study the mechanisms behind the disease. From this material it has been possible to monitor the progression of the cellular phenotype and to compile information about the observed defects (De Sandre-Giovannoli *et al.* 2003, Eriksson *et al.* 2003, Goldman *et al.* 2004). However, since HGPS is an extremely rare disease, and due to the frailty of the children bearing the condition, there are many obstacles hampering the access to samples. This problem was attenuated with the development of induced pluripotent stem cells from HGPS patient's fibroblasts (HGPS-iPSCs) (Liu *et al.* 2011, Zhang *et al.* 2011), rendering conditions to maintain cells with HGPS phenotype for an undetermined period of time. The HGPS-iPSCs were shown to not accumulate progerin nor develop features of the disease while undifferentiated but, as soon as they were differentiated in specific lineages, it was observed that they started to express the mutant protein (Liu *et al.* 2011).

To confirm the findings obtained with *in vitro* models it is frequently necessary to support them with *in vivo* studies. Several animal models have been proposed in the past years that mimic part of the HGPS phenotype features (Zhang *et al.* 2013, Swahari and Nakamura 2016).

The first lamin A mutant mouse created was a null mutant for lamin A and C that carried a deletion of the LMNA gene (Sullivan *et al.* 1999) and showed various defects

including growth retardation, loss of fat and cardiac arrhythmia. But this model did not represent what happens in HGPS given that it does not produce progerin or any other LMNA gene product.

Later, it was created a mouse model in which the mice only produced progerin due to a deletion of the introns 10 and 11, and also the last 150 nucleotides of the exon 11, in the LMNA gene (Yang *et al.* 2006). The phenotype of the mice was similar to the one seen in children with HGPS but it lacked one important feature: cardiovascular abnormalities were absent (Yang *et al.* 2006). Moreover, the production of progerin was accomplished with a bypass of the processing of prelamin A, which is the altered mechanism underlying HGPS. This way, the model did not copy the process that leads to the disease and it was not possible to modulate those steps seeking a therapeutic strategy.

Other approach to develop a HGPS mouse model was carried out by Varga *et al*. 2006 by introducing a bacterial artificial chromosome conveying the human mutated LMNA gene (G608G) in mice. The characterization of these animals revealed that external features of the disease were not evident, but they developed progressive loss of vascular smooth muscle cells like it is seen in HGPS patients (Varga *et al.* 2006). In addition, with similar strategies, it is attainable to induce the expression of human progerin in specific tissues. For instance, it was developed a transgenic mouse model expressing progerin only in the basal layer of the epidermis taking advantage of the keratin-14 promoter, allowing a focus on particular symptoms and features of the disease (Wang *et al.* 2008).

Taking into account that the absence of the ZMPSTE24 cleavage site in prelamin A is the trigger to develop the disease (Eriksson *et al.* 2003), an alternative to models with exogenous expression of human progerin was presented. Knockout mice for ZMPSTE24 were shown to synthesize and accumulate farnesylated prelamin A (Bergo *et al.* 2002, Pendas *et al.* 2002) and, despite appearing normal at birth, they begin to exhibit many characteristics of the HGPS patients such as growth retardation, alopecia, lipodystrophy and premature death (Bergo *et al.* 2002, Pendas *et al.* 2002). Additionally, they also present dilated cardiomyopathy and muscle dystrophy. Still, there is no production and accumulation of progerin, one of the main features of the cellular HGPS phenotype, and consequently do not properly represents HGPS phenotype (Pendas *et al.* 2002).

1.3.5.1. *Lmna*$^{G609G/G609G}$ mice

The most recent mouse model created, and the one that most accurately represents HGPS and its features, consists of *Lmna*$^{G609G/G609G}$ mice, that carry a mutation in the LMNA gene (1827C>T; Gly609Gly) analogous to the one found in HGPS patients and express lamin A, C and also progerin (Osorio *et al.* 2011).

These animals seem normal until 3 weeks after birth when they start to present the main clinical features of the disorder, including cardiovascular and bone

abnormalities, impaired growth rate, low body weight, lipodystrophy and alopecia. Their lifespan is, on average, 103 days, while the wild type mice usually live for more than 2 years.

Several biochemical and hormonal alterations were described in *Lmna*$^{G609G/G609G}$ mice, including extreme hypoglycemia, decreased levels of circulating IGF-1, insulin and leptin, whereas it was observed an increase in the levels of GH and adiponectin (Osorio *et al.* 2011).

Most organs from the homozygous mice are proportional to the reduced body weight, however, the spleen and thymus display a striking involution, which can be associated with impairment of the immune function. The skin of these animals is characterized by a pronounced loss of subcutaneous fat and attrition of the hair follicles. It was also shown a premature cellular senescence in liver and kidney sections, probably as a result of an enhanced p53 signaling (Osorio *et al.* 2011). The understanding of what is happening in other organs, and even in these ones in further detail, is limited, and studies aiming a more exhaustive characterization of the model are of extreme importance.

At the cellular level, fibroblasts obtained from the *Lmna*$^{G609G/G609G}$ mice accumulate progerin, show nuclear abnormalities and present increased DNA double-strand breaks compared to wild type mice. Pathways involved in responses to stress, such as p53 and ATM, are upregulated, while the ones related with metabolic processes, including fatty acid metabolism, oxidative phosphorylation and mitochondria biogenesis are downregulated (Osorio *et al.* 2011).

Despite the fact that the human HGPS is caused by a mutation in a single allele, the model that better mimics the disorder in mice is homozygous for the defective gene instead of heterozygous. This can be due to the higher tolerance of mice to accumulation of prelamin A forms (Osorio *et al.* 2011). The great similarities with the molecular mechanisms of the disease have been allowing the search for therapies involving the processing of prelamin A.

1.3.6. Potential therapies

The models described above allowed an intense quest for therapeutic strategies to thwart this severe premature aging condition, as well as to understand the normal aging process. It was through their study that the molecular mechanisms that are behind the clinical manifestations of the disease have been unraveled, along with the recognition of promising potential targets to correct the phenotype. Different approaches have been considered aiming gene, cell and tissue levels, trying to correct the protein function, RNA splicing and even the LMNA gene mutation (Gordon *et al.* 2014, Vidak and Foisner 2016).

Therapeutics envisaging the processing steps of prelamin A were shown to be potentially successful strategies to work against HGPS progression. The first indications in that direction were given by the results obtained with the administration of

farnesyltransferase inhibitors to cultured HGPS cells (Toth *et al.* 2005, Yang *et al.* 2005) and progeria mouse models (Fong *et al.* 2006, Yang *et al.* 2006). These molecules attach reversibly to the farnesyltransferase binding site, hence, blocking the farnesylation of progerin and its strong association with the nuclear membrane (Cox and Der 2002). In fact, it was proposed that the farnesyl group was the deleterious component of progerin (Young *et al.* 2005), and the prevention of its linkage with progerin ameliorated the cellular phenotype of the disease, as shown by improvements of the nuclear shape and cell proliferation. It also ameliorated clinical features in mice such as the loss of body weight, bone integrity and lifespan (Yang *et al.* 2005, Young *et al.* 2005, Fong *et al.* 2006, Yang *et al.* 2006). Given the encouraging results in preclinical studies, a clinical trial using lonafarnib, a farnesyltransferase inhibitor, was conducted (Gordon *et al.* 2012) with only 9 of the 25 patients achieving a primary outcome success (predefined as a 50 % increase over pretherapy in the rate of weight gain). It was observed that upon farnesyltransferase inhibitors administration, cells use an alternative prenylation pathway, called geranylation that reduces the efficacy of the treatment (Yang *et al.* 2008). This alternative prenylation confers to progerin, as farnesylation, the ability to interact strongly with the nuclear membrane. To overcome this barrier it has been tested the inhibition of synthesis of the farnesyl moieties, through the combination of aminophosponate and statins, which hinder the activity of farnesyl-pyrophosphatase synthase and 3-hydroxy-3-methylglutaryl-coenzyme A (HMG-CoA) reductase, respectively, in a progeria mouse model (Varela *et al.* 2008). This combination of molecules is able to avoid effectively the farnesylation and geranylation of progerin reverting many of the clinical manifestations of the disease in the animals, including the growth impairments, lipodystrophy, alopecia and lifespan (Varela *et al.* 2008). Furthermore, it was shown that by interfering with the post-translational methylation step in the processing of prelamin A it was improved HGPS cellular premature senescence (Ibrahim *et al.* 2013). Another clinical trial was conducted taking in consideration these studies, using a combination of 3 different drugs, namely lonafarnib, and 2 prenylation inhibitors, zoledronic acid and pravastatin (Gordon *et al.* 2016). However, the results did not represent a solid improvement in comparison with the clinical trial using lonafarnib alone (Gordon *et al.* 2016).

Recently, it was found that serine-arginine family of proteins (SR) regulate the local where the cleavage of prelamin A predominantly occurs, thus, influencing the proportion of healthy lamin A and progerin (Vautrot *et al.* 2016). Serine/arginine-rich splicing factor 5 (SRSF5) is among this family of proteins and its enhanced expression decreased the progerin levels in human HGPS fibroblasts, by promoting the utilization of the normal lamin A splicing site (Vautrot *et al.* 2016). Furthermore, others members of the SR protein family were associated with the regulation of the splicing of prelamin A, namely, serine/arginine-rich splicing factor 6 (SRSF6) that was shown to directly repress the progerin splicing site, and its reduction, using small interfering RNA

(siRNA), enhanced the utilization of this site with a concomitant decrease in the normal lamin A one (Lopez-Mejia *et al.* 2011).

All the therapies described so far focused in impairing or correcting the processing of prelamin A with the goal of avoiding the farnesylation of progerin or the utilization of the cryptic splicing site. However, there are other promising tools under study in order to neutralize the progression of the disease. The mutation in LMNA gene underlying HGPS phenotype leads, as already explained, to the activation of a supposedly alternative cryptic splicing site (Eriksson *et al.* 2003). Despite of its activation, the mutant allele continues to express normal lamin A (Reddel and Weiss 2004), which means that the original cleavage site is still used, albeit in much lower frequency. Using a short antisense morpholino oligonucleotide it was possible to block the cryptic splice site that produced progerin with the consequent decrease in progerin levels. This strategy successfully reversed the cellular and clinical HGPS phenotype, with the treated animals presenting an extended lifespan and improved body weight (Scaffidi and Misteli 2005, Osorio *et al.* 2011). Although this is a very exciting and promising tool it is not easy to convey such oligonucleotides to human patients, which can represent an obstacle to the application of this strategy in clinical scope.

Some studies have tried to deal directly with the reversal of specific altered features in the hope that such corrections may act in the general phenotype. For instance, it is described a downregulation of IGF-1, and an upregulation of GH, in progeroid mouse models that is associated with a deregulation of the somatotropic axis with deleterious effects to the animals (Marino *et al.* 2010). Treating Zmpste24$^{-/-}$ mice with a recombinant IGF-1 molecule ameliorated the clinical features seen in the disease and extended their lifespan when compared to non-treated Zmpste24$^{-/-}$ mice (Marino *et al.* 2010).

One molecule that revealed itself as an option to thwart HGPS is resveratrol, an activator of SIRT1, a deacetylase involved in a great variety of processes (Lavu *et al.* 2008). This molecule had already been characterized as a potential treatment against aging and was found to be beneficial in the treatment of Zmpste24$^{-/-}$ mice (Liu *et al.* 2012); however, the specific mechanisms leading to its effects are not fully understood. It is suggested that resveratrol could enhance the binding of SIRT1 to lamin A promoting its activity. In this study, it was observed a retardation of the body weight loss and an extension of the lifespan of treated mice (Liu *et al.* 2012). The effects of SIRT1 are, anyway, under debate with a recent study finding no evidence of its beneficial effects (Strandgren *et al.* 2015).

The idea that a decrease in progerin levels, through its degradation, may represent a promising therapeutic strategy is supported by the finding of Chojnowski and colleagues which confirmed that the severity of the induced HGPS phenotype in normal fibroblasts is dependent on the magnitude of progerin expressed (Chojnowski *et al.* 2015). Therefore, the question whether reducing progerin to levels below a certain threshold could be sufficient to attenuate the phenotype arises. Activation of

autophagy is considered to be one way to enhance clearance of progerin, with some molecules being described as autophagy-activators, and, as a result, it has been studied their effect on counteracting the HGPS phenotype. Sulphorane, an antioxidant molecule, stimulates autophagic and proteasomal degradation and by this means was able to enhance progerin clearance and to reverse several cellular hallmarks of HGPS cells (Gabriel *et al.* 2015). Another molecule that activates autophagy, in this case by inhibition of MTOR, is rapamycin. Cao and colleagues showed that treatment of cultured HGPS cells with rapamycin leads to progerin clearance and rescue of some of the senescent phenotype features, including the nuclear shape, the levels of DNA damage and normalization of gene expression (Cao *et al.* 2011, Cenni *et al.* 2011). Unfortunately, even though the many valuable advantages of this molecule, it conveys also many adverse effects (Salmon 2015). It was described the appearance of metabolic defects, including hyperglycemia, hyperlipidemia, insulin resistance and type 2 diabetes, during chronic rapamycin treatment (Liu *et al.* 2014, Miller *et al.* 2014).

Taking into account the potential that the stimulation of autophagy has to treat the disease, there is an urge to find possible alternatives that recapitulate the beneficial effects of rapamycin but with absence of its side effects.

1.4. Ghrelin

Ghrelin is a 28 amino acid peptide, purified for the first time from rat stomach extracts, that was found to be the only known endogenous ligand for the growth hormone secretagogue receptor 1a (GHS-R1a) (Kojima *et al.* 1999). Until recently, ghrelin was considered as the “hunger hormone” that modulates food intake and energy expenditure, but increasing evidence has challenged this limited view and unveiled broader functions for this peptide at central and peripheral levels (Pradhan *et al.* 2013, Muller *et al.* 2015).

1.4.1. Ghrelin synthesis and processing

Human GHRL gene encodes for ghrelin and is present in chromosome 3p25–26, consisting of four coding exons (1-4) and a short, 20 base pairs long, exon 0 (Kojima and Kangawa 2005, Seim *et al.* 2007). Two different mRNA molecules arise from the expression of GHRL gene, transcript A and B, due to the existence of two different transcription initiation sites (Kojima and Kangawa 2005). Transcript B lacks a glutamine at position 14 and it is termed des-gln14 acyl ghrelin (Hosoda *et al.* 2000). On the other hand, transcript A is translated into a precursor of ghrelin, named preproghrelin, with 117 aminoacids, from which are removed the first 23 aminoacids corresponding to the signal peptide. This step originates proghrelin peptide, with 94 aminoacids, which is further processed by prohormone convertase 1/3 (Zhu *et al.* 2006) resulting in the production of ghrelin (Figure 1.5). Simultaneously, it is synthesized an additional small peptide called obestatin (Kojima and Kangawa 2005, Zhang *et al.* 2005, Muller *et al.* 2015). The aminoacid sequence of ghrelin is well conserved among mammals including

mouse, rat and humans, and the 10 aminoacids in the N terminal are, actually, identical, suggesting a critical role of this region for ghrelin activity (Kojima and Kangawa 2005).

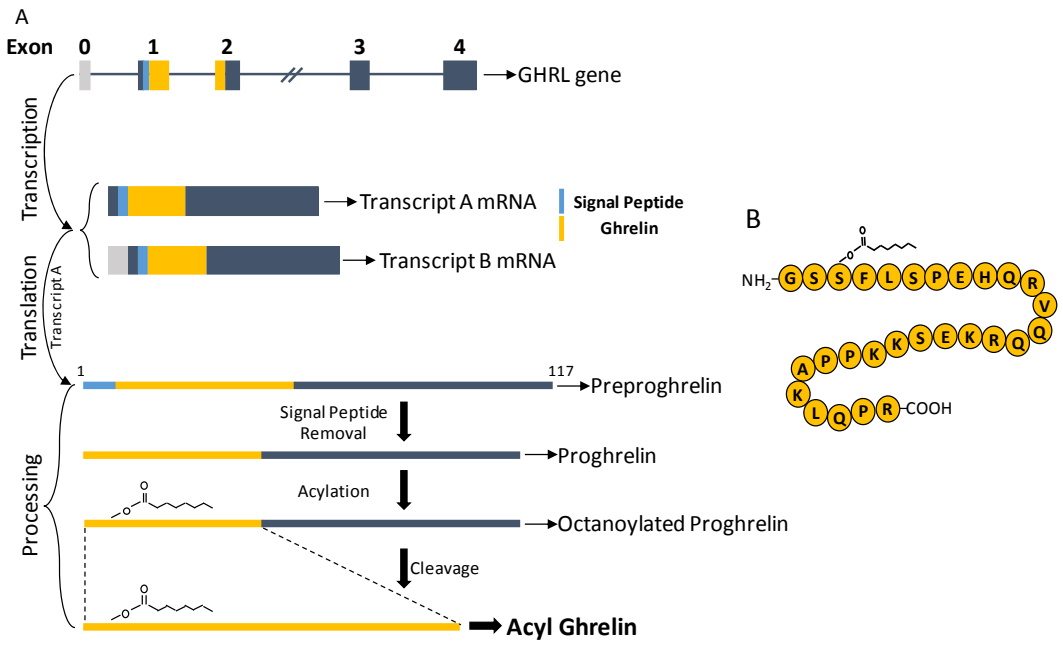

Figure 1.5. **Ghrelin Synthesis**. (A) Illustration of the events leading to ghrelin synthesis, including transcription, translation and posttranslational steps. (B) Representation of acyl ghrelin aminoacid sequence. Adapted from: (Kojima and Kangawa 2005)

In order to become fully mature, and activate GHS-R1a, ghrelin needs to undergo another processing step. More specifically, it needs to be acylated by ghrelin O-acyl-transferase (GOAT) at its serine 3 residue (Gutierrez *et al.* 2008, Yang *et al.* 2008). In addition, it was shown that glycine 1 and phenylalanine 4 are critical residues to the recognition sequence of GOAT (Yang *et al.* 2008) and their mutation leads to the impairment of ghrelin octanoylation or decanoylation. The lipids involved in this processing step are directly derived from the ingested food (Nishi *et al.* 2005, Kirchner *et al.* 2009) and their length appears to be important in the regulation of the effects promoted by ghrelin (Heppner *et al.* 2012).

Ghrelin is mainly synthesized in the stomach (Kojima *et al.* 1999) but can also be found in smaller amounts in the intestine (Ariyasu *et al.* 2001), pancreas, kidney (Mori *et al.* 2000), immune cells (Ariyasu *et al.* 2001), pituitary gland (Korbonits *et al.* 2001), hippocampus and hypothalamus (Horvath *et al.* 2001), where its expression, within the central nervous system (CNS), is more significant (Ferrini *et al.* 2009).

1.4.2. Ghrelin release

Ghrelin is predominantly synthesized in the stomach (Kojima *et al.* 1999) by the oxyntic glands (Date *et al.* 2000) and it is secreted into the bloodstream. Ghrelin levels

are elevated in preprandial times and decrease to basal levels within 1 hour after meals (Cummings *et al.* 2001), suggesting a role in meal initiation. The fall in ghrelin levels seems to be proportional to the caloric intake, and it appears that meals containing carbohydrates cause greater drops in ghrelin levels than fat meals (Monteleone *et al.* 2003).

After 72 hours of food deprivation, young adult male rats presented increased ghrelin expression in the stomach, but not in the pituitary nor the hypothalamus (Torsello *et al.* 2003). In concordance, caloric restriction in mice fed 60 % of the normal calories for 10 days increased circulating ghrelin levels (Lutter *et al.* 2008). Ghrelin secretion into the bloodstream appears to decrease with age since its levels in the plasma were found to be decreased in diverse studies with older humans (Rigamonti *et al.* 2002, Kozakowski *et al.* 2008, Nass *et al.* 2014)

1.4.3. Growth hormone secretagogue receptor

The discovery and isolation of GHS-R occurred prior to the recognition of its endogenous ligand, ghrelin, with the study of the biological activity of the receptor being performed recurring to synthetic molecules until that moment. The first studies linked GHS-R to the induction of GH secretion (Laviano *et al.* 2012). GHS-R receptor belongs to G-protein coupled receptors (GPCR) superfamily, characterized by seven transmembrane spanning helix domains (Laviano *et al.* 2012). Human GHSR gene, similarly to the ghrelin gene, is located on chromosome 3, at position 3q26.2, and is composed of 2 exons and 1 intron (McKee *et al.* 1997). Exon 1 codes for the GHS-R region from the extracellular N-terminal end to the 5th transmembrane helix, while exon 2 codes for the rest of the receptor (McKee *et al.* 1997). Two spliced variants of GHS-R have been identified: GHS-R1a, a 366 aa protein containing 7 transmembrane helix domains, and GHS-R1b, a 289 aa protein containing only 5 transmembrane helix domains (McKee *et al.* 1997); however, only GHS-R1a was described to transduce ghrelin signaling (Laviano, Molfino et al. 2012). GHS-R can signal through activation of G(q) or G(s) proteins pathways leading to an increase in intracellular calcium upon ligand binding.

GHS-R1a is distributed across the body, both centrally and peripherally, with special emphasis in the pituitary gland and the hypothalamus (Guan *et al.* 1997, Gnanapavan *et al.* 2002). This wide tissue distribuition suggests that the function of this receptor goes beyond the central regulation of feeding behaviour, energy expenditure and GH secretion. The effect of GHS-R1a activation vary according to the tissue type and also with the formation of homo or heterodimers (Laviano *et al.* 2012).

GHSR-1b is a truncated form of the GHS-R1a that does not bind to ghrelin but is thought to act as a dominant-negative receptor precisely by heterodimerizing with GHS-R1a receptor and sequestering it inside the cell, not allowing its translocation to the membrane (Leung *et al.* 2007).

1.4.3.1. GHS-R1a signaling pathways

The GHS-R1a, upon ligand binding, undegoes a dramatic adjustment in its conformation, which predisposes the receptor to interact with G-proteins (Yin *et al.* 2014). This event activates G-proteins subunits through the exchange of guanosine diphosphate (GDP) for guanosine triphosphate (GTP) and triggers different intracellular signaling cascades (Camina 2006).

One of the major outcomes derived from GHS-R1a activation is the increase in intracellular calcium that can, for instance, enhance the excitability of neurons regulating their activity (Camina 2006, Yin *et al.* 2014). It was shown that ghrelin can instigate the rise in intracellular calcium by two mechanisms, depending on the cell type. In somatotroph cells, the ghrelin-dependent calcium mobilisation is mediated by phospholipase C (PLC) that generates inositol 1,4,5-triphosphate (IP_3) and diacylglycerol (DAG) through the cleavage of phosphatidylinositol 4,5-biphosphate (PIP_2). Subsequently, IP_3 stimulates the release of calcium from intracellular stores within the endoplasmic reticulum while DAG activates protein kinase C (PKC). This kinase inhibits potassium channels, hence promoting membrane depolarization and extracellular calcium influx (Camina 2006, Yin *et al.* 2014). On the other hand, in neuropeptide Y (NPY) neurons, ghrelin promotes the calcium influx through the cyclic adenosine monophosphate (cAMP)-protein kinase A (PKA) pathway. The entrance of calcium to the neurons occurs via the N-type calcium channels that are activated following the coupling of a Gαs protein to the GHS-R1a (Kohno *et al.* 2003).

Besides its role in enhancing neuronal depolarization, GHS-R1a activity was described to also have an impact on the proliferative capacity of different cell types (Camina 2006, Yin *et al.* 2014). The activation of the mitogen activated protein kinase (MAPK) signaling cascade seems to be implicated in the proliferative action of ghrelin in human and rat adrenal zona glomerulosa cells, and this effect was shown to be dependent on tyrosine kinase (TK) and MAPK p42/p44 and independent of PKA or PKC activities (Mazzocchi *et al.* 2004). Furthermore, in 3T3-L1 preadipocytes, ghrelin exerts similar effects in the proliferation capacity of these cells, however, in this model, besides MAPK cascade, the mechanism also involves phosphatidylinositol 4,5-biphosphate 3-kinase (PI3K) pathway (Kim *et al.* 2004). Additionally, ghrelin was shown to promote proliferation in pancreatic adenocarcinoma and hepatoma cells through the PI3K/Akt and MAPK cascades, respectively. It was also observed that ghrelin was able to modulate insulin receptor substrate-1 (IRS-1) associated PI3K activity in the hepatoma cells (Murata *et al.* 2002, Duxbury *et al.* 2003).

Another signaling pathway that is modulated by GHS-R1a and is engaged on the regulation of energy metabolism is the AMPK cascade. However, this modulation seems to be tissue-specific (Yin *et al.* 2014). AMPK activity in the hypothalamus is stimulated by ghrelin administration with a consequent increase of food intake, and, concomitantly, ghrelin was shown to sustain NPY/agouti related protein (AgRP) neurons firing in an AMPK dependent manner (Camina 2006, Andrews *et al.* 2008, Yin

et al. 2014). On the contrary, in the rat liver, it was observed that ghrelin inhibits AMPK activity and facilitates the expression of lipogenic and glucogenic genes, therefore increasing the triglyerides levels in this organ (Barazzoni *et al.* 2005). In addition, it was suggested that the the afforded protection to cardiomyocytes, hepatocytes and neurons by ghrelin is also mediated by AMPK (Yin *et al.* 2014). Interestingly, central administration of ghrelin increases AMPK as well as MTOR signaling in the hypothalamus and rapamycin, a MTOR inhibitor, abolishes the orexigenic effect of ghrelin (Martins *et al.* 2012). In accordance, knockout mice for the ribosomal protein S6 kinase beta-1 (S6K1), a downstream substrate of MTOR, do not undergo an increase in body weight, fat mass and food efficiency upon chronic peripheral ghrelin administration (Stevanovic *et al.* 2013). Nevertheless, these observations are still under debate since evidences indicating the opposite also exist. One considered explanation for these antagonistic behaviors is that hypothalamic neurons may respond differently to GHS-R1a activity according to the energy state of the organism (Yin *et al.* 2014).

GHS-R1a presents a strong constitutive activity that triggers diverse intracellular signaling pathways. This constitutive activity is suggested to have an important physiological role in regulation of energy metabolism by providing a positive signaling tone, stimulating appetite, against which leptin and insulin may have to act (Camina 2006). Moreover, it also appears to be significant in the control of GH release (Yin *et al.* 2014).

1.4.3.2. Regulation of GHS-R1a activity

It has been demonstrated that GHS-R1a levels are under a tight regulation, with its agonists, including ghrelin, being capable of rapidly decrease its expression and protein levels upon binding, suggesting a potential negative feedback (Bennett *et al.* 1997, Kineman *et al.* 1999, Luque *et al.* 2004). In addition, ghrelin binding to the receptor results in its rapid desensitization and attenuation of its signaling pathways via endocytosis (Camina *et al.* 2004). This internalization occurs in a time-dependent manner and it was shown that the effect is maximal 20 minutes after ghrelin stimulus, with GHS-R1a being moved to endosomal compartments. It was also verified that the receptor is recycled to the cell membrane and its levels on the surface are completely replenished after 6 hours following agonist removal (Camina *et al.* 2004). These mechanisms are suggested to provide protection of the cells regarding receptor overstimulation (Yin *et al.* 2014), and it is possible that this desensitization underlies somehow the pulsatile effects of ghrelin signaling.

The GHS-R1a has been shown to interact and dimerize with several other receptors with effects on its response to ligands. For instance, it was observed that GHS-R1a homodimerization (Leung *et al.* 2007, Chow *et al.* 2012) may ensure a way to maximize the response to agonist stimuli. Moreover, its interaction with dopamine, adenosine and melanocortin-3 (MC3) receptors has been reported (Carreira *et al.*

2004, Jiang *et al.* 2006, Rediger *et al.* 2011), resulting in different patterns of intracellular signaling pathways activation. GHS-R1b also heterodimerizes with GHS-R1a and is thought to act as a dominant-negative mutant of the ghrelin receptor (Leung *et al.* 2007). These GHS-R1a/GHS-R1b heterodimers are localized, and enriched, in the endoplasmic reticulum, whereas GHS-R1a homodimers are present evenly on cell surface and intracellular compartments. It has been suggested that GHS-R1b traps GHS-R1a in the endoplasmic reticulum mitigating its trafficking to the cell membrane and thus decreasing its activity (Leung *et al.* 2007, Chow *et al.* 2012).

All these mechanisms influence and determine the effects of ghrelin stimulation and in some way may elucidate the diverse results of GHS-R1a signaling.

1.4.4. Biological functions of ghrelin

1.4.4.1. Growth hormone and food Intake

Ghrelin was firstly reported as the molecule responsible for the GH release from the pituitary. Actually, it can promote GH secretion from the somatotropic cells by targeting directly this structure (Kojima *et al.* 1999). In addition, GHS-R is also expressed in GH-releasing hormone (GHRH) neurons in the hypothalamus (Guan *et al.* 1997), where its activation facilitates the formation of action potentials by decreasing gamma-aminobutyric acid (GABA) inhibitory inputs, and allowing the boost in GHRH secretion in the hypothalamus. Subsequently, GHRH promotes the release of GH in the pituitary (Laviano *et al.* 2012). Kojima and collaborators described the GH-releasing properties of ghrelin, both *in vitro* and *in vivo*, using primary cultures of pituitary cells and anaesthetized rats, respectively (Kojima *et al.* 1999). In accordance, it was shown that ghrelin administration to humans also induces acute GH release (Arvat *et al.* 2000, Peino *et al.* 2000) and, further support came from the association between the impairment of the constitutive activity of GHS-R and familial short stature (Pantel *et al.* 2006).

The presence of this receptor in the arcuate nucleus of the hypothalamus, a key center for regulation of food intake and satiety (Willesen *et al.* 1999) suggests a role for ghrelin in the regulation of appetite. Indeed, intracerebroventricular injections of ghrelin strongly stimulated food intake and body weight gain in rats, and the effect was dependent on NPY and AgRP (Nakazato *et al.* 2001). NPY and AgRP neurons harbor GHS-R and have their activity increased upon ghrelin signaling, while pro-opiomelanocortin (POMC) neurons experience the opposite effect (Cowley *et al.* 2003). It is not surprising that ghrelin administration increases food intake in both mice and rats (Tschop *et al.* 2000). The effects of ghrelin in food intake are dependent on NPY and AgRP since single knockout mice for both genes do not present the orexigenic effects upon ghrelin administration (Chen *et al.* 2004).

Since HGPS patients, as well as *Lmna*$^{G609G/G609G}$ mice, show a severe growth impairment that in the mouse model is accompanied by increased levels of circulating GH and low levels of IGF-1, suggesting GH resistance, ghrelin modulation of the GH

pathway could be positive to thwart such phenotype. Besides, given the difficulties that the children have to accumulate fat, the effects of ghrelin in food intake and adipogenesis are also promising in improving this feature of the disease.

1.4.4.2. Glucose metabolism

Pancreas constitutes an important structure in the regulation of glucose metabolism given that it secretes insulin. Interestingly, both ghrelin mRNA and protein are present in pancreatic β-cells, as shown by Volante and colleagues (Volante *et al.* 2002). Using mouse models it was observed that ghrelin inhibits insulin secretion (Reimer *et al.* 2003, Dezaki *et al.* 2004) and the blockade of GHS-R with a specific antagonist, ablating the signaling by endogenous ghrelin, resulted in the opposite effects: lowered fasting glucose concentrations and enhanced insulin responses (Dezaki *et al.* 2004). Ghrelin deficient mice showed augmented insulin secretion and it was proposed that the inhibitory effect of ghrelin in insulin secretion may be related with an observed decrease in mitochondrial uncoupling protein 2 (UCP2) expression in the pancreatic β-cells of these mice (Sun *et al.* 2006). By decreasing ATP production, UCP2 lowers the ATP:ADP ratio, a crucial signal required for insulin secretion (Senniappan *et al.* 2013). Moreover, re-expression of GHS-R exclusively in AgRP neurons of genetically modified mice that did not express the receptor was able to rescue the lowered blood glucose levels upon caloric restriction (Wang *et al.* 2014).

In a physiological context, when in fasting state, the increase in ghrelin signaling seems to promote the increase in circulatory ghrelin and to inhibit insulin secretion, in order to counteract the lowering of glucose in the bloodstream due to the negative energy state. As previously described, *Lmna*$^{G609G/G609G}$ mice experience extreme hypoglycemia which is argued to contribute for the impairment in the cardiovascular function of these animals (Osorio *et al.* 2011). Taking this in consideration, ghrelin's effects on glucose metabolism can be advantageous in the context of HGPS.

1.4.4.3. Adiposity

The GHS-R1a has a wide distribution, including adipocytes, and a role for ghrelin in the control of the metabolism of these cells has been demonstrated. Tschöp and colleagues, in 2000, reported that peripheral administration of ghrelin caused weight gain in mice and rats by decreasing the fat utilization (Tschop *et al.* 2000). Furthermore, central administration of ghrelin in Wistar rats led to several cellular adaptations in white and brown adipose tissues. In white adipocytes, it was observed an increase in the expression of many enzymes involved in the synthesis and storage of lipids, along with a higher rate of glucose utilization, while a rate-limiting enzyme for the fatty acids oxidation was down-regulated (Theander-Carrillo *et al.* 2006). Interestingly, the authors noticed that these alterations in the gene expression were independent of ghrelin-induced hyperphagia. The rate of glucose utilization was also increased in brown adipose tissue and it was observed a decrease in the expression of

mitochondrial uncoupling protein 1 (UCP1), suggesting a decline in the energy expenditure attributed to this tissue (Theander-Carrillo *et al.* 2006). Moreover, old mice with ablation of GHS-R1a show reduced body weight when compared to their wild type littermates, mainly because of reduced adiposity (Lin *et al.* 2011). In the study, it was observed that these mice have increased energy expenditure, with a concomitant elevation in the expression of thermogenic genes in brown adipose tissue. In the white adipose tissue, it was described a reduction in the fat synthesis (Lin *et al.* 2011).

With these studies it has been uncovered the capacity of ghrelin to induce adipogenesis and accumulation of fat in several models. HGPS patients, and *Lmna*$^{G609G/G609G}$ mice, are lipodystrophic and have problems in sustaining body weight which makes ghrelin a potential target to counteract the progression of the disease's features.

1.4.4.4. Cardiovascular system

Another system that widely expresses GHS-R, and thus can be influenced by ghrelin signaling, is the cardiovascular system. In fact, the receptor is present in aorta and other arteries as well as in cardiomyocytes (Katugampola *et al.* 2001, Nagaya and Kangawa 2003).

In vitro studies showed that ghrelin can inhibit doxorubicin-induced, and serum starvation-induced, apoptosis in H9c2 cardiomyocytes, and it also prevented apoptosis stimulated by anti-FAS agonist antibodies in primary culture of adult cardiomyocytes. It was suggested that this was accomplished through activation of extracellular signal–regulated kinase (ERK) 1/2 and RAC-alpha serine/threonine-protein (PKB/AKT) kinase (Baldanzi *et al.* 2002). Ghrelin was shown to have also inhibitory effects on tumor necrosis factor (TNF)-α-induced cytokine release in human umbilical vein endothelial cells (HUVECs) (Li *et al.* 2004) as well as attenuated NF-kB activation induced by TNF-α.

Ghrelin also acts on the vagal nerves and prevents excessive activation of the cardiac sympathetic nerves. This avoids the deleterious effects of arrhythmia, improving the survival prognosis after myocardial infarctions in mice (Mao *et al.* 2012). Experiments performed in rat models have shed light on beneficial effects of ghrelin administration in the heart structure and function. Indeed, ghrelin delayed the development of cardiac cachexia in treated animals (Nagaya *et al.* 2001). Additionally, in rat models of myocardial infarction, ghrelin treatment increased VEGF expression and angiogenesis (Yuan *et al.* 2012). Furthermore, ghrelin has been shown to have beneficial effects in patients with heart failure, where its administration leads to a decrease in vascular resistance and ameliorates cardiac output (Nagaya *et al.* 2001).

The effects of ghrelin in the cardiovascular system are thought to be mediated by activation of GHS-R in the heart and vessels and also through GH dependent mechanisms (Laviano *et al.* 2012). All these findings are very promising and support

the potential role of ghrelin as a treatment for HGPS since the worst features of the disease are related with defects in the cardiovascular system.

1.4.4.5. Skeletal muscle and bone

There are several studies connecting ghrelin to beneficial effects on muscle and bone health. By ameliorating the nutritional status, through increases in food intake, and stabilizing the GH/IGF-1 axis, ghrelin was shown to indirectly improve skeletal muscle catabolism in cachexic mice (Sugiyama *et al.* 2012). In an *in vitro* study using C2C12 skeletal myoblasts it was determined the capacity of, either acylated or des-acylated, ghrelin to promote their fusion and differentiation into multinucleated myotubes. Surprisingly, these cells do not express GHS-R1a, hence suggesting the existence of an additional unknown receptor. Furthermore, it was demonstrated that these events were mediated by p38 activation (Filigheddu *et al.* 2007). Supporting these results, a study in mice with cachexia revealed the protective role of ghrelin, independent of GHS-R1a, against skeletal muscle atrophy. Both acylated and des-acylated ghrelin were able to counteract the dexamethasone-induced muscle atrophy, and it was observed that p38, MTOR complex 2 (MTORC2) and phosphatidylinositol-4,5-bisphosphate 3-kinase beta (PI3Kβ) pathways underlie this effect (Porporato *et al.* 2013).

Growing evidence support the idea that ghrelin can also be beneficial to bone health. Ghrelin was shown to have a stimulatory effect on the proliferation and differentiation of osteoblasts, cells responsible for the formation of bone, while inhibiting cell apoptosis (Delhanty *et al.* 2014). For instance, Fukushima and colleagues observed that ghrelin increased the expression of osteoblast differentiation markers and the number of osteoblast-like cells. Moreover, ghrelin-administered rats showed increased bone mineral density, suggesting that it can directly stimulate bone formation (Fukushima *et al.* 2005). Ghrelin also leads to the phosphorylation, and consequent activation, of AMPK that was shown to play a role in skeletal physiology and can be on the basis of ghrelin effects on bone (Shah *et al.* 2010). Osteoclasts are also under the influence of ghrelin signaling, which enhances bone-resorption activity (Costa *et al.* 2011). These apparently contradictory roles can lead to an improved bone turnover, which can ultimately represent a benefit to the health of the skeleton.

These discoveries can be relevant to the improvement of HGPS features related to muscle and bone abnormalities.

1.4.4.6. Other functions

Ghrelin presents many other functions that were not covered in the previous sections, related with learning and memory, stress, mood and anxiety, depression and sleep/wake rhythms. Moreover, ghrelin was also implicated to play a neuroprotective role in neurodegenerative disorders (Muller *et al.* 2015).

Ghrelin's effects on cellular proliferation have also been extensively studied in diverse models, including in adrenal zona glomerulosa cells, pancreatic adenocarcinoma and hepatoma cells, small intestinal IEC-6 cells, 3T3-L1 preadipocytes, primary osteoblasts and diverse osteoblastic cell lines (Murata *et al.* 2002, Duxbury *et al.* 2003, Kim *et al.* 2004, Mazzocchi *et al.* 2004, Kim *et al.* 2005, Yu *et al.* 2013). Furthermore, ghrelin administration was shown to stimulate proliferation and neuronal differentiation in adult hippocampal progenitor cells in the subgranular zone (SGZ) (Moon *et al.* 2009). Its immunoneutralization reduced proliferation and differentiation in the same population of cells (Moon *et al.* 2009). Later, using ghrelin deficient mice, it was confirmed the role of endogenous ghrelin in this process (Li *et al.* 2013). Similar results were obtained in the subventricular zone (SVZ), where ghrelin-KO mice presented lower number of neural progenitor cells that were restored to wild-type levels upon ghrelin administration (Li *et al.* 2014). The work from another group supported the idea that ghrelin administration stimulates neurogenesis in the hippocampus (Zhao *et al.* 2014), however, in order to achieve these effects, ghrelin had to be systemically administered, since its direct infusion in the CA1 region of the hippocampus did not lead to any alterations in neurogenesis.

Recently, it was reported the ability of ghrelin to promote autophagy in rat cortical neurons through the canonical inhibition of MTOR activity (Ferreira-Marques *et al.* 2016). This action is, however, blunted in the presence of a GHS-R1a antagonist. Since HGPS is caused by the accumulation of progerin, it is tempting to speculate if the enhancement of autophagy promoted by ghrelin would not be successful in ameliorating this condition. In line with this, our group showed that ghrelin treatment increases autophagic flux and enhances progerin clearance, rescues nuclear abnormalities, decreases DNA damage, increases cell proliferative capacity and delays cellular senescence of HGPS cells. Altogether, these results show that ghrelin reverses cellular hallmarks of premature aging of HGPS fibroblasts and strongly support that ghrelin can be considered a promising strategy to delay or block the premature aging of HGPS as well as normal cellular aging.

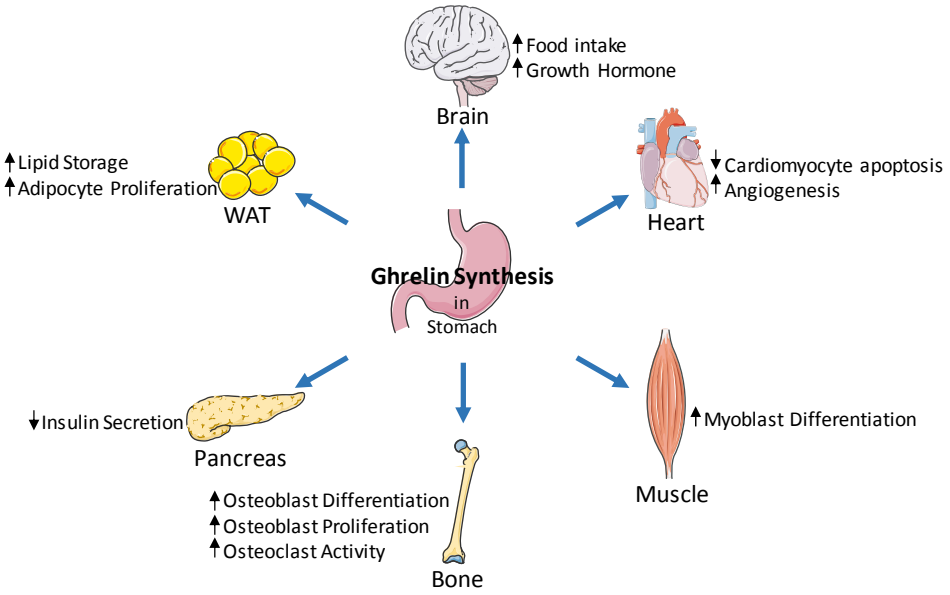

Figure 1.6. **Summary of ghrelin biological functions.** Ghrelin is produced in the stomach and travels in the bloodstream to target different regions of the body, where it exerts a wide range of functions. Adapted from: (Muller *et al.* 2015)

1.5. Hypothalamus

In the previous chapter we focused our attention on ghrelin and its broad spectrum of actions within our organism. However, despite the wide expression of its receptor, GHS-R1a still is mainly present in the hypothalamus and pituitary gland (Guan *et al.* 1997, Gnanapavan *et al.* 2002), unraveling the crucial role of ghrelin in the actions carried out by this structure.

The hypothalamus is found underneath the thalamus and consists of several nuclei, each one composed of different types of neurons that communicate between each other, and with different brain regions, to regulate physiological functions and maintain the homeostasis in animals (Pearson and Placzek 2013, Biran *et al.* 2015). Among these functions lie the regulation of metabolism, water balance, satiety, reproductive behaviours, circadian rythms, emotional responses (Machluf *et al.* 2011, Pearson and Placzek 2013) and aging (Zhang *et al.* 2013). The hypothalamus integrates and processes internal and external sensory inputs, subsequently providing regulatory autonomic and neuroendocrine responses in order to keep the physiological balance of the organism and its survival (Pearson and Placzek 2013).

The hypothalamus establishes an intimate relation with the pituitary gland, representing a fundamental part for the neural control of this endocrine organ (Markakis and Swanson 1997, Simerly 2004).

1.5.1. Hypothalamic nuclei

The hypothalamus is found ventrally to the thalamus and dorsally to the pituitary gland, in the medio-basal region of the mammalian brain (Machluf *et al.* 2011). At the

morphological level, it is divided in three distinct longitudinal zones: namely the periventricular, medial and lateral; and into four rostrocaudal levels: the preoptic, anterior, tuberal and mammilary regions (Simerly 2004); where all the hypothalamic nuclei are accommodated.

There are diverse nuclei within the hypothalamus (Figure 1.7), consisting of segregated agglomeration of cell bodies that present particular connections with other hypothalamic and brain regions (Simerly 2004), and consequently, being important for different functions. Among these are included, the arcuate nucleus (ARC), paraventricular nucleus (PVN), ventromedial hypothalamus (VMH), dorsomedial hypothalamus (DMH) the suprachiasmatic nucleus (SCN), and the medial preoptic (MPO), anterior (AH), posterior (PHA) and lateral (LHA) hypothalamic areas.

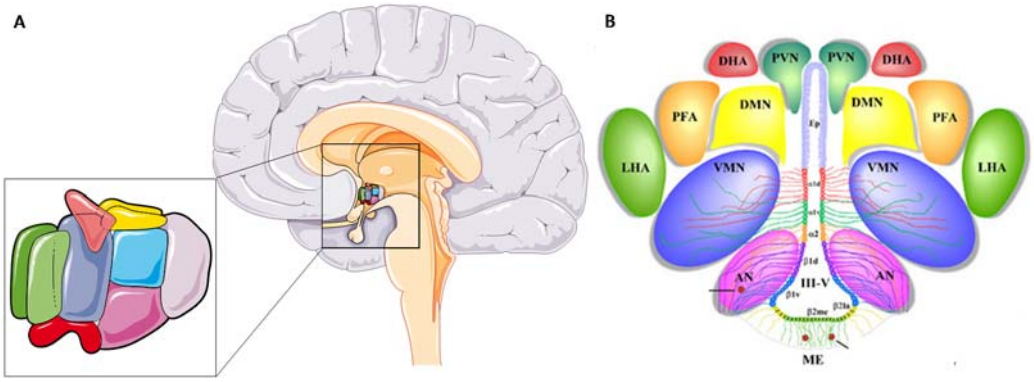

Figure 1.7. **Hypothalamic Nuclei.** Schematic representation of the hypothalamic nuclei in sagittal (A) and coronal (B) sections. Adapted from (Elizondo-Vega *et al.* 2015) and Selvier Medical Art.

1.5.1.1. Arcuate nucleus (ARC)

The ARC resides on the base of the hypothalamus, on either side of the third ventricle (Kalra *et al.* 1999), and the fact that the blood brain barrier in this zone is semi-permeable (Broadwell and Brightman 1976) reflects the potential of this nucleus to be in direct communication with peripheral signals, such as leptin, insulin or ghrelin (Kalra *et al.* 1999).

Besides integrating signals from the periphery, it also receives inputs from the brainstem (Minor *et al.* 2009). ARC first-order neurons convey the integrated information to various hypothalamic nuclei, including the PVN, DMH and VMH (Kalra *et al.* 1999, Minor *et al.* 2009). In addition, ARC extends its projections to regions of the forebrain, thalamus, midbrain, pons and medulla (Sapru 2013). It contains some neurons that project to the median eminence where they release hypophysiotropic hormones that are targeted to the pituitary (Simerly 2004, Sapru 2013).

ARC is a critical structure for food intake regulation (Minor *et al.* 2009), possessing two important populations of neurons controlling appetite: neurons co-expressing NPY and AgRP, that when activated stimulate food intake (Broberger *et al.* 1998, Hahn *et al.* 1998); and neurons co-expressing POMC and cocaine-and-

amphetamine-regulated transcript (CART), that have the opposite effect (Elias *et al.* 1998, Kristensen *et al.* 1998).

Using immunocytochemical studies, ghrelin was reported to be synthesized in ARC neurons, which interact with POMC and NPY expressing neurons (Lu *et al.* 2002, Ferrini *et al.* 2009). Its receptor, GHS-R1a, is also abundantly expressed in this nucleus (Ferrini *et al.* 2009), and it is co-expressed in NPY and GHRH expressing neurons (Tannenbaum *et al.* 1998, Willesen *et al.* 1999), which suggests a role for ghrelin in the modulation of the activity of these neurons.

ARC is also a fundamental region in the regulation of GH. Indeed, GHRH neurons are present in ARC and its activity, along with the secretion of GHRH to the pituitary, control the circulating levels of GH (Mano-Otagiri *et al.* 2006). Ghrelin was shown to have an impact in GHRH neurons in the ARC since the attenuation of the expression of GHS-R1a decreased their number (Mano-Otagiri *et al.* 2006).

1.5.1.2. Paraventricular nucleus (PVN)

The PVN is located in the periventricular zone, next to the third ventricle, and is considered an integration center for the autonomic nervous system (Argiolas and Melis 2005). It receives afferent inputs from diverse centers within the hypothalamus, namely the ARC, the LHA and the SCN, as well as from the pons, medulla and the nucleus of tractus solitarius (Hill 2012). Projections from the PVN extend to the brainstem and to regions containing preganglionic autonomic neurons (Simerly 2004, Hill 2012). This nucleus contains also parvocellular neuroendocrine neurons that project to the median eminence, as well as to the pituitary, and express regulating peptides, like corticotropin-releasing hormone (CRH) or thyrotropin-releasing hormone (TRH), which will subsequently stimulate the production of hormones in the anterior pituitary implicated in several physiological axes (Simerly 2004, Pearson and Placzek 2013). Furthermore, it is observed another neuronal type, the magnocellular neuroendocrine neurons, that send their axons to the pituitary, delivering vasopressin or oxytocin to the systemic circulation (Hill 2012). Altogether, by these means, PVN is thought to: participate in autonomic responses; regulate growth, development and reproductive axes; mediate the hypothalamic response to stress; and also to play a crucial role in feeding and drinking behaviors (Simerly 2004, Hill 2012, Pearson and Placzek 2013).

1.5.1.3. Ventromedial nucleus (VMH)

The VMH sits at the base of the diencephalon, above the median eminence and the pituitary (McClellan *et al.* 2006) and represents the largest nucleus in the tuberal region of the hypothalamus (Simerly 2004). This nucleus establishes connections with several regions of the brain (Simerly 2004, McClellan *et al.* 2006). It receives inputs from other hypothalamic nuclei of the medial and lateral zones, the posterior hypothalamic area and also from the SCN. In addition, it integrates information coming

from thalamic and epithalamic areas, the amygdala, the ventral subiculum and the parabrachial nucleus (Fahrbach *et al.* 1989, Canteras *et al.* 1994, Simerly 2004). The VMH also presents a vast amount of both intra and extra hypothalamic efferents. It projects to the medial zone of the hypothalamus, including the MPO and the AH, to the bed nucleus of the stria terminalis, the amygdala, as well as to the periaqueductal gray (Saper *et al.* 1976, Canteras *et al.* 1994).

VMH appears to be involved in a variety of homeostatic and behavioral functions (McClellan *et al.* 2006). KO mice lacking steroidogenic factor 1 exhibit abnormalities in the VMH, which were associated with the manifestation of obesity in adulthood of these animals (Majdic *et al.* 2002), implicating VMH in ingestive behaviors. Moreover, lesion of neurons containing steroid hormone receptors in the VMH was sufficient to inhibit lordosis behavior in rats (Emery and Moss 1984), highlighting the importance of this nucleus in the production of reproductive actions. It was also linked to the regulation of cardiovascular function since stimulation of neurons within the VMH caused decreases in blood pressure and heart rate in rats (Hirasawa *et al.* 1996).

1.5.1.4. Dorsomedial nucleus (DMH)

The DMH is adjacent to the third ventricle, and surrounded by the PVN, VMH, LHA, AH and PHA (Fontes *et al.* 2011). It has been shown that DMH possesses afferent arising in the telencephalon, including from the ventral subiculum, the prefrontal cortex, lateral septal nucleus and the bed nucleus of the stria terminalis. The brainstem, the periaqueductal gray, parabrachial nucleus and the ventrolateral medulla project to this nucleus (Thompson and Swanson 1998). However, the vast majority of the inputs coming to the DMH have their origin within the hypothalamus (Thompson and Swanson 1998). Regarding the efferents of the DMH, they seem to be mostly intrahypothalamic (Thompson *et al.* 1996), although it also innervates the periaqueductal gray, the parabrachial nucleus and the nucleus of the solitary tract.

Within the hypothalamus, the interaction between SCN and the DMH, and subsequent connection to other nuclei, is considered important for the regulation of several behaviors influenced by the circadian rhythms (Chou *et al.* 2003). Indeed, it was shown that lesions in DMH reduced circadian rhythm of sleep-wake behavior and total wakefulness. Furthermore, it was also observed that the temporal patterns of feeding were also affected, as well as the circadian rhythmicity of adrenal corticosteroids (Chou *et al.* 2003). This disruption in the circadian rhythm of ingestive behavior was corroborated by another study, where DMH-lesioned rats showed a decrease in food-anticipatory locomotor activity and a reduction in preprandial wakefulness (Gooley *et al.* 2006). It is also suggested a role for DMH in the cardiovascular activity since inhibition of neurons within this nucleus was able to abolish increases in heart rate elicited by stress (Stotz-Potter *et al.* 1996)

1.5.1.5. Suprachiasmatic nucleus (SCN)

The SCN is adjacent to the third ventricle, above the medial portion of the optic chiasm, and is formed by a group of small, closely packed, neurons (Simerly 2004, Nakamura *et al.* 2016). It receives inputs from the retina and the geniculate nucleus of the thalamus (Simerly 2004, Moore 2013), and the main efferents reach the thalamus and other hypothalamic regions, including the DMH (Moore 2013, Vujovic *et al.* 2015). These links suggest a role in the regulation of circadian rhythms, that is supported by the observation that experimental lesion of this nucleus leads to the abolishment of circadian rhythmicity and photic entrainment (Stephan and Zucker 1972). Moreover, it was also shown that the circadian output from the SCN decreases with age, and can be related to the sleep disorders observed in aged people (Nakamura *et al.* 2011).

1.5.1.6. Medial preoptic nucleus (MPO)

The MPO is located in the preoptic region and holds some of the most complex connections of the hypothalamus (Simerly 2004). Regarding the inputs, MPO displays extensive intrahypothalamic connections from several nuclei, including the PVN and ARC, which may be related to autonomic and neuroendocrine functions (Saper and Levisohn 1983, McKinley *et al.* 2015). It also receives information from several extrahypothalamic regions such as: the subfornical organ, with this pathway being activated by osmotic stimuli and circulating angiotensin II (Saper and Levisohn 1983, Gutman *et al.* 1988); midbrain neurons, for instance from the parabrachial nucleus, thought to participate in thermoregulatory control (Saper and Levisohn 1983, Nakamura and Morrison 2008, Nakamura and Morrison 2010); the nucleus of the solitary tract and the ventrolateral medulla, relevant regions for cardiovascular and body fluid regulation (Saper and Levisohn 1983, Simerly 2004); and the amygdala (Simerly 2004). The MPO has also broad projections that include several hypothalamic nuclei, the parabrachial nucleus, locus coeruleus, among others. These connections are thought to mediate neuroendocrine, autonomic and somatomotor responses associated with this nucleus (Simerly 2004, McKinley *et al.* 2015).

1.5.1.7. Anterior nucleus (AH)

The AH lies near the rostral end of the SCN and is bordered by the PVN, MPO, VMH and the DMH (Simerly 2004). The connections of this nucleus seem to be a subset of those of the MPO, consisting of complex inputs from nuclei of the medial zone of the hypothalamus, scarce afferents from the lateral zone and a smaller portion coming from telencephalic regions, like the ventral subiculum, the bed nucleus of the stria terminalis and the lateral septal nucleus (Simerly 2004). The AH project to several regions in the hypothalamus, with particularly dense focus to the perifornical region, the paraventricular nucleus of the thalamus and also to the periaqueductal gray (Simerly 2004). It is thought that this region is implicated in thermoregulatory responses (Ishiwata *et al.* 2001).

1.5.1.8. Posterior hypothalamic area (PHA)

The PHA comprises the most caudal and dorsal hypothalamic region (Simerly 2004). It receives inputs from the amygdala, the hippocampal formation, the septum and also from the other regions of the hypothalamus (Abrahamson and Moore 2001, Cavdar *et al.* 2001). Interestingly, it conveys information to cortical regions related with limbic structures, and to subcortical regions in the hypothalamus, thalamus, amygdala, septum and basal forebrain (Vertes *et al.* 1995). It is hypothesized that due to its strong interaction with forebrain regions connected to the hippocampus PHA can be important in the context of emotional behavior (Vertes *et al.* 1995, Simerly 2004). Additionally, it has also been attributed to PHA a role in the control of sleep-wake cycles (Vanni-Mercier *et al.* 1984, Lin *et al.* 1989), cardiovascular regulation (Buccafusco and Brezenoff 1979, Spencer *et al.* 1990) and defensive-aggressive behaviors (Yardley and Hilton 1986, Shekhar and DiMicco 1987).

1.5.2. Hypothalamic functions

Even though the hypothalamic nuclei consist of segregated cell populations, they cannot be interpreted as independent. In order to carry out the functions exerted by the hypothalamus, each nucleus needs to communicate with the remaining and with several other brain regions, working on an orchestrated manner to maintain the homeostasis of the organism.

Diverse functions were recognized for the hypothalamus including regulation of energy and fluid balance (Muroi and Ishii 2016), triggering of stress responses (Ulrich-Lai and Herman 2009), control of growth (Guan *et al.* 1997) and reproductive behaviors through the stimulation of GH and GnRH release, respectively, and it was also credited with a role in emotional and social behaviors (Pearson and Placzek 2013).

1.5.2.1. Energy balance

The hypothalamus is crucial for keeping an appropriate balance between energy intake and expenditure, which is an essential feature for the survival of animals (Muroi and Ishii 2016). In particular, the ARC is reckoned as a perfectly suited nucleus for sensing the organism energy and hormonal status due to its localization next to the median eminence, the third ventricle and the hypophyseal portal system, which renders it free access to circulating nutrients and hormones (Minor *et al.* 2009, Roh and Kim 2016).

As previously explained, there are two important neuronal populations controlling appetite in the ARC: NPY/AgRP and POMC/CART expressing neurons, that activate and inhibit food intake, respectively (Broberger *et al.* 1998, Elias *et al.* 1998, Hahn *et al.* 1998, Kristensen *et al.* 1998) (Figure 1.8). These first-order neurons then innervate second-order neurons in other hypothalamic nuclei, including the PVN, VMH and LHA, and to preganglionic neurons in the brain stem and spinal cord (Sternson *et*

al. 2005, Krashes *et al.* 2014, Muroi and Ishii 2016, Roh and Kim 2016) that will subsequently trigger adaptive responses (increasing/decreasing food intake, energy expenditure) that depend on which neuronal type activity prevails.

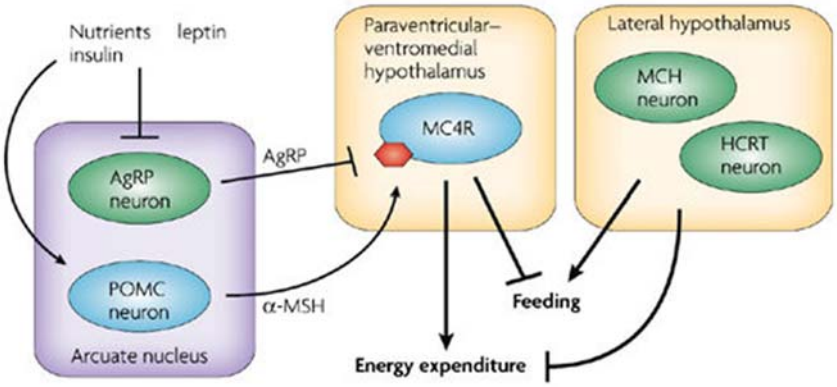

Figure 1.8. **Energy balance regulation**. Schematic representation of the circuit regulating feeding and food intake within the hypothalamus. Adapted from (Bishop and Guarente 2007).

The peripheral tissues transmit the information about energy levels through the circulating levels of glucose and hormones, such as leptin, insulin and ghrelin, that are sensed by the NPY/AgRP and POMC/CART neurons (MacDougald *et al.* 1995, Toshinai *et al.* 2001) (Figure 1.8). Leptin consists of an anorexigenic hormone synthesized in the adipose tissue under energy-rich conditions (Zhang *et al.* 1994), while insulin, also an anorexigenic hormone, is secreted from the beta cells of the pancreas (Muroi and Ishii 2016). In fact, both neuronal populations express the receptors for each of these molecules (Marks *et al.* 1992, Cheung *et al.* 1997, Baskin *et al.* 1999, Konner *et al.* 2007, Muroi and Ishii 2016), and it is known that ghrelin activates NPY/AgRP neurons (Andrews *et al.* 2008), whereas insulin and leptin have the opposite effect (Cowley *et al.* 2003). Glucose was also shown to directly inhibit NPY/AgRP, while activating POMC/CART, expressing neurons (Ibrahim *et al.* 2003, Lee *et al.* 2005). Reinforcing this antagonistic effect, NPY/AgRP GABAergic neurons innervate POMC/CART neurons inhibiting their activity (Cowley *et al.* 2001). Overall, NPY/AgRP neurons are activated by low energy conditions, whereas POMC/CART neurons are inhibited in these circumstances (Muroi and Ishii 2016).

In conditions of high energy levels, the anorexigenic POMC/CART neurons produce α-melanocyte stimulating hormone (α-MSH) that will activate its receptors, MC3R and MC4R, in second-order neurons of the PVN, consequently activating catabolic pathways that ultimately lead to a reduced food intake and increased energy expenditure (Cowley *et al.* 1999, Roh and Kim 2016). On the other hand, in low-energy conditions, NPY/AgRP neurons antagonize POMC action, thereby increasing food intake and reducing energy expenditure (Kim *et al.* 2014).

The diverse hypothalamic nuclei involved in the energy balance also establish an interaction with the SCN and DMH, and other regions that participate in circadian

rhythms, in order to adjust the temporal patterns of feeding to external cues (Chou *et al.* 2003, Gooley *et al.* 2006).

1.5.2.2. Stress response

Stress is defined as internal or external challenges that demand appropriate reactions in order for an organism to survive (Koch *et al.* 2017). Because of its significance for the fitness of an individual, an intricate system, activated by stress, and eliciting adequate responses has evolved (Ulrich-Lai and Herman 2009).

The stress response is initiated when sensory systems collect signals about stressful situations and relay the information to the brainstem (Ulrich-Lai and Herman 2009), which activates sympathetic responses by communicating with the medulla and preganglionic sympathetic neurons in the spinal cord. Additionally, the brainstem also communicates with the PVN, which subsequently triggers the HPA axis mediated response (Ulrich-Lai and Herman 2009). PVN also integrates stress signals from other regions, such as the hippocampus, prefrontal cortex and amygdala (Koch *et al.* 2017). After integration of the stress signals by the PVN, parvocellular hypothalamic neurons release CRH into the median eminence, which reaches the pituitary and stimulates the release of adrenocorticotropic hormone (ACTH) to the bloodstream (Mains *et al.* 1977, Roberts and Herbert 1977, Romanov *et al.* 2017). Ultimately, glucocorticoids are produced and secreted from the cortex of the adrenal gland upon binding of ACTH to the MC2 receptor (Koch *et al.* 2017, Romanov *et al.* 2017). Thereafter, glucocorticoids act through mineralocorticoid (MR) and glucocorticoid (GR) receptors (Gustafsson *et al.* 1987), widely distributed across the body, to induce changes in cellular states, leading to integrative-protective responses against noxious conditions, and promoting energy utilization with the goal of overcoming metabolic compromise (Koch *et al.* 2017, Romanov *et al.* 2017). The acute stress response is concluded by parasympathetic activation, for the autonomic response, and also by a mechanism of negative feedback where glucocorticoids, at concentrations over a given threshold, inhibit further release of CRH and ACTH from hypothalamic and pituitary cells, disrupting the loop (Nader *et al.* 2010). Since glucocorticoids have to be synthesized upon ACTH stimulus, HPA axis promotes a delayed response, taking several minutes. This suggests that the autonomic, sympathetic, response to stress, which occurs within seconds, can mediate the reaction for imminent danger, like a possible life-threatening situation, for instance, loss of blood or pain stimuli.

This complex process, along with the regulation of energy balance, underpins the organized manner by which hypothalamus interacts with a vast number of regions throughout the body to maintain homeostasis, and supports the notion that central and peripheral organs cannot be seen as independent organizations. Moreover, taking this into account, it is clear that what happens in the brain has systemic implications, and, more importantly, the reverse holds also true.

1.5.2.3. Aging

In the past years, the idea that age-associated hypothalamic dysfunction represents a significant intervenient in whole-body aging evolution has gained strength (Satoh *et al.* 2013, Zhang *et al.* 2013, Satoh *et al.* 2015, Cavadas *et al.* 2016). Moreover, hypothalamic–pituitary–GH axis is intimately related with the regulation of physiological processes involved in longevity (Brown-Borg 2015).

During the process of aging many alterations occur in the hypothalamus, at the cellular level, that interfere with its normal function, including defective autophagy, impaired neurogenesis, microglia activation, upregulation of inflammatory cytokines and activation of NF-kB signaling (Kaushik *et al.* 2012, Newton *et al.* 2013, Zhang *et al.* 2013, Kermath *et al.* 2014).

In 2013, Zhang and colleagues presented a study pinpointing the importance of hypothalamic inflammation on aging (Zhang *et al.* 2013). NF-kB had been previously implicated in the control of gene expression during aging, mediating immune cell communication and inflammatory responses (Adler *et al.* 2007). Taking this into account, it was observed that hypothalamic NF-kB, along with increased expression of several cytokines, was activated in old mice (Zhang *et al.* 2013). The initiation of inflammatory events involving microglia-induced TNF-α, neuronal NF-kB and IKK-β, culminates in a feed-forward loop that produces epigenetic changes, for instance, in neuroendocrine genes, compromising hypothalamic function (Gabuzda and Yankner 2013, Zhang *et al.* 2013). One of the genes affected is the GnRH, which may contribute to the characteristic decline in muscle and bone fitness, skin atrophy, reduced neurogenesis and memory impairment, observed during aging (Zhang *et al.* 2013). Noteworthy, other brain regions tested were not as sensitive to aging-related NF-kB activity as the mediobasal part of the hypothalamus (Zhang *et al.* 2013)

Another strong hint pointing to a connection between hypothalamic dysregulation and aging comes from the study conducted by Mariño and collaborators (Marino *et al.* 2010), where it is verified that Zmpste24$^{-/-}$ mice, an animal model of accelerated aging, present a dysfunction of the somatotroph axis signaling. In healthy conditions, GH released from the pituitary in response to hypothalamic GHRH stimulates the production of IGF-1 in the liver, however, it was observed that these mice undergo a progressive increase in circulating GH but IGF-1 levels do not follow this tendency, thus suggesting a phenomenon of GH resistance (Marino *et al.* 2010). Proving that this decrease in IGF-1 is detrimental for the individuals, treatment with recombinant IGF-1 was sufficient to improve the aging features of the animals and extend their lifespan (Marino *et al.* 2010).

Despite these valuable contributions, considerable efforts to understand the hypothalamic changes occurring with aging are still necessary in order to ascertain if targeting hypothalamus constitutes a realistic therapeutic strategy to delay the deteriorations that occur with whole-body aging.

1.5. Objectives

HGPS is a condition characterized by premature and accelerated aging. The patients develop cardiovascular disease that results in their death by myocardial infarction (Ullrich and Gordon 2015). Currently there is no treatment for HGPS despite all the efforts implemented.

An extensive description of the clinical features observed in HGPS patients has been performed (Gordon *et al.* 2007, Merideth *et al.* 2008, Ullrich and Gordon 2015), nonetheless, besides the finding that miR9 protects neurons and glial cells from progerin accumulation (Nissan *et al.* 2012), few studies have focused on the CNS in the context of the disease. In line with this, and given the role of hypothalamic dysfunction in the development of whole-body aging (Satoh *et al.* 2013, Zhang *et al.* 2013, Satoh *et al.* 2015, Cavadas *et al.* 2016), the first aim of our study is to investigate potential alterations in the hypothalamus in a HGPS mouse model, the *Lmna*$^{G609G/G609G}$ mice.

Ghrelin is an orexigenic hormone that is produced mainly in the stomach and travels to the hypothalamus where it stimulates food intake and GHRH release (Muller *et al.* 2015). Ghrelin can therefore modulate hypothalamic function, with particular emphasis in the regulation of NPY production (Cowley *et al.* 2003). Besides central functions, ghrelin also possesses a wide variety of effects in peripheral tissues, namely in the cardiovascular system, bones, muscle and adipose tissue (Nagaya and Kangawa 2003, Pradhan *et al.* 2013, Delhanty *et al.* 2014, Muller *et al.* 2015). Moreover, recent findings of our group demonstrate ghrelin's ability to promote autophagy in dermal fibroblasts of HGPS patients and counteract several of the cellular HGPS features including progerin accumulation, dysmorphic nuclei, accumulation of DNA damage and cellular senescence. Therefore, given the plethora of actions of ghrelin and the promising results obtained in HGPS fibroblasts, the second objective of this study is to assess the effect of peripheral administration of ghrelin on HGPS premature aging phenotype, using *Lmna*$^{G609G/G609G}$ mice. In particular, we intend to investigate the treatment outcome on *Lmna*$^{G609G/G609G}$ mice peripheral aging (heart, aorta, spleen, thymus, liver, kidney, white and brown adipose tissues, muscle and skin).

With this study we expect to shed light on how accelerated aging impacts hypothalamus structure and function and whether these alterations contribute to HGPS phenotype, unravelling a role for hypothalamus on HGPS progression. We also expect to provide ghrelin as an innovative therapeutic strategy for the treatment of HGPS. Moreover, given the similarities between HGPS phenotype and normal aging phenotype, the results will also contribute to a better understanding of ghrelin as an anti-aging molecule.

Chapter 2

Materials and Methods

2. Materials and Methods

2.1. Animals

In the present study wild-type C57BL/6 mice (*Lmna*$^{+/+}$), *Lmna*$^{G609G/+}$ and *Lmna*$^{G609G/G609G}$ mice (C57BL/6 genetic background) were used to perform all experiments. These different genotypes were obtained through heterozygous males and females crossings, as *Lmna*$^{G609G/G609G}$ mice are infertile. Mice were housed two to four per cage, in a 12 hours light/dark, with controlled temperature and humidity with ad libitum access to water and standard chow diet.

All the experiments were performed under the European Community directive for the care and use of animals in laboratory (2010/63/EU) which was translated to the Portuguese law in 2013 (Decree-law 113/2013). The animals were housed in our licensed animal facility (International Animal Welfare Assurance number 520.000.000.2006). All investigators who handled the mice have received an appropriate education (FELASA course) and are credited to perform animal experimentation as required by the Portuguese authorities. The present study is included in a project approved and financed by the Progeria Research foundation that approved the utilization of animals for this project (PRF2014-53).

2.1.1. Impact of premature aging on the hypothalamus of *Lmna*$^{G609G/G609G}$ mice

To characterize the alterations that occur in the hypothalamus of *Lmna*$^{G609G/G609G}$ mice along the aging process, mice of the three genotypes were sacrificed at different time points: *Lmna*$^{+/+}$ and *Lmna*$^{G609G/+}$ mice were sacrificed at 1.5, 3 and 8 months of age while *Lmna*$^{G609G/G609G}$ mice were sacrificed at 1.5 and 3 months of age, as depicted in Figure 2.1A. Mice whole brain or hypothalamus was collected for immunohistochemistry or gene expression analysis, respectively. A total of 3-6 animals were used per time point, for each genotype.

2.1.2. Effect of daily peripheral administration of ghrelin in *Lmna*$^{G609G/G609G}$ mice premature aging phenotype

To investigate the effect of ghrelin treatment on the aging phenotype of *Lmna*$^{G609G/G609G}$ mice, *Lmna*$^{+/+}$ (wild-type), *Lmna*$^{G609G/+}$ (heterozygous) and *Lmna*$^{G609G/G609G}$ mice (all 1.5 month old) were randomly distributed into two groups (4-5 mice per each experimental group): saline-treated or ghrelin-treated mice. Ghrelin (50 µg/kg) or saline (0.9 M NaCl) was administered for 1.5 months (daily; subcutaneous injection). During the time of treatment, mice body weight and food intake was evaluated twice a week. In the end of the trial mice behavior and glucose levels (under fed and fasting conditions) were evaluated. Mice were then euthanized and several organs and tissues were collected for histological, biochemical and molecular analysis of age-related alterations and cellular hallmarks of aging, as depicted in Figure 2.1B.

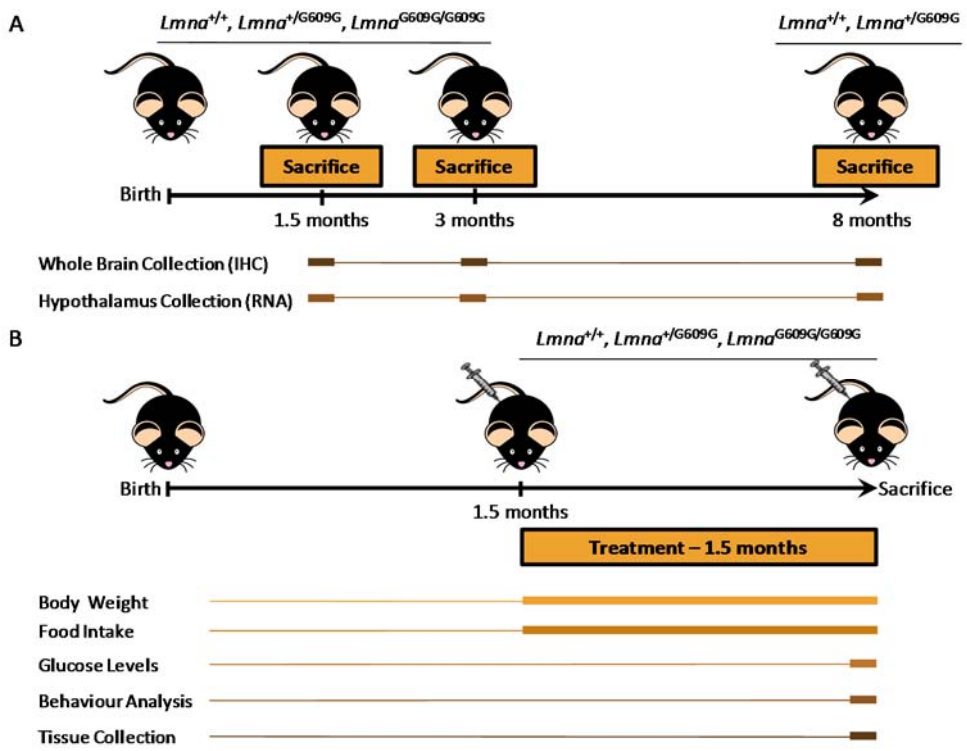

Figure 2.1. **Schematic representation of the experimental design.** A) Impact of premature aging on the hypothalamus of Lmna$^{G609G/G609G}$ mice. B) Effect of daily peripheral administration of ghrelin in Lmna$^{G609G/G609G}$ mice premature aging phenotype.

2.2. Genotyping

To determine the genotype of each mouse, mice were genotyped through standard procedures before the beginning of the study with, on average, 1 month of age. Mice were then housed according to their genotype and gender.

2.2.1. DNA extraction and purification

DNA was extracted and purified from a 20 mg ear sample from each mouse, using the GeneJet Genomic DNA Purification kit (Thermo Fisher) and following the manufacturer's instructions. Briefly, ear tissue was cut into small pieces and incubated in a digestion solution containing proteinase K for 6 hours at 56 °C. After digestion, samples were lysed with a proprietary Lysis buffer containing RNase to eliminate RNA from samples. The lysates were then mixed with ethanol and loaded on purification columns with silica membranes with high affinity for DNA molecules, where DNA molecules bind and are retained. Subsequently, samples were subjected to several wash steps with proprietary washing buffers through centrifugation to eliminate impurities from samples. Finally, genomic DNA was eluted from purification column with a proprietary elution buffer. After extraction and purification, DNA concentration was measured in a NanoDrop Lite Spectrophotometer (Thermo Fisher) and samples were frozen at -20 °C until use.

2.2.2. Polymerase Chain Reaction (PCR)

PCR was performed to amplify the Lmna gene region of interest (encompassing exon 11) using the following primers: DNA-Mm-Lmna forward: 5'-GGTTCCCACTGCAGCGGCTC-3' (exon 11), and DNA-Mm-Lmna reverse: 5'-GGACCCCACTCCCTTGGGCT-3' (intron 11).

For each PCR reaction (25 µL), a master mix containing 50 ng DNA, dNTPs mix (200 µM each), reverse and forward primers (400 nM each), 1.25 U DreamTaq DNA Polymerase (Thermo Fisher) and 1x DreamTaq buffer (Thermo Fisher) containing 2 mM $MgCl_2$ was prepared. PCR reactions were performed in a Doppio thermal cycler (VWR) with the following protocol: an initial denaturation step of 95 °C for 3 minutes followed by 30 cycles at 95 °C for 30 seconds, 60 °C for 30 seconds and 72 °C for 1 minute per kilobase, corresponding to the denaturation, annealing and extension steps, respectively. Ultimately, the final extension took place at 72 °C for 10 minutes. PCR products were stored at -20 °C until use.

PCR products were run on a 1.5 % agarose gel, at 90V for approximately 30 minutes. A Gel Doc EZ Imager (Biorad) was used to analyze the bands and confirm the correct size of the amplification products (342 pb).

2.2.3. Clean-up

To purify the PCR products from enzymatic reactions, a Nucleospin Gel and PCR Clean-up kit (Macherey-Nagel) was used. This step is critical to avoid errors of contamination with oligomers formed throughout the reaction, or the nucleotides and primers present in the solution, as these may interfere in the DNA sequencing. PCR samples purification was performed according to the manufacturer instructions. Briefly, samples were mixed with a proprietary Binding Buffer, then DNA was bound to the silica membranes of NucleoSpin® Gel and PCR Clean-up columns and contaminants were removed by two washing steps with proprietary Wash Buffer. Finally, the pure DNA was eluted under low salt conditions with a proprietary Elution Buffer.

2.2.4. Sequencing

DNA sequencing was performed at GATC Biotech (Germany). Purified PCR products from each sample were mixed with the forward primer and sent to the company for Sanger sequencing. Results were made available through their website (https://www.gatc-biotech.com/en/index.html). Using the GATC Viewer software (GATC Biotech) the presence or absence of the c.1827C>T;p.Gly609Gly mutation, homologous the human HGPS c.1824C>T;p.Gly608Gly mutation, was confirmed, and the genotype of each animal determined (Figure 2.2).

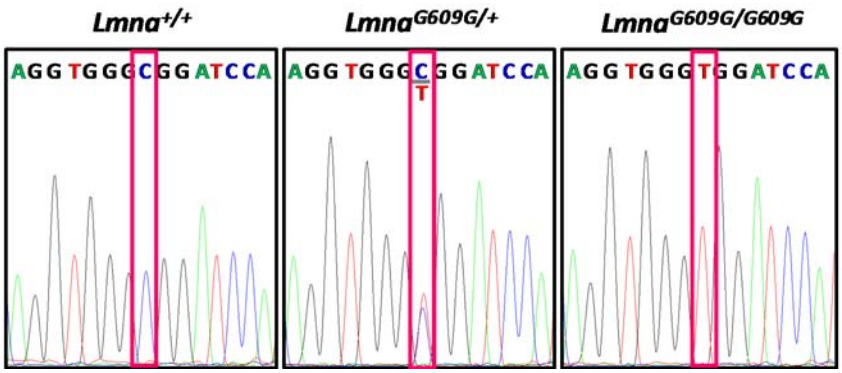

Figure 2.2. **Mice genotyping.** Examples of genomic sequencing of *Lmna* exon 11 showing the wild-type sequence or heterozygous/homozygous mutations respectively in *Lmna*$^{+/+}$, *Lmna*$^{G609G/+}$ and *Lmna*$^{G609G/G609G}$ mice.

2.3. Food intake and body weight analysis

During the course of ghrelin treatment, mice body weight and food intake of were evaluated twice a week. Body weight gain was calculated as the percentage of weight gain since the beginning of the treatment. Food intake was measured as a ratio of total food ingested over the study (g) per total weight gained (g). This ratio was calculated for each cage and then multiplied for the body weight of each mouse within to calculate food intake for each mouse.

2.4. Blood glucose levels determination

Blood glucose levels were measured by using a FreeStyle Precison Neo glucometer (Abbott) under fed (normal ad libitum conditions) and fasting (8 hours fasting during the night) conditions. Blood sampling was performed in the mouse tail tip. Glucose levels measurements were performed early in the morning, before the daily administration of ghrelin or vehicle to the animals, in order to avoid significant alterations in the blood glucose levels due to their manipulation.

2.5. Behavioral analysis

2.5.1. Open field test

For the assessment of mice horizontal locomotor activity and anxiety-like behaviors, open field tests were performed at the 43rd day of treatment.

Mice were acclimated to the test room for a 12 h period before the experiment. Mice were placed individually in the center of a 50 x 50cm arena with 50 cm high walls and their movement activity was recorded for 40 minutes using the Acti-Track System (Panlab, Barcelona, Spain). Several parameters were analyzed: activity tracing between the peripheral and central zone of the arena, total distance travelled, mean velocity, resting time and permanence in the central zone of the arena.

2.6. Tissue and Blood Collection

Animals from each experimental group were randomly selected either for whole brain removal for immunohistochemistry experiments, or for collection of blood, hypothalamic tissue for RNA extraction and peripheral organs extraction for histological and RNA/protein analysis.

For immunohistochemistry, mice were euthanazied with an overdose of avertin (tribromoethanol; 2.5 times 14 uL/g; 250 mg/Kg intraperitoneal) and then intracardially perfused with 4 % (w/v) paraformaldeheyde/0.1 M phosphate buffered saline (PBS; 137 mM NaCl; 2.7 mM KCl; 10 mM Na_2PO_4; 1.8 mM KH_2PO_4; pH 7.4) fixative solution. After decapitation, the whole brain was collected and fixed for 48 hours in 4 % paraformaldehyde (w/v) in PBS and then cryopreserved in 30 % sucrose/PBS solution (w/v) for 72 hours. Brains were dried and stored at -80 °C until use.

For tissue and blood analysis, mice were first anesthetized with isofluorane (Abbot) and then decapitated. Blood was collected upon decapitation and kept on ice until serum separation by centrifugation (2,000 g for 15 minutes at 4 °C). Serum samples were stored at -20 °C until use. After decapitation, brain was removed and the hypothalamus dissected and stored at -80 °C for posterior processing. After removal of the brain, several organs and tissues (liver, heart, kidney, spleen, thymus, gonadal white adipose tissue (WAT) and intrascapular brown adipose tissue (BAT)) were collected and weighed. Samples from other organs and tissues were also collected (skeletal muscle, aorta, pancreas, gut, bone, skin, testis and ovaries). For histological analysis, tissues' samples were fixed in 10 % neutral buffered formalin solution (VWR), for 72 hours, before further processing. For protein and gene expression analysis, small samples of tissue were isolated from the collected organs and stored at -80 °C until use.

2.7. Gene expression analysis

2.7.1. Purification and quantification of total RNA

Total RNA was isolated using the RNeasy Mini Kit (Qiagen) according to the manufacturer's instructions. Briefly, cells were lysed, the total RNA was adsorbed to a silica matrix, washed with the recommended buffers and eluted with 30 µL of RNase-free water by centrifugation. Total RNA amount was quantified by optical density (OD) measurements using a ND-1000 Nanodrop Spectrophotometer (Thermo Scientific), and the purity was evaluated by measuring the ratio of OD at 260 and 280 nm. RNA samples were treated with RNase-free DNAse (Qiagen) to eliminate any contamination with genomic DNA. RNA samples were kept at -80 °C until use.

2.7.2. Reverse transcription

Reverse transcription into cDNA was carried out using the iScript cDNA Synthesis Kit (Bio-Rad) following the manufacturer's instructions. Briefly, 1 µg of total RNA from

each sample was reverse transcribed into cDNA in a 30 µL reaction containing 1x iScript reaction buffer, and 1 µL of iScript reverse transcriptase. Reverse transcription reactions were performed in a thermocycler at 25 °C for 5 minutes, 46 °C for 30 minutes, 95 °C for 5 minutes, and 4 °C for 5 minutes. cDNA samples were then stored at -20 °C until use.

2.7.3. Quantitative real-time polymerase chain reaction (qPCR)

qPCR was performed in the StepOne Plus Real-Time PCR System (Applied Biosystems) using 96-well microliter plates and the SsoAdvanced SYBR Green Supermix (Bio-Rad). All primers used were designed using PrimerBlast Software and produced by Invitrogen. Primers' sequences are listed below (Table 2.1). For each primer set, qPCR reactions were carried out in 10 µL reaction volume containing 5 µL of 2× SsoAdvanced SYBR Green Supermix, 0.5 µL of forward primer (500 nM), 0.5 µL of reverse primer (500 nM) and 4 µL of template cDNA. Appropriate negative controls were also prepared. All reactions were performed in duplicate and according to the manufacturer's recommendations: 95 °C for 30 seconds, followed by 45 cycles at 95 °C for 5 seconds and 56 – 60 °C for 30 seconds. The melting curve protocol started immediately after amplification with the following protocol: 65 °C to 95 °C with 0.5 °C increments, 5 seconds /step and 95 °C for 10 seconds. For each primer set, the specific annealing temperature and the quantity of cDNA used are described in Table 2.1. The amplification efficiency for each gene and the threshold values for threshold cycle determination (Ct) were determined automatically by the StepOne Software (Applied Biosystems). Relative mRNA quantification was performed using the ΔCt method for genes with the same amplification efficiency using hypoxanthine-guanine phosphoribosyltransferase (HPRT) as the endogenous housekeeping gene. The results are expressed as the relative amount compared to vehicle-treated experimental group.

2.8. Protein expression analysis

2.8.1. Western Blotting

2.8.1.2. Lysates preparation

Liver protein extracts were obtained by the mechanical disruption, on ice, of the tissue using a microcentrifuge tube adapted pestle (Eppendorf), in radio-immunoprecipitation assay (RIPA) buffer (50 mM Tris-HCl, pH 7.4; 150 mM NaCl; 5 mM EDTA; 1 % Triton X-100; 0.5 % deoxycholate; 0.1 % sodium dodecyl sulphate (SDS); 200 µM phenylmethylsulphonylfluoride (PMSF); 1 mM dithiothreitol (DDT); 1 mM Na_3VO_4; 10 mM NaF) supplemented with Complete™ Mini Protease Inhibitor Cocktail tablet (Roche). The samples were then sonicated (Amplitude: 40; 5 pulses of 5 seconds), always on ice, and centrifuged for 10 minutes at full speed, at 4 °C for deposition of the insoluble material. Each supernatant was collected into a new tube and liver lysates were stored at -20 °C until protein determination.

Skin protein extracts were obtained using the above protocol however, skin samples were incubated in RIPA buffer, on ice, for 30 minutes before mechanical disruption.

WAT protein extracts were obtained using the above protocol with minor modifications. After mechanical disruption and sonication in RIPA buffer, tissue lysates were centrifuged for 5 minutes at 1,000x *g* at 10 °C, and the soluble fraction (supernatant) was collected using a syringe to a new tube, without disturbing the fat layer. This soluble fraction was centrifuged a second time for 5 minutes at 3,300x *g* at 8 °C. The obtained soluble fraction was collected with a syringe to a new tube and stored at -20 °C until use.

Table 2.1. **Primers used for gene expression analysis.**

Primer	Sequence	Temperature	Function
NPY	F:CACCAGACAGAGATATGGCAAGA R: TGTTCTGGGGGCGTTTTCTG	60 °C	Orexigenic neuropeptide
AgRP	F: TCCCAGAGTTCCCAGGTCTAA R: CGCGGTTCTGTGGATCTAGC	56 °C	Orexigenic neuropeptide
POMC	F: CAACCTGCTGGCTTGCATC R: CGTACTTCCGGGGGTTTTCA	56 °C	Anorexigenic neuropeptide
CART	F: CGCTATGTTGCAGATCGAAGC R: GCGTCACACATGGGGACTT	60 °C	Anorexigenic neuropeptide
Y1R	F: CCCATCTGACTCTCACAGGC R: AGCGAATGTATATCTTGAAGTAGCA	58 °C	NPY receptor
Y2R	F: CGCAAGAGTCAATACAGCCAA R: CCCATAGGGCTCCACTTTCA	58 °C	NPY receptor
Y5R	F: TTCCATCTCAAGCAGAAGCGA R: CATACTAGAGTCCTCGGGATGC	58 °C	NPY receptor
GFAP	F: AGAAAACCGCATCACCATTCCT R: CTTGTGACTTTTTGGCCTTCCC	60°C	Astrocyte marker
CD11b	F: TCGCTACGTAATTGGGGTGG R: TAGATGCGATGGTGTCGAGC	60 °C	Immune cells marker
IL-1β	F: GCCACCTTTTGACAGTGATGAG R: GACAGCCCAGGTCAAAGGTT	58 °C	Pro-inflammatory marker
IL-10	F: ACCTGGTAGAAGTGATGCCC R: ACAGGGGAGAAATCGATGACAG	56 °C	Anti-inflammatory marker
SOX2	F: CCTACAGCATGTCCTACTCGC R: AGTGGGAGGAAGAGGTAACCA	58 °C	Pluripotency marker
GnRH	F: AGGAGGTGGATCAAATGGCAG R: AATCAGACTTTCCAGAGCTCCTC	56 °C	HPG-axis regulation
BDNF	F: GCAAAGCCGAACTTCTCACAT R: TGGTGGAACATTGTGGCTTTG	56 °C	Neurotrophic factor
Hprt	F: GCTTACCTCACTGCTTTCCG R: CATCATCGCTAATCACGACGC	58 °C	Control

Protein concentration of each sample was determined by the bicinchoninic acid (BCA) protein assay (Thermo Fisher) according with the manufacturer's instructions.

Bovine serum albumin solution (BSA) (2 $mg.mL^{-1}$) serial dilutions was used as standard curve. The samples were then denatured by adding 6x concentrated sample buffer (0.5 M Tris, 30 % glycerol, 10 % SDS, 0.6 M DTT, 0.012 % bromophenol blue) and heated at 95°C for 5 minutes. Samples were equalized for protein concentration (60 µg/30 µL) to minimize variations when resolving the protein extracts, and stored at -20 °C until use.

2.8.1.3. Western blotting analysis

Western Blotting technique was used in order to immunodetect the expression of several proteins in the tissues of interest (liver, WAT, BAT and skin).

Equal amounts of total protein were loaded per lane (60-80 µg) and separated by electrophoresis in 4-10 % or 4-12 % sodium dodecyl sulphate-polyacrylamide gels (SDS-PAGE) on a Tris-Bicine buffer (25 mM Tris; 25 mM Bicine; 1 % (w/v) SDS; pH 8.3) at 120-140 V until proper separation of the proteins of interest, according with their molecular weight. Next, proteins were electro-transferred to previously methanol-activated polyvinylidene fluoride (PVDF) membranes (Merck Milipore), in CAPS transfer buffer (10 mM CAPS, pH 11.0; 10 % (v/v) methanol), at a constant current of 1,000 mA for 2 hours and 15 minutes, at 4 °C. The membranes were then blocked, for 1 hour at room temperature, with 5 % (m/v) low-fat milk in Tris-buffered saline (TBS: 137 mM NaCl; 20 mM Tris-HCl; pH 7.6) containing 0.1 % (v/v) Tween 20 (TBS-T) and incubated overnight with the respective primary antibodies (listed on Table 2.2) in TBS-T with 5 % (w/v) skim milk or BSA at 4 °C. Afterwards, the membranes were washed three times for 10 minutes in TBS-T and incubated for 1 hour at room temperature with a rabbit or mouse IgG-specific alkaline phosphatase-linked secondary antibody (all from PIERCE), in a dilution of 1:10,000 in the same blocking solution as the respective primary antibody. The membranes underwent another washing step and then the protein immunoreactive bands were visualized by chemifluorescence using the ECF substrate (GE Healthcare) on a Versa Doc Imaging System (Bio-Rad). The optical density of the bands was quantified with the Quantity One Software 4.6.9 (Bio-Rad). Membranes were reprobed with a monoclonal anti-β-tubulin (1:10,000; Sigma) or anti-β-actin (1:5,000; Sigma) for equal protein load control. The specific optical density was then normalized with respect to the amount of β-actin or β-tubulin loaded in the corresponding lane of the same gel. Results were normalized to the mean value of each experimental control condition (vehicle-treated mice), and expressed as relative amount compared with the experimental control group.

Table 2.2. **List of the primary antibodies used in the western blot experiments.**

Antibody	Supplier	Host	Dilution	Blocking Solution
Anti-lamin A/C	Santa Cruz Biotechnology	Goat Polyclonal	1:500	5 % low-fat milk
Anti-SQSTM1/P62	Cell Signaling	Rabbit Polyclonal	1:1,000	5 % BSA
Anti-LC3B	Cell Signaling	Rabbit Polyclonal	1:1,000	5 % BSA
Anti-PCNA	Santa Cruz Biotechnology	Mouse Monoclonal	1:500	5 % low-fat milk
Anti-p53	Santa Cruz Biotechnology	Rabbit Polyclonal	1:500	5 % low-fat milk

2.8.2. Immunohistochemistry

Brains collected for the immunohistochemistry studies were included in Tissue-Tek optimum cutting temperature (OCT) compound (Sakura Finetek) and then sectioned into 30 µm coronal sections at -20 °C using a cryostat-microtome Leica CM3050S (Leica Microsystems Nussloch GmbH, Nußloch, Germany). Sections were collected and stored in 48-well plates, free floating in 0.1 M PBS supplemented with 0.05 % (v/v) sodium azide, and stored at 4 °C until use. The Paxino's Mouse Brain Atlas was used to define the coordinates for the beginning (1.18 mm Bregma) and end (-2.92 mm Bregma) of the sectioning in order to assure the representation of the whole hypothalamus.

Hypothalamic NPY, POMC, NeuN, GFAP and Iba-1 protein levels were assessed by immunohistochemistry on mice brain sections. For that, coronal sections of approximately equal spacing were sampled over the anterior–posterior extent of the hypothalamus (approximately between Bregma -0.46 mm to -2.80 mm using The Paxino's Mouse Brain Atlas). For immunohistochemistry processing, brain coronal sections were washed three times with PBS (137 mM NaCl; 2.7 mM KCl; 10 mM Na_2PO_4; 1.8 mM KH_2PO_4; pH 7.4) and then blocked and permeabilized for 1 hour at room temperature, in PBS supplemented with 10 % goat serum (GS; Sigma) and 0.3 % (v/v) triton X-100 (Merk Millipore). Afterwards, brain coronal sections were incubated with the primary antibodies (listed in Table 2.3) diluted in the blocking solution, overnight at 4 °C. Sections were washed three times in PBS and then incubated with the respective secondary antibodies for 2 hours, at room temperature. Nuclei were stained with Hoechst 33342 (2 µg/mL; Invitrogen). After incubation, brain sections were washed four times in PBS and mounted in slides with Mowiol mounting medium (Sigma-Aldrich). Brain coronal sections were analyzed on an Axio Imager Z2 (Carl Zeiss). For hypothalamic protein immunoreactivity determination, tiles images encompassing the hypothalamus were acquired using a Plan-Apochromat 20x/0.8 M27 objective.

Table 2.3. **List of the primary and secondary antibodies used for imunohistochemistry studies**

Antibody	Supplier	Host	Dilution
Anti-NeuN	Chemicon	Mouse Monoclonal	1:500
Anti-NPY	Sigma	Rabbit Polyclonal	1:5000
Anti-POMC	Abcam	Chicken Polyclonal	1:1000
Anti-GFAP	Merck Millipore	Mouse Monoclonal	1:500
Anti-Iba1	WAKO	Rabbit Polyclonal	1:1000
Anti-Chicken (Alexa-Fluor 488)	Life Technologies	Goat	1:250
Anti-Mouse (Alexa-Fluor 488)	Life Technologies	Goat	1:200
Anti-Mouse (Alexa-Fluor 594)	Life Technologies	Goat	1:500
Anti-Rabbit (Alexa-Fluor 488)	Life Technologies	Goat	1:1000
Anti-Rabbit (Alexa-Fluor 594)	Life Technologies	Goat	1:500

2.8.2.1. Quantification of NeuN, NPY, POMC, GFAP and Iba-1 immunoreactivity in the mouse hypothalamic nuclei

For protein immunoreactivity quantification, the ARC, VMH, DMH and PVN nuclei area were defined using The Paxino's Mouse Brain Atlas. For each brain section, an area including each nucleus in one hemisphere was delimited as depicted in Figure 2.3 and the integrated density (the product of area and mean grey value; arbitrary units) of 5 (for ARC), 3 (for VMH and DMH) and 2 (for PVN) sections was measured using the Fiji (Fiji is Just ImageJ) software (NIH - National Institutes of Health, Bethesda, MD, USA). For each nucleus, the integrated density values of each section were summed to yield total integrated density values for each animal, and the mean of the total integrated density values was calculated for each experimental group. The results are represented as mean values for each experimental group and are relative to one hemisphere.

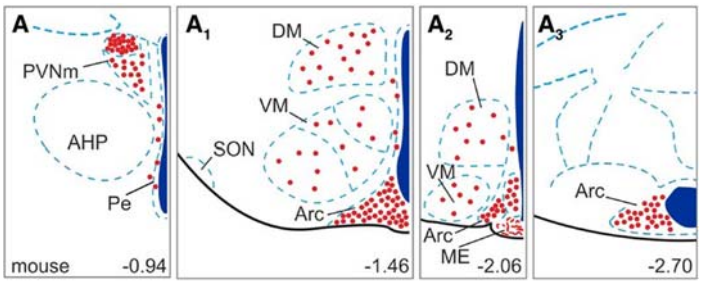

Figure 2.3. **Schematic representation of hypothalamic nuclei area delimitation along the anterior-posterior length of hypothalamus used for protein immunoreactivity quantification in paraventricular, dorsolateral, ventromedial, and arcuate nuclei of the mouse hypothalamus (Paxinos & Franklin, 2001).** A: Bregma -0.94; A1: Bregma -1.46; A2: Bregma -2.06; A3: Bregma: -2.70. AHP, anterior hypothalamus; Arc, arcuate nucleus; DM, dorsomedial nucleus; ME, median eminence; Pe, periventricular nucleus; PVN, paraventricular nucleus, PVNm, magnocellular part; SON, supraoptic nucleus; VM, ventromedial nucleus. Adapted from (Romanov *et al.*, 2014).

2.9. Histological analysis

2.9.1. Tissue preparation for histological analysis

After fixation in formalin, tissue samples were cut in smaller pieces and then submitted to several steps for paraffin (Merck Millipore) embedding: 70 % ethanol (v/v) (Fisher Scientific) for 1 hour; two series of 95 % ethanol (v/v), for 40 minutes each; two series of 100% ethanol (v/v), for 1 hour each; two series of xylene (Fisher Scientific), for 1 hour each, and two series of paraffin (Histosec, Millipore) at 56 °C, for 1 hour each. After dehydration, clearing and infiltration, tissue samples were mounted in embedding molds filled with melted paraffin (56 °C) and oriented as desired. A tissue cassette was placed on top and the block was allowed to cool down and hardened. Afterwards, the block was removed from the mold and stored at room temperature in a dry place until use. Paraffin blocks were sectioned in sections with 3 µm of thickness in a HM 325 Rotary Microtome (Thermo Fisher) at room temperature. Sections were placed into gelatin-coated microscopy slides and stored at room temperature until use.

2.9.2. Hematoxylin-eosin staining

For histological analysis, hematoxylin-eosin staining was performed according to the manufacturer's instructions, in tissue paraffin sections. Sections were deparaffinized in xylene and rehydrated in 100 % ethanol (v/v) and then 95 % ethanol (v/v)). Sections were incubated with hematoxylin solution modified according to Gill III (Merck Milipore) for 30 seconds and then washed in distilled water. Sections were then counterstained with 0.5 % aqueous Eosin Y solution (Merck Milipore) for 1 minute, washed with distilled water and dehydrated with 95 % ethanol (v/v), 100 % ethanol (v/v) and xylene. After staining, sections were mounted in slides with Richard-Allan Scientific Mounting Medium (HM325, Thermo Fisher Scientific) and analyzed by microscopy.

2.9.3. Masson Trichrome staining

To evaluate alterations in collagen fibers or potential signs of fibrosis, Masson's trichrome staining (Thermo Scientific) was performed in paraffin liver and skin sections following the manufacturer's instructions. In summary, sections were dewaxed and rehydrated as previously described and incubated with Bouin's solution (Thermo Scientific) for 1 hour at 56 °C. The sections were cooled down and then washed in distilled water. Then sections were placed in the Weigert's Iron Hematoxylin stain solution for 10 minutes, washed with water, placed in Biebrich Scarlet-Acid Fucshin stain solution for 10 minutes and washed in water. For differentiation, sections were placed in Phosphotungstic/Phosphomolybdic Acid Solution for 5 minutes. Then, sections were transferred to an Aniline Blue stain solution and incubated for 10 minutes. Color was differentiated upon incubation in a 1 % acetic acid solution for 1

minute. Sections were then rinsed in water, dehydrated in 95 % ethanol (v/v) and 100 % ethanol (v/v), cleared in xylene and then mounted as described above.

With Masson's trichrome staining, collagen fibers will be stained blue, the nuclei will be stained dark brown/black and the background (keratin, muscle fibers and cell's cytoplasm) is stained red or light pink. Tissue sections images were acquired on a Zeiss Axio Imager Z2 microscope (Zeiss) using the Plan-Apochromat 20x/0.8 M27 objective and alterations in collagen fibers were evaluated by qualitative assessment.

2.9.4. Hoechst staining

For aorta wall cell density analysis, Hoechst staining was performed in aorta paraffin sections. Sections were first deparaffinized and rehydrated as described and then washed in distilled water. Sections were incubated with Hoechst solution (2µg/µL in didtilled water) for 15 minutes and then washed twice in distilled water for 5 minutes. After staining, sections were let to dry and then were mounted in slides with Mowiol mounting medium. Aorta sections were then analyzed by microscopy.

2.9.5. White adipose tissue analysis

Images of hematoxylin-eosin stained WAT (at least 5 different fields per mouse) were acquired in the Axio Scan Z1 (Carl Zeiss) and Axio Imager Z2 (Carl Zeiss), using the Plan-Apochromat 20x/0.8 M27 objective.

Adipocytes (300 per animal) with intact cellular membranes were chosen for determination of the cross-sectional area (adipocyte size) using Fiji software (NIH, Bethesda, MD, USA). For each mouse, the mean of adipocytes area was calculated from all the WAT images analyzed. The results are represented as mean values for each experimental group. Adipocye size distribution was also determined. For each mouse, the obtained adipocyte area values were grouped by size range and adipocytes size distribution was determined as percentage of total number of adipocytes analyzed. The number of adipocytes per area in WAT tissue was also determined using the Cell counter plugin of Fiji software and the adipocyte density was estimated by dividing the number of adipocytes by the analyzed tissue area. For each mouse, the mean of adipocytes number per area was calculated from all the WAT images analyzed. The results are represented as mean values for each experimental group.

2.9.6. Skeletal muscle analysis

Images of hematoxylin-eosin stained skeletal muscle (at least 5 different fields per mouse) were acquired in the Axio Scan Z1 (Carl Zeiss) or Axio Imager Z2 (Carl Zeiss), using the Plan-Apochromat 20x/0.8 M27 objective.

Skeletal muscle fibers (~200 per mouse; cross-section cut) with intact cellular membranes were chosen for determination of the cross-sectional area (muscle fiber size) using Fiji software. Elongated fibers indicating an oblique or longitudinal muscle section were excluded. For each mouse, the mean of muscle cross-sectional area was

calculated from all the skeletal muscle images analyzed. The results are represented as mean values for each experimental group. Muscle fiber size distribution was also determined. For each mouse, the obtained muscle area values were grouped by size range and muscle fibers size distribution was determined as percentage of total number of muscle fibers analyzed.

2.9.7. Liver analysis

Images of hematoxylin-eosin stained liver sections (at least 5 different fields per mouse liver) were acquired in the Axio Imager Z2 microscope (Zeiss) using the Plan-Apochromat 20x/0.8 M27 objective. The number of hepatocytes per area in the liver was determined using the Cell counter plugin of Fiji software (NIH, Bethesda, MD, USA) and the hepatocyte density was estimated by dividing the number of hepatocytes by the analyzed tissue area. For each mouse, the mean of hepatocytes number per area was calculated from all the liver images analyzed. The results are represented as mean values for each experimental group.

2.9.8. Aorta analysis

Images (tiles images) of hematoxylin-eosin stained proximal descending thoracic aorta sections (two sections per mouse) were acquired in the Axio Imager Z2 microscope (Zeiss) using the Plan-Apochromat 20x/0.8 M27 objective.

Aortic medial (tunica media) thickness was measured from the internal elastic lamina to the adventitial border, using Fiji software. For each aorta section, 5 random thickness length measurements were made and the mean of measurements was calculated. For each mouse, the mean of aorta medial thickness was calculated from the aorta sections analyzed. The results are represented as mean values for each experimental group. Cell density (in cells/mm^2) in the aortic wall was also determined in by counting the number of nuclei per area of medial tissue from Hoechst-stained aorta sections mice and dividing by the total area of tissue examined. The results are represented as mean values for each experimental group.

2.9.9. Spleen analysis

Images (tiles images) of hematoxylin-eosin stained spleen sections (4 per mouse) were obtained in the the Axio Scan Z1 (Carl Zeiss) or Axio Imager Z2 (Carl Zeiss), using the Plan-Apochromat 20x/0.8 M27 objective.

White pulp area of each spleen section was measured using the Fiji software (NIH) and expressed as the percentage of the total area of the spleen section. For each mouse, the mean percentage of white pulp area was calculated. The results are represented as mean values for each experimental group.

2.9.10. Kidney analysis

Images (tiles images) of hematoxylin-eosin stained kidney sections (at least 2 sections per mouse) were acquired in the Axio Scan Z1 (Carl Zeiss) or Axio Imager Z2 (Carl Zeiss) using the Plan-Apochromat 20x/0.8 M27 objective.

The renal corpuscle area was measured using Fiji software. For the renal corpuscle area assessment, 6-8 random fields were analyzed per kidney section (~100 glomeruli per mouse). For each mouse, the mean of renal corpuscle area was calculated from all fields analyzed. The results are represented as mean values for each experimental group.

2.9.11. Skin analysis

Images (tiles images) of hematoxylin-eosin stained skin sections (at least 3 skin sections per mouse) were acquired in the Axio Imager Z2 microscope (Zeiss) using the Plan-Apochromat 20x/0.8 M27 objective.

The thicknesses of epidermis, dermis and subcutaneous fat layer were determined by histomorphometric analysis using Fiji software (NIH, Bethesda, MD, USA). For each skin layer thickness measurement, at least 30 length measurements were made in each skin section (measurements were randomly done throughout each skin section). For each skin section, the mean of measurements for each layer was calculated. Finally, for each mouse, the mean of each skin layer thickness was calculated from all the skin sections analyzed. The results are represented as mean values for each experimental group.

2.10. Statistical analysis

All the results are expressed as mean ± standard error of the mean (SEM). The statistical analysis was performed using two-way analysis of variance (ANOVA), one-way ANOVA followed by Dunnett's or Bonferroni's multiple comparisons test or unpaired Student's *t* test, depending on the number of experimental groups or the number of variables to be analyzed in each experiment. For the statistical analysis Prism 6.01 (GraphPad Software) was used.

Chapter 3
Results

3. Results

3.1. Impact of premature aging on the hypothalamus of *Lmna*$^{G609G/G609G}$ mice

One puzzling observation in HGPS patients is the absence of cognitive impairment, despite the systemic and dramatic premature aging exhibited. In fact, the CNS of these children is thought to be protected from the deleterious effects of progerin accumulation, a hypothesis that is supported by the finding that neural-specific miR9 negatively regulates lamin A and progerin expression, decreasing progerin levels in HGPS cells (Nissan *et al.* 2012). However, besides this observation, there is a lack of knowledge about the alterations that occur in the brain of HGPS patients and what may be the impact of premature aged peripheral organs and systems on CNS structure and function and whether the crosstalk between periphery and CNC is compromised.

In recent years, hypothalamus has emerged as a key player in whole-body aging (Satoh *et al.* 2013, Zhang *et al.* 2013, Satoh *et al.* 2015, Cavadas *et al.* 2016). This brain region regulates body homeostasis through specialized neurons that sense and integrate central and peripheral signals to properly coordinate several survival functions, including development, reproduction, sleep, immunity, food intake, metabolism and neuroendocrine axis (Cowley *et al.* 2003, Pearson and Placzek 2013, Biran *et al.* 2015). Therefore, a decline in hypothalamic neurons responsiveness with age may adversely affect body physiological functions. In fact, some studies show that age-related hypothalamic dysfunction leads to metabolic and neuroendocrine homeostatic imbalance, accelerating whole-body aging (Kaushik *et al.* 2012, Newton *et al.* 2013, Zhang *et al.* 2013, Kermath *et al.* 2014).

In line with hypothalamus role on whole-body aging and given that HGPS is characterized by a premature aging, we investigate the impact of premature aging on the hypothalamus of *Lmna*$^{G609G/G609G}$ mice. For that, brains of *Lmna*$^{+/+}$, *Lmna*$^{G609G/+}$ and *Lmna*$^{G609G/G609G}$ mice were collected at 1.5, 3 and 8 months (at 8 months only *Lmna*$^{+/+}$ and *Lmna*$^{G609G/+}$ were used given the reduced lifespan of *Lmna*$^{G609G/G609G}$ mice) and processed for immunohistochemistry (protein immunoreactivity) or gene expression analysis (qPCR) of several proteins involved in hypothalamic function and structure. Protein immunoreactivity was evaluated in four hypothalamic nuclei, namely ARC, VMH, DMH and PVN. The ARC is a vital hypothalamic nucleus involved in the sensing of signals from the periphery and triggering of the correct adaptive responses. Along with DMH, VMH and PVN, it plays a key role in the regulation of food intake and energy homeostasis. Gene expression analysis was performed in whole hypothalamus.

3.1.1. Premature aging effect on hypothalamic NPY immunoreactivity

NPY is abundantly expressed throughout the brain, with a special emphasis in the hypothalamus (Adrian *et al.* 1983). It is a potent orexigenic peptide that plays a key role in the regulation food intake and body weight (Chee and Colmers 2008).

In the ARC (Figure 3.1A and B), we observed a tendency towards an increase in NPY protein levels in both *Lmna*$^{+/+}$ (1.5 months: 6.32±0.99 (x10^6); 3 months: 7.88±0.40 (x10^6); 8 months: 8.69±0.56 (x10^6)) and *Lmna*$^{G609G/G609G}$ (1.5 months: 6.85±0.54 (x10^6); 3 months: 7.85±0.71 (x10^6)) mice across time, however this effect was not statistically different. At 1.5 and 3 months of age, NPY protein levels in the ARC of *Lmna*$^{G609G/G609G}$ were similar to *Lmna*$^{+/+}$ mice (Figure 3.1B). However, a significant decrease in NPY protein levels was observed in *Lmna*$^{G609G/+}$ mice at 3 (6.33±0.30 (x10^6)) and 8 (6.22±0.24 (x10^6)) months of age comparing with age-matched *Lmna*$^{+/+}$ mice (Figure 3.1B).

In the VMH (Figure 3.1A and C), a tendency towards NPY immunoreactivity increase over time was also observed in *Lmna*$^{+/+}$ (1.5 months: 1.55±0.09 (x10^6); 3 months: 1.63±0.11 (x10^6); 8 months: 2.16±0.22 (x10^6)) and *Lmna*$^{G609G/G609G}$ (1.5 months: 1.88±0.14 (x10^6); 3 months: 2.33±0.21 (x10^6)) mice, although not statistical different. *Lmna*$^{G609G/G609G}$ mice show higher NPY protein levels in VMH than age-matched *Lmna*$^{+/+}$ mice being this increase more pronounced at 3 months of age. VMH NPY immunoreactivity was similar between *Lmna*$^{G609G/+}$ and *Lmna*$^{+/+}$ mice at 1.5 and 3 months of age. At 8 months, *Lmna*$^{G609G/+}$ showed lower NPY protein levels (1.64±0.10 (x10^6)) than age-matched *Lmna*$^{+/+}$ mice, however this effect was not statistical different.

We did not observe significant alterations in NPY protein levels in the DMH over time (Figure 3.1A and D), although a small tendency towards an increase of NPY immunoreactivity with age was shown by the three genotypes (*Lmna*$^{+/+}$ - 1.5 months: 4.15±0.66 (x10^6); 3 months: 4.99±0.50 (x10^6); 8 months: 5.03±0.53 (x10^6); *Lmna*$^{G609G/+}$ - 1.5 months: 3.84±0.11 (x10^6); 3 months: 4.03±0.32 (x10^6); 8 months: 4.48±0.53 (x10^6); *Lmna*$^{G609G/G609G}$ - 1.5 months: 3.94±0.32 (x10^6); 3 months: 4.65±0.63 (x10^6)). No significant changes in NPY immunoreactivity were observed between genotypes for each time point, however, *Lmna*$^{G609G/+}$ mice showed lower NPY levels than age-matched *Lmna*$^{+/+}$ mice at 3 and 8 months of age.

Premature aging had also an impact on NPY immunoreactivity in the PVN of *Lmna*$^{G609G/+}$ and *Lmna*$^{G609G/G609G}$ mice (Figure 3.1A and E). NPY protein levels did not significantly change along time in *Lmna*$^{+/+}$ (1.5 months: 2.64±0.23 (x10^6); 3 months: 2.58±0.16 (x10^6); 8 months: 2.22±0.35 (x10^6)) and *Lmna*$^{G609G/+}$ (1.5 months: 1.89±0.21 (x10^6); 3 months: 1.84±0.13 (x10^6); 8 months: 1.44±0.12 (x10^6)) mice along time although a tendency towards a decrease in NPY levels was observed at 8 months of age. On the other hand, *Lmna*$^{G609G/G609G}$ mice showed higher NPY levels with age (1.5 months: 1.80±0.04 (x10^6); 3 months: 2.42±0.31 (x10^6)), but this effect was not statistical different. Interestingly, when comparing the levels of NPY immunoreactivity between genotypes at each time-point, *Lmna*$^{G609G/G609G}$ mice showed decreased NPY levels than *Lmna*$^{+/+}$ mice at 1.5 months but not at 3 months of age, while *Lmna*$^{G609G/+}$ mice showed decreased levels of NPY than *Lmna*$^{+/+}$ mice at 1.5, 3 and 8 months of age.

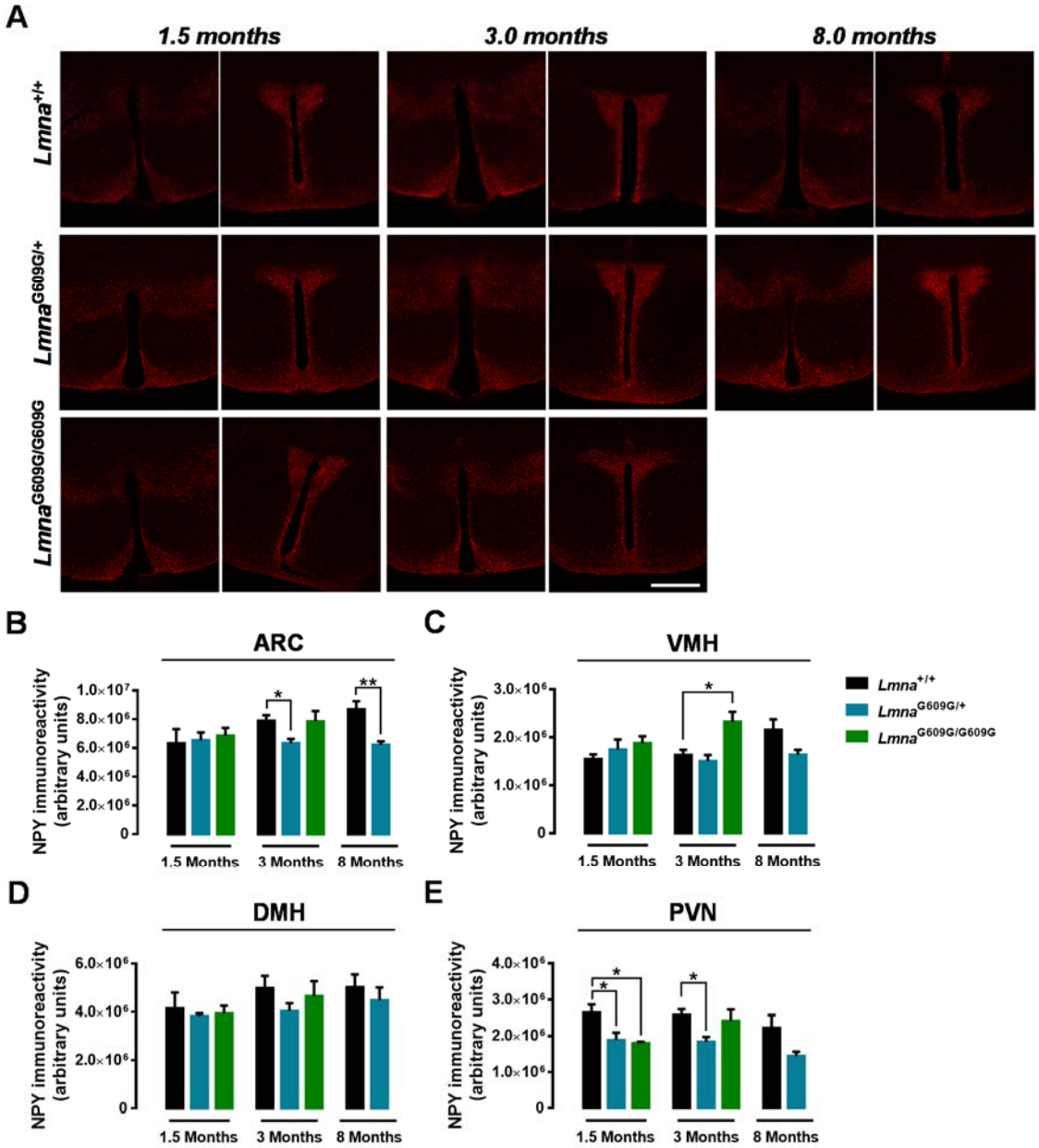

Figure 3.1. **NPY immunoreactivity in the hypothalamus of *Lmna*$^{+/+}$, *Lmna*$^{G609G/+}$ and *Lmna*$^{G609G/G609G}$ mice along time**. (A) Representative images of NPY immunoreactivity in the ARC, VMH, DMH and PVN of 1.5, 3 and 8 months-old *Lmna*$^{+/+}$ and *Lmna*$^{G609G/+}$ mice and 1.5 and 3 months-old *Lmna*$^{G609G/G609G}$ mice. (B-E) Quantification of NPY immunoreactivity in the ARC (B), VMH (C), DMH (D) and PVN (E) through the anterior-posterior length of the mouse ARC. The results represent the mean ± SEM of the total integrated density (n=3-6 mice per group for each nuclei). *p<0.05, **p<0.01 significantly different compared to *Lmna*$^{+/+}$, as determined by one-way ANOVA, followed by Dunnett's multiple comparison test or Student's unpaired t test.

3.1.2. Premature aging effect on hypothalamic POMC protein levels

We also assessed the immunoreactivity of POMC, an anorexigenic neuropeptide, in hypothalamic ARC, VMH, DMH and PVN in *Lmna*$^{+/+}$, *Lmna*$^{G609G/+}$ and *Lmna*$^{G609G/G609G}$ mice (Figure 3.2).

In the ARC (Figure 3.2A and B), we observed that POMC levels showed a tendency to increase over time in *Lmna*$^{+/+}$ mice (1.5 months: 4.50±0.40 (x10^6); 3 months: 5.04±0.41 (x10^6); 8 months: 6.20±0.64 (x10^6)) while the opposite was observed in both *Lmna*$^{G609G/+}$ (1.5 months: 5.64±0.00 (x10^6); 3 months: 5.07±0.27 (x10^6); 8 months: 4.90±0.36 (x10^6)) and *Lmna*$^{G609G/G609G}$ (1.5 months: 5.65±0.59 (x10^6); 3 months: 4.57±0.15 (x10^6)) mice. At 1.5 months, protein levels of POMC in the ARC of *Lmna*$^{G609G/+}$ and *Lmna*$^{G609G/G609G}$ mice were higher when comparing with *Lmna*$^{+/+}$ mice, although this difference is not statistically different. Interestingly, at 3 months of age, no significant differences were observed on POMC levels between the three genotypes but at 8 months, *Lmna*$^{G609G/+}$ showed a decrease, of POMC immunoreactivity comparing to age-matched *Lmna*$^{+/+}$ mice.

In the VMH (Figure 3.2A and C), POMC immunoreactivity significantly increased from 3 to 8 months, in both *Lmna*$^{+/+}$ (1.5 months: 6.33±1.00 (x10^6); 3 months: 5.98±0.80 (x10^6); 8 months: 9.33±8.64 (x10^6)) and *Lmna*$^{G609G/+}$ (1.5 months: 7.14±0.00 (x10^6); 3 months: 5.78±0.62 (x10^6); 8 months: 7.38±0.35 (x10^6)) mice. In *Lmna*$^{G609G/G609G}$ mice (1.5 months: 7.02±1.61 (x10^6); 3 months: 7.29±0.49 (x10^6)), however, POMC levels remained constant along time. At 1.5 months, there were no differences in POMC immunoreactivity between the three genotypes, however, at 3 months, *Lmna*$^{G609G/G609G}$ mice showed a tendency towards an increase in POMC levels when compared to *Lmna*$^{+/+}$ mice. At 8 months, POMC levels in *Lmna*$^{G609G/+}$ were decreased relative to age-matched *Lmna*$^{+/+}$ mice, although not statistically different.

In the DMH (Figure 3.2A and D), we observed a significant increase in POMC immunoreactivity in *Lmna*$^{+/+}$ mice with 8 months of age (1.5 months: 6.46±1.34 (x10^6); 3 months: 6.56±0.49 (x10^6); 8 months: 11.09±0.79 (x10^6)). POMC levels in the DMH of *Lmna*$^{G609G/+}$ (1.5 months: 9.81±0.00 (x10^6); 3 months: 7.75±1.07 (x10^6); 8 months: 8.00±0.34 (x10^6)) and *Lmna*$^{G609G/G609G}$ (1.5 months: 8.39±1.19 (x10^6); 3 months: 8.58±0.16 (x10^6)) mice were similar across time. At 1.5 months, we observed that POMC levels in the DMH of *Lmna*$^{G609G/G609G}$ and *Lmna*$^{G609G/+}$ mice were increased comparing to *Lmna*$^{+/+}$ mice, although not statistically significant. The same trend was observed at 3 months. At 8 months, though, *Lmna*$^{G609G/+}$ showed a marked decrease in values of POMC immunoreactivity when compared to age-matched *Lmna*$^{+/+}$ mice.

In the PVN (Figure 3.2A and E), we observed an increase along time in POMC levels of *Lmna*$^{+/+}$ mice (1.5 months: 1.00±0.06 (x10^6); 3 months: 1.19±0.08 (x10^6); 8 months: 1.85±0.16 (x10^6)), being more marked at 8 months. On the other hand, we did not detect significant alterations in POMC immunoreactivity along time in the PVN of *Lmna*$^{G609G/G609G}$ (1.5 months: 1.63±0.29 (x10^6); 3 months: 1.45±0.17 (x10^6) nor *Lmna*$^{G609G/+}$ (1.5 months: 1.06±0.00 (x10^6); 3 months: 1.20±0.07 (x10^6); 8 months:

1.09±0.14 (x10^6)) mice. We found a tendency towards increased POMC levels in the PVN of *Lmna*$^{G609G/G609G}$ mice compared to *Lmna*$^{+/+}$ mice at 1.5 months of age, as well as at 3 months. At 8 months, in contrast, *Lmna*$^{G609G/+}$ mice show decreased POMC immunoreactivity comparing to *Lmna*$^{+/+}$ mice, but it was not possible to perform statistical analysis at this timepoint given the fact that only two *Lmna*$^{G609G/+}$ animals were analyzed.

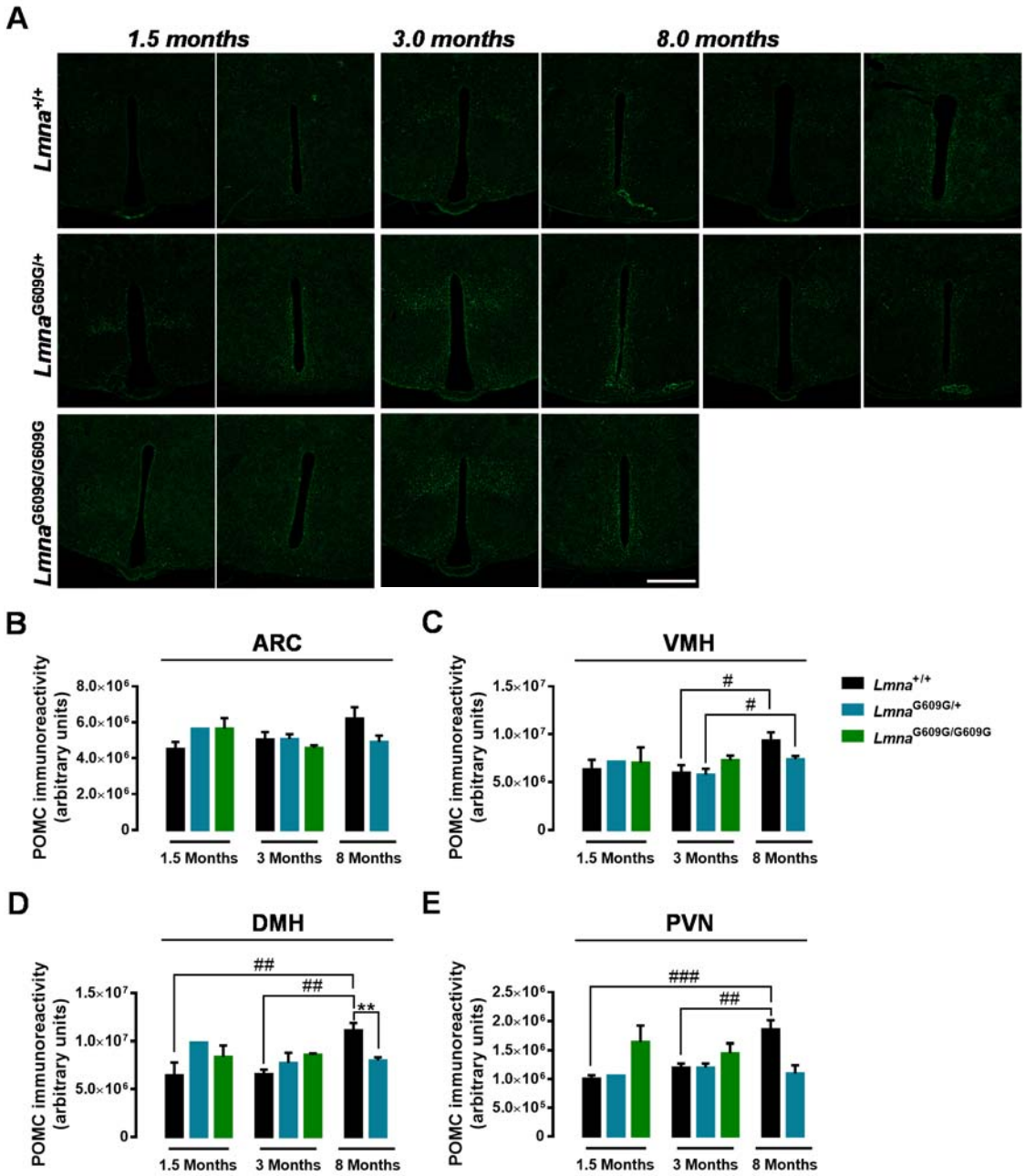

Figure 3.2. **POMC immunoreactivity in the hypothalamus of *Lmna*$^{+/+}$, *Lmna*$^{G609G/+}$ and *Lmna*$^{G609G/G609G}$ mice along time.** (A) Representative images of POMC immunoreactivity in the ARC, VMH, DMH and PVN of 1.5, 3 and 8 months-old *Lmna*$^{+/+}$ and *Lmna*$^{G609G/+}$ mice and 1.5 and 3 months-old *Lmna*$^{G609G/G609G}$ mice. (B-E) Quantification of POMC immunoreactivity in the ARC (B), VMH (C), DMH (D) and PVN (E) through the anterior-posterior length of the mouse ARC. The results represent the mean ± SEM of the total integrated density (n=3-6 mice per group for each nuclei). **p<0.01 significantly different compared to

Lmna$^{+/+}$, as determined by Student's unpaired t test. $^{\#}p<0.05$, $^{\#\#}p<0.01$, $^{\#\#\#}p<0.001$ significantly different as determined by one-way ANOVA, followed by Bonferroni's multiple comparison test.

3.1.3. Premature aging effect on the levels of NeuN in the hypothalamus of *Lmna*$^{+/G609G}$ and *Lmna*$^{G609G/G609G}$ mice

To understand whether HGPS premature aging alters *Lmna*$^{G609G/G609G}$ mice hypothalamic neuronal structure, the immunoreactivity of NeuN, a marker of mature neurons was analyzed.

In the ARC (Figure 3.3A and B), we observed a general tendency of NeuN immunoreactivity to increase along time in *Lmna*$^{+/+}$ mice (1.5 months: 5.40±1.12 (x10^6); 3 months: 7.57±0.71 (x10^6); 8 months: 7.10±0.52 (x10^6)), *Lmna*$^{G609G/G606G}$ (1.5 months: 5.61±0.83 (x10^6); 3 months: 6.35±0.82 (x10^6)) and *Lmna*$^{G609G/+}$ (1.5 months: 4.76±0.74 (x10^6); 3 months: 5.74±0.35 (x10^6); 8 months: 7.31±0.69 (x10^6)) mice. At 1.5 months, the animals from the three genotypes show similar levels of NeuN. At 3 months, however, both *Lmna*$^{G609G/G609G}$ and *Lmna*$^{G609G/+}$ mice show a slight decrease in NeuN immunoreactivity comparing to *Lmna*$^{+/+}$ mice. At 8 months, we observed similar NeuN levels in the ARC of *Lmna*$^{G609G/+}$ and *Lmna*$^{+/+}$ mice.

In the VMH (Figure 3.3A and C), NeuN levels in *Lmna*$^{+/+}$ (1.5 months: 8.68±0.87 (x10^6); 3 months: 9.51±0.45 (x10^6); 8 months: 10.09±0.53 (x10^6)) and *Lmna*$^{G609G/G609G}$ (1.5 months: 11.16±1.00 (x10^6); 3 months: 11.33±1.43 (x10^6)) mice are almost constant over time. The same was observed regarding *Lmna*$^{G609G/+}$ mice (1.5 months: 8.72±1.31 (x10^6); 3 months: 8.03±0.82 (x10^6); 8 months: 7.48±0.60 (x10^6)). At 1.5 months, NeuN immunoreactivity in the ARC of *Lmna*$^{G609G/G609G}$ mice showed a tendency for an increase in comparison to age-matched *Lmna*$^{+/+}$ mice. Moreover, the tendency was maintained also at 3 months of age. In contrast, at 3 months, *Lmna*$^{G609G/+}$ mice have decreased NeuN levels comparing to *Lmna*$^{+/+}$ mice, and this decrease is statistically significant at 8 months of age.

In the DMH (Figure 3.3A and D), we observed that NeuN immunoreactivity decreased significantly in *Lmna*$^{+/+}$ mice (1.5 months: 6.80±1.05 (x10^6); 3 months: 5.25±0.16 (x10^6); 8 months: 4.63±0.43 (x10^6)) across time. A similar trend was detected in *Lmna*$^{G609G/+}$ mice (1.5 months: 4.89±0.35 (x10^6); 3 months: 4.41±0.61 (x10^6); 8 months: 3.63±0.30 (x10^6)). On the other hand, NeuN levels did not change in *Lmna*$^{G609G/G609G}$ mice (1.5 months: 4.90±0.87 (x10^6); 3 months: 5.25±0.40 (x10^6)) along time. At 1.5 months, NeuN levels in *Lmna*$^{G609G/G609G}$ and *Lmna*$^{G609G/+}$ mice seem to be decreased comparing to *Lmna*$^{+/+}$, although this difference did not reach statistical significance. At 3 months, we found similar NeuN immunoreactivity in the three genotypes, but at 8 months, *Lmna*$^{G609G/+}$ mice show a tendency for a reduction in NeuN when compared to age-matched *Lmna*$^{+/+}$ mice.

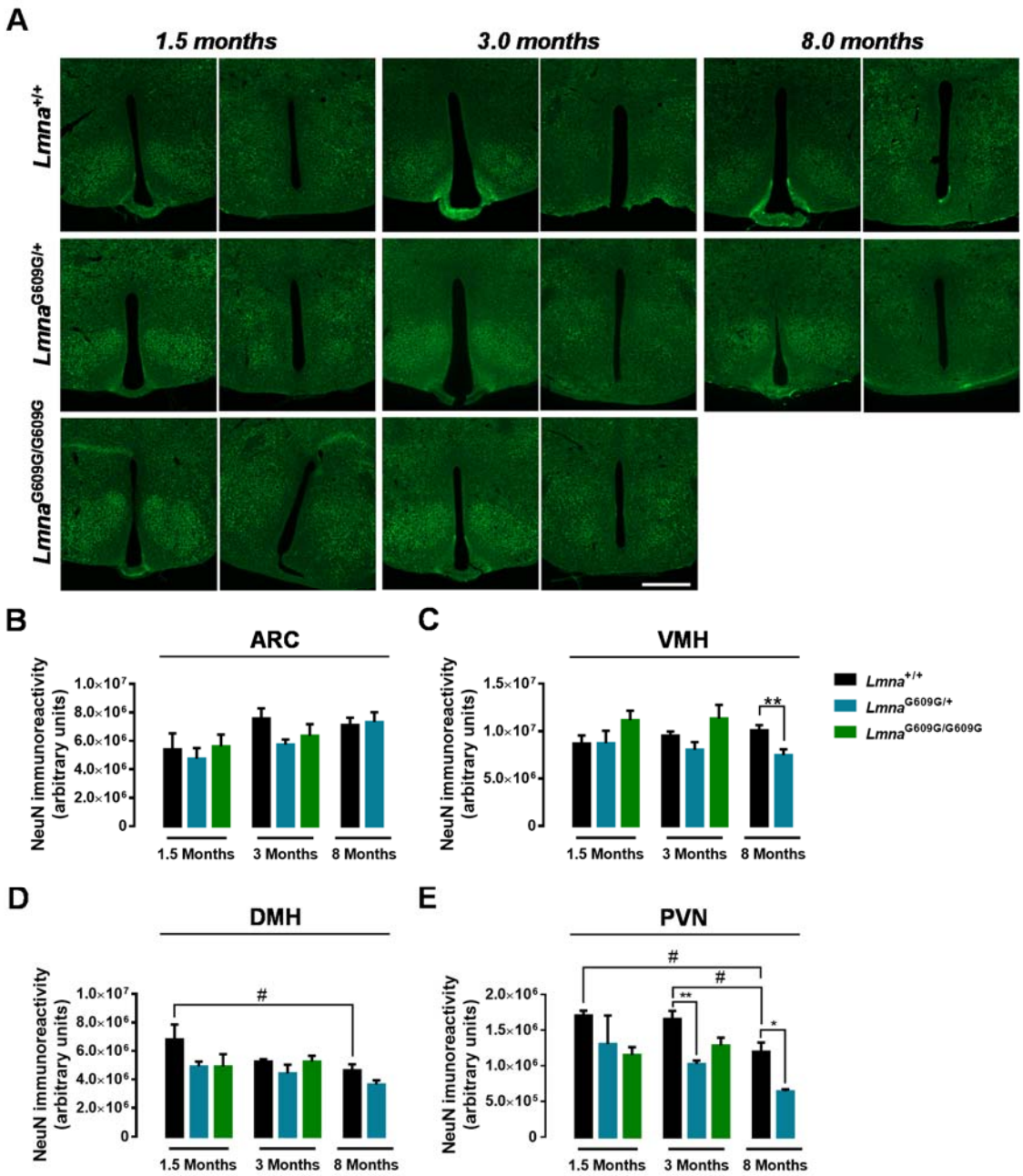

Figure 3.3. **NeuN immunoreactivity in the hypothalamus of *Lmna*$^{+/+}$, *Lmna*$^{G609G/+}$ and *Lmna*$^{G609G/G609G}$ mice along time.** (A) Representative images of NeuN immunoreactivity in the ARC, VMH, DMH and PVN of 1.5, 3 and 8 months-old *Lmna*$^{+/+}$ and *Lmna*$^{G609G/+}$ mice and 1.5 and 3 months-old *Lmna*$^{G609G/G609G}$ mice. (B-E) Quantification of NeuN immunoreactivity in the ARC (B), VMH (C), DMH (D) and PVN (E) through the anterior-posterior length of the mouse ARC. The results represent the mean ± SEM of the total integrated density (n=3-6 mice per group for each nuclei). *p<0.05, **p<0.01 significantly different compared to *Lmna*$^{+/+}$, as determined by Student's unpaired t test or by one-way ANOVA, followed by Dunnett's multiple comparison test. $^{\#}$p<0.05 significantly different as determined by one-way ANOVA, followed by Bonferroni's multiple comparison test.

In the PVN (Figure 3.3A and E) we observed that NeuN immunoreactivity in *Lmna*$^{+/+}$ (1.5 months: 1.71±0.07 (x10^{6}); 3 months: 1.66±0.12 (x10^{6}); 8 months: 1.19±0.13 (x10^{6})) and *Lmna*$^{G609G/+}$ (1.5 months: 1.30±0.40 (x10^{6}); 3 months: 1.02±0.05 (x10^{6}); 8 months: 0.64±0.03 (x10^{6})) mice decreased with time. However, in the PVN of

Lmna$^{G609G/G609G}$ mice (1.5 months: 1.15±0.11 (x10^6); 3 months: 1.28±0.11 (x10^6)), NeuN levels remained unaltered. At 1.5 months, *Lmna*$^{G609G/G609G}$ and *Lmna*$^{G609G/+}$ mice show a tendency to have reduced NeuN levels comparing to age-matched *Lmna*$^{+/+}$ mice. At 3 months, the NeuN immunoreactivity in the PVN of *Lmna*$^{G609G/G609G}$ mice is also decreased compared to *Lmna*$^{+/+}$ mice, although not statistical different. At this timepoint, NeuN levels in *Lmna*$^{G609G/+}$ mice are significantly decreased in comparison to *Lmna*$^{+/+}$ mice. At 8 months, *Lmna*$^{G609G/+}$ mice also exhibit a significant reduction in NeuN levels comparing to age-matched *Lmna*$^{+/+}$ mice.

3.1.4. Premature aging effect on hypothalamic inflammation

Inflammation in the hypothalamus has been pointed as one important process involved in the development of whole-body aging (Zhang *et al.* 2013). To investigate if *Lmna*$^{G609G/G609G}$ mice show signs of inflammation within hypothalamus, we evaluated the protein immunoreactivity of two neuroinflammatory markers: GFAP, an astrocyte marker, and Iba1, a marker of microglia, the resident macrophages of the CNS, as shown in Figures 3.4 and 3.5, respectively.

3.1.4.1. Effect of premature aging on hypothalamic GFAP immunoreactivity

In the ARC (Figure 3.4 A and B), we observed that GFAP immunoreactivity increased along time in *Lmna*$^{+/+}$ (1.5 months: 1.76±0.12 (x10^6); 3 months: 2.38±0.29 (x10^6); 8 months: 2.27±0.26 (x10^6)) and *Lmna*$^{G609G/+}$ (1.5 months: 1.47±0.004 (x10^6); 3 months: 2.96±0.20 (x10^6); 8 months: 3.66±0.43 (x10^6)) mice. On the other hand, *Lmna*$^{G609G/G609G}$ mice (1.5 months: 1.75±0.06 (x10^6); 3 months: 1.81±0.19 (x10^6)) presented similar GFAP levels along time. At 1.5 months, GFAP immunoreactivity was similar in the three genotypes. At 3 months, however, the levels of GFAP in the ARC of *Lmna*$^{G609G/G609G}$ mice appeared to be decreased, while in the *Lmna*$^{G609G/+}$ mice they were increased, compared to age-matched *Lmna*$^{+/+}$ mice, although the differences in any of the cases were statistically significant. At 8 months, *Lmna*$^{G609G/+}$ mice showed a significant increase in NeuN immunoreactivity compared to *Lmna*$^{+/+}$ mice.

In the VMH (Figure 3.4A and C), we observed that GFAP levels increased along time in *Lmna*$^{+/+}$ (1.5 months: 0.84±0.08 (x10^6); 3 months: 0.94±0.07 (x10^6); 8 months: 1.05±0.08 (x10^6)) and *Lmna*$^{G609G/+}$ (1.5 months: 0.90±0.09 (x10^6); 3 months: 1.24±0.06 (x10^6); 8 months: 1.36±0.04 (x10^6)) mice, with the differences being statistical significant in the latter. GFAP levels in *Lmna*$^{G609G/G609G}$ mice (1.5 months: 0.93±0.08 (x10^6); 3 months: 0.90±0.13 (x10^6)), however, remained stable along time. At 1.5 months, we found that GFAP levels were similar among the three genotypes. Similarly, at 3 months, *Lmna*$^{G609G/G609G}$ mice showed similar GFAP immunoreactivity to age-matched *Lmna*$^{+/+}$ mice. Also at 3 months, GFAP levels in the VMH of *Lmna*$^{G609G/+}$ mice were significantly increased compared to *Lmna*$^{+/+}$ mice, and this increase was also observed at 8 months.

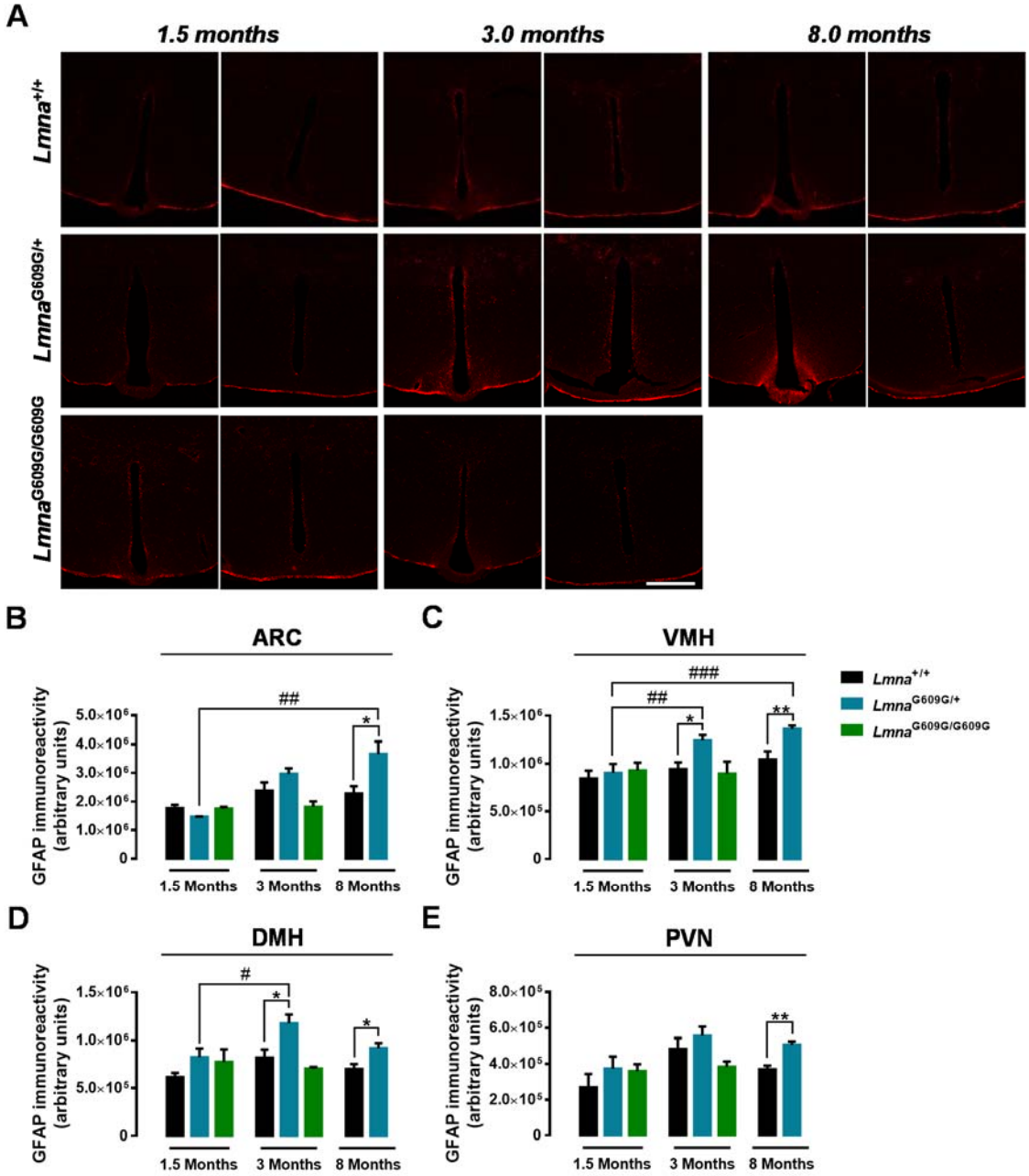

Figure 3.4. **GFAP immunoreactivity in the hypothalamus of *Lmna*$^{+/+}$, *Lmna*$^{G609G/+}$ and *Lmna*$^{G609G/G609G}$ mice along time.** (A) Representative images of GFAP immunoreactivity in the ARC, VMH, DMH and PVN of 1.5, 3 and 8 months-old *Lmna*$^{+/+}$ and *Lmna*$^{G609G/+}$ mice and 1.5 and 3 months-old *Lmna*$^{G609G/G609G}$ mice. (B-E) Quantification of GFAP immunoreactivity in the ARC (B), VMH (C), DMH (D) and PVN (E) through the anterior-posterior length of the mouse ARC. The results represent the mean ± SEM of the total integrated density. (n=2-6 mice per group for each nuclei). *p<0.05, **p<0.01 significantly different compared to *Lmna*$^{+/+}$, as determined by Student's unpaired *t* test or by one-way ANOVA, followed by *Dunnett's* multiple comparison test. $^{\#}$p<0.05, $^{\#\#}$<0.01, $^{\#\#\#}$<0.001 significantly different as determined by one-way ANOVA, followed by Bonferroni's multiple comparison test.

In the DMH (Figure 3.4A and D), we observed that GFAP immunoreactivity in *Lmna*$^{+/+}$ mice (1.5 months: 0.62±0.04 (x10^{6}); 3 months: 0.82±0.09 (x10^{6}); 8 months: 0.70±0.05 (x10^{6})) slightly increased at 3 months of age, but at 8 months GFAP levels returned to levels similar to those found at 1.5 months. In the DMH of *Lmna*$^{G609G/G609G}$

mice (1.5 months: 0.77±0.13 (x10^6); 3 months: 0.70±0.02 (x10^6)) GFAP levels did not change with age. GFAP immunoreactivity in *Lmna*$^{G609G/+}$ mice (1.5 months: 0.82±0.09 (x10^6); 3 months: 1.18±0.09 (x10^6); 8 months: 0.92±0.05 (x10^6)) significantly increased with time, although it slightly declined from 3 to 8 months. At 1.5 months, *Lmna*$^{G609G/G609G}$, as well as *Lmna*$^{G609G/+}$, mice showed a tendency towards an increase in GFAP levels comparing to age-matched *Lmna*$^{+/+}$ mice. However, at 3 months, GFAP immunoreactivity in the DMH of *Lmna*$^{G609G/G609G}$ mice was decreased relatively, to *Lmna*$^{+/+}$ mice, but the difference was not significant. In contrast, at this timepoint, *Lmna*$^{G609G/+}$ mice exhibited a significant increase in the levels of GFAP when compared to *Lmna*$^{+/+}$ of the same age, and this was increase was maintained at 8 months.

Regarding PVN (Figure 3.4A and E), we observed a tendency for an increase in GFAP levels of *Lmna*$^{+/+}$ mice (1.5 months: 0.27±0.07 (x10^6); 3 months: 0.48±0.06 (x10^6); 8 months: 0.37±0.02 (x10^6)) at 3 months, with a subsequent subtle decrease at 8 months. *Lmna*$^{G609G/G609G}$ mice (1.5 months: 0.36±0.04 (x10^6); 3 months: 0.38±0.03 (x10^6)) showed similar levels of GFAP along time. On the other hand, GFAP immunoreactivity in the PVN of *Lmna*$^{G609G/+}$ mice (1.5 months: 0.37±0.07 (x10^6); 3 months: 0.56±0.05 (x10^6); 8 months: 0.51±0.02 (x10^6)) increased along time, although it was not statistically significant. At 1.5 months, *Lmna*$^{G609G/G609G}$ and *Lmna*$^{G609G/+}$ mice showed a tendency to have increased levels of GFAP compared to age-matched *Lmna*$^{+/+}$ mice. However, at 3 months, GFAP levels in the PVN of *Lmna*$^{G609G/G609G}$ were shown to be decreased, with no statistical significance, relative to *Lmna*$^{+/+}$ mice, while in *Lmna*$^{G609G/+}$ mice we observed an increase, but due to the low number of *Lmna*$^{G609G/+}$ mice analyzed at this timepoint, we could not perform statistical analysis. At 8 months, we observed that GFAP immunoreactivity was significantly increased in *Lmna*$^{G609G/+}$ mice comparing to age-matched *Lmna*$^{+/+}$ mice.

3.1.4.2. Effect of premature aging on hypothalamic Iba-1 immunoreactivity

Within the ARC (Figure 3.5A and B), we observed a tendency for the Iba-1 immunoreactivity in *Lmna*$^{+/+}$ (1.5 months: 3.26±0.23 (x10^6); 3 months: 3.68±0.13 (x10^6); 8 months: 4.15±0.27 (x10^6)) and *Lmna*$^{G609G/+}$ (1.5 months: 3.33±0.13 (x10^6); 3 months: 4.03±0.23 (x10^6); 8 months: 3.94±0.28 (x10^6)) mice to increase along time. Conversely, in the ARC of *Lmna*$^{G609G/G609G}$ mice (1.5 months: 3.94±0.24 (x10^6); 3 months: 3.03±0.32 (x10^6)) we found a decrease in Iba-1 levels with time, although not statistically significant. At 1.5 months, we found that Iba-1 levels in *Lmna*$^{G609G/G609G}$ mice are increased, but not significantly, when compared to age-matched *Lmna*$^{+/+}$ mice. Interestingly, this tendency was inverted at 3 months, where *Lmna*$^{G609G/G609G}$ mice present decreased levels of Iba-1 comparing to *Lmna*$^{+/+}$ mice. Also at 3 months, we observed that Iba-1 immunoreactivity had a tendency for an increase in *Lmna*$^{G609G/+}$ compared to age-matched *Lmna*$^{+/+}$ mice. However, this difference was blunted at 8 months.

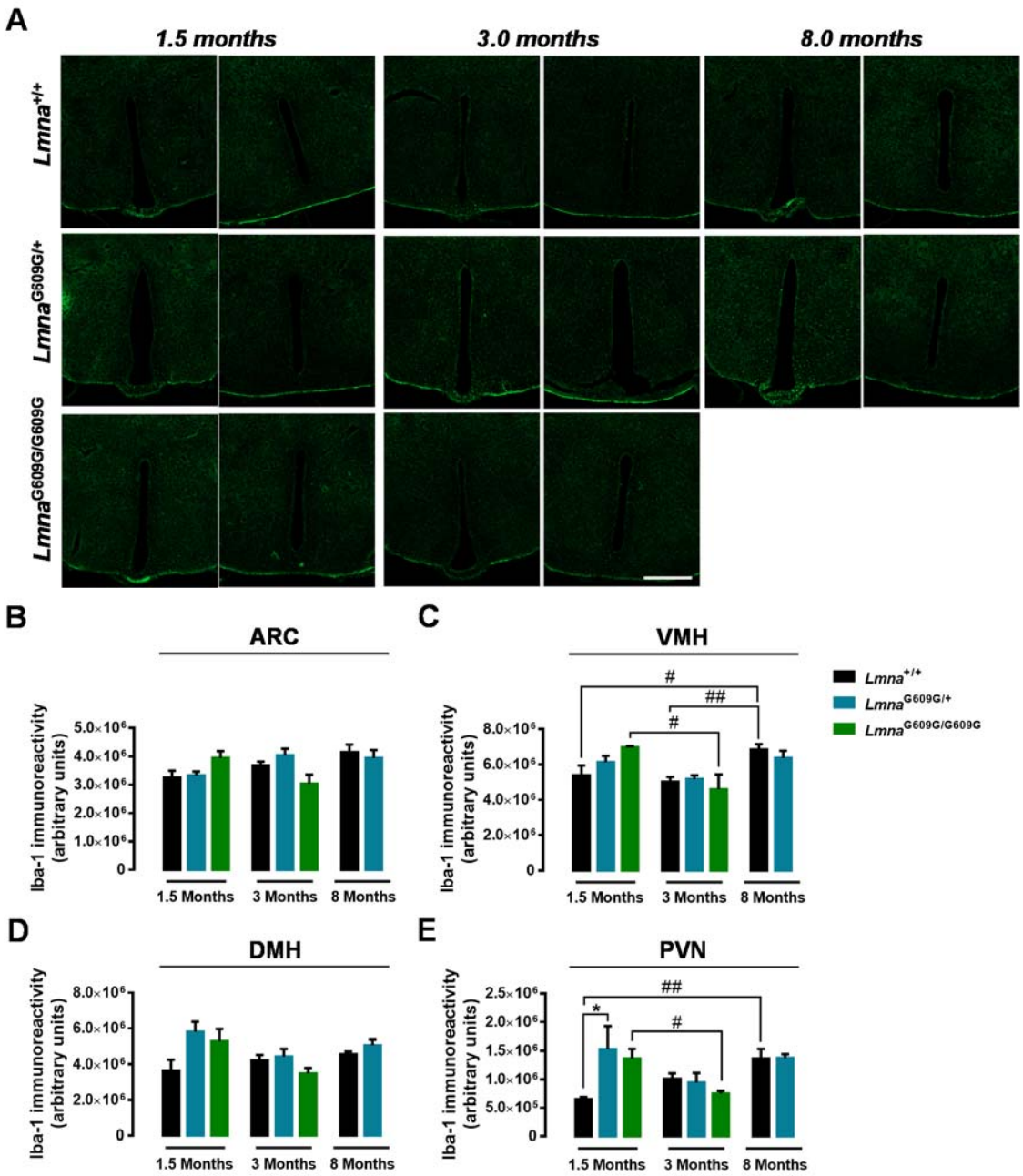

Figure 3.5. **Iba-1 immunoreactivity in the hypothalamus of *Lmna*$^{+/+}$, *Lmna*$^{G609G/+}$ and *Lmna*$^{G609G/G609G}$ mice along time.** (A) Representative images of Iba-1 immunoreactivity in the ARC, VMH, DMH and PVN of 1.5, 3 and 8 months-old *Lmna*$^{+/+}$ and *Lmna*$^{G609G/+}$ mice and 1.5 and 3 months-old *Lmna*$^{G609G/G609G}$ mice. (B-E) Quantification of Iba-1 immunoreactivity in the ARC (B), VMH (C), DMH (D) and PVN (E) through the anterior-posterior length of the mouse ARC. The results represent the mean ± SEM of the total integrated density (n=2-6 mice per group). *p<0.05 significantly different compared to *Lmna*$^{+/+}$, as determined by one-way ANOVA, followed by *Dunnett's* multiple comparison test. $^{\#}$p<0.05, $^{\#\#}$<0.01 significantly different as determined by one-way ANOVA, followed by Bonferroni's multiple comparison test or Student's unpaired *t* test.

In the VMH (Figure 3.5A and C), *Lmna*$^{+/+}$ mice showed a statistically significant increase in Iba-1 levels at 8 months, compared to earlier timepoints (1.5 months: 5.39±0.55 (x10^6); 3 months: 5.03±0.27 (x10^6); 8 months: 6.84±0.31 (x10^6)). In contrast, *Lmna*$^{G609G/G609G}$ mice (1.5 months: 6.97±0.05 (x10^6); 3 months: 4.60±0.84 (x10^6))

exhibited a significant decrease of Iba-1 immunoreactivity with time. In the VMH of *Lmna*$^{G609G/+}$ mice (1.5 months: 6.13±0.36 (x10^6); 3 months: 5.17±0.21 (x10^6); 8 months: 6.37±0.41 (x10^6)), however, Iba-1 levels decreased from 1.5 to 3 months, but were recovered at 8 months. At 1.5 months, both *Lmna*$^{G609G/G609G}$ and *Lmna*$^{G609G/+}$ mice have a tendency to show higher Iba-1 levels compared to age-matched *Lmna*$^{+/+}$ mice. However, at 3 months, Iba-1 immunoreactivity was similar in the three genotypes. At 8 months, we also did not detect differences in Iba-1 levels between *Lmna*$^{G609G/+}$ and *Lmna*$^{+/+}$ mice.

In the DMH (Figure 3.5A and D), we observed that Iba-1 immunoreactivity had a tendency towards an increase in *Lmna*$^{+/+}$ mice (1.5 months: 3.65±0.62 (x10^6); 3 months: 4.22±0.31 (x10^6); 8 months: 4.58±0.14 (x10^6)) along time. However, *Lmna*$^{G609G/G609G}$ mice (1.5 months: 5.30±0.67 (x10^6); 3 months: 3.49±0.31 (x10^6)) Iba-1 levels seem to decrease, although not significantly, with age. Iba-1 levels in the DMH of *Lmna*$^{G609G/+}$ mice (1.5 months: 5.80±0.58 (x10^6); 3 months: 4.44±0.58 (x10^6); 8 months: 5.08±0.31 (x10^6)) also showed a tendency to decrease with time, but this was attenuated at 8 months. At 1.5 months, we found that both *Lmna*$^{G609G/G609G}$ and *Lmna*$^{G609G/+}$ mice have a non-significant increase in Iba-1 levels comparing to age-matched *Lmna*$^{+/+}$ mice. At 3 months, however, *Lmna*$^{G609G/G609G}$ mice showed reduced Iba-1 levels compared to age-matched *Lmna*$^{+/+}$ mice, although the difference was not statistically different. At 8 months, *Lmna*$^{G609G/+}$ present similar levels of Iba-1 to *Lmna*$^{+/+}$ mice.

In the PVN (Figure 3.5A and E), we found that Iba-1 levels in *Lmna*$^{+/+}$ mice (1.5 months: 0.65±0.04 (x10^6); 3 months: 1.01±0.10 (x10^6); 8 months: 1.67±0.17 (x10^6)) were increased along time. In opposition, in the PVN of *Lmna*$^{G609G/G609G}$ mice (1.5 months: 1.37±0.17 (x10^6); 3 months: 0.75±0.05 (x10^6)), we observed a significant decline in Iba-1 immunoreactivity with time. Iba-1 levels in *Lmna*$^{G609G/+}$ mice (1.5 months: 1.53±0.40 (x10^6); 3 months: 0.94±0.17 (x10^6); 8 months: 1.38±0.07 (x10^6)) also showed a tendency for decreasing from 1.5 to 3 months, but at 8 months we detected a moderate recovery in these values. At 1.5 months, we observed an increase in Iba-1 levels in *Lmna*$^{G609G/G609G}$ mice comparing to *Lmna*$^{+/+}$ mice, but this difference was not statistical different. Moreover, *Lmna*$^{G609G/+}$ mice display a significant increase in Iba-1 levels relative to *Lmna*$^{+/+}$ mice, at 1.5 months. At 3 months, we observed a tendency towards a decrease in Iba-1 immunoreactivity in *Lmna*$^{G609G/G609G}$ mice relatively to age-matched *Lmna*$^{+/+}$ mice, and *Lmna*$^{G609G/+}$ presented similar levels to the latter. At 8 months, we did not detect differences between *Lmna*$^{G609G/+}$ and *Lmna*$^{+/+}$ mice in the levels of Iba-1.

3.1.5. Premature aging alters the temporal pattern of gene expression in the hypothalamus of *Lmna*$^{G609G/G609G}$ mice

In addition to immunohistochemistry studies, we also assessed whether premature aging alters hypothalamic gene expression in *Lmna*$^{G609G/G609G}$ mice. Whole

hypothalami were collected from *Lmna*$^{+/+}$ and *Lmna*$^{G609G/G609G}$ mice at 1.5 and 3 months of age for RNA extraction. Gene expression analysis was assessed by qPCR. Hypothalamic function is dependent on the expression of both orexigenic and anorexigenic neuropeptides such as NPY and AgRP, and POMC and CART, respectively. Therefore, we evaluated whether the expression of these hypothalamic neuropeptides were altered in *Lmna*$^{G609G/G609G}$ mice.

As shown in Figure 3.6A, a decrease in NPY mRNA levels was observed in *Lmna*$^{+/+}$ mice at 3 months of age (0.48±0.05) comparing with *Lmna*$^{+/+}$ with 1.5 months of age (0.88±0.10). On the other hand, *Lmna*$^{G609G/G609G}$ mice showed an increase in NPY gene expression at 3 months of age (1.43±0.14) compared with 1.5 months littermates (0.74±0.03). Although at 1.5 months of age the expression of NPY was similar in *Lmna*$^{+/+}$ and *Lmna*$^{G609G/G609G}$ mice, a significant decrease in NPY mRNA levels was observed *Lmna*$^{G609G/G609G}$ mice at 3 months of age. Similar alterations were observed in AgRP gene expression in both *Lmna*$^{+/+}$ and *Lmna*$^{G609G/G609G}$ with time (Figure 3.6A).

With increasing age, *Lmna*$^{+/+}$ mice showed an increase in POMC mRNA levels (1.5 months: 0.05±0.01; 3 months: 0.09±0.01) while the opposite was observed in *Lmna*$^{G609G/G609G}$ mice (1.5 months: 0.05±0.01; 3 months: 0.02±0.01), as shown in Figure 3.6A. Nevertheless, these differences did not reach statistical difference. POMC expression was similar between both genotypes at 1.5 months of age. However, *Lmna*$^{G609G/G609G}$ showed a significant reduction in POMC mRNA levels at 3 months when comparing with age-matched *Lmna*$^{+/+}$ mice (Figure 3.6A). Regarding CART, no significant alterations were observed along time for both genotypes or between genotypes in each time-point analyzed (Figure 3.6A).

We also analyzed whether NPY receptors, namely Y_1R, Y_2R and Y_5R, gene expression was altered in the hypothalamus of *Lmna*$^{G609G/G609G}$ mice. NPY Y_1R, Y_2R and Y_5R mRNA levels were similar between *Lmna*$^{+/+}$ and *Lmna*$^{G609G/G609G}$ mice and did not change with time (Figure 3.6B). Despite the lack of significant differences, 3-months old *Lmna*$^{G609G/G609G}$ mice showed a decrease in NPY Y_1R and Y_5R mRNA levels when compared to 1.5 months-old *Lmna*$^{G609G/G609G}$ littermates. In addition, we tried also to evaluate GHS-R gene expression in the hypothalamus of *Lmna*$^{+/+}$ and *Lmna*$^{G609G/G609G}$ mice, but at the time we were not successful. However, the expression of ghrelin receptors as well as insulin and leptin receptors is is something we would like to investigate in the near future.

The gene expression of several proteins involved in the inflammatory process such as GFAP, an astrocyte marker, CD11b, a marker of macrophage and microglia, IL-1β, a pro-inflammatory cytokine, and IL-10, an anti-inflammatory cytokine, was also analyzed, as shown in Figure 3.6C.

Both *Lmna*$^{+/+}$ (0.010±0.001) and *Lmna*$^{G609G/G609G}$ (0.011±0.001) mice showed a significant reduction in GFAP mRNA levels at 3 months of age comparing with 1.5 months old matched genotype littermates (*Lmna*$^{+/+}$: 0.025±0.002; *Lmna*$^{G609G/G609G}$:

0.023±0.003) (Figure 3.6C). However, GFAP expression was similar between genotypes at 1.5 or 3 months of age (Figure 3.6C).

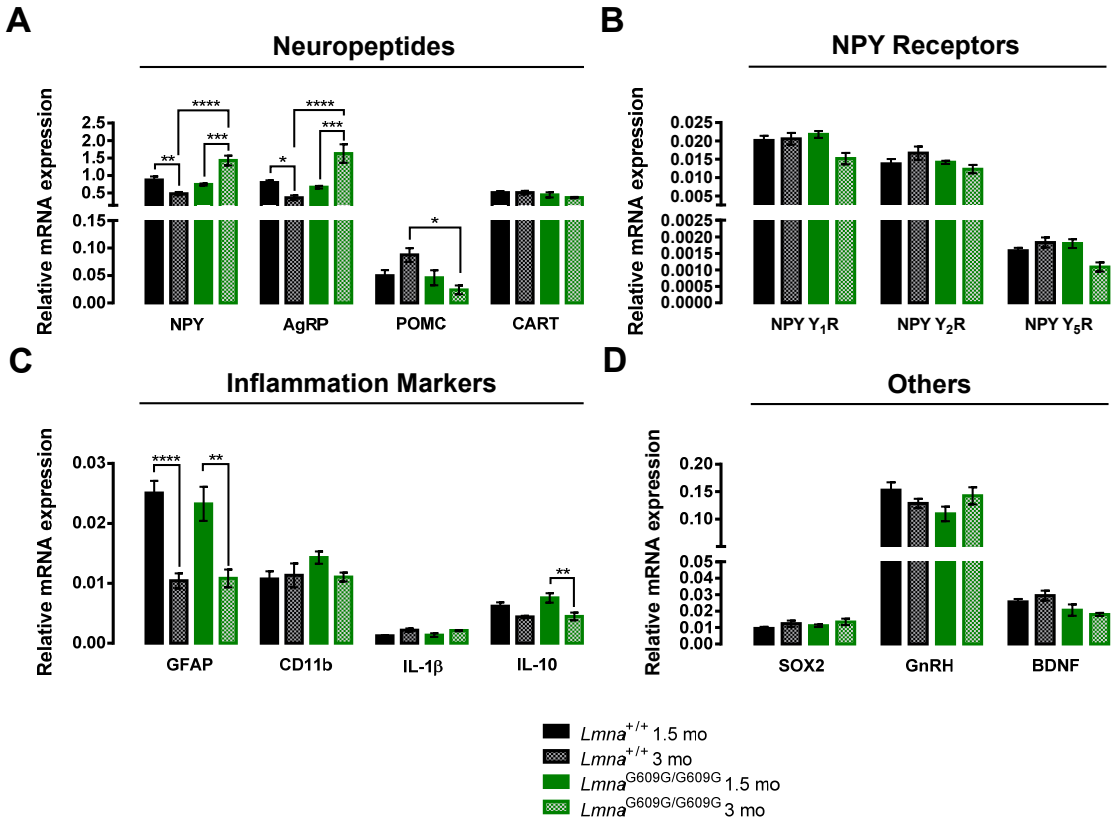

Figure 3.6. **Comparative analysis of hypothalamic gene expression of 1.5 and 3 months-old *Lmna*$^{+/+}$ and *Lmna*$^{G609G/G609G}$ mice.** Gene expression analysis of (A) orexigenic, NPY and AgRP, and anorexigenic, POMC and CART, neuropeptides; (B) NPY Y_1R, Y_2R and Y_5R, receptors; (C) inflammatory markers GFAP, CD11b, IL-1β and IL-10; (D) SOX2, GnRH and BDNF in the hypothalamus of 1.5, 3 and 8 months-old *Lmna*$^{+/+}$ and *Lmna*$^{G609G/+}$ mice and 1.5 and 3 months-old *Lmna*$^{G609G/G609G}$ mice. The results represent the mean ± SEM of the relative expression normalized to Hprt gene. (n=4-11 mice per group). *p<0.05, **p<0.01, ***p<0.001, ****p<0.0001 significantly different as determined by one-way ANOVA, followed by Bonferroni's multiple comparisons test.

As shown in Figure 3.6C, no significant alterations were observed in CD11b expression with time or between *Lmna*$^{+/+}$ and *Lmna*$^{G609G/G609G}$ mice. Interestingly, CD11b mRNA levels were higher in 1.5 month-old *Lmna*$^{G609G/G609G}$ mice when comparing with age-matched *Lmna*$^{+/+}$ mice, but this difference was not observed at 3 months of age.

Similar to CD11b, we did not observe significant alterations in IL-1β gene expression between genotypes or with time (Figure 3.6C). However, a tendency towards an increase in IL-1β mRNA levels was observed in both *Lmna*$^{+/+}$ and *Lmna*$^{G609G/G609G}$ mice at 3 months of age comparing with age-matched genotype littermates (Figure 3.6C).

IL-10 mRNA levels were similar between *Lmna*$^{+/+}$ and *Lmna*$^{G609G/G609G}$ mice at 1.5 and 3 months of age (Figure 3.6C). However, with time, IL-10 expression decreases in both *Lmna*$^{+/+}$ and *Lmna*$^{G609G/G609G}$ mice (figure 3.6C).

We also analyzed whether premature aging altered SOX2, a transcription factor involved in the regulation of pluripotency, critical for directing the differentiation of pluripotent stem cells to neural progenitors and for maintaining the properties of neural progenitor stem cells, GnRH, a hypothalamic trophic peptide hormone that regulates the hypothalamic–pituitary–gonadal axis, and BDNF, a neurotrophic factor.

SOX2 expression was similar between *Lmna*$^{+/+}$ and *Lmna*$^{G609G/G609G}$ mice and did not change with time in both genotypes (Figure 3.6D). Although no significant alterations were observed in GnRH expression (Figure 3.6D), with time, we observed a tendency towards a decrease in GnRH mRNA levels in *Lmna*$^{+/+}$ mice while the opposite was observed in *Lmna*$^{G609G/G609G}$ mice. In addition, *Lmna*$^{G609G/G609G}$ mice showed lower levels of GnRH mRNA that *Lmna*$^{+/+}$ at 1.5 months of age but this difference was not observed at 3 months of age (Figure 3.6D). BDNF expression was also similar between genotypes and did not change with time. Although not significant, we did notice that *Lmna*$^{G609G/G609G}$ mice showed lower levels of BDNF mRNA than *Lmna*$^{+/+}$ mice (Figure 3.6D).

3.2. Effect of daily peripheral administration of ghrelin in *Lmna*$^{G609G/G609G}$ mice premature aging phenotype

Lmna$^{G609G/G609G}$ mice carry the c.1827C>T;p.Gly609Gly mutation which is equivalent to the HGPS c.1824C>T;p.Gly608Gly mutation within exon 11 in the human LMNA gene and recapitulate most of the described alterations associated with HGPS phenotype including progerin accumulation, reduced growth rate and body weight, lipodystrophy, bone and cardiovascular abnormalities, dysregulation of glucose and lipid metabolism, and shortened lifespan, as described previously by Osorio and colleagues (Osorio *et al.* 2011). The features presented by this animal model make it valuable for the study of HGPS as well as for the preclinical evaluation of approaches aimed at preventing the pathological features of this condition.

To investigate the effect of daily peripheral administration of ghrelin on the premature aging phenotype of *Lmna*$^{G609G/G609G}$ mice, *Lmna*$^{+/+}$, *Lmna*$^{+/G609G}$ and *Lmna*$^{G609G/G609G}$ mice, at the age of 1.5 months were distributed into two groups: vehicle-treated and ghrelin-treated mice, as follows: vehicle-treated *Lmna*$^{+/+}$ mice (n=5; 3 females and 2 males), ghrelin-treated *Lmna*$^{+/+}$ mice (n=5; 3 males and 2 females), vehicle-treated *Lmna*$^{+/G609G}$ mice (n=5; 3 females and 2 males), ghrelin-treated *Lmna*$^{+/G609G}$ mice (n=4; all males), vehicle-treated *Lmna*$^{G609G/G609G}$ mice (n=5; 3 females and 2 males) and ghrelin-treated and *Lmna*$^{G609G/G609G}$ mice (n=4; 2 females and 2 males).

Ghrelin (50 µg/kg) or saline was administered for 1.5 months (daily; subcutaneous injection). During the time of treatment, mice body weight was

evaluated twice a week. In the end of the trial, after mice behavior and blood glucose levels evaluation, mice were sacrificed and several organs and tissues were collected for histological and molecular analysis of age-related alterations and cellular hallmarks of aging.

3.2.1. Ghrelin administration increased body weight gain in *Lmna*$^{+/+}$ and *Lmna*$^{G609G/G609G}$ mice

At birth, *Lmna*$^{G609G/G609G}$ mice are morphologically similar to wild-type and heterozygous littermates and seemed healthy until the third week of age. Then they started to show a reduction in growth rate (Figure 3.7A) and body weight gain (Figure 3.7B, C and D).

At 1.5 months of age, *Lmna*$^{G609G/G609G}$ mice have a lower body weight (16.99±0.63 g) than wild-type *Lmna*$^{+/+}$ (20.96±0.79 g) and *Lmna*$^{G609G/+}$ (20.57±1.41 g) mice. Until 3 months of age, *Lmna*$^{G609G/G609G}$ show a progressive reduction in body weight gain (Figure 3.7D) while their wild-type and heterozygous littermates showed a sustained increase in body weight gain (Figure 3.7B and C, respectively). Consequently, at 3 months of age we observed a significant decrease in body weight of *Lmna*$^{G609G/G609G}$ mice (14.83±0.31 g; ~12 % of body weight reduction) when compared with *Lmna*$^{+/+}$ (22.24±1.03 g; ~15 % body weight increase) and *Lmna*$^{G609G/+}$ (22.87±1.99 g; ~15% of body weight increase) as shown in Figure 3.7E.

After 1.5 months of ghrelin treatment, *Lmna*$^{+/+}$ mice showed a significant body weight gain (~30 %; 26.19±1.09 g) compared to the saline-treated mice (Figure 3.7B and E). However, ghrelin had no effect on body weight gain in *Lmna*$^{G609G/+}$ mice (Figure 3.7C and E). Interestingly, ghrelin induced an increase, although modest, in body weight gain in *Lmna*$^{G609G/G609G}$ mice (~10 %; Figure 3.7D) and prevented the loss of weight observed in saline-treated *Lmna*$^{G609G/G609G}$ mice (17.50±0.64 g; Figure 3.7E).

The alterations in body weight between genotypes and upon ghrelin treatment could be due to alterations in food intake. In fact, we observed that *Lmna*$^{G609G/G609G}$ (2.65±0.10 g) mice eat less than their wild-type (3.13±0.10 g) or heterozygous (3.28±0.27 g) littermates, although this difference was not statistical different (Figure 3.7F). Ghrelin-treated *Lmna*$^{+/+}$ mice (3.72±0.06 g) showed a significant increase in food intake comparing with vehicle-treated *Lmna*$^{+/+}$ mice (3.13±0.10 g) (Figure 3.7F). Upon ghrelin treatment, *Lmna*$^{G609G/+}$ mice and *Lmna*$^{G609G/G609G}$ mice also showed higher food consumption, however this effect was not statistical different from vehicle-treated matched genotype mice (Figure 3.7F).

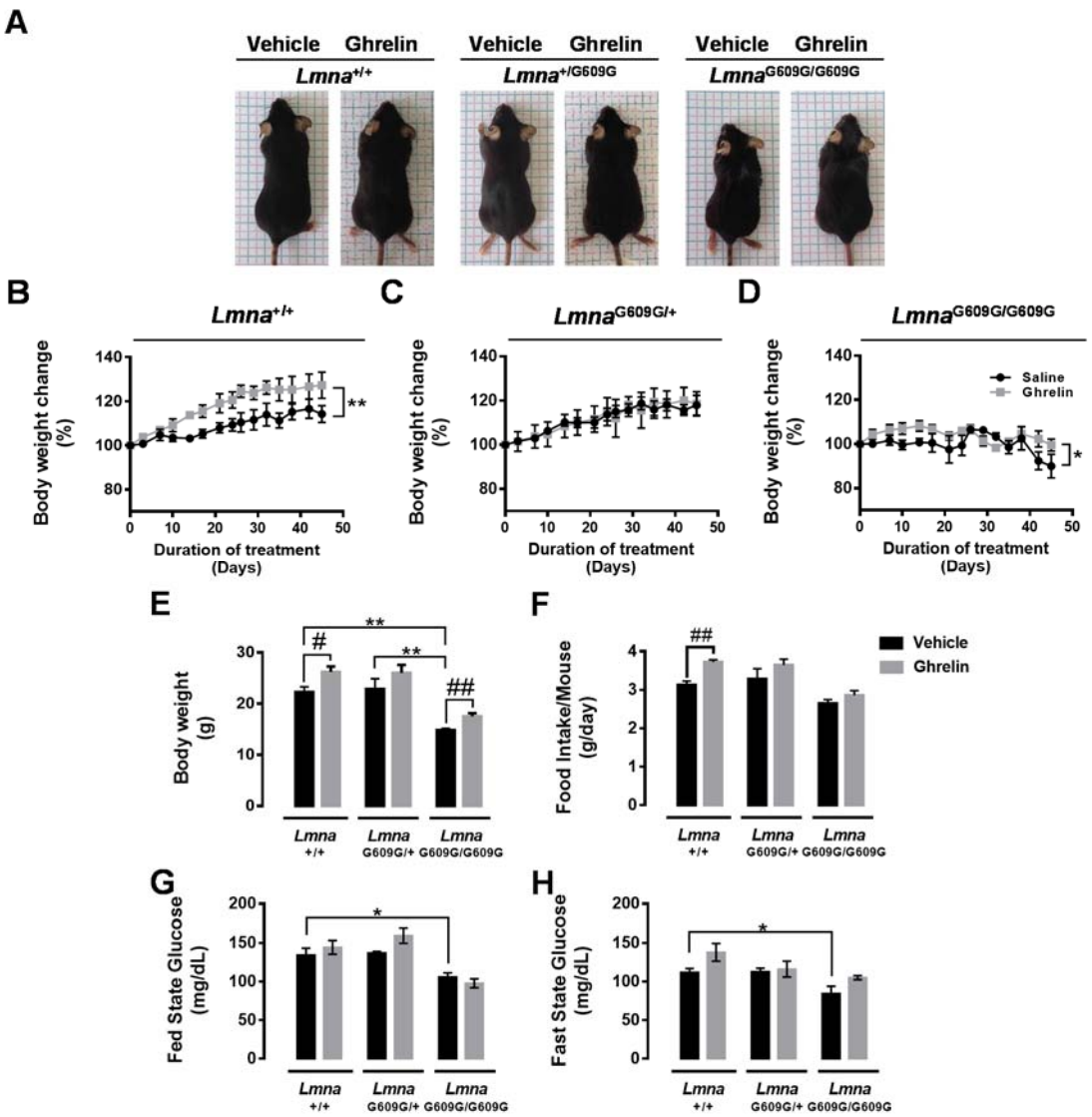

Figure 3.7. **Phenotypic characterization of vehicle- and ghrelin-treated *Lmna*$^{+/+}$, *Lmna*$^{G609G/+}$ and *Lmna*$^{G609G/G609G}$ mice.** (A) Representative photographs of 3 months-old vehicle- or ghrelin-treated *Lmna*$^{+/+}$, *Lmna*$^{G609G/+}$ and *Lmna*$^{G609G/G609G}$ mice. (B-D) Cumulative body weight gain of vehicle- and ghrelin-treated *Lmna*$^{+/+}$ (B), *Lmna*$^{G609G/+}$ (C) and *Lmna*$^{G609G/G609G}$ (D) mice, as the percentage of weight gain between the beginning and the end of the study. (E) Body weight (g) of vehicle- and ghrelin-treated *Lmna*$^{+/+}$, *Lmna*$^{G609G/+}$ and *Lmna*$^{G609G/G609G}$ mice at 3 months of age. (F) Daily food intake (g) of vehicle- and ghrelin-treated *Lmna*$^{+/+}$, *Lmna*$^{G609G/+}$ and *Lmna*$^{G609G/G609G}$ mice, expressed as g/day (G-H) Serum glucose concentrations (mg/dL) of 3 months-old vehicle- and ghrelin-treated *Lmna*$^{+/+}$, *Lmna*$^{G609G/+}$ and *Lmna*$^{G609G/G609G}$ mice, under fed (G) and fast (H) states. The results represent the mean ± SEM (n=4-5 per group). *p<0.05, **p<0.01 significantly different compared to vehicle-treated control or *Lmna*$^{+/+}$, as determined by unpaired Student's *t* test or by one-way ANOVA, followed by Dunnett's multiple comparison test, respectively. $^{\#}$p<0.05, $^{\#\#}$p<0.01 significantly different compared to matched genotype vehicle-treated control, as determined by unpaired Student's *t* test.

As described, we also observed that *Lmna*$^{G609G/G609G}$ mice (vehicle-treated *Lmna*$^{G609G/G609G}$: 84.50±9.44 mg/dL) showed lower blood glucose levels under fasting conditions than *Lmna*$^{+/+}$ (vehicle-treated *Lmna*$^{+/+}$: 112.10±4.76 mg/dL) and *Lmna*$^{G606G/+}$ (vehicle-treated *Lmna*$^{G609G/+}$: 112.60±4.61 mg/dL) mice, as shown in Figure 3.7G).

Ghrelin administration increased blood glucose levels in *Lmna*$^{+/+}$ (ghrelin-treated *Lmna*$^{+/+}$: 137.9±11.45 mg/dL; Figure 3.7G). Ghrelin-treated *Lmna*$^{G609G/G609G}$ mice showed a slight improvement in serum glucose levels in fasting conditions (105.00±2.65 mg/dL) however, this effect was not statistical different from vehicle-treated *Lmna*$^{G609G/G609G}$ mice (Figure 3.7G). Ghrelin had no effect on blood glucose levels in heterozygous mice. We also analyzed potential changes in blood glucose levels in mice under fed conditions (Figure 3.7). As in fasting conditions, *Lmna*$^{G609G/G609G}$ (vehicle-treated *Lmna*$^{G609G/G609G}$: 105.80±5.53 mg/dL) showed lower blood glucose levels than *Lmna*$^{+/+}$ (vehicle-treated *Lmna*$^{+/+}$: 134.38±8.91 md/dL) and *Lmna*$^{G609G/+}$ (vehicle-treated *Lmna*$^{G609G/+}$: 137.00±2.27 mg/dL) under fed conditions (Figure 3.7H). Upon ghrelin treatment, a tendency towards an increase in blood glucose levels in fed conditions was observed in both *Lmna*$^{+/+}$ (ghrelin-treated *Lmna*$^{+/+}$: 144.20±8.95 mg/dL) and *Lmna*$^{G609G/+}$ (ghrelin-treated *Lmna*$^{G609G/+}$: 159.50±9.85 mg/dL) mice but not in *Lmna*$^{G609G/G609G}$ mice (ghrelin-treated *Lmna*$^{G609G/G609G}$: 97.75±5.69 mg/dL) (Figure 3.7H).

At 3 months of age *Lmna*$^{G609G/G609G}$ mice display a marked curvature of the spine and an abnormal posture, and this was not observed in ghrelin-treated mice (Figure 3.7A).

These results suggest that ghrelin has beneficial effects on *Lmna*$^{G609G/G609G}$ mice, namely in overall appearance, body weight gain and blood glucose levels.

3.2.2. Ghrelin administration increased WAT weight in *Lmna*$^{G609G/G609G}$ mice

As shown in Figure 3.8, the weight of the heart (Figure 3.8A), liver (Figure 3.8B), kidney (Figure 3.8C), BAT (Figure 3.8D) and thymus (Figure 3.8F) of vehicle-treated *Lmna*$^{G609G/G609G}$ mice was similar to vehicle-treated *Lmna*$^{+/+}$ and *Lmna*$^{G609G/+}$ mice, when normalized for their percentage of body weight. The main difference observed was in the weight of perigonadal WAT, which was significantly decreased in vehicle-treated *Lmna*$^{G609G/G609G}$ mice (0.18±0.11 % total body weight), when compared to vehicle-treated *Lmna*$^{+/+}$ (1.22±0.16 % total body weight) and *Lmna*$^{G609G/+}$ (1.00±0.09 % total body weight) mice (Figure 3.8E). Although not significant, the weight of WAT was lower in heterozygous mice than wild-type mice. We also observed a significant decrease in the spleen weight in *Lmna*$^{G609G/G609G}$ mice (0.26±0.035 % total body weight) when compared with vehicle-treated wild-type mice (0.37±0.018 % total body weight) (Figure 3.8G). *Lmna*$^{G609G/+}$ mice (0.34±0.021 % total body weight) also showed a lower spleen weight however not significantly different from wild-type mice (Figure 3.8G). Ghrelin administration had no effect on the weight of heart, liver, kidney and BAT in any of the three genotypes (Figure 3.8A, B, C and D). However, ghrelin increased the weight of WAT in both *Lmna*$^{G609G/+}$ (1.288±0.05 % total body weight) and *Lmna*$^{G609G/G609G}$ (0.70±0.06 % total body weight) mice, but not in *Lmna*$^{+/+}$ mice (1.23±0.10 % total body weight) (Figure 3.8E). This result suggests that ghrelin administration could thwart the lipodystrophy observed in *Lmna*$^{G609G/G609G}$ mice.

Unexpectedly, ghrelin treatment decreased, although not significantly, the weight of thymus and spleen of *Lmna*$^{+/+}$ and *Lmna*$^{G609G/+}$ mice compared to the vehicle-treated matched genotype mice group (Figure 3.8F and G). However, this tendency was not observed in ghrelin-treated *Lmna*$^{G609G/G609G}$ mice (Figure 3.8F and G).

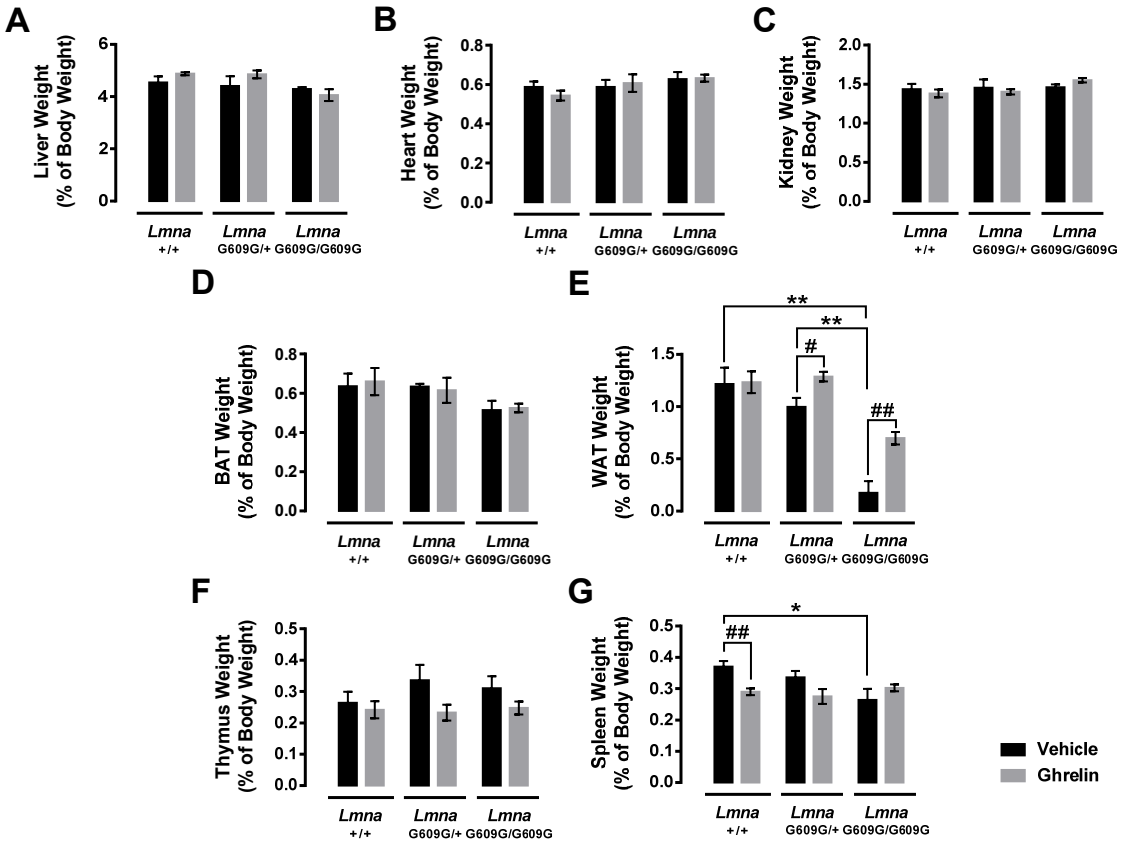

Figure 3.8. **Organ weight of vehicle- and ghrelin-treated *Lmna*$^{+/+}$, *Lmna*$^{G609G/+}$ and *Lmna*$^{G609G/G609G}$ mice.** (A-G) Size of the liver (A), heart (B), kidney (C), BAT (D), WAT (E), thymus (F) and spleen (G), expressed as percentage of total body weight in 3 months-old vehicle- and ghrelin-treated *Lmna*$^{+/+}$, *Lmna*$^{G609G/+}$ and *Lmna*$^{G609G/G609G}$ mice. The results represent the mean ± SEM (n=4-5 per group). *p<0.05, **p<0.01 significantly different compared to vehicle-treated control or *Lmna*$^{+/+}$, as determined by one-way ANOVA, followed by Dunnett's multiple comparisons test. $^{\#}$p<0.05, $^{\#\#}$p<0.01 significantly different compared to matched genotype vehicle-treated control, as determined by unpaired Student's *t* test.

3.2.3. Ghrelin administration effect on locomotor activity of *Lmna*$^{+/+}$, *Lmna*$^{G609G/+}$ and *Lmna*$^{G609G/G609G}$ mice

To investigate potential behavioral effects of the daily peripheral administration of ghrelin in *Lmna*$^{+/+}$, *Lmna*$^{G609G/+}$ and *Lmna*$^{G609G/G609G}$ mice, we performed open-field tests.

As shown in Figure 3.9A and B, vehicle-treated *Lmna*$^{G609G/+}$ and *Lmna*$^{G609G/G609G}$ mice showed a decrease in the distance covered (*Lmna*$^{G609G/+}$: 6147.34±1130.78 cm; *Lmna*$^{G609G/G609G}$: 5351.72±637.95 cm) and mean velocity (*Lmna*$^{G609G/+}$: 2.58±0.47 cm/s; *Lmna*$^{G609G/G609G}$: 2.24±0.27 cm/s) comparing to vehicle-treated *Lmna*$^{+/+}$ (distance covered: 7654.76±1347.96 cm; mean velocity: 3.20±0.56 cm/s). However, these

differences are not statistical different. Unexpectedly, ghrelin treatment led to a decrease in the total distance traveled and mean velocity of mice of the three genotypes, although this effect was not statistical different. No significant alterations were observed in the resting time during the test period between the three genotypes and between vehicle- and ghrelin-treated mice. However, we observed that *Lmna*$^{G609G/G609G}$ mice spent more time resting than wild-type and heterozygous littermates (Figure 3.9C) which could account to the observed decrease in the distance travelled by these mice. Interestingly, vehicle-treated *Lmna*$^{G609G/+}$ and *Lmna*$^{G609G/G609G}$ mice showed a tendency for spending more time in the center region of the arena when compared to vehicle-treated *Lmna*$^{+/+}$ mice. Ghrelin-treated *Lmna*$^{G609G/+}$ and *Lmna*$^{G609G/G609G}$ mice showed a tendency to spend less time in the center region of the arena (Figure 3.9D).

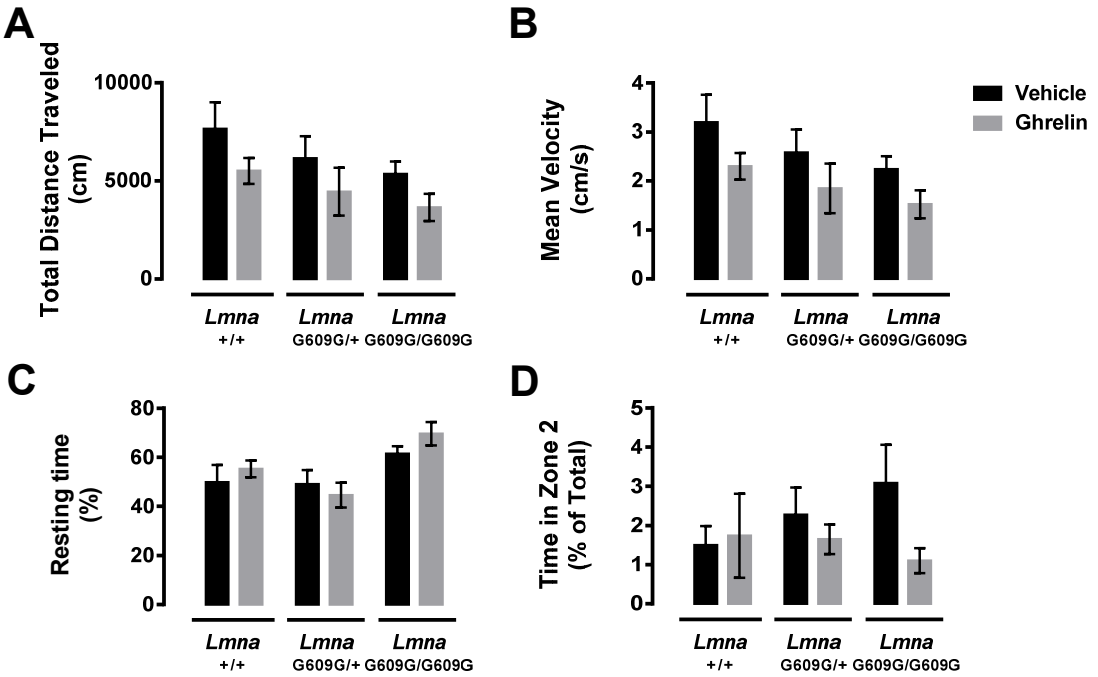

Figure 3.9. **Horizontal locomotor activity of vehicle- and ghrelin-treated *Lmna*$^{+/+}$, *Lmna*$^{G609G/+}$ and *Lmna*$^{G609G/G609G}$ mice.** Locomotor activity was assessed by the open field test. (A) Total distance travelled, in cm. (B) Mean velocity, in cm/s. (C) Time spent resting, as the % relative to total time of the test. (D) Time spent in the center region of the arena, as the % relative to total time of the test. The results represent the mean ± SEM (n=4-5 per group).

3.2.4. Ghrelin administration increased white adipocyte size in *Lmna*$^{G609G/G609G}$ mice

Lmna$^{G609G/G609G}$ mice, similarly to HGPS patients, develop a severe lipodystrophy (Osorio 2011) that contributes to the decreased body weight and other metabolic complications. Taking this into account, and given that ghrelin increased WAT weight, WAT samples were collected from vehicle-treated and ghrelin-treated mice of the three genotypes and processed for histological and molecular analysis to further understand how premature aging and ghrelin impact on WAT.

To assess alterations in the architecture of WAT, hematoxylin-eosin staining was performed in WAT paraffin sections and the area and number of adipocytes/area was determined (Figure 3.10B and C).

We observed a pronounced decrease in the adipocyte area of vehicle-treated *Lmna*$^{G609G/G609G}$ mice (194.55±42.44 µm^2), when compared to vehicle-treated *Lmna*$^{+/+}$ (1302.86±261.04 µm^2,) or *Lmna*$^{G609G/+}$ mice (989.27±97.65 µm^2) (Figures 3.10B). Although ghrelin treatment did not alter the size of adipocytes in *Lmna*$^{+/+}$ and *Lmna*$^{G609G/+}$ mice, it did promote a significant increase in the adipocyte area of *Lmna*$^{G609G/G609G}$ (874.09±149.86 µm^2) when compared to vehicle-treated mice (Figure 3.10B). We further explored the alterations observed in white adipocytes size. For that, we distributed adipocyte in classes, according to their size (Figure 3.10D). Vehicle-treated *Lmna*$^{G609G/G609G}$ mice show a higher number of small adipocytes, with areas below 500 µm^2 (<100: 35.88±10.97 %; 100-500: 58.14±11.88 %), and a concomitant lower number of fibers of higher caliber (500-900: 4.07±2.49 %; 900-1300: 1.61±1.61 %; 1300-1700: 0.19±0.19%) than vehicle-treated *Lmna*$^{+/+}$ (<100: 4.65±3.60 %; 100-500: 18.43±5.69 %; 500-900: 19.78±4.04 %; 900-1300: 14.96±2.15 %; 1300-1700: 14.10±2.95 %) (Figure 3.10D). In *Lmna*$^{G609G/G609G}$ mice, ghrelin treatment rescued the distribution of the adipocytes along the size classes to a pattern very similar to the one observed in vehicle-treated *Lmna*$^{+/+}$ mice (Figure 3.10D).

Lmna$^{G609G/G609G}$ mice showed a significant increase in adipocyte density when compared with *Lmna*$^{+/+}$ and *Lmna*$^{G609G/+}$ (Figure 3.10C) as a consequence of the reduced adipocyte size. However, ghrelin treatment, by increasing adipocyte area, reverted this effect (Figure 3.10B) to values similar to wild-type mice.

To better understand the mechanisms underlying ghrelin effects on WAT in *Lmna*$^{G609G/G609G}$, we analyzed putative alterations in some key proteins related with mechanisms known to be altered or compromised with aging, namely autophagy, a mechanism involved in cell proteostasis, and cell proliferation. To investigate the effect of ghrelin on autophagy we monitored measured the protein levels of the transient autophagosomal membrane-bound form of LC3B (LC3B-II) and sequestosome 1 (SQSTM1, also known as p62), widely used as markers of the autophagic process (Klionsky *et al.* 2016). We observed that ghrelin treatment led to a decrease of LC3B-II levels in both *Lmna*$^{+/+}$ (55±19 % of vehicle-treated *Lmna*$^{+/+}$) and *Lmna*$^{+/G609G}$ mice (48±13 % of vehicle-treated *Lmna*$^{G609G/+}$), as shown in Figure 3.11A and B. However, ghrelin effect was only statistical significant on heterozygous mice. A similar tendency was observed in ghrelin-treated *Lmna*$^{G609G/G609G}$ mice (72±8 % of vehicle-treated *Lmna*$^{G609G/G609G}$).

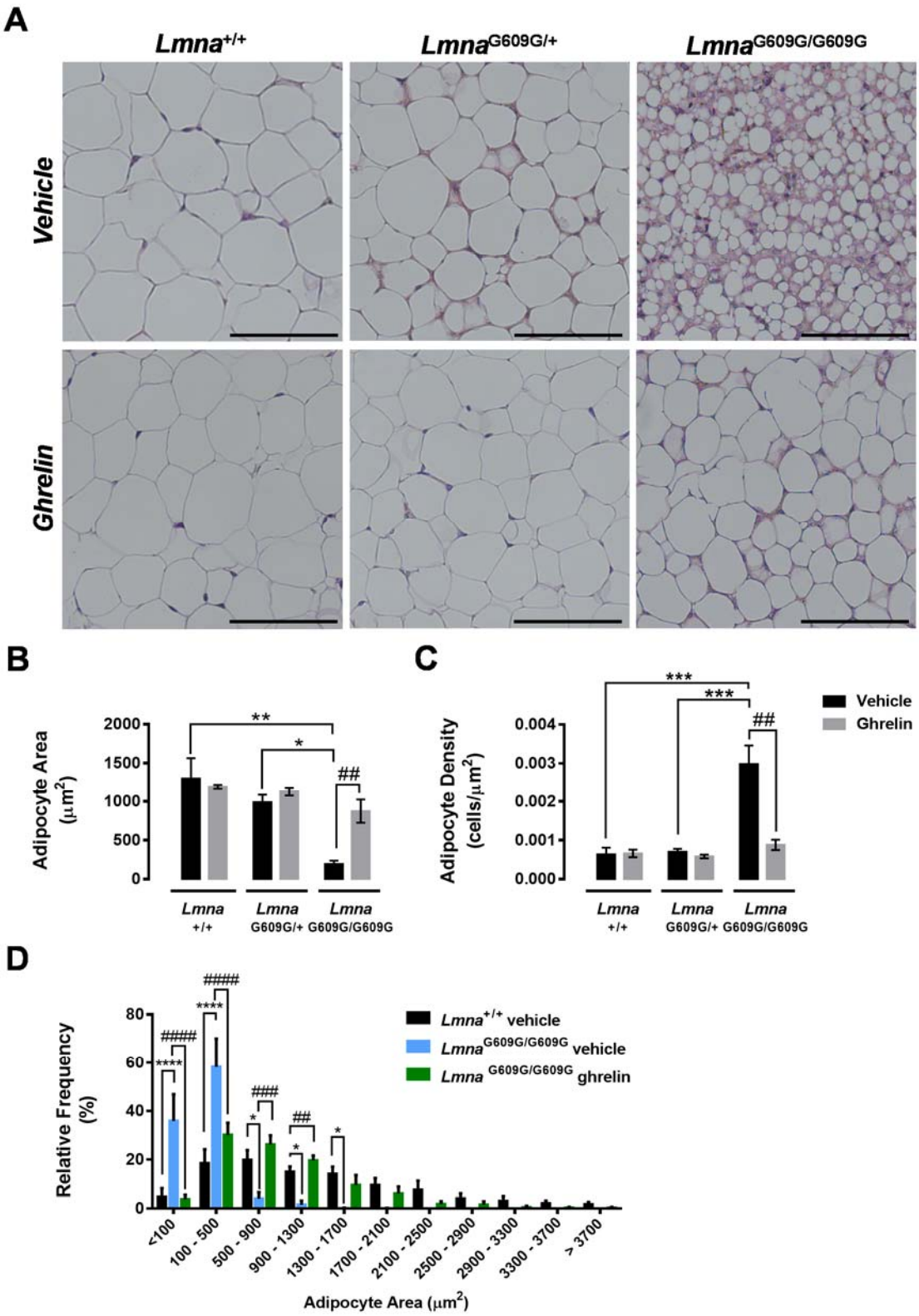

Figure 3.10. **Ghrelin effect in white adipose tissue histology of *Lmna*$^{G609G/G609G}$ mice.** (A) Representative images of hematoxylin-eosin-stained sections of gonadal white adipose tissue of vehicle- and ghrelin-treated *Lmna*$^{+/+}$, *Lmna*$^{G609G/+}$ and *Lmna*$^{G609G/G609G}$ mice. (B) Quantification of adipocyte area (µm^2) of vehicle- and ghrelin-treated *Lmna*$^{+/+}$, *Lmna*$^{G609G/+}$ and *Lmna*$^{G609G/G609G}$ mice. (D) Quantification of adipocyte density (cells/µm^2) of vehicle- and ghrelin-treated *Lmna*$^{+/+}$, *Lmna*$^{G609G/+}$ and *Lmna*$^{G609G/G609G}$ mice. (D) Adipocyte distribution along size classes, as the relative frequency (%) of the total adipocytes

analyzed, in vehicle- and ghrelin-treated *Lmna*$^{+/+}$, *Lmna*$^{G609G/+}$ and *Lmna*$^{G609G/G609G}$ mice. The results represent the mean ± SEM (n=4-5 per group). *p<0.05, **p<0.01, ***p<0.001, ****p<0.0001 significantly different, as determined by one-way ANOVA, followed by Bonferroni's multiple comparisons test or by two-way ANOVA, followed by Bonferroni's multiple comparisons test. ##p<0.01, ###p<0.001, ####p<0.0001 significantly different, as determined by two-way ANOVA, followed by Bonferroni's multiple comparisons test or by unpaired Student's *t* test (compared to vehicle-treated control). Scale bar 100 µm.

In addition, ghrelin-treated *Lmna*$^{+/+}$ mice showed a significant decrease in the protein levels of SQSTM1 (43±9 % of vehicle-treated *Lmna*$^{+/+}$) (Figure 3.11A and C), and a similar tendency was observed in ghrelin treated *Lmna*$^{G609G/G609G}$ mice (57±11 % of vehicle-treated *Lmna*$^{G609G/G609G}$). However, ghrelin treatment did not alter SQSTM1 protein levels in *Lmna*$^{G609G/+}$ mice (107±14 % of vehicle-treated *Lmna*$^{G609G/+}$; Figure 3.11C).

Proliferating cell nuclear antigen (PCNA) protein levels are used as a marker of cellular proliferation (Kubben *et al.* 1994) and therefore were used in this study to assess potential ghrelin effects on adipocyte proliferation. Ghrelin-treated *Lmna*$^{G609G/+}$ mice show an increase in the protein levels of PCNA (179±20 % of vehicle-treated *Lmna*$^{G609G/+}$) (Figure 3.11D). Ghrelin-treated *Lmna*$^{+/+}$ (124±16 % of vehicle-treated *Lmna*$^{+/+}$) and *Lmna*$^{G609G/G609G}$ mice (121±19 % of vehicle-treated *Lmna*$^{G609G/G609G}$) showed a tendency for increased levels of PCNA, however this effect did not reach statistical significance (Figure 3.11D).

Of note, given the severe lipodystrophy observed in *Lmna*$^{G609G/G609G}$ mice, we could only obtain one WAT sample from one vehicle-treated *Lmna*$^{G606G/G609G}$ mice for molecular analysis. Therefore, we did not perform statistical analysis between vehicle- and ghrelin-treated *Lmna*$^{G609G/G609G}$ mice and we must be cautious in drawing any conclusions from the results obtained regarding molecular changes in these mice.

3.2.5. Ghrelin administration increased cross sectional area of muscle fibers in *Lmna*$^{G609G/G609G}$ mice

Lmna$^{G609G/G609G}$ mice show a reduced body weight (Osorio *et al.* 2011), that can be aggravated by muscular atrophy. However, the alterations occurring at the level of skeletal muscle in these animals have not been studied in detail. To assess possible alterations in the skeletal muscle of *Lmna*$^{G609G/G609G}$ mice, and ghrelin effects on this tissue, we performed hematoxylin-eosin staining in skeletal muscle section samples from vehicle- and ghrelin-treated mice of each genotype and measured the cross-sectional area of the muscular fibers. We did not observe gross alterations in skeletal muscle histological structure in *Lmna*$^{G609G/+}$ and *Lmna*$^{G609G/G609G}$ mice comparing with *Lmna*$^{+/+}$ mice (Figure 3.12A), showing polygonal or round muscle fibers with peripheral nuclei. However, skeletal muscle fibers seem smaller in *Lmna*$^{G609G/G609G}$ mice. In fact, as illustrated in Figure 3.12B, the cross-sectional area of muscular fibers (muscle fibers size) is decreased in vehicle-treated *Lmna*$^{G609G/G609G}$ mice (1266.06±105.25 µm^2) when compared to vehicle-treated *Lmna*$^{+/+}$ mice (2016.36±70.43 µm^2). Ghrelin treatment

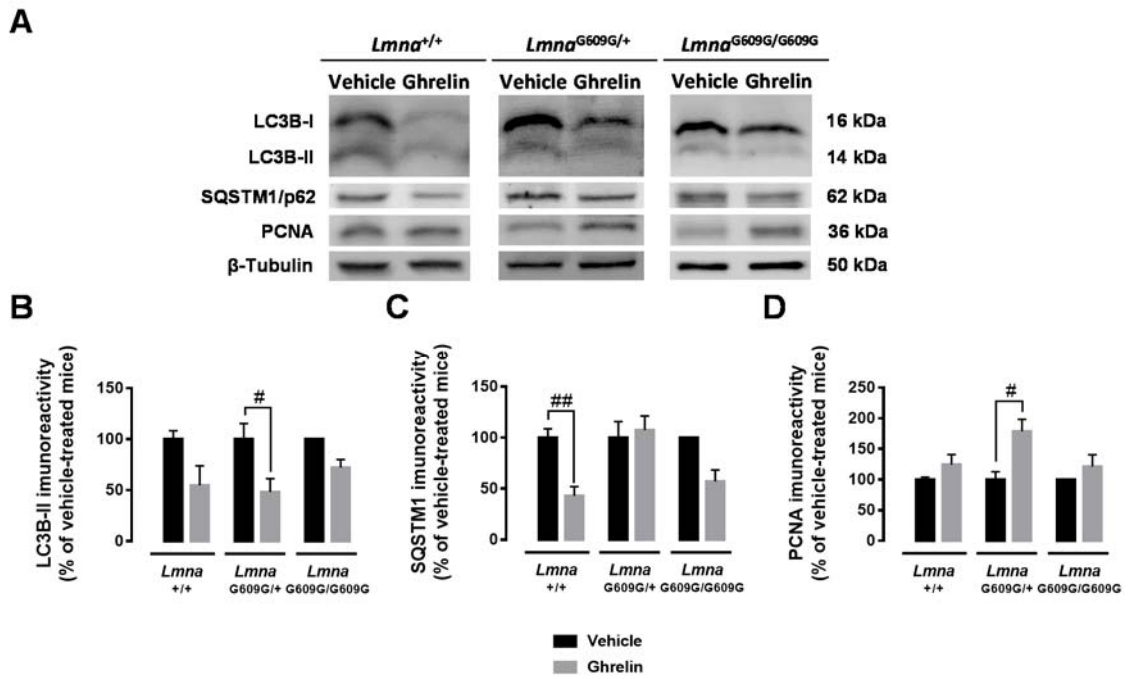

Figure 3.11. **Ghrelin effect in autophagy and cell proliferation markers in the white adipose tissue of *Lmna*$^{G609G/G609G}$ mice.** WAT protein lysates from *Lmna*$^{+/+}$, *Lmna*$^{G609G/+}$ and *Lmna*$^{G609G/G609G}$ mice were assayed for LC3B (B), SQSTM1/p62 (C), PCNA (D) and β-tubulin (loading control) immunoreactivity through Western blotting analysis. Representative Western blots for each protein are presented (A). The results represent the mean ± SEM (n=4-5 per group) and are expressed as percentage of matched genotype vehicle-treated mice. $^{\#}p<0.05$, $^{\#\#\#}p<0.001$ significantly different compared to matched genotype vehicle-treated control, as determined by unpaired Student's *t* test.

had no effect on the cross-sectional area of the muscular fibers in *Lmna*$^{+/+}$ mice (2106.53±129.70 µm^2) comparing to the vehicle-treated *Lmna*$^{+/+}$ mice. However, in *Lmna*$^{G609G/G609G}$ mice, ghrelin treatment increased skeletal muscle fiber size (1971.26±140.11 µm^2) when compared to vehicle-treated *Lmna*$^{G609G/G609G}$ mice (Figure 3.12B). In fact, ghrelin administration rescued the cross-sectional area of the muscle fibers of *Lmna*$^{G609G/G609G}$ mice to levels similar to the vehicle-treated *Lmna*$^{+/+}$ mice. Ghrelin-treated *Lmna*$^{G609G/+}$ mice show a tendency towards an increase in muscle fiber cross-sectional area (2364.25±160.83 µm^2) when compared to vehicle-treated controls (1784.53±226.17 µm^2), however, this difference is not statistically significant. To examine in more detail these results, muscle fibers were distributed into classes according to their cross sectional area. Vehicle-treated *Lmna*$^{G609G/G609G}$ mice show a higher number of small fibers, with areas below 1500µm^2 (<500: 12.62±3.53 %; 500-1000: 26.57±2.52 %; 1000-1500: 28.15±3.80 %), and a concomitant lower number of fibers of higher caliber (2000-2500: 7.56±1.87 %; 2500-3000: 4.25.15±1.82 %) than vehicle-treated *Lmna*$^{+/+}$ (<500: 2.88±0.99 %; 500-1000: 19.64±6.02 %; 1000-1500: 18.49±2.52 %; 2000-2500: 16.80±3.11 %; 2500-3000: 12.95±3.70 %) (Figure 3.12C). Ghrelin treatment rescued the distribution of muscle fibers along size classes in *Lmna*$^{G609G/G609G}$ mice to a pattern similar to vehicle-treated *Lmna*$^{+/+}$ mice.

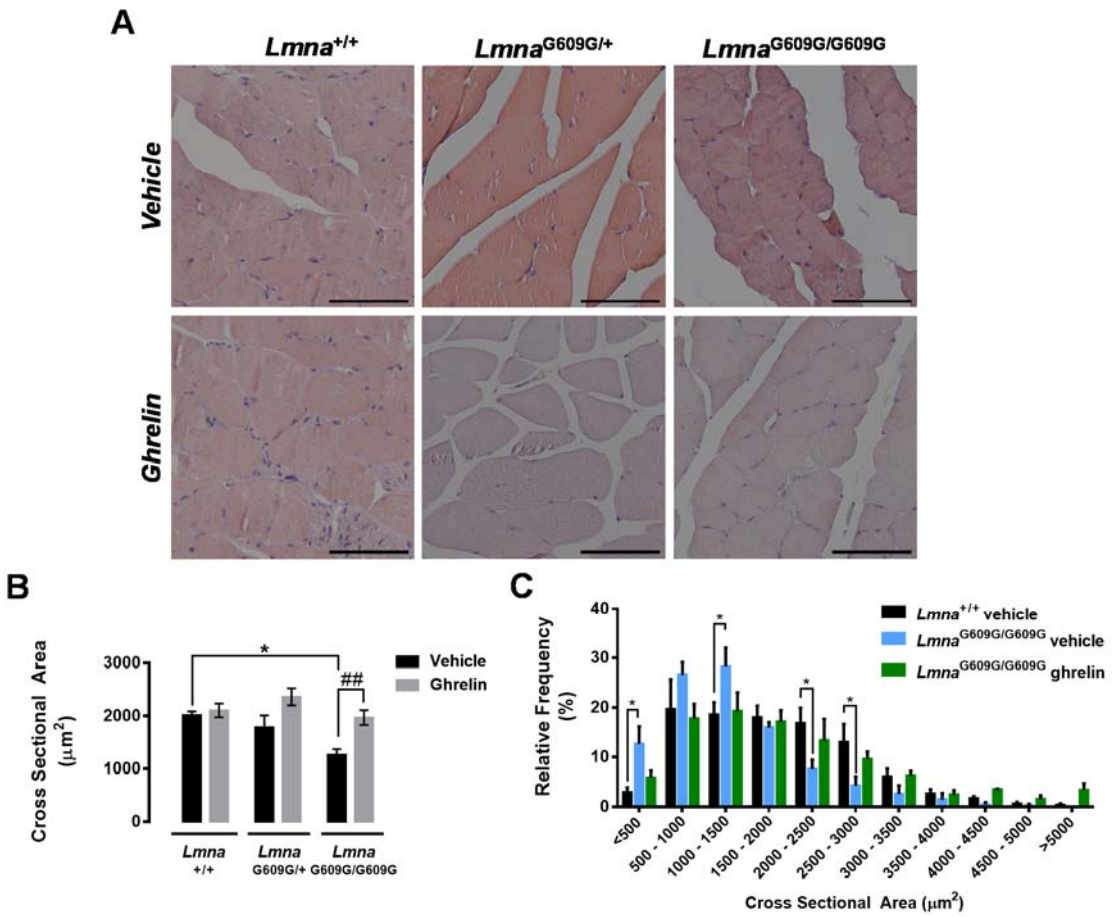

Figure 3.12. **Ghrelin effect in skeletal muscle histology of *Lmna*$^{G609G/G609G}$ mice.** (A) Representative images of hematoxylin-eosin-stained sections of skeletal muscle of vehicle- and ghrelin-treated *Lmna*$^{+/+}$, *Lmna*$^{G609G/+}$ and *Lmna*$^{G609G/G609G}$ mice. (B) Muscle fiber cross-sectional area (µm^2) of vehicle- and ghrelin-treated *Lmna*$^{+/+}$, *Lmna*$^{G609G/+}$ and *Lmna*$^{G609G/G609G}$ mice. (C) Muscle fibers distribution along size classes, as the relative frequency (%) of the total fibers analyzed, in vehicle- and ghrelin-treated *Lmna*$^{+/+}$, *Lmna*$^{G609G/+}$ and *Lmna*$^{G609G/G609G}$ mice. The results represent the mean ± SEM (n=3-5 per group). *p<0.05 significantly different, as determined by one-way ANOVA, followed by Bonferroni's multiple comparisons test or by two-way ANOVA, followed by Bonferroni's multiple comparisons test. ##p<0.01 significantly different compared to vehicle-treated control, as determined by unpaired Student's *t* test. Scale bar 100 µm.

3.2.6. Ghrelin administration increased hepatocyte number in *Lmna*$^{+/+}$, *Lmna*$^{G609G/+}$ and *Lmna*$^{G609G/G609G}$ mice

Liver is a poorly studied organ in the context of HGPS. In *Lmna*$^{G609G/G609G}$ mice, Osorio and colleagues, 2011, showed increased senescence-associated β-galactosidase staining in liver sections, which suggests an increase in cellular senescence in the liver of these mice. Apart from this, histological alterations occurring in the liver of *Lmna*$^{G609G/G609G}$ mice are currently unknown.

To assess potential alterations in the structure of the liver in *Lmna*$^{G609G/G609G}$ mice and the impact of ghrelin on this tissue, paraffin liver sections were stained with hematoxylin-eosin. We observed some differences in the liver histological structure between the three genotypes (Figure 3.13A). First, the size of the hepatocytes appears

to be bigger in vehicle-treated *Lmna*$^{+/+}$ and *Lmna*$^{G609G/+}$ mice than in vehicle-treated *Lmna*$^{G609G/G609G}$ mice. This difference may be related with the high number of lipid vacuoles present within hepatocytes from *Lmna*$^{+/+}$ and *Lmna*$^{G609G/+}$ mice livers. These lipid vacuoles also occur in hepatocytes from *Lmna*$^{G609G/G609G}$ mice, however in reduced number and size. Moreover, the size and shape of hepatocytes' nuclei of vehicle-treated *Lmna*$^{G609G/G609G}$ mice are altered, being smaller and irregular. We did not find gross alterations in hepatic structure, but we did observe that sinusoidal capillaries lumen was larger in *Lmna*$^{G609G/G609G}$ mice than in *Lmna*$^{+/+}$ and *Lmna*$^{G609G/+}$ mice (Figure 3.13A). Ghrelin-treated mice did not show visible differences in liver histological structure when comparing to vehicle-treated mice in three genotypes (Figure 3.13A). With aging the liver regenerative capacity is decreased, therefore, we decided to analyze if the number of hepatocytes was altered in vehicle-treated *Lmna*$^{G609G/G609G}$ mice. We observed a tendency for vehicle-treated *Lmna*$^{G609G/G609G}$ mice having a higher number of hepatocytes/area (1182.60±46.53) than the vehicle-treated *Lmna*$^{+/+}$ mice (1045.54±74.42) and vehicle-treated *Lmna*$^{G609G/+}$ mice (952.69±94.45) (Figure 3.13B). Interestingly, ghrelin administration significantly increased the number of hepatocytes/area in the three genotypes, being this effect more pronounced in *Lmna*$^{G609G/G609G}$ mice (Figure 3.13B).

Masson's trichrome staining was performed in liver sections in order to assess if there are alterations in collagen levels induced by the accelerated aging process and to evaluate ghrelin's effect on collagen deposition. We observed that vehicle-treated *Lmna*$^{G609G/G609G}$ and *Lmna*$^{G609G/+}$ mice present a visible decrease in collagen staining, more prominent in the first, around the blood vessels, comparing to vehicle-treated *Lmna*$^{+/+}$ (Figure 3.13C). This decrease was abolished by ghrelin treatment in *Lmna*$^{G609G/G609G}$ and *Lmna*$^{G609G/+}$ mice, suggesting that ghrelin increases collagen synthesis in these mice.

To better understand the impact of the aging in the liver of *Lmna*$^{G609G/G609G}$ mice, we analyzed the protein levels of SQSTM1 and PCNA as markers of autophagy and cellular proliferation, mechanisms known to be impaired with aging. We also evaluated the protein levels of p53, a protein involved in cell cycle arrest and DNA damage repair. We observed a decrease in the levels of SQSTM1 in ghrelin-treated *Lmna*$^{+/+}$ mice (65.7±14.5 % of vehicle-treated *Lmna*$^{+/+}$) (Figure 3.14A and B), however this difference did not reach statistical difference. On the other hand, ghrelin-treated *Lmna*$^{G609G/+}$ showed an increase in SQSTM1 protein levels (135.3±26.9 % of vehicle-treated *Lmna*$^{G609G/+}$), although not statistically significant. Ghrelin had no effect on SQSTM1 protein levels in *Lmna*$^{G609G/G609G}$ mice (100.0±8.0 % vehicle-treated *Lmna*$^{G609G/G609G}$) (Figure 3.14A and B). We also tried to analyze alterations in the protein levels of LC3B-II, an important autophagic marker, but we could no detect this protein in the liver samples analyzed. Regarding PCNA protein levels, ghrelin treatment did not have any effect in *Lmna*$^{+/+}$ (105.4±29.6 % of vehicle-treated *Lmna*$^{+/+}$) and *Lmna*$^{G609G/+}$ (92.5±18.6 % of vehicle-treated *Lmna*$^{G609G/+}$) mice (Figure 3.14A and C), however, ghrelin-treated

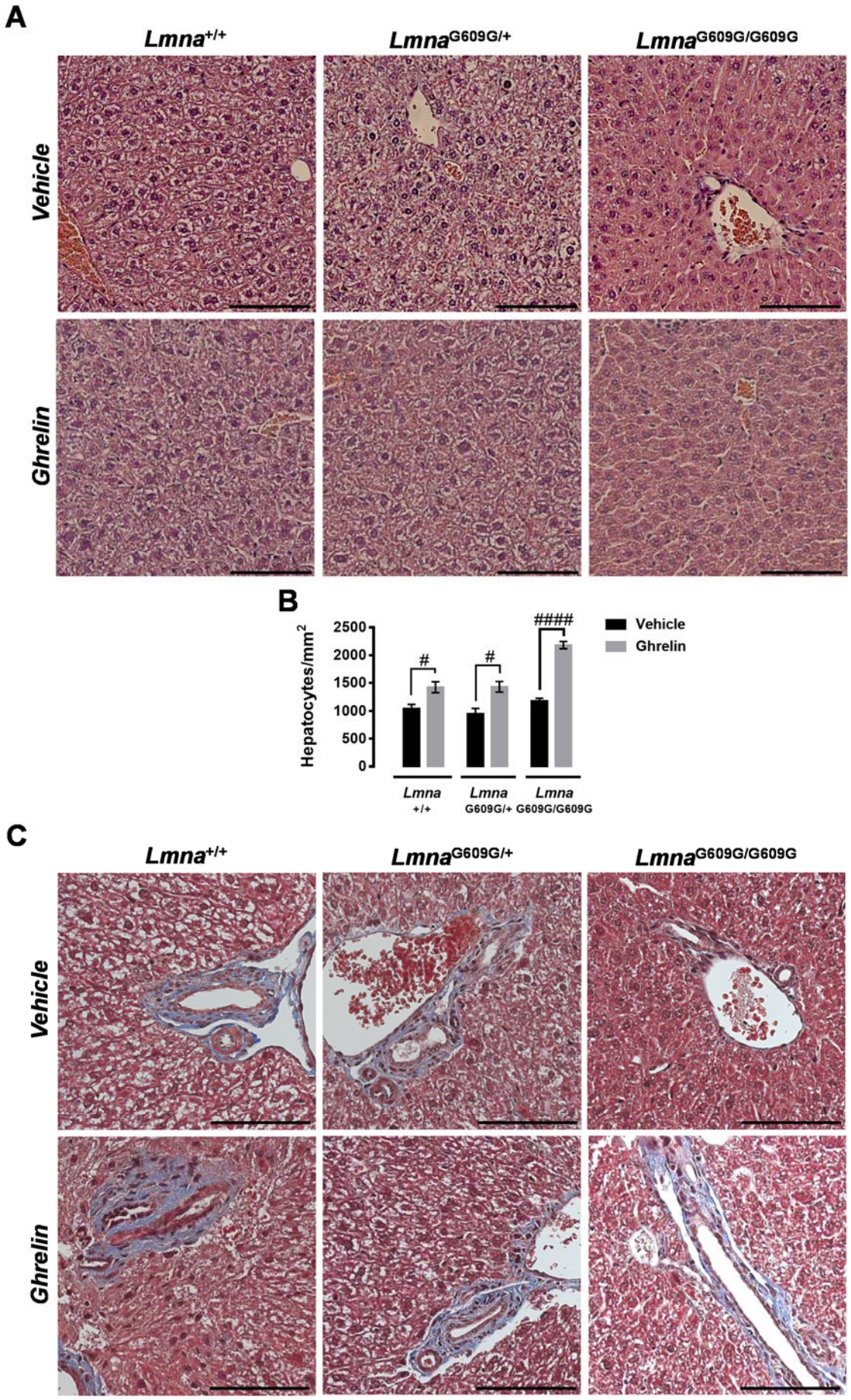
A
Lmna+/+
LmnaG609G/+
LmnaG609G/G609G
Vehicle
Ghrelin
B
Hepatocytes/mm2
2500
2000
1500
1000
500
0
#
#
####
Vehicle
Ghrelin
Lmna +/+
Lmna G609G/+
Lmna G609G/G609G
C
Lmna+/+
LmnaG609G/+
LmnaG609G/G609G
Vehicle
Ghrelin

Figure 3.13. **Ghrelin effect in liver histology of *Lmna*$^{G609G/G609G}$ mice.** (A) Representative images of hematoxylin-eosin-stained sections of liver of vehicle- and ghrelin-treated *Lmna*$^{+/+}$, *Lmna*$^{G609G/+}$ and *Lmna*$^{G609G/G609G}$ mice. (B) Quantification of the hepatocyte number, expressed as hepatocytes/mm^2, in the liver of vehicle- and ghrelin-treated *Lmna*$^{+/+}$, *Lmna*$^{G609G/+}$ and *Lmna*$^{G609G/G609G}$ mice. (C) Representative images of Masson's trichrome-stained sections of liver of vehicle- and ghrelin-treated *Lmna*$^{+/+}$, *Lmna*$^{G609G/+}$ and *Lmna*$^{G609G/G609G}$ mice. The results represent the mean ± SEM (n=4-5 per group). $^{\#}p<0.05$, $^{\#\#\#}p<0.001$ significantly different compared to matched genotype vehicle-treated control, as determined by unpaired Student's *t* test. Scale bar 100 µm.

Lmna$^{G609G/G609G}$ mice (79.6±12.4 % vehicle-treated *Lmna*$^{G609G/G609G}$) show a slight decrease in PCNA levels, although it did not reach statistical significance (Figure 3.14A and C). Ghrelin treatment resulted in a significant decrease in p53 levels both in *Lmna*$^{+/+}$ (48.7±9 % of vehicle-treated *Lmna*$^{+/+}$) and *Lmna*$^{G609G/+}$ (65.5±11.4 % of vehicle-treated *Lmna*$^{G609G/+}$) mice. However, it only had a mild effect on p53 protein levels of *Lmna*$^{G609G/G609G}$ mice (89.8±20.7 % vehicle-treated *Lmna*$^{G609G/G609G}$), that were slightly reduced (Figure 3.14A and D).

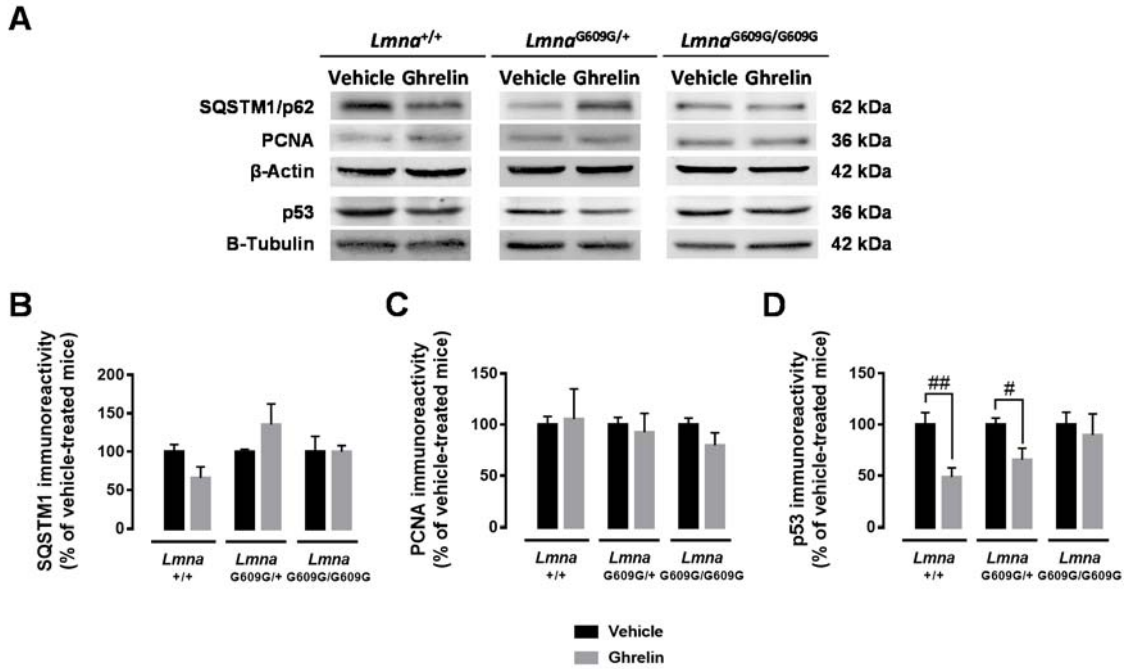

Figure 3.14. **Ghrelin effect in autophagy and cell proliferation markers in the liver of *Lmna*$^{G609G/G609G}$ mice.** Liver protein lysates from *Lmna*$^{+/+}$, *Lmna*$^{G609G/+}$ and *Lmna*$^{G609G/G609G}$ mice were assayed for SQSTM1 (B), PCNA (C), p53 (D) and β-tubulin (loading control) immunoreactivity through Western blotting analysis (A). Representative Western blots for each protein are presented. The results represent the mean ± SEM (n=3-5 per group) and are expressed as percentage of matched genotype vehicle-treated mice. $^{\#}p<0.05$, $^{\#\#\#}p<0.001$ significantly different compared to matched genotype vehicle-treated control, as determined by unpaired Student's *t* test.

3.2.7. Ghrelin administration had no effect on the wall thickness or nuclei number in the aorta of *Lmna*$^{+/+}$, *Lmna*$^{G609G/+}$ and *Lmna*$^{G609G/G609G}$ mice

The cardiovascular system is extremely affected in HGPS patients, with myocardial infarction being the most frequent death cause (Ullrich and Gordon 2015). *Lmna*$^{G609G/G609G}$ mice recapitulate to a certain extent the abnormalities described in these patients, having a depletion of VSMCs in the aortic arch, which may underlie the dysfunctions observed in their cardiovascular system (Osorio *et al.* 2011).

In order to evaluate ghrelin's effect on the cardiovascular system, hematoxylin-eosin staining was performed in mice aorta paraffin sections. We did not find gross histological structure differences in the aorta (Figure 3.15A) among genotypes as well as upon ghrelin treatment. We measured aortic medial (tunica media) thickness, a parameter often altered with aging or cardiovascular disease. We found a slight, but not significant, increase in the aortic medial thickness of vehicle-treated *Lmna*$^{G609G/G609G}$ mice (62.95±3.491 µm) comparing to vehicle-treated *Lmna*$^{+/+}$ animals (58.65±5.148 µm) (Figure 3.15A and B). Ghrelin had no effect on the thickness of aortic tunica media in the three genotypes (Figure 3.13B).

In addition, to investigate if our model showed a decrease in the aortic cell number, as reported by Osorio and collaborators, we stained sections of aorta with Hoechst in order to measure nuclei density of the aortic walls (Figure 3.15C). We observed a decrease in cell number in aortic wall in vehicle-treated *Lmna*$^{G609G/G609G}$ mice (2940.00±331.06 cells/mm^2) compared with vehicle-treated *Lmna*$^{+/+}$ mice (3880.00±549.91 cells/mm^2) (Figure 3.15C and D), although this difference is not statistical significant. Ghrelin-treated mice showed a tendency towards an increase in cell density in aortic wall in the three genotypes, though this effect was not statistical different from vehicle-treated mice.

In addition, we also analyzed the histological structure of the heart, but we did not detect alterations between the genotypes. Moreover, ghrelin treatment did not cause any effect in any of the groups.

3.2.8. Ghrelin administration increases splenic white pulp area in *Lmna*$^{G609G/G609G}$ mice

Spleen is a major lymphoid organ and plays a vital role in the immune system. *Lmna*$^{G609G/G609G}$ mice were described to have a marked splenic involution relative to wild-type controls (Osorio *et al.* 2011), and it was suggested that this feature could be associated with defects in the immune system of these animals.

To investigate the effect of ghrelin in the spleen, and a possible impact on immune function, of *Lmna*$^{G609G/G609G}$ mice, we performed hematoxylin-eosin staining in paraffin spleen sections and measured the white pulp area, splenic lymphatic tissue that mainly consists of B-lymphocytes and T-lymphocytes.

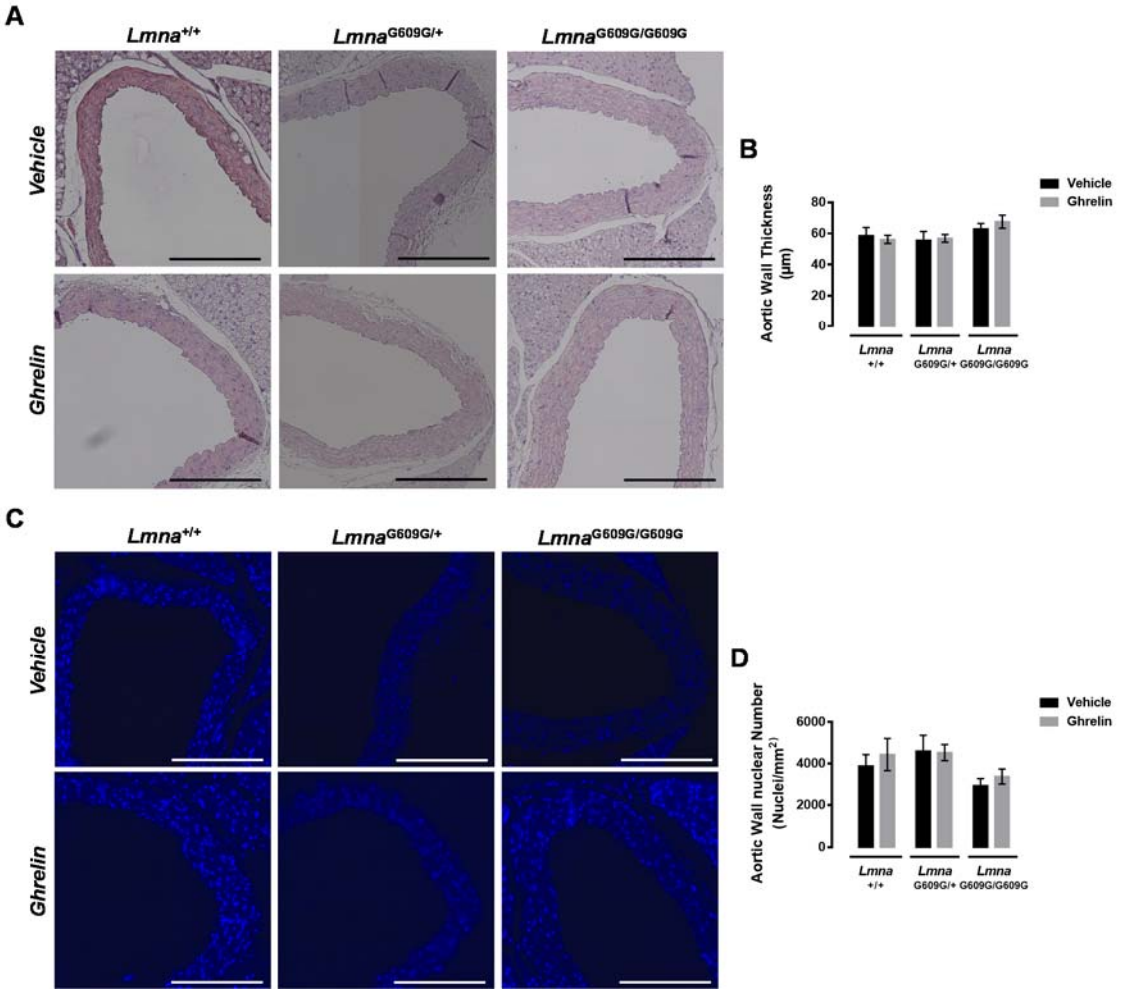

Figure 3.15. **Ghrelin effect in aorta histology of *Lmna*$^{G609G/G609G}$ mice.** (A) Representative images of hematoxylin-eosin-stained cross sections of the aorta of vehicle- and ghrelin-treated *Lmna*$^{+/+}$, *Lmna*$^{G609G/+}$ and *Lmna*$^{G609G/G609G}$ mice. (B) Quantification of the aorta medial thickness, expressed in µm, in the aorta of vehicle- and ghrelin-treated *Lmna*$^{+/+}$, *Lmna*$^{G609G/+}$ and *Lmna*$^{G609G/G609G}$ mice. (C) Representative images of Hoechst-stained cross sections of the aorta of vehicle- and ghrelin-treated *Lmna*$^{+/+}$, *Lmna*$^{G609G/+}$ and *Lmna*$^{G609G/G609G}$ mice. (D). Quantification of aortic wall nuclei number, expressed as aortic wall nuclei number/mm^2, in the aorta of vehicle- and ghrelin-treated *Lmna*$^{+/+}$, *Lmna*$^{G609G/+}$ and *Lmna*$^{G609G/G609G}$ mice. The results represent the mean ± SEM (n=4-5 per group). $^{\#}p<0.05$, $^{\#\#\#}p<0.001$ significantly different compared to matched genotype vehicle-treated control, as determined by unpaired Student's *t* test. Scale bar 100 µm.

No visible alterations were observed in the spleen histological structure between the three genotypes (Data not shown). Although vehicle-treated *Lmna*$^{G609G/G609G}$ mice show a slight decrease in splenic white pulp area (29.03±2.51 %) when compared to vehicle-treated *Lmna*$^{+/+}$ mice (33.45±2.77), no significant differences were found (Figure 3.16A). Interestingly, ghrelin-treated *Lmna*$^{G609G/G609G}$ mice present an increase in the white pulp area (38.24±1.88 %) relative to vehicle-treated *Lmna*$^{G609G/G609G}$ mice (Figure 3.16A). Ghrelin-treated *Lmna*$^{G609G/+}$ mice showed a similar tendency, however, this difference was not statistically significant. Ghrelin had no effect on white pulp area in *Lmna*$^{+/+}$ mice.

3.2.9. Ghrelin administration had no impact in the renal corpuscle area of *Lmna*$^{+/+}$, *Lmna*$^{G609G/+}$ and *Lmna*$^{G609G/G609G}$ mice

Similarly to liver, kidney structure, function and possible modifications in *Lmna*$^{G609G/G609G}$ mice were not studied in detail. So far, it is only known that kidney sections from *Lmna*$^{G609G/G609G}$ mice show increased senescence-associated β-galactosidase staining when compared to wild-type controls (Osorio *et al.* 2011).

In an attempt to increase our knowledge about the consequences of the accelerated HGPS aging phenotype in the kidney of *Lmna*$^{G609G/G609G}$ mice, kidney sections from the three genotypes were stained with hematoxylin-eosin and the renal corpuscle area was measured, since these are important structures for the correct functioning of nephrons, the renal function units, known to be affected during aging process. Among these alterations, it is included the hypertrophy of the renal corpuscle (Denic *et al.* 2016).

We did not notice any evident histological changes in the kidney of vehicle-treated *Lmna*$^{G609G/G609G}$ and *Lmna*$^{G609G/+}$ mice, namely in the cortical thickness, medulla organization and structure of the renal corpuscles, comparing to vehicle-treated *Lmna*$^{+/+}$ mice (data not shown). In fact, the area of the renal corpuscles was not altered in vehicle-treated *Lmna*$^{G609G/G609G}$ mice (2738.79±170.31 µm$^{2)}$, when compared to vehicle-treated *Lmna*$^{+/+}$ mice (2960.23±76.31 µm^2) (Figure 3.16B). Moreover, the renal corpuscle area of ghrelin-treated animals from the three genotypes was also identical to their respective vehicle-treated littermates (Figure 3.16B).

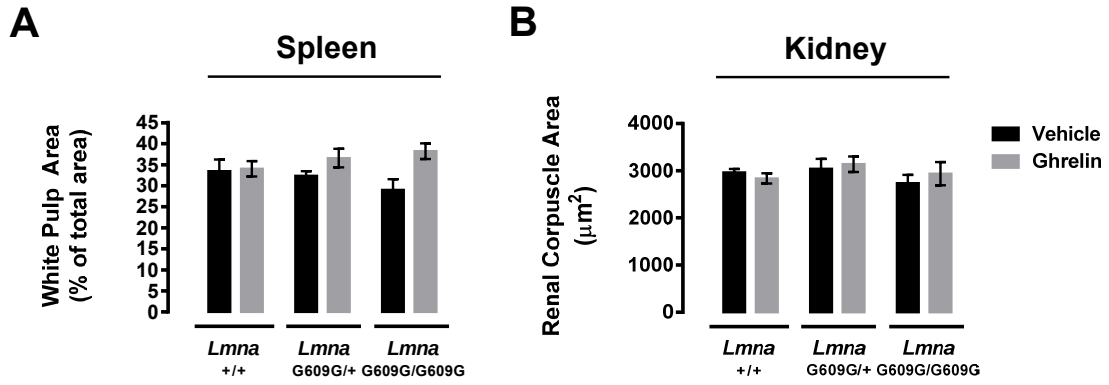

Figure 3.16. **Ghrelin effect in spleen and kidney histology of of *Lmna*$^{G609G/G609G}$ mice.** (A) Quantification of the white pulp area, expressed as the % of total area, of the spleen of vehicle- and ghrelin-treated *Lmna*$^{+/+}$, *Lmna*$^{G609G/+}$ and *Lmna*$^{G609G/G609G}$ mice. (B) Quantification of the renal corpuscle area, expressed in µm^2, of vehicle- and ghrelin-treated *Lmna*$^{+/+}$, *Lmna*$^{G609G/+}$ and *Lmna*$^{G609G/G609G}$ mice. The results represent the mean ± SEM (n=4-5 per group).

3.2.10. Ghrelin administration rescued the hypodermal thickness of *Lmna*$^{G609G/G609G}$ mice to similar values observed in *Lmna*$^{+/+}$ mice

In HGPs patients the skin is one of the organs that harbors the most evident alterations. Among these are included the appearance of regions of hyper- and hypopigmentation, gradual loss of the subcutaneous fat layer, which makes the skin extremely thin, and loss of hair (Hennekam 2006). *Lmna*$^{G609G/G609G}$ mice were also reported to exhibit some of these alterations in the skin, namely the decrease in the subcutaneous fat layer and hair follicle attrition (Osorio *et al.* 2011). However, these assumptions were drew based on qualitatively assessments. To better understand the impact of HGPS phenotype in this structure, and assess the result of ghrelin treatment, samples of the dorsal skin were stained with hematoxylin-eosin and the thickness of the dermis, epidermis and hypodermis was evaluated.

The thickness of the epidermis of vehicle-treated *Lmna*$^{G609G/G609G}$ mice (10.21±0.93 µm) was shown to be slightly decreased when compared to vehicle-treated *Lmna*$^{+/+}$ (13.05±0.77 µm) and *Lmna*$^{G609G/+}$ (11.85±0.37 µm) mice, but the difference was not statistically significant (Figure 3.17A and B). Ghrelin-treatment led to a significant increase in epidermal thickness of *Lmna*$^{G609G/G609G}$ mice (13.17±0.84 µm) compared to vehicle-treated *Lmna*$^{G609G/G609G}$ mice, but had no effect on *Lmna*$^{+/+}$ and *Lmna*$^{G609G/+}$.

We did not observe alterations in thickness of the dermis between vehicle-treated *Lmna*$^{G609G/G609G}$ (180.03±31.61 µm), *Lmna*$^{G609G/+}$ (238.87±39.31 µm) and *Lmna*$^{+/+}$ (236.32±40.44 µm) mice (Figure 3.17C). Ghrelin-treated *Lmna*$^{+/+}$ (267.64±41.00 µm) and *Lmna*$^{G609G/+}$ (330.07±43.36 µm) mice showed a tendency for an increase in the thickness of the dermis when compared to vehicle-treated matched controls. Ghrelin treatment, however, did not result in any changes in *Lmna*$^{G609G/G609G}$ mice.

We also found that the subcutaneous fat layer, also known as the hypodermis, of vehicle-treated *Lmna*$^{G609G/G609G}$ mice (18.44±11.63 µm) was significantly decreased when compared to vehicle-treated *Lmna*$^{+/+}$ mice (232.18±68.46 µm) (Figure 3.17D). Ghrelin treatment resulted in an increase in the hypodermis thickness in *Lmna*$^{G609G/G609G}$ mice (118.75±59.08 µm) when compared to vehicle-treated *Lmna*$^{G609G/G609G}$ mice (Figure 3.17D). In contrast, ghrelin-treated *Lmna*$^{+/+}$ (192.98.75±30.56 µm) and *Lmna*$^{G609G/+}$ (132.75±41.13 µm) mice showed decreased thickness of the hypodermis when compared to the respective vehicle-treated controls, although the differences were not statistically significant.

We observed a great variability in the thickness of the different layers of the skin between genders, which may explain the absence of significance in some of our evaluations. In fact, we observed that the dermis was thicker in males, while the subcutaneous fat layer was thicker in females. However, due to the low number of animals, we could not perform statistical analysis, or take any conclusions, independently for each gender.

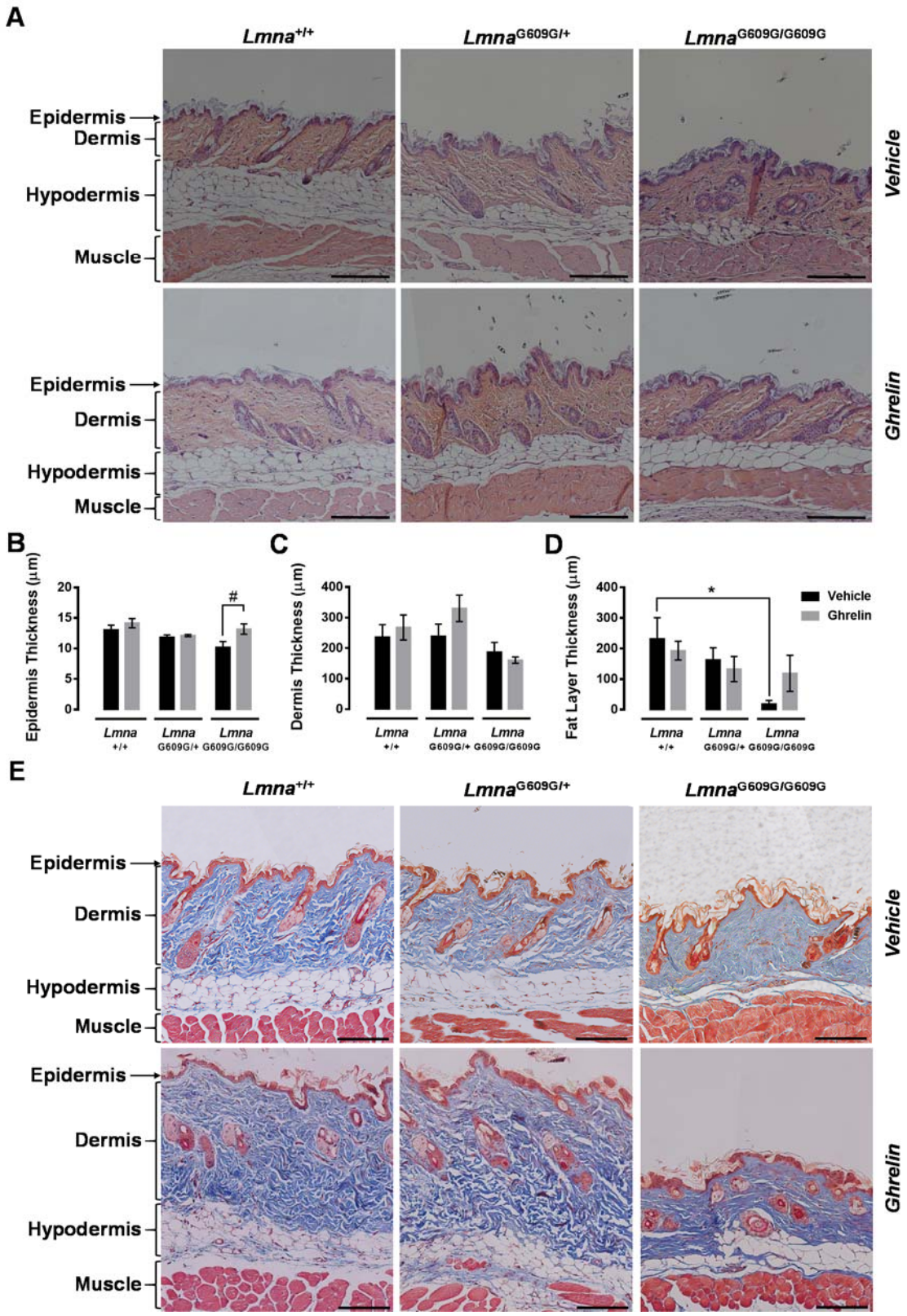

Figure 3.17. **Ghrelin effect in skin histology of *Lmna*$^{G609G/G609G}$ mice.** (A) Representative images of hematoxylin-eosin-stained sections of dorsal skin of vehicle- and ghrelin-treated *Lmna*$^{+/+}$, *Lmna*$^{G609G/+}$ and *Lmna*$^{G609G/G609G}$ mice. (B-D) Quantification of the epidermis (B), dermis (C) and hypodermis (D) thickness, expressed in µm, of the dorsal skin of vehicle- and ghrelin-treated *Lmna*$^{+/+}$, *Lmna*$^{G609G/+}$ and *Lmna*$^{G609G/G609G}$ mice. (E) Representative images of Masson's trichrome-stained sections of dorsal skin of

vehicle- and ghrelin-treated *Lmna*$^{+/+}$, *Lmna*$^{G609G/+}$ and *Lmna*$^{G609G/G609G}$ mice. The results represent the mean ± SEM (n=4-5 per group). *p<0.05 significantly different compared to vehicle-treated control or *Lmna*$^{+/+}$, as determined by one-way ANOVA, followed by Dunnett's multiple comparisons test. #p<0.05 significantly different compared to matched genotype vehicle-treated control, as determined by unpaired Student's *t* test. Scale bar 100 µm.

We also performed Masson's trichrome staining of skin sections to investigate alterations in collagen deposition, the major component of the skin dermal matrix, induced by premature aging and ghrelin. As shown in Figure 3.17E, in general, collagen deposition seems to be similar among mice of the different genotypes, with a homogeneous bluish staining, and similar collagen fiber orientation with open spaces interspersed between fiber bundles. However, we did observe a small decrease in the collagen staining intensity in *Lmna*$^{G609G/G609G}$ mice, in particular in male mice. In these mice, collagen fiber bundles seem thicker with less open space within and between bundles in the dermis (Figure 3.17E). Ghrelin-treated *Lmna*$^{G609G/G609G}$ mice, however, showed increased collagen staining compared to vehicle-treated mice, suggesting a that ghrelin may increase collagen synthesis or remodeling in *Lmna*$^{G609G/G609G}$ mice., similarly to what was observed in the liver of these mice.

To further understand the impact of ghrelin treatment in the alterations observed in skin structure and function occurring in *Lmna*$^{G609G/G609G}$ mice we analyzed the levels of LC3B-II and SQSTM1, autophagy markers, PCNA, cell proliferation marker, and p53, a protein involved in cell cycle arrest and DNA damage repair.

LC3b-II levels in ghrelin-treated *Lmna*$^{G609G/G609G}$ mice (74±21.6 % of vehicle-treated *Lmna*$^{G609G/G609G}$) decreased (Figure 3.18A and B), however, due to the fact that only two animals from the vehicle-treated group were analyzed it was not possible to perform statistical analysis. Ghrelin-treated *Lmna*$^{G609G/+}$ mice presented similar levels of LC3B-II (102.6± 3.1 % of vehicle-treated *Lmna*$^{G609G/+}$) to vehicle-treated controls (Figure 3.18A and B). We were not able to detect LC3B-II protein levels in the samples of *Lmna*$^{+/+}$ mice. We observed a significant increase of SQSTM1 levels in ghrelin-treated *Lmna*$^{G609G/G609G}$ mice (141.3±13.1 % of vehicle-treated *Lmna*$^{G609G/G609G}$) (Figure 3.18 A and C). Conversely, SQSTM1 levels in skin lysates from ghrelin-treated *Lmna*$^{G609G/+}$ mice (75.3±7.9 % of vehicle-treated *Lmna*$^{G609G/+}$) were significantly reduced in comparison to vehicle-treated controls (Figure 3.18A and C). A similar tendency was observed in ghrelin-treated *Lmna*$^{+/+}$ mice (79.7± 24.5 % of vehicle-treated *Lmna*$^{+/+}$), but the decrease was not significant. These conflicting results may be explained by the fact that autophagy is a very dynamic process, and the levels of this protein depend on the balance between autophagosome formation and degradation (Weidberg *et al.* 2011). Then, we would expect an increase in P62 levels in the case of autophagy blockade, but also if the formation of autophagosomes was stimulated in such a manner that lysosomal degradation could not degrade at the same rate the autophagolysosomes. To better understand the autophagic process in the skin further experiments need to be performed.

Ghrelin treatment induced a significant increase in PCNA protein levels in the skin of *Lmna*$^{G609G/G609G}$ mice (363.9±57.6 % of vehicle-treated *Lmna*$^{G609G/G609G}$), suggesting an increase in cell proliferation (Figure 3.18A and D). On the other hand, we did not observe any alterations of the PCNA protein levels in the skin of *Lmna*$^{+/+}$ or *Lmna*$^{G609G/+}$ mice upon ghrelin treatment (Figure 3.18A and D).

Regarding p53, we observed a decrease in its levels in ghrelin-treated *Lmna*$^{G609G/G609G}$ mice (77.1±14.7 % of vehicle-treated *Lmna*$^{G609G/G609G}$) compared to vehicle-treated animals, but this reduction did not reach statistical significance (Figure 3.18A and E). We could not detect P53 protein levels in the samples of *Lmna*$^{+/+}$ and *Lmna*$^{G609G/+}$ mice.

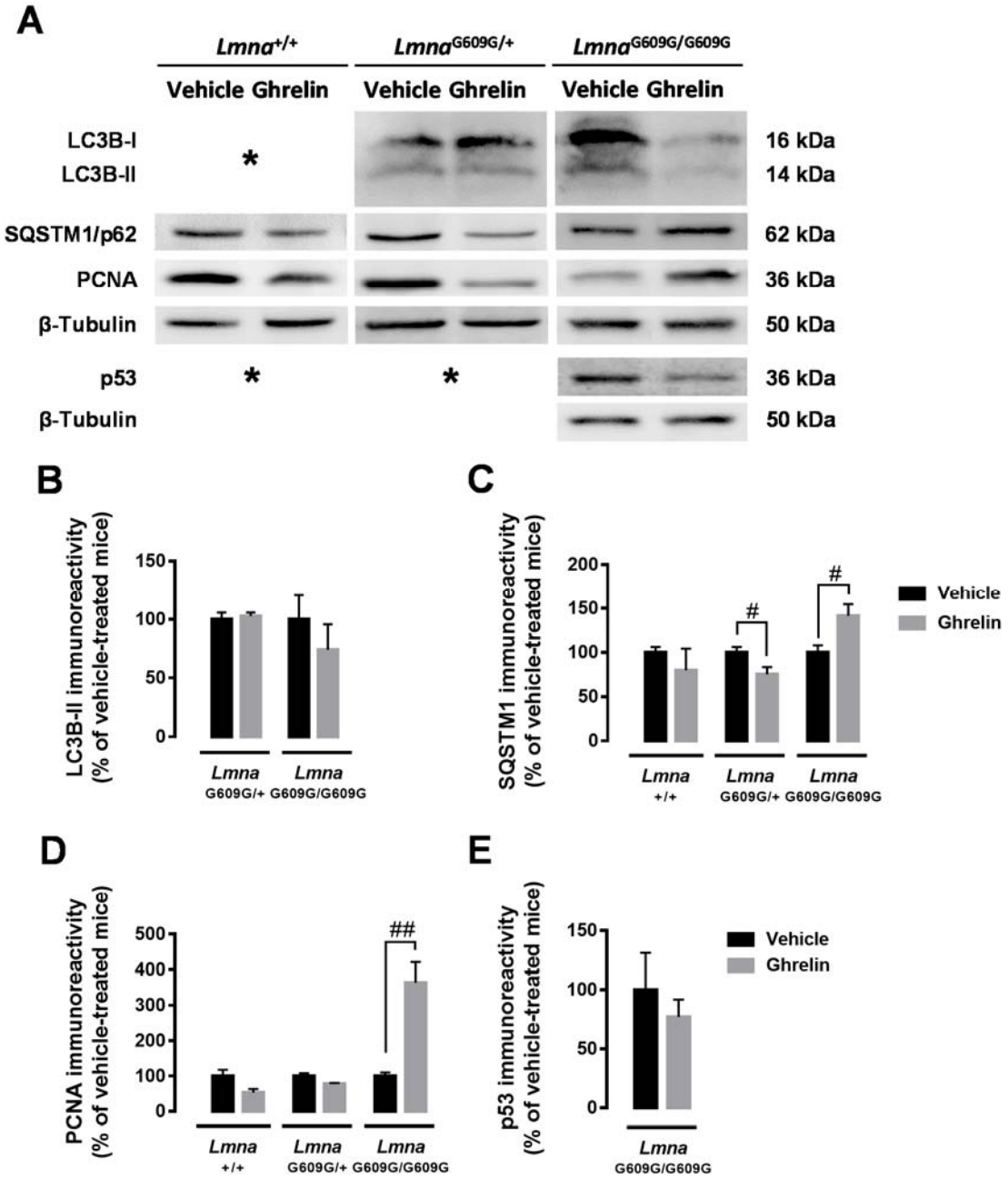

Figure 3.18. **Ghrelin effect in autophagy and cell proliferation markers in the skin of *Lmna*$^{G609G/G609G}$ mice.** Skin protein lysates from *Lmna*$^{+/+}$, *Lmna*$^{G609G/+}$ and *Lmna*$^{G609G/G609G}$ mice were assayed for LC3B (B), SQSTM1 (C), PCNA (D), p53 (E) and β-tubulin (loading control) immunoreactivity through Western blotting analysis. Representative Western blots for each protein are presented (A). The results represent the mean ± SEM (n=3-5 per group) and are expressed as percentage of matched genotype vehicle-treated mice. $^{\#}p<0.05$, $^{\#\#\#}p<0.001$ significantly different compared to matched genotype vehicle-treated control, as determined by unpaired Student's *t* test. * We could not detect LC3B-II in *Lmna*$^{+/+}$ mice and p53 in *Lmna*$^{+/+}$and *Lmna*$^{G609G/+}$ mice.

3.2.11. Ghrelin administration has an impact on hypothalamic gene expression of *Lmna*$^{+/+}$ and *Lmna*$^{G609G/G609G}$ mice

Ghrelin is mainly produced in the stomach but it travels to the CNS where it triggers several responses, regulating GH release, food intake and energy expenditure (Kojima 1999). Hypothalamus is the structure where ghrelin initiates most of its central actions and therefore, although no overt neurological symptoms are described in HGPS patients or in *Lmna*$^{G609G/G609G}$ mice, in order to evaluate the impact of ghrelin on the hypothalamus in these mice, we performed quantitative analysis of the expression of several genes related to hypothalamic function, inflammation, neurogenesis and neurotrophic factors.

Regarding hypothalamic function, we evaluated the gene expression of neuropeptides known to be crucial for food intake and energy metabolism regulation. We observed that ghrelin treatment caused an increase in the expression of NPY in *Lmna*$^{+/+}$ mice (1.48±0.15 of vehicle-treated *Lmna*$^{+/+}$), although this was not statistical different. Unexpectedly, in ghrelin-treated *Lmna*$^{G609G/G609G}$ mice (0.75±0.06 of vehicle-treated *Lmna*$^{G609G/G609G}$) the NPY expression was shown to be decreased relatively to vehicle-treated controls (Figure 3.19A), but the difference was not significant. Ghrelin treatment resulted, similarly, in a tendency towards an increase in AgRP expression in *Lmna*$^{+/+}$ mice (1.54±0.24 of vehicle-treated *Lmna*$^{+/+}$), while decreasing the expression of this peptide in *Lmna*$^{G609G/G609G}$ mice (0.78±0.10 of vehicle-treated *Lmna*$^{G609G/G609G}$), but these differences were not statistically significant. Moreover, we observed that POMC gene expression was, not significantly, decreased in *Lmna*$^{+/+}$ mice (0.56±0.10 of vehicle-treated *Lmna*$^{+/+}$) upon ghrelin treatment, and a similar tendency was found in ghrelin-treated *Lmna*$^{G609G/G609G}$ mice (0.84±0.14 of vehicle-treated *Lmna*$^{G609G/G609G}$), however, in any of the two cases the differences were significant. Surprisingly, ghrelin treatment caused a tendency for an increase in the expression of CART in both *Lmna*$^{+/+}$ (1.45±0.14 of vehicle-treated *Lmna*$^{+/+}$) and *Lmna*$^{G609G/G609G}$ (1.15±0.12 of vehicle-treated *Lmna*$^{G609G/G609G}$) mice (Figure 3.19A).

We also analyzed the effects of ghrelin on the expression of NPY receptors, namely NPY Y_1R, Y_2R and Y_5R. Interestingly, ghrelin-treated *Lmna*$^{+/+}$ (0.62±0.08 of vehicle-treated *Lmna*$^{+/+}$) and *Lmna*$^{G609G/G609G}$ (0.69±0.08 of vehicle-treated *Lmna*$^{G609G/G609G}$) mice showed a significant decrease in the expression of the NPY receptor Y2R (Figure 3.19B). Similar tendencies were obtained, upon ghrelin

treatment, in *Lmna*$^{+/+}$ and *Lmna*$^{G609G/G609G}$ for the expression of the receptors Y1R and Y5R, but the differences were not statistically significant (Figure 3.19B).

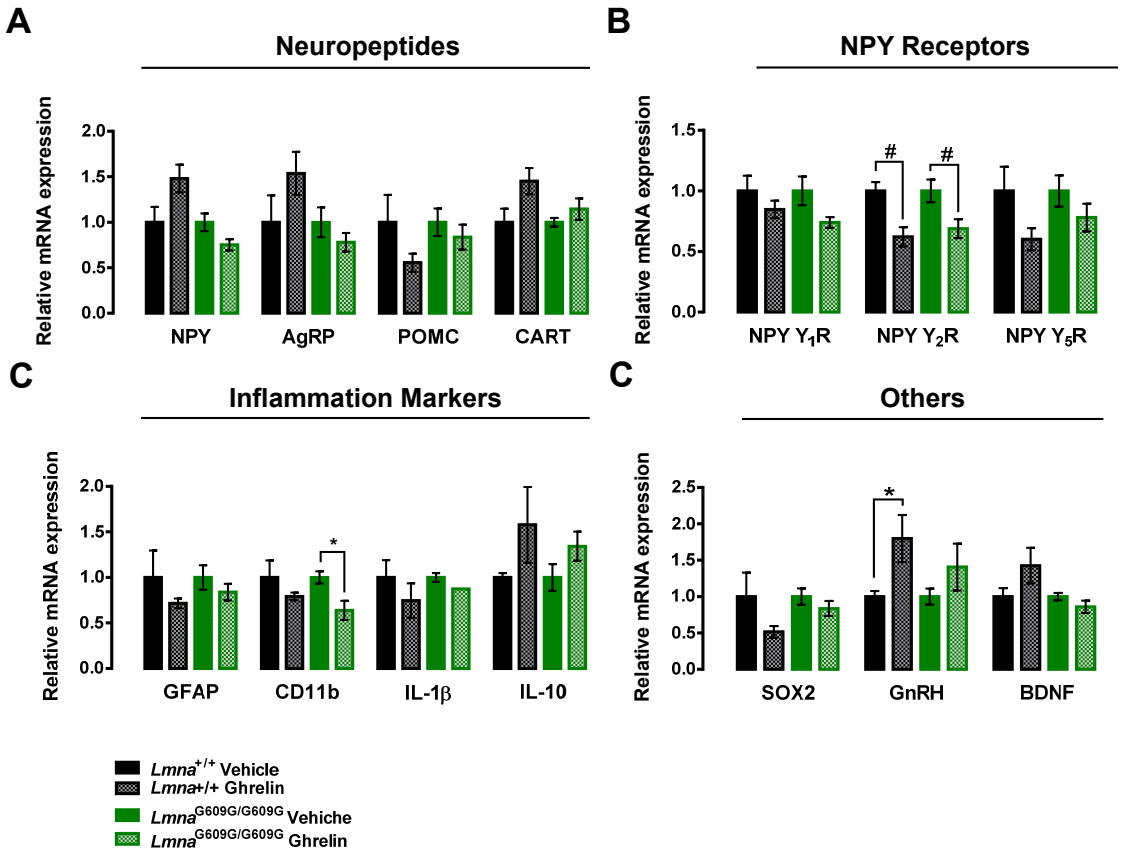

Figure 3.19. **Comparative analysis of hypothalamic gene expression of vehicle- and ghrelin-treated *Lmna*$^{+/+}$ and *Lmna*$^{G609G/G609G}$ mice.** Gene expression analysis of (A) orexigenic, NPY and AgRP, and anorexigenic, POMC and CART, neuropeptides; (B) NPY Y_1R, Y_2R and Y_5R receptors; (C) inflammatory markers GFAP, CD11b, IL-1β and IL-10; (D) SOX2, GnRH and BDNF, in the hypothalamus of in ghrelin-treated *Lmna*$^{+/+}$ and *Lmna*$^{G609G/G609G}$ mice, expressed as mRNA expression relative to vehicle-treated control. The results represent the mean ± SEM of the relative expression normalized to Hprt gene (n=4-5 per group). $^{\#}p<0.05$ significantly different compared to matched genotype vehicle-treated control, as determined by unpaired Student's *t* test.

We evaluated the expression of some genes known to be involved in inflammatory processes. We observed that ghrelin-treated *Lmna*$^{+/+}$ (0.72±0.05 of vehicle-treated *Lmna*$^{+/+}$) and *Lmna*$^{G609G/G609G}$ (0.84±0.09 of vehicle-treated *Lmna*$^{G609G/G609G}$) mice had a slight decrease, although not significant, in the expression of GFAP (Figure 3.19C). Ghrelin treatment led to a significant decrease in the gene expression of CD11b in *Lmna*$^{G609G/G609G}$ mice (0.64±0.11 of vehicle-treated *Lmna*$^{G609G/G609G}$), and ghrelin-treated *Lmna*$^{+/+}$ mice (0.79±0.04 of vehicle-treated *Lmna*$^{+/+}$) followed this trend, although the decrease was not statistical different. It was also observed a tendency towards a decrease in IL-1β expression, after ghrelin treatment, in both *Lmna*$^{+/+}$ (0.75±0.19 of vehicle-treated *Lmna*$^{+/+}$) and *Lmna*$^{G609G/G609G}$ (0.88±0.00 of vehicle-treated *Lmna*$^{G609G/G609G}$) mice (Figure 3.19C). Due to the limited number of *Lmna*$^{G609G/G609G}$ mice analyzed for IL-1β expression it was not possible to

perform statistical analysis for this gene. We observed that ghrelin-treated *Lmna*$^{G609G/G609G}$ (1.34±0.16 of vehicle-treated *Lmna*$^{G609G/G609G}$), as well as ghrelin-treated *Lmna*$^{+/+}$ (1.56±0.42 of vehicle-treated *Lmna*$^{+/+}$), mice show an increment in the expression of IL-10, although the differences are not significant (Figure 3.19C).

We further analyzed the gene expression of SOX2 and found that ghrelin treatment led to a tendency for a decrease in its expression in *Lmna*$^{+/+}$ mice (0.52±0.08 % of vehicle-treated *Lmna*$^{+/+}$) comparing to their controls, but it was not significant (Figure 3.19D). A similar tendency was observed for ghrelin treated *Lmna*$^{G609G/G609G}$ (0.84±0.10 of vehicle-treated *Lmna*$^{G609G/G609G}$). The expression of GnRH was also measured and it was observed that ghrelin treatment resulted in a significant increase in its expression in *Lmna*$^{+/+}$ mice (1.80±0.32 % of vehicle-treated *Lmna*$^{+/+}$) (Figure 3.19D). Ghrelin-treated *Lmna*$^{G609G/G609G}$ mice also displayed a tendency towards increased expression of GnRH (1.41±0.32 % of vehicle-treated *Lmna*$^{G609G/G609G}$), but it was not statistical different. The gene expression of BDNF appears to be increased in ghrelin-treated *Lmna*$^{+/+}$ mice (1.43±0.24 % of vehicle-treated *Lmna*$^{+/+}$) relative to vehicle-treated controls, however, this increase was not statistically significant (Figure 3.19D). In *Lmna*$^{G609G/G609G}$ mice, on the other hand, ghrelin treatment did not alter the expression of BDNF.

Chapter 4
Discussion

4.Discussion

HGPS is a very rare and fatal condition that is characterized by a premature and accelerated aging that culminates with the death of the patients, commonly due to myocardial infarction or stroke, at an average age of 14.6 years (Ullrich and Gordon 2015). It is caused by a *de novo* point mutation in the LMNA gene, which results in the production of a truncated lamin A, named progerin, that remains permanently farnesylated (De Sandre-Giovannoli *et al.* 2003, Eriksson *et al.* 2003).

The accumulation of this mutant protein leads to the development of several common features in the patients which include growth impairment allied to a reduced body weight, alterations in the skin with progressive appearance of alopecia, problems in the bones and joints, severe lipodystrophy and cardiovascular complications, that ultimately lead to their death (Hennekam 2006, Gordon *et al.* 2007, Ullrich and Gordon 2015).

Several attempts have been made in order to treat this condition, and two independent clinical trials have already been performed using lonafarnib, farnesyltransferase inhibitor, (Gordon *et al.* 2012) and a combination of pravastatin and zeledronate (Gordon *et al.* 2014). Although treated patients showed some improvements, including the ability to gain additional weight, increased flexibility of blood vessels, decreased incidence of strokes, improved bone structure and an extension of mean survival of 1.6 years (Gordon *et al.* 2012), to date, there is no cure or treatment for this disease.

In order to investigate the mechanisms underlying HGPS and potential therapeutic strategies to thwart its progression, several experimental models have been produced. The *Lmna*$^{G609G/G609G}$ mice were engineered to harbor a mutation at the LMNA gene (1827C>T; Gly609Gly) analogous to the one found in HGPS patients (Osorio *et al.* 2011), and phenocopy most of the features that characterize HGPS patients, including the accumulation of progerin, lipodystrophy, bone and cardiovascular defects and reduced lifespan (Osorio *et al.* 2011). *Lmna*$^{G609G/+}$ mice also recapitulate the disease, but they display an intermediate phenotype (Osorio *et al.* 2011).

To develop our study, we established a colony of *Lmna*$^{G609G/G609G}$ mice in our animal facility, by the intercrossing of *Lmna*$^{G609G/+}$ mice. Given that we were generating these mice for the first time, it was necessary to first assess if *Lmna*$^{G609G/G609G}$ mice obtained at our animal facility recapitulated the phenotype described by Osorio and colleagues.

We found that *Lmna*$^{G609G/G609G}$ mice were apparently normal at first, however, at 1.5 months of age they already manifested a growth impairment and lower body weight, which was aggravated at 3 months, and at this age, they had already acquired an abnormal posture and curvature of the spine. We further examined the phenotype of *Lmna*$^{G609G/G609G}$ mice, and observed that the blood glucose levels were decreased relatively to *Lmna*$^{+/+}$ mice. The weight of WAT was decreased, suggesting that *Lmna*$^{G609G/G609G}$ mice are lipodystrophic. Spleen size was also diminished, pointing to

the development of immune defects. All these features were reported by Osorio and colleagues, which led us to the conclusion that the *Lmna*$^{G609G/G609G}$ mice generated at our animal facility were recapitulating the phenotype previously reported (Osorio 2011), allowing us to move forward with our study.

One puzzling fact about HGPS is that despite the fact that it resembles normal aging in diverse aspects, mimicking several processes occurring during this process. HGPS patients do not exhibit overt neurological symptoms besides those resulting from the accumulated damage caused by the occurrence of "silent" infarcts (Ullrich and Gordon 2015). It is thought that miR9 prevents the accumulation of progerin in neural cells, thereby protecting neurons from the deleterious effects of this process (Nissan *et al.* 2012), and this may explain the lack of clinically evident symptoms at the level of the CNS. Another hypothesis is the fact that HGPS patients may not live long enough in order to undergo evident alterations in their brain. Apart from this study, our perception of what occurs in the CNS of these patients is diminutive and it is necessary to understand it in more detail.

A growing body of evidences has been linking hypothalamic dysfunction with whole-body aging (Satoh, Brace et al. 2013, Zhang, Li et al. 2013, Satoh, Brace et al. 2015, Cavadas, Aveleira et al. 2016), and this led us to hypothesize whether the hypothalamus of *Lmna*$^{G609G/G609G}$ mice could be altered due to the premature aging process. Therefore, the first aim of our study was to investigate potential alterations in the hypothalamus of *Lmna*$^{G609G/G609G}$ mice.

To this end, we first analyzed the levels of orexigenic and anorexigenic hypothalamic-derived neuropeptides in different hypothalamic nuclei, since hypothalamic function is strongly dependent on the concerted action of these molecules and hypothalamic neuronal populations within these nuclei. We know from previous reports that NPY levels are decreased with age in rodents and elderly humans (Gruenewald *et al.* 1994, Chiodera *et al.* 2000, Veyrat-Durebex *et al.* 2013). Using immunohistochemistry experiments we found that NPY protein levels were differently altered in the hypothalamus of *Lmna*$^{G609G/G609G}$ mice. We observed that NPY levels appear to be upregulated with the progression of the disease in *Lmna*$^{G609G/G609G}$ mice, in contrast to what is described in normal aging (Gruenewald *et al.* 1994, Veyrat-Durebex *et al.* 2013). Interestingly, *Lmna*$^{G609G/+}$ mice showed no evident changes in the levels of this neuropeptide along time, however, when we compared with age-matched *Lmna*$^{+/+}$ mice we observed a decrease in NPY levels, especially at later stages, concordant to what is described to occur in normal aging (Gruenewald *et al.* 1994, Veyrat-Durebex *et al.* 2013). We cannot explain the differences between *Lmna*$^{G609G/G609G}$ and *Lmna*$^{G609G/+}$ mice in the NPY levels as the disease progresses, but one hypothesis is that this may be caused by the different severity of the phenotypes, and alterations in the metabolic machinery.

Lmna$^{G609G/G609G}$ mice exhibited a tendency to have higher POMC levels than age-matched *Lmna*$^{+/+}$ mice in the PVN, DMH and, to some extent, ARC. These nuclei are

crucial for the regulation of food intake and energy expenditure. POMC, being an anorexigenic neuropeptide, decreases food intake (Elias, Lee et al. 1998, Kristensen, Judge et al. 1998), and its upregulation in *Lmna*$^{G609G/G609G}$ mice may contribute to the observed decrease in food intake of these mice. Moreover, POMC in the PVN is also involved in the regulation of energy expenditure, triggering responses that lead to higher energy consumption (Williams and Elmquist 2012) and thus, it may also be related with the lipodystrophy observed in *Lmna*$^{G609G/G609G}$ mice. On the other hand, *Lmna*$^{G609G/+}$ mice showed lower levels of POMC with increasing age when compared to *Lmna*$^{+/+}$ mice. This decline was in accordance to the findings that normal aged mice have decreased POMC mRNA expression in the hypothalamus (Nelson *et al.* 1988). Interestingly, the regulation of orexigenic and anorexigenic neuropeptides seems to be differentially regulated in *Lmna*$^{G609G/+}$ and *Lmna*$^{G609G/G609G}$ mice. Further studies should be done to explore the underlying regulatory mechanisms of hypothalamic neuropetides.

To support our results, and further explore the alterations occurring in hypothalamic neuropepides in *Lmna*$^{G609G/G609G}$ mice, we analyzed NPY and AgRP, orexigenic neuropeptides, and POMC and CART, anorexigenic neuropeptides, gene expression within hypothalamus by qPCR. Similar to NPY immunoreactivity, we observed an increase in NPY, and also AgRP, expression in *Lmna*$^{G609G/G609G}$ mice. On the other hand, POMC gene expression was decreased in these mice, in opposition to what was observed for POMC protein immunoreactivy in the different hypothalamic nuclei, which may be the derive from the fact that gene expression was evaluated in whole-hypothalamus lysates. Moreover, with age, the alterations in the expression of these genes goes in opposite directions in *Lmna*$^{+/+}$ and *Lmna*$^{G609G/G609G}$ mice, which pinpoints a possible dysregulation of the hypothalamic function and may have impact on energy balance regulation and lipodystrophy progression observed in *Lmna*$^{G609G/G609G}$ mice.

Interestingly, NPY Y_1R and Y_5R receptors gene expression modestly decreases with age in *Lmna*$^{G609G/G609G}$ mice, which could constitute a compensatory mechanism, to prevent excessive receptor activation, triggered by the upregulation of NPY (Babilon *et al.* 2013). These receptors are widely expressed in the CNS, including the hypothalamus (Fetissov *et al.* 2004), with NPY Y_1R being expressed in magnocellular and parvocellular neurons. The activation of these receptors is important for the regulation of feeding.

We also observed alterations in hypothalamic neuronal structure in *Lmna*$^{G609G/G609G}$ mice. The immunoreactivity of NeuN, a neuron-specific marker found only in postmitotic, differentiated, neurons (Gusel'nikova and Korzhevskiy 2015), had a tendency to be increased (VMH) or decreased (DMH, PVN) when comparing to age-matched *Lmna*$^{+/+}$ mice. NeuN immunoreactivity was not altered in the ARC. These results suggest that in the DMH and PVN there is a lower number of differentiated neurons than in *Lmna*$^{+/+}$, while in the VMH the opposite holds true. Interestingly, *Lmna*$^{G609G/+}$ mice showed a decrease in the levels of NeuN with increasing age

comparing to *Lmna*$^{+/+}$ mice. What caused this differential effect is currently unknown, but may be due to the differences in the phenotype or neuronal density in each nuclei. To strengthen our observations, we could determine the number of positive cells for NeuN in each nucleus. Moreover, to further elucidate this process it would be interesting to evaluate cellular death and neurogenesis in the hypothalamus of these mice or hypothalamic neuronal primary cultures derived from Lmna$^{G609/G609G}$ mice.

Inflammation in the hypothalamus has been associated with the progress of systemic aging (Zhang *et al.* 2013). To investigate whether inflammation occur in the hypothalamus of *Lmna*$^{G609G/G609G}$ we analyzed potential alterations in GFAP, a widely used marker for the labeling of reactive astrocytes (Sofroniew and Vinters 2010), and Iba-1, a marker used for the identification of microglial cells (Jeong *et al.* 2013), since these cells participate and mediate, along with neurons, brain inflammatory processes (Jeong *et al.* 2013). We observed that GFAP immunoreactivity did not change with disease progression in *Lmna*$^{G609G/G609G}$ mice, showing no signs of astrogliosis. In fact, we observed a decrease in GFAP expression in the hypothalamus of these mice. On the other hand, at 1.5 months of age, *Lmna*$^{G609G/G609G}$ mice showed increased Iba-1 levels when compared to *Lmna*$^{+/+}$ mice, suggesting microglia reactivity. However, a decline in Iba-1 levels occurs with increasing age, which points to an impairment of immune responses in these mice. These results are supported by the finding that CD11b expression, a marker of microglia and macrophages, was also upregulated at 1.5 months in *Lmna*$^{G609G/G609G}$ mice, but it declined over time. We also measured the gene expression of an anti-inflammatory cytokine, IL-10, and found that it decreased with the phenotype progression, further suggesting a dysregulation of the immune responses. Signals from the altered periphery, observed in these mice, may affect inflammatory markers in the hypothalamus which can subsequently have an impact on hypothalamic responses.

Interestingly, GFAP immunoreactivity increased in the hypothalamus of *Lmna*$^{G609G/+}$ with the progression of the phenotype, being higher than those observed in *Lmna*$^{+/+}$ mice, particularly at later stages. Iba-1 immunoreactivity was also upregulated in these mice relatively to *Lmna*$^{+/+}$ mice, in most nuclei, at early stages, however, with age they declined to similar levels of wild-type mice.

As previously explained, neural cells appear to be protected from the deleterious effects of progerin accumulation due to the activity of miR9 (Nissan *et al.* 2012). Neural precursor cells originate not only neurons, but also glial cells, in which astrocytes are included (Qian *et al.* 2000, Asano *et al.* 2009), and therefore, these are also spared from progerin toxic consequences. Conversely, even though also present in the CNS, microglia are not derived from the same precursor cells of neurons and astrocytes and are, probably, affected by HGPS cellular aging phenotype. This way, astrocytes may remain at constant levels with the progression of HGPS phenotype in *Lmna*$^{G609G/G609G}$ mice, while microglial cells undergo the aging phenotype observed in HGPS cells. The divergent results obtained between *Lmna*$^{G609G/+}$ and *Lmna*$^{G609G/G609G}$ mice regarding

GFAP and Iba-1 levels could be based on the difference in the severity of the phenotype presented by these animals (Osorio *et al.* 2011). One hypothesis is that signals from the aged periphery and CNS may activate microglia cells in *Lmna*$^{G609G/+}$ mice, which are not so severely affected as in *Lmna*$^{G609G/G609G}$, and consequently, astrocytes would be recruited to mediate inflammatory responses (Jeong *et al.* 2013), explaining the observed upregulation of GFAP levels. In *Lmna*$^{G609G/G609G}$ mice, however, microglia could be already unable to trigger such mechanisms, thereby, GFAP levels in the hypothalamus of these animals would not vary, while Iba-1 would decline with time. The decrease in Iba-1 levels may also be related with the immune system defects thought to occur in these mice. These are just hypothesis that need further studies to be confirmed.

This was the first study to show alterations in the hypothalamus in this HGPS mouse model, and to diverge from the well-established idea that CNS is not affected in this disease. Many of the results are difficult to explain due to the lack of studies focused on the CNS in HGPS scope. This was a really exploratory study and numerous questions are still to be answered, and most of all, to be made. We need to increase the number of animals in order to strengthen our analysis. Furthermore, it is also necessary to perform metabolic and biochemical studies to understand the interconnection between hypothalamus, aging and metabolism in these mice.

Although HGPS is an extremely rare disease, affecting one in four million newborns (Gordon *et al.* 2014), many efforts are being made in order to find therapies that could improve the life quality of these children, or even its cure. In line with this, our second aim was to investigate the potential of ghrelin administration as a therapeutic strategy to thwart HGPS aging phenotype in *Lmna*$^{G609G/G609G}$ mice.

Why ghrelin? Ghrelin is a hormone mainly produced in the stomach (Kojima *et al.* 1999) that is synthesized and secreted into the bloodstream in preprandial periods (Cummings *et al.* 2001), targeting several tissues in the organism, including the CNS. Diverse functions have been attributed to ghrelin besides its classical role in the induction of GH release (Kojima *et al.* 1999) and stimulation of food intake and body weight gain (Nakazato *et al.* 2001). Among these lie several actions that pinpoint the potentiality of ghrelin to counteract HGPS progression namely the stimulation of proliferative capacity of the cells (Murata *et al.* 2002, Duxbury *et al.* 2003, Kim *et al.* 2004, Mazzocchi *et al.* 2004, Kim *et al.* 2005, Yu *et al.* 2013), regulation of glucose metabolism (Reimer *et al.* 2003, Dezaki *et al.* 2004), energy expenditure and adiposity (Tschop *et al.* 2000, Theander-Carrillo *et al.* 2006) its protective effects on cardiovascular system (Nagaya *et al.* 2001, Baldanzi *et al.* 2002), and the impact on muscle (Sugiyama *et al.* 2012, Porporato *et al.* 2013, Reano *et al.* 2017) and bones (Fukushima *et al.* 2005). Moreover, recent data obtained by our group shows the beneficial effects of ghrelin in fibroblasts obtained from HGPS patients, where it was able to revert the major hallmarks of cellular aging in HGPS cells, supporting ghrelin as a potential therapeutic strategy for HGPS.

To investigate whether ghrelin could ameliorate or delay the progression of HGPS phenotype, *Lmna*$^{+/+}$, *Lmna*$^{G609G/+}$ and *Lmna*$^{G609G/G609G}$ were subjected to a chronic treatment with ghrelin (daily administration for 1.5 months). Upon mice sacrifice, and an extensive analysis of ghrelin treatment outcomes on mice phenotype and histopathological and molecular alterations in several peripheral organs and tissues, including hypothalamus, was performed.

Lmna$^{G609G/G609G}$ mice displayed an overall healthier aspect upon treatment, with no signs of kyphosis of the spine. We observed that ghrelin treatment increased body weight gain in *Lmna*$^{+/+}$, and the increase in the food intake may have contributed to this effect, as expected (Nakazato *et al.* 2001). In *Lmna*$^{G609G/G609G}$ mice, ghrelin induced a modest increase in the body weight gain, however, it did not significantly stimulate food intake in these mice, which may suggest that food intake is not the only process responsible for the accumulation of body weight. Ghrelin, in addition to stimulate ingestion of food, thereby promoting weight gain, plays also a role in decreasing energy expenditure (Tschop *et al.* 2000, Theander-Carrillo *et al.* 2006). This way, the administration of ghrelin could be increasing body weight gain through two independent mechanisms. Although the treatment did not completely rescue the weight of *Lmna*$^{G609G/G609G}$ mice to similar values of *Lmna*$^{+/+}$, it prevented the progressive weight loss observed in vehicle-treated *Lmna*$^{G609G/G609G}$ mice at later stages, which was a very promising result in the context of HGPS pathology.

Ghrelin treatment increased blood glucose levels in both *Lmna*$^{+/+}$ and *Lmna*$^{G609G/G609G}$ mice, and this may be related with an inhibition of insulin secretion, already described for ghrelin (Dezaki *et al.* 2004). Ghrelin effect on blood glucose levels may constitute a protective mechanism by which, in fasting periods when glucose levels are low, it may minimize hypoglycemia by decreasing glucose uptake by the different tissues. Since *Lmna*$^{G609G/G609G}$ mice show hypoglycemia (Osorio 2011) that could aggravate the cardiovascular abnormalities observed in these animals (Wright and Frier 2008, Frier *et al.* 2011), ghrelin effect on blood glucose levels can have a beneficial impact on cardiovascular functions and therefore minimize disease's progression.

HGPS patients do not display any neurological symptoms, and cognitively, are considered normal children (Ullrich and Gordon 2015). Supporting this notion, transgenic mice engineered to express HGPS mutation in the brain, skin, bone and heart did not reveal any alterations in behavioral tests (Baek *et al.* 2015). Our observations, however, although not statistically significant, showed alterations in the locomotor activity of these mice. *Lmna*$^{G609G/G609G}$ mice have a tendency to travel shorter distances, with an associated decrease in the mean velocity, than *Lmna*$^{+/+}$ mice. One hypothesis that needs to be confirmed is that *Lmna*$^{G609G/G609G}$ mice may present muscular atrophy and bone alterations that could interfere with their locomotor performance. This is supported by the discovery that the skeletal muscle fibers are smaller in *Lmna*$^{G609G/G609G}$ mice compared to *Lmna*$^{+/+}$ mice. Interestingly, we

observed that *Lmna*$^{G609G/G609G}$ mice spent more time in the center region of the arena than *Lmna*$^{+/+}$ mice, which may suggest that they present lower anxiety levels.

Upon ghrelin treatment, mice of the three genotypes had a tendency to travel shorter distances, with decreased mean velocity. In addition, ghrelin treated mice spent less time on the center of the arena than vehicle-treated mice. This behavior may suggest anxiogenic processes, but this hypothesis needs to be further investigated with other behavioral tests, like the elevated plus maze, and the analysis of stress markers, like corticosterone, for instance. In addition, it would be interesting to evaluate motor function and coordination in these mice through rotarod and horizontal bars test. Although there are no reports on memory impairments in HGPS, it would be also pertinent to evaluate potential memory alterations in these mice by performing Y-maze test or novel object recognition tests.

Ghrelin is known to be involved in the modulation of stress and anxiety (Bali and Jaggi 2016), although diverse conflicting studies addressing the specific effects exist. Exogenous administration of ghrelin was shown to increase CRH mRNA expression in the hypothalamus of mice (Asakawa *et al.* 2001, Cabral *et al.* 2012), and cortisol and ACTH in humans (Takaya *et al.* 2000, Arvat *et al.* 2001). However, the elucidation of the biological significance of these data is still under debate, with authors finding evidences that ghrelin promotes anxiolytic-like behaviors (Lutter *et al.* 2008, Spencer *et al.* 2012, Huang *et al.* 2017), while authors indicate the opposite (Hansson *et al.* 2011, Currie *et al.* 2012). It has been hypothesized that ghrelin may play a dual role in anxious behavior, with differential effects under basal or stressed conditions. Under basal conditions, ghrelin seems to trigger anxiety-like behaviors, but after stress, ghrelin may further enhance the rise in glucocorticoids to activate HPA axis negative feedback loop, preventing its overstimulation and deleterious effects (Spencer *et al.* 2012, Bali and Jaggi 2016). Despite this interaction with the HPA axis, ghrelin has been used in clinical trials without harmful effects being described (Collden *et al.* 2017).

The size of most organs did not change significantly with ghrelin treatment. However, we did find changes in WAT, spleen and thymus in ghrelin-treated *Lmna*$^{G609G/G609G}$ mice.

The most prominent effect of ghrelin treatment was at the level of WAT. We found that the adipocytes of *Lmna*$^{G609G/G609G}$ mice were smaller when compared to *Lmna*$^{+/+}$ and *Lmna*$^{G609G/+}$ adipocytes which may suggest an impaired capacity of these cells to store lipids, and may represent one of the causes for the lipodystrophy of these animals. Capanni and colleagues reported the *in vivo* interaction between prelamin A and SREBP1, a transcription factor upstream of PPARγ, essential for adipocyte differentiation. This interaction resulted in the sequestration of SREBP1 at the nuclear periphery with a concomitant downregulation of its target genes (Capanni *et al.* 2005). This process may be shared by progerin which is known to sequester several transcriptional factors at the nuclear periphery through the same mechanism (Scaffidi and Misteli 2008, Ghosh *et al.* 2015). Taking this into account, we can hypothesize that

the structural changes that we observed in the WAT of *Lmna*$^{G609G/G609G}$ mice may be caused by impairment of the adipogenic process. On the other hand, other mechanism that could explain this alteration would be the browning of the WAT (Wu *et al.* 2013), given the similarities between WAT adipocytes in *Lmna*$^{G609G/G609G}$ WAT with BAT adipocytes. However, to explore both theories, further experiments using specific preadipocytes, BAT and mitochondrial markers, like Pref-1, UCP-1, and PGC-1, and PGC-1α, respectively, should be performed to better understand WAT physiology.

In *Lmna*$^{G609G/+}$ and *Lmna*$^{G609G/G609G}$ mice, the gonadal WAT weight significantly increased upon ghrelin treatment. This effect may be explained by the well described ghrelin's action on adiposity (Tschop *et al.* 2000, Theander-Carrillo *et al.* 2006) and energy expenditure inhibition, with the consequent accumulation of energy in adipose tissue in the form of lipids. Nevertheless, to confirm this hypothesis further studies should be performed, namely metabolic studies as well as biochemical analysis of lipids and hormones involved in metabolism and energy expenditure regulation.

One major finding of our study was that ghrelin treatment was able to rescue, almost completely, the structural abnormalities found in the WAT adipocytes in *Lmna*$^{G609G/G609G}$ mice. We did observe that adipocyte size increased in Lmna$^{G609G/G609G}$ mice upon ghrelin treatment, and this may be related with an increase in adipocyte differentiation and lipid accumulation. Ghrelin can directly act on adipocytes which express GHSR, and was shown to increase proliferation of 3T3-L1 preadipocytes (Kim *et al.* 2004). Its administration in rats resulted in cellular adaptations in white adipocytes related with increased expression of genes involved in the synthesis and storage of lipids (Theander-Carrillo *et al.* 2006). We also observed that ghrelin treatment also had an impact on molecular mechanisms in adipocytes. In fact, we analyzed potential alterations in some key proteins related with mechanisms known to be altered or compromised with aging, namely autophagy and cell proliferation. The levels of LC3B-II and SQSTM1, autophagy markers (Klionsky *et al.* 2016) were both decreased in *Lmna*$^{+/+}$ and *Lmna*$^{G609G/G609G}$ mice, suggesting that ghrelin is enhancing autophagy in WAT adipocytes. In accordance, ghrelin's effects on autophagy stimulation have been previously reported by our group in cortical neurons (Ferreira-Marques *et al.* 2016) and also in HGPS fibroblasts. These results raise the possibility that ghrelin treatment may lead to progerin clearance by autophagy, improving cell structure and function. Unfortunately, we were not able to measure progerin levels which could be crucial in order to assess if ghrelin was indeed stimulating its clearance. We also evaluated PCNA levels, a marker of cell proliferation (Kubben *et al.* 1994), and found that ghrelin induced a tendency towards an increase in its protein levels in the three genotypes. This may indicate that ghrelin is increasing cellular proliferation in this tissue, which is in accordance to what is described in the literature (Kim *et al.* 2004).

Here we show that ghrelin stimulated WAT accumulation and improved the observed histological alterations in *Lmna*$^{G609G/G609G}$ mice, thwarting the characteristic

lipodystrophy in this model, supporting ghrelin as a potential therapeutic strategy for HGPS.

Ghrelin administration led to a reduction of thymus size in *Lmna*$^{G609G/+}$ and *Lmna*$^{G609G/G609G}$ mice, an observation that was surprising taking into account the findings of Dixit and colleagues, where it is shown that ghrelin improved age-associated changes of the thymus, attenuating its involution and promoting thymopoiesis (Dixit *et al.* 2007). We cannot exclude the hypothesis that ghrelin impact on anxiety and stress may be causing an effect on the immune system of these mice. This reinforces the idea that it will be necessary the execution of specific experiments focused on the evaluation of the stress and anxiety markers, and anxiety-like behaviors.

The spleen weight of *Lmna*$^{+/+}$ and *Lmna*$^{G609G/+}$ mice was also shown to be decreased upon ghrelin treatment. One possible explanation may be a decrease in the proliferation of splenic lymphocytes (Xia *et al.* 2004) that could provoke a reduction in spleen size. However, in ghrelin-treated *Lmna*$^{G609G/G609G}$ mice we observed a tendency for an increase of the spleen. Ghrelin's differential effect can be caused by the already identified involution of the *Lmna*$^{G609G/G609G}$ mice spleen. Although our data regarding spleen and thymus sizes may suggest a detrimental role for ghrelin in immune activity, through histological analysis we found that the *Lmna*$^{G609G/G609G}$ mice spleen showed an increase in the white pulp area, the splenic lymphoid tissue, in ghrelin-treated animals. Since white pulp is the region of the spleen devoted to the proliferation and maturation of lymphocytes (Mebius and Kraal 2005) this result may suggest an increment in lymphocytes production and consequent strengthening of the immune function. Interestingly, it was described an atrophy of the white pulp in the spleen of aged rats, and it is tempting to speculate if ghrelin can exhibit the same effects on naturally aged mice. In addition, several studies support an overall improvement of immune function and inflammatory profiles with ghrelin administration (Himmerich and Sheldrick 2010, Taub *et al.* 2010, Baatar *et al.* 2011).

The accumulation of adipose tissue, *per se*, cannot explain the full extent of increased body weight gain in *Lmna*$^{G609G/G609G}$ mice. We were not able to weigh muscle and bone but alterations in the weight of both tissues certainly may contribute to weight gain upon ghrelin treatment. Ghrelin has been shown to have protective properties against skeletal muscle atrophy in cachexic mice (Porporato *et al.* 2013), to reduce muscle degeneration and improve muscle function in dystrophic mice (Reano *et al.* 2017) and to increase mineral bone density in ghrelin-administered rats (Fukushima *et al.* 2005), supporting the contribution of these tissues to the overall increase in body weight. Although we did not find gross histological alteration in the skeletal muscle tissue of *Lmna*$^{G609G/G609G}$ mice, we did find that skeletal muscle fibers were smaller in these mice compared to *Lmna*$^{+/+}$, suggesting muscle fiber atrophy, which may indicate reduced muscle function in these mice (Maughan *et al.* 1983, Organ *et al.* 2016). Interestingly, ghrelin administration rescued muscle fiber size in

Lmna$^{G609G/G609G}$ mice and this effect may result of ghrelin stimulation of myocyte fusion and differentiation into myotubes, which was already described in C2C12 skeletal myoblasts (Filigheddu, Gnocchi et al. 2007). This process may underlie the beneficial effects of ghrelin in skeletal muscle observed also in models of cachexic mice (Sugiyama *et al.* 2012). Given ghrelin's action in bone metabolism, and the fact that *Lmna*$^{G609G/G609G}$ show signs of osteoporosis, we are also analyzing ghrelin's effect on the bone histopatholical alterations in these mice.

The liver is one of the most important metabolic organs and its function is deteriorated with age. In fact, during aging, the size and volume of the liver declines as well as its regenerative capacity, due to inhibition of hepatocyte proliferation (Schmucker 2005, Schmucker and Sanchez 2011). We performed histological analysis in liver sections in order to assess possible alterations in its structure and we did not observe major alterations between *Lmna*$^{G609G/G609G}$ mice and *Lmna*$^{+/+}$ animals. However, the hepatocytes of *Lmna*$^{G609G/G609G}$ mice were smaller than in *Lmna*$^{+/+}$ and *Lmna*$^{G609G/+}$ mice, and this difference may be related with the higher number of lipid vacuoles present within hepatocytes from *Lmna*$^{+/+}$ and *Lmna*$^{G609G/+}$ mice. This may result from the fact that mice were subjected to 8 hours of fasting before sacrifice. Fasting is known to promote lipolysis and release of fatty acids from the adipose tissue to liver and muscle, where they are used to produce energy (muscle) or be stored as triglycerides (liver) (Browning *et al.* 2012). We also detected these lipid vacuoles in hepatocytes of *Lmna*$^{G609G/G609G}$ mice, however, they were in low number and smaller. One hypothesis for these differences may be the fact that *Lmna*$^{G609G/G609G}$ mice are lipodystrophic, and do not accumulate lipid stores, therefore, their response to fasting mobilizing lipids may be compromised. In addition, we also noticed that the nuclei of hepatocytes from *Lmna*$^{G609G/G609G}$ mice were smaller and irregular. We also observed decreased collagen staining around the blood vessels which can be related to age-associated dysfunctions. This organ is poorly studied in the HGPS context, with patients not showing symptoms related with its functions (Ullrich and Gordon 2015). However, since the liver regenerative capacity is decreased with aging (Schmucker and Sanchez 2011), we decided to analyze the hepatocytes density in these mice. We did not find significant alterations between the different genotypes, however, upon ghrelin treatment the number of hepatocytes was significantly increased in *Lmna*$^{+/+}$, *Lmna*$^{G609G/+}$ and *Lmna*$^{G609G/G609G}$ mice. We hypothesized that this may reflect an improvement in the liver regenerative capacity, since hepatocytes constitute a quiescent population of cells that proliferate during the normal liver regenerative process (Schmucker and Sanchez 2011). For this to occur, it is required the activation of mitogenic genes, along with the repression of cell cycle repressors (Schmucker and Sanchez 2011). Osorio and colleagues showed that the expression of p53 targets is upregulated in the liver of *Lmna*$^{G609G/G609G}$ mice and sections of this tissue present increased senescence-associated β-galactosidase staining (Osorio *et al.* 2011), suggesting that disease progression may in fact inhibit hepatocyte proliferation, and

therefore impair liver regenerative capacity To explore this hypothesis, we assessed, by western blot, the protein levels of PCNA in liver lysates. Interestingly, ghrelin treatment did not increase the levels of this proliferation marker. Data from our group, show however that PCNA levels are highly increased in the liver of *Lmna*$^{G609G/G609G}$ mice, when compared to *Lmna*$^{+/+}$, which does not necessarily mean augmented rates of proliferation. Actually, a recent paper reports that progerin sequesters PCNA in HGPS cells, thus affecting DNA replication (Hilton *et al.* 2017). Therefore, PCNA can be upregulated as a compensatory mechanism of the cells, and this would explain its exacerbated levels in the liver of *Lmna*$^{G609G/G609G}$ mice. If this holds true, ghrelin treatment may actually be thwarting this process, normalizing PCNA levels. Since the gene expression of several p53 targets was described to be incremented in *Lmna*$^{G609G/G609G}$ mice (Osorio *et al.* 2011), we also evaluated p53 levels in this tissue. In fact, p53 is an important molecular player involved in cell cycle arrest and in the cellular response to DNA damage (Rufini *et al.* 2013). We observed that ghrelin treatment significantly reduced the levels of p53 in *Lmna*$^{+/+}$ and *Lmna*$^{G609G/+}$ mice, which may contribute to the increased number of hepatocytes assessed in liver sections. On the other hand, ghrelin treatment did not alter p53 protein levels in *Lmna*$^{G609G/G609G}$ mice. Further studies are necessary to better understand these results, and the reasons behind the increase in hepatocyte number upon ghrelin treatment. Although we did not observe modifications in p53 levels in ghrelin-treated *Lmna*$^{G609G/G609G}$ mice comparing to vehicle-treated animals, that does not mean that its activity is not altered. It would be interesting to evaluate p53 downstream targets, like p21, to understand if its activity is, indeed, altered. Altogether, our results imply that ghrelin may play a role in thwarting liver cellular senescence and promote the regenerative capacity of this organ, which may be useful in normal aging.

Since HGPS is characterized by severe cardiovascular defects (Ullrich and Gordon 2015), features that are shared by *Lmna*$^{G609G/G609G}$ mice (Osorio *et al.* 2011), we also evaluated histological parameters in the aorta of *Lmna*$^{G609G/G609G}$ mice. We found that the aorta of *Lmna*$^{G609G/G609G}$ mice comprised a lower number of cells in its walls compared to *Lmna*$^{+/+}$ mice. This is in agreement with the report made by Osorio and colleagues, where they describe a loss of VSMCs in the aortic arch (Osorio *et al.* 2011), that is suggested to be related with cardiovascular abnormalities in these mice. Ghrelin treatment provoked a subtle amelioration of this parameter. The lack of visible effects of ghrelin in the aorta is surprising, since this system is one of the targets of this hormone, where it was shown to have protective roles in cardiomyocytes (Baldanzi, Filigheddu et al. 2002) and delay cardiac cachexia (Nagaya, Uematsu et al. 2001). However, to fully assess the impact of ghrelin in this system, it would be important to analyze not only the aorta, but also perform a deper analysis of heart histopathology and to perform functional studies in these structures. In addition, it would be interesting to evaluate inflammation markers and alterations in cardiac stem cells.

The kidney of *Lmna*$^{G609G/G609G}$ mice show increased senescence-associated β-galactosidase staining when compared to wild-type controls (Osorio *et al.* 2011), but besides this observation, the impact of premature aging on this organ in poorly understood. In fact, HGPS patients do not show alterations in kidney function (Ullrich and Gordon 2015), however, during normal aging, this structure is affected, with a decrease in the functional glomeruli and a consequent compensatory hypertrophy in the remaining (Denic *et al.* 2016). In agreement with previous reports, we did not find any histological alterations in the kidney of *Lmna*$^{G609G/G609G}$ mice, compared to *Lmna*$^{+/+}$ mice. Moreover, ghrelin treatment had no effect on the structure of the kidney or in the renal corpuscle area.

The skin of HGPS patients is extremely affected by disease progression (Hennekam 2006). Alterations in the skin of *Lmna*$^{G609G/G609G}$ mice were also reported (Osorio *et al.* 2011), including the loss of subcutaneous fat layer and attrition of hair follicles, however, these observations were only based on qualitative assessments, without being further studied.

To understand how premature aging impacts the skin of *Lmna*$^{G609G/G609G}$ mice we performed histomorphometric analysis of this tissue. We observed that *Lmna*$^{G609G/G609G}$ mice show a general decrease in the thickness of the epidermis, dermis and hypodermis, comparing to *Lmna*$^{+/+}$ mice. However, the alterations in hypodermis are more pronounced, which is probably related with the severe lipodystrophy of these animals (Osorio *et al.* 2011). These results are concomitant with the reports describing that HGPS patients have thinner skin, which makes their veins salient (Hennekam 2006). In fact, with normal aging process, skin also thins progressively due to a decline in epidermal cell numbers, reduction of the vascularity and cellularity in the dermis, and also diminished subcutaneous fat in the hypodermis (Farage *et al.* 2013). Our group showed that *Lmna*$^{G609G/G609G}$ mice have decreased levels of PCNA in the skin compared to wild-type animals. We can therefore speculate if the thinning in the skin layers of this model is not aggravated by decreased cellular proliferation, as it occurs in normal aging.

In this study we found that ghrelin treatment rescued the thinning of the epidermal layer in *Lmna*$^{G609G/G609G}$ mice which can be triggered by an enhancement of cellular proliferation. This idea is strongly supported by the protein levels analysis. Ghrelin-treated *Lmna*$^{G609G/G609G}$ mice exhibited a marked increase in the levels of PCNA compared to vehicle-treated controls, which suggests an increment in cellular proliferation. Moreover, p53 levels in these animals also presented a tendency to be decreased, therefore diminishing its role in cell cycle arrest.

One hypothesis to explain the observed beneficial effects of ghrelin treatment in the thickness of the epidermal layer of the skin of *Lmna*$^{G609G/G609G}$ mice is that ghrelin may be the induction of the proliferation of preexisting keratinocytes, given its well-established role in promoting cell proliferation (Murata *et al.* 2002, Duxbury *et al.* 2003, Kim *et al.* 2004, Mazzocchi *et al.* 2004, Kim *et al.* 2005, Yu *et al.* 2013). Another

possible mechanism underlying this effect may also consist in the potential role of ghrelin to increase stem cell proliferation and differentiation, which has already been described in diverse models (Moon *et al.* 2009, Gao *et al.* 2013). It would be interesting to further study whether ghrelin is indeed promoting proliferation in the epidermis of the *Lmna*$^{G609G/G609G}$ mice skin through the study of other markers, for instance Ki67, and to also assess its effect on the proliferation and differentiation capacity of skin stem cells.

Ghrelin also promoted the thickening of the subcutaneous fat layer in *Lmna*$^{G609G/G609G}$ mice, thus counteracting one of the most important HGPS features (Merideth *et al.* 2008, Osorio *et al.* 2011). These results are probably associated with the accumulation of adipose tissue observed in these animals upon ghrelin treatment, and support the idea that ghrelin is having an important contribution for the rescue of the lipodystrophy observed in *Lmna*$^{G609G/G609G}$ mice.

Age-associated changes in the skin also include decreases in the extracellular matrix components, for that reason, we investigated whether deposition of collagen, the most abundant component of skin, was altered in *Lmna*$^{G609G/G609G}$ mice. For that we performed Masson's trichrome staining in skin sections, and observed that collagen staining intensity was diminished in *Lmna*$^{G609G/G609G}$ mice comparing to *Lmna*$^{+/+}$ mice, as well as the collagen fiber bundles appeared to be thicker. This result may suggest that HGPS alters the synthesis, turnover and organization of collagen fibers (Farage *et al.* 2013). Ghrelin administration attenuated the collagen loss, suggesting that it may be increasing the collagen synthesis or turnover. To further elucidate these processes, we could perform, in addition, a Sirius red staining to better distinguish the collagen fibers. Collagen levels could also be measured by western blotting techniques.

The knowledge that ghrelin exerts its effects both at peripheral and central levels, and that in fact, food intake and energy expenditure are processes under the central modulation of ghrelin (Nakazato *et al.* 2001), led us to investigate the impact of ghrelin treatment on hypothalamic function, by gene expression analysis. We found that ghrelin administration in *Lmna*$^{+/+}$ mice caused an expected increase in NPY and AgRP gene expression, and a concomitant decrease in POMC expression, which was in accordance to the described functions of ghrelin (Cowley *et al.* 2003). However, ghrelin-treated *Lmna*$^{G609G/G609G}$ mice displayed a tendency to have decreased levels of NPY and AgRP gene expression than vehicle-treated *Lmna*$^{G609G/G609G}$ mice, which does not coincide with the common effects of ghrelin administration (Cowley *et al.* 2003). In the first part of our work, we had identified some hypothalamic alterations at the level of gene expression, between *Lmna*$^{+/+}$ and *Lmna*$^{G609G/G609G}$ mice, including the greater NPY/AgRP, and decreased POMC, expression in 3 months-old *Lmna*$^{G609G/G609G}$ mice than age-matched *Lmna*$^{+/+}$. This suggested a dysregulation of the hypothalamic function. Taking this into account, it seems that ghrelin treatment is somehow reverting the observed alterations in the expression of these neuropeptides, which could be a beneficial action. Moreover, we also evaluated the gene expression of three

NPY receptors, and found that, in general, ghrelin treatment downregulated Y_1R, Y_2R and Y_5R expression, with more pronounced effects on Y_2R, in *Lmna*$^{G609G/G609G}$ mice. This decrease may be occurring as a compensatory mechanism since NPY levels in *Lmna*$^{G609G/G609G}$ mice are upregulated (Babilon *et al.* 2013).

Since we had also observed some signs that suggested an eventual inflammatory process in the hypothalamus of *Lmna*$^{G609G/G609G}$ mice, we also assessed the impact of ghrelin treatment in the expression of genes associated with these responses. We found that ghrelin administration led to a decline in CD11b, a marker of immune cells, in *Lmna*$^{G609G/G609G}$ and *Lmna*$^{+/+}$ mice, and to an increase of IL-10 expression, an anti-inflammatory cytokine. These results suggest that ghrelin treatment may be promoting an anti-inflammatory environment in the hypothalamus of *Lmna*$^{+/+}$ and *Lmna*$^{G609G/G609G}$ mice. In fact, it is known that ghrelin exerts anti-inflammatory roles in diverse models (Dixit *et al.* 2004, Li *et al.* 2004, Waseem *et al.* 2008, Moon *et al.* 2009).

We also analyzed the potential beneficial effects of ghrelin on neurogenesis and hormone or neurotrophic factors release in the hypothalamus *Lmna*$^{G6909G/G609G}$ mice. Ghrelin treatment decreased the expression of SOX2 in *Lmna*$^{+/+}$ mice. In Lmna$^{G609G/G609G}$ mice, however, ghrelin did not change SOX2 levels. One hypothesis is that ghrelin may be inducing neuronal differentiation (Moon *et al.* 2009), thereby decreasing SOX2 expression. However, this observation is conflicting with previous reports showing the role of ghrelin in the induction of neurogenesis (Zhao *et al.* 2014). Ghrelin treatment provoked a tendency to increased expression of BDNF in the hypothalamus of *Lmna*$^{+/+}$ mice, which suggests a potential role in neuronal survival. We also observed that ghrelin administration enhanced the expression of GnRH in *Lmna*$^{+/+}$ and, to a lesser extent, in *Lmna*$^{G609G/G609G}$ mice. This result was surprising since ghrelin was shown to decrease the firing of GnRH neurons (Farkas *et al.* 2013). One possible explanation for this observation is that ghrelin may in fact be exerting an inhibitory effect on GnRH neurons, but this action could trigger compensatory mechanisms that would eventually stimulate GnRH gene expression. One should keep in mind that *Lmna*$^{G609G/G609G}$ mice present elevated levels of circulating GH, but they show GH resistance, which results in lower IGF1 levels (Osorio *et al.* 2011). These observations suggest that they have alterations in the somatotropic axis, and therefore, GnRH increasing upon ghrelin treatment may have beneficial regulatory effects on this axis. Interestingly, it was previously described that the decline in GnRH may represent an important feature in the driving of systemic aging (Zhang *et al.* 2013). Therefore, the ghrelin-induced increase in GnRH expression in *Lmna*$^{G609G/G609G}$ mice may play a role in the beneficial effects observed upon ghrelin treatment. More studies regarding ghrelin and its impact on hypothalamus have to be carried out in order to further understand how this hormone regulates metabolism and energy expenditure. Moreover, it is also necessary to perform more studies focused on ghrelin and how it affects, and is affected by, whole-body aging.

In conclusion, ghrelin treatment resulted in a healthier appearance in *Lmna*$^{G609G/G609G}$ mice, with increased body weight gain. It stimulated the accumulation of adipose tissue, thwarting the severe lipodystrophy observed in this HGPS model, both in WAT and in the subcutaneous fat layer of the skin. Ghrelin-treated *Lmna*$^{G609G/G609G}$ mice showed some promising improvements in several organs, including in the WAT, skeletal muscle, where ghrelin increased cross-sectional area of the muscle fibers, and skin.

However, there were some aspects that could have improved our work, and helped clarify some of the results. For instance, we were not able to measure progerin levels in the organs studies, which could have given us an idea if ghrelin treatment was indeed promoting progerin clearance. Moreover, we also need to repeat some experiments in order to have a higher sample size, namely in the western blot analysis of WAT of *Lmna*$^{G609G/G609G}$ mice. Most importantly, due to the scarcity of animals, we did not have the opportunity to test different doses of ghrelin in order to find the ideal concentration. The evaluation of lifespan of these mice upon ghrelin treatment would also be of utmost importance in order to ascertain whether ghrelin may extend both health- and lifespan in *Lmna*$^{G609G/G609G}$ mice.

In summary this was the first study to identify hypothalamic alterations in *Lmna*$^{G609G/G609G}$ mice, and to perform an extensive report on histological changes occurring in diverse organs of this mouse model. Moreover, we present promising results pointing ghrelin administration as a potential therapeutic strategy for HGPS. However, there is the need to further understand what are the mechanisms underlying ghrelin's effects in order to establish ghrelin as a promising therapeutic strategy to block HGPS progression.

Chapter 5
References

5. References

Abrahamson, E. E. and R. Y. Moore (2001). "The posterior hypothalamic area: chemoarchitecture and afferent connections." Brain Res **889**(1-2): 1-22.

Adler, A. S., et al. (2007). "Motif module map reveals enforcement of aging by continual NF-kappaB activity." Genes Dev **21**(24): 3244-3257.

Adrian, T. E., et al. (1983). "Neuropeptide Y distribution in human brain." Nature **306**(5943): 584-586.

Andrews, Z. B., et al. (2008). "UCP2 mediates ghrelin's action on NPY/AgRP neurons by lowering free radicals." Nature **454**(7206): 846-851.

Argiolas, A. and M. R. Melis (2005). "Central control of penile erection: role of the paraventricular nucleus of the hypothalamus." Prog Neurobiol **76**(1): 1-21.

Ariyasu, H., et al. (2001). "Stomach is a major source of circulating ghrelin, and feeding state determines plasma ghrelin-like immunoreactivity levels in humans." J Clin Endocrinol Metab **86**(10): 4753-4758.

Armanios, M. (2013). "Telomeres and age-related disease: how telomere biology informs clinical paradigms." J Clin Invest **123**(3): 996-1002.

Armanios, M., et al. (2009). "Short telomeres are sufficient to cause the degenerative defects associated with aging." Am J Hum Genet **85**(6): 823-832.

Arvat, E., et al. (2000). "Preliminary evidence that Ghrelin, the natural GH secretagogue (GHS)-receptor ligand, strongly stimulates GH secretion in humans." J Endocrinol Invest **23**(8): 493-495.

Arvat, E., et al. (2001). "Endocrine activities of ghrelin, a natural growth hormone secretagogue (GHS), in humans: comparison and interactions with hexarelin, a nonnatural peptidyl GHS, and GH-releasing hormone." J Clin Endocrinol Metab **86**(3): 1169-1174.

Asakawa, A., et al. (2001). "A role of ghrelin in neuroendocrine and behavioral responses to stress in mice." Neuroendocrinology **74**(3): 143-147.

Asano, H., et al. (2009). "Astrocyte differentiation of neural precursor cells is enhanced by retinoic acid through a change in epigenetic modification." Stem Cells **27**(11): 2744-2752.

Baatar, D., et al. (2011). "The effects of ghrelin on inflammation and the immune system." Mol Cell Endocrinol **340**(1): 44-58.

Babilon, S., et al. (2013). "Towards improved receptor targeting: anterograde transport, internalization and postendocytic trafficking of neuropeptide Y receptors." Biol Chem **394**(8): 921-936.

Baek, J. H., et al. (2015). "Expression of progerin in aging mouse brains reveals structural nuclear abnormalities without detectible significant alterations in gene expression, hippocampal stem cells or behavior." Hum Mol Genet **24**(5): 1305-1321.

Baker, D. J., et al. (2016). "Naturally occurring p16(Ink4a)-positive cells shorten healthy lifespan." Nature **530**(7589): 184-189.

Baker, D. J., et al. (2011). "Clearance of p16Ink4a-positive senescent cells delays ageing-associated disorders." Nature **479**(7372): 232-236.

Balch, W. E., et al. (2008). "Adapting proteostasis for disease intervention." Science **319**(5865): 916-919.

Baldanzi, G., et al. (2002). "Ghrelin and des-acyl ghrelin inhibit cell death in cardiomyocytes and endothelial cells through ERK1/2 and PI 3-kinase/AKT." J Cell Biol **159**(6): 1029-1037.

Bali, A. and A. S. Jaggi (2016). "An Integrative Review on Role and Mechanisms of Ghrelin in Stress, Anxiety and Depression." Curr Drug Targets **17**(5): 495-507.

Barazzoni, R., et al. (2005). "Ghrelin regulates mitochondrial-lipid metabolism gene expression and tissue fat distribution in liver and skeletal muscle." Am J Physiol Endocrinol Metab **288**(1): E228-235.

Baskin, D. G., et al. (1999). "Leptin receptor mRNA identifies a subpopulation of neuropeptide Y neurons activated by fasting in rat hypothalamus." Diabetes **48**(4): 828-833.

Beck, L. A., et al. (1990). "Isoprenylation is required for the processing of the lamin A precursor." J Cell Biol **110**(5): 1489-1499.
Bennett, P. A., et al. (1997). "Hypothalamic growth hormone secretagogue-receptor (GHS-R) expression is regulated by growth hormone in the rat." Endocrinology **138**(11): 4552-4557.
Benson, E. K., et al. (2010). "Role of progerin-induced telomere dysfunction in HGPS premature cellular senescence." J Cell Sci **123**(Pt 15): 2605-2612.
Bergo, M. O., et al. (2002). "Zmpste24 deficiency in mice causes spontaneous bone fractures, muscle weakness, and a prelamin A processing defect." Proc Natl Acad Sci U S A **99**(20): 13049-13054.
Biran, J., et al. (2015). "Role of developmental factors in hypothalamic function." Front Neuroanat **9**: 47.
Bishop, N. A. and L. Guarente (2007). "Genetic links between diet and lifespan: shared mechanisms from yeast to humans." Nat Rev Genet **8**(11): 835-844.
Blackburn, E. H., et al. (2006). "Telomeres and telomerase: the path from maize, Tetrahymena and yeast to human cancer and aging." Nat Med **12**(10): 1133-1138.
Blasco, M. A. (2007). "Telomere length, stem cells and aging." Nat Chem Biol **3**(10): 640-649.
Bodnar, A. G., et al. (1998). "Extension of life-span by introduction of telomerase into normal human cells." Science **279**(5349): 349-352.
Bridger, J. M., et al. (1993). "Internal lamin structures within G1 nuclei of human dermal fibroblasts." J Cell Sci **104 (Pt 2)**: 297-306.
Broadwell, R. D. and M. W. Brightman (1976). "Entry of peroxidase into neurons of the central and peripheral nervous systems from extracerebral and cerebral blood." J Comp Neurol **166**(3): 257-283.
Broberger, C., et al. (1998). "The neuropeptide Y/agouti gene-related protein (AGRP) brain circuitry in normal, anorectic, and monosodium glutamate-treated mice." Proc Natl Acad Sci U S A **95**(25): 15043-15048.
Bronshtein, I., et al. (2015). "Loss of lamin A function increases chromatin dynamics in the nuclear interior." Nat Commun **6**: 8044.
Brown-Borg, H. M. (2015). "The somatotropic axis and longevity in mice." Am J Physiol Endocrinol Metab **309**(6): E503-510.
Browning, J. D., et al. (2012). "The effect of short-term fasting on liver and skeletal muscle lipid, glucose, and energy metabolism in healthy women and men." J Lipid Res **53**(3): 577-586.
Buccafusco, J. J. and H. E. Brezenoff (1979). "Pharmacological study of a cholinergic mechanism within the rat posterior hypothalamic nucleus which mediates a hypertensive response." Brain Res **165**(2): 295-310.
Burke, B. and C. L. Stewart (2006). "The laminopathies: the functional architecture of the nucleus and its contribution to disease." Annu Rev Genomics Hum Genet **7**: 369-405.
Burtner, C. R. and B. K. Kennedy (2010). "Progeria syndromes and ageing: what is the connection?" Nat Rev Mol Cell Biol **11**(8): 567-578.
Cabral, A., et al. (2012). "Ghrelin indirectly activates hypophysiotropic CRF neurons in rodents." PLoS One **7**(2): e31462.
Calderwood, S. K., et al. (2009). "The shock of aging: molecular chaperones and the heat shock response in longevity and aging--a mini-review." Gerontology **55**(5): 550-558.
Camina, J. P. (2006). "Cell biology of the ghrelin receptor." J Neuroendocrinol **18**(1): 65-76.
Camina, J. P., et al. (2004). "Desensitization and endocytosis mechanisms of ghrelin-activated growth hormone secretagogue receptor 1a." Endocrinology **145**(2): 930-940.
Canteras, N. S., et al. (1994). "Organization of projections from the ventromedial nucleus of the hypothalamus: a Phaseolus vulgaris-leucoagglutinin study in the rat." J Comp Neurol **348**(1): 41-79.
Cao, K., et al. (2011). "Rapamycin reverses cellular phenotypes and enhances mutant protein clearance in Hutchinson-Gilford progeria syndrome cells." Sci Transl Med **3**(89): 89ra58.

Capanni, C., et al. (2005). "Altered pre-lamin A processing is a common mechanism leading to lipodystrophy." Hum Mol Genet **14**(11): 1489-1502.
Carreira, M. C., et al. (2004). "Agonist-specific coupling of growth hormone secretagogue receptor type 1a to different intracellular signaling systems. Role of adenosine." Neuroendocrinology **79**(1): 13-25.
Cavadas, C., et al. (2016). "The pathophysiology of defective proteostasis in the hypothalamus - from obesity to ageing." Nat Rev Endocrinol **12**(12): 723-733.
Cavdar, S., et al. (2001). "The afferent connections of the posterior hypothalamic nucleus in the rat using horseradish peroxidase." J Anat **198**(Pt 4): 463-472.
Cenni, V., et al. (2011). "Autophagic degradation of farnesylated prelamin A as a therapeutic approach to lamin-linked progeria." Eur J Histochem **55**(4): e36.
Chee, M. J. and W. F. Colmers (2008). "Y eat?" Nutrition **24**(9): 869-877.
Chen, H. Y., et al. (2004). "Orexigenic action of peripheral ghrelin is mediated by neuropeptide Y and agouti-related protein." Endocrinology **145**(6): 2607-2612.
Cheung, C. C., et al. (1997). "Proopiomelanocortin neurons are direct targets for leptin in the hypothalamus." Endocrinology **138**(10): 4489-4492.
Chiodera, P., et al. (2000). "Decline in circulating neuropeptide Y levels in normal elderly human subjects." Eur J Endocrinol **143**(5): 715-716.
Choi, A. M., et al. (2013). "Autophagy in human health and disease." N Engl J Med **368**(7): 651-662.
Chojnowski, A., et al. (2015). "Progerin reduces LAP2alpha-telomere association in Hutchinson-Gilford progeria." Elife **4**.
Chondrogianni, N. and E. S. Gonos (2012). "Structure and function of the ubiquitin-proteasome system: modulation of components." Prog Mol Biol Transl Sci **109**: 41-74.
Chou, T. C., et al. (2003). "Critical role of dorsomedial hypothalamic nucleus in a wide range of behavioral circadian rhythms." J Neurosci **23**(33): 10691-10702.
Chow, K. B., et al. (2012). "The truncated ghrelin receptor polypeptide (GHS-R1b) is localized in the endoplasmic reticulum where it forms heterodimers with ghrelin receptors (GHS-R1a) to attenuate their cell surface expression." Mol Cell Endocrinol **348**(1): 247-254.
Collden, G., et al. (2017). "Therapeutic Potential of Targeting the Ghrelin Pathway." Int J Mol Sci **18**(4).
Colman, R. J., et al. (2009). "Caloric restriction delays disease onset and mortality in rhesus monkeys." Science **325**(5937): 201-204.
Costa, J. L., et al. (2011). "Ghrelin is an Osteoblast Mitogen and Increases Osteoclastic Bone Resorption In Vitro." Int J Pept **2011**: 605193.
Coutinho, H. D., et al. (2009). "Molecular ageing in progeroid syndromes: Hutchinson-Gilford progeria syndrome as a model." Immun Ageing **6**: 4.
Cowley, M. A., et al. (1999). "Integration of NPY, AGRP, and melanocortin signals in the hypothalamic paraventricular nucleus: evidence of a cellular basis for the adipostat." Neuron **24**(1): 155-163.
Cowley, M. A., et al. (2001). "Leptin activates anorexigenic POMC neurons through a neural network in the arcuate nucleus." Nature **411**(6836): 480-484.
Cowley, M. A., et al. (2003). "The distribution and mechanism of action of ghrelin in the CNS demonstrates a novel hypothalamic circuit regulating energy homeostasis." Neuron **37**(4): 649-661.
Cox, A. D. and C. J. Der (2002). "Farnesyltransferase inhibitors: promises and realities." Curr Opin Pharmacol **2**(4): 388-393.
Cummings, D. E., et al. (2001). "A preprandial rise in plasma ghrelin levels suggests a role in meal initiation in humans." Diabetes **50**(8): 1714-1719.
Currie, P. J., et al. (2012). "Ghrelin is an orexigenic peptide and elicits anxiety-like behaviors following administration into discrete regions of the hypothalamus." Behav Brain Res **226**(1): 96-105.

Dahl, K. N., et al. (2010). "Mechanobiology and the microcirculation: cellular, nuclear and fluid mechanics." Microcirculation **17**(3): 179-191.
Date, Y., et al. (2000). "Ghrelin, a novel growth hormone-releasing acylated peptide, is synthesized in a distinct endocrine cell type in the gastrointestinal tracts of rats and humans." Endocrinology **141**(11): 4255-4261.
De Sandre-Giovannoli, A., et al. (2003). "Lamin a truncation in Hutchinson-Gilford progeria." Science **300**(5628): 2055.
Dechat, T., et al. (2010). "Lamina-independent lamins in the nuclear interior serve important functions." Cold Spring Harb Symp Quant Biol **75**: 533-543.
Dechat, T., et al. (2007). "Alterations in mitosis and cell cycle progression caused by a mutant lamin A known to accelerate human aging." Proc Natl Acad Sci U S A **104**(12): 4955-4960.
Delhanty, P. J., et al. (2014). "Ghrelin and bone." Biofactors **40**(1): 41-48.
Denic, A., et al. (2016). "Structural and Functional Changes With the Aging Kidney." Adv Chronic Kidney Dis **23**(1): 19-28.
Dezaki, K., et al. (2004). "Endogenous ghrelin in pancreatic islets restricts insulin release by attenuating Ca2+ signaling in beta-cells: implication in the glycemic control in rodents." Diabetes **53**(12): 3142-3151.
Dixit, V. D., et al. (2004). "Ghrelin inhibits leptin- and activation-induced proinflammatory cytokine expression by human monocytes and T cells." J Clin Invest **114**(1): 57-66.
Dixit, V. D., et al. (2007). "Ghrelin promotes thymopoiesis during aging." J Clin Invest **117**(10): 2778-2790.
Dorner, D., et al. (2006). "Lamina-associated polypeptide 2alpha regulates cell cycle progression and differentiation via the retinoblastoma-E2F pathway." J Cell Biol **173**(1): 83-93.
Duxbury, M. S., et al. (2003). "Ghrelin promotes pancreatic adenocarcinoma cellular proliferation and invasiveness." Biochem Biophys Res Commun **309**(2): 464-468.
Eckersley-Maslin, M. A., et al. (2013). "Lamin A/C is expressed in pluripotent mouse embryonic stem cells." Nucleus **4**(1): 53-60.
Elias, C. F., et al. (1998). "Leptin activates hypothalamic CART neurons projecting to the spinal cord." Neuron **21**(6): 1375-1385.
Elizondo-Vega, R., et al. (2015). "The role of tanycytes in hypothalamic glucosensing." J Cell Mol Med **19**(7): 1471-1482.
Emery, D. E. and R. L. Moss (1984). "Lesions confined to the ventromedial hypothalamus decrease the frequency of coital contacts in female rats." Horm Behav **18**(3): 313-329.
Eriksson, M., et al. (2003). "Recurrent de novo point mutations in lamin A cause Hutchinson-Gilford progeria syndrome." Nature **423**(6937): 293-298.
Espada, J., et al. (2008). "Nuclear envelope defects cause stem cell dysfunction in premature-aging mice." J Cell Biol **181**(1): 27-35.
Fahrbach, S. E., et al. (1989). "Studies of ventromedial hypothalamic afferents in the rat using three methods of HRP application." Exp Brain Res **77**(2): 221-233.
Farage, M. A., et al. (2013). "Characteristics of the Aging Skin." Adv Wound Care (New Rochelle) **2**(1): 5-10.
Farkas, I., et al. (2013). "Ghrelin decreases firing activity of gonadotropin-releasing hormone (GnRH) neurons in an estrous cycle and endocannabinoid signaling dependent manner." PLoS One **8**(10): e78178.
Feldman, D. E. and J. Frydman (2000). "Protein folding in vivo: the importance of molecular chaperones." Curr Opin Struct Biol **10**(1): 26-33.
Ferreira-Marques, M., et al. (2016). "Caloric restriction stimulates autophagy in rat cortical neurons through neuropeptide Y and ghrelin receptors activation." Aging (Albany NY).
Ferrini, F., et al. (2009). "Ghrelin in central neurons." Curr Neuropharmacol **7**(1): 37-49.
Fetissov, S. O., et al. (2004). "Distribution of NPY receptors in the hypothalamus." Neuropeptides **38**(4): 175-188.

Filigheddu, N., et al. (2007). "Ghrelin and des-acyl ghrelin promote differentiation and fusion of C2C12 skeletal muscle cells." Mol Biol Cell **18**(3): 986-994.
Finley, D. (2009). "Recognition and processing of ubiquitin-protein conjugates by the proteasome." Annu Rev Biochem **78**: 477-513.
Fong, L. G., et al. (2006). "A protein farnesyltransferase inhibitor ameliorates disease in a mouse model of progeria." Science **311**(5767): 1621-1623.
Fontana, L., et al. (2010). "Extending healthy life span--from yeast to humans." Science **328**(5976): 321-326.
Fontes, M. A., et al. (2011). "The dorsomedial hypothalamus and the central pathways involved in the cardiovascular response to emotional stress." Neuroscience **184**: 64-74.
Freije, J. M. and C. Lopez-Otin (2012). "Reprogramming aging and progeria." Curr Opin Cell Biol **24**(6): 757-764.
Frier, B. M., et al. (2011). "Hypoglycemia and cardiovascular risks." Diabetes Care **34 Suppl 2**: S132-137.
Fukushima, N., et al. (2005). "Ghrelin directly regulates bone formation." J Bone Miner Res **20**(5): 790-798.
Fumagalli, M., et al. (2012). "Telomeric DNA damage is irreparable and causes persistent DNA-damage-response activation." Nat Cell Biol **14**(4): 355-365.
Furukawa, K., et al. (1994). "Identification and cloning of an mRNA coding for a germ cell-specific A-type lamin in mice." Exp Cell Res **212**(2): 426-430.
Gabriel, D., et al. (2015). "Sulforaphane enhances progerin clearance in Hutchinson-Gilford progeria fibroblasts." Aging Cell **14**(1): 78-91.
Gabuzda, D. and B. A. Yankner (2013). "Physiology: Inflammation links ageing to the brain." Nature **497**(7448): 197-198.
Gao, M., et al. (2013). "Ghrelin induces cardiac lineage differentiation of human embryonic stem cells through ERK1/2 pathway." Int J Cardiol **167**(6): 2724-2733.
Garinis, G. A., et al. (2008). "DNA damage and ageing: new-age ideas for an age-old problem." Nat Cell Biol **10**(11): 1241-1247.
Gerhard-Herman, M., et al. (2012). "Mechanisms of premature vascular aging in children with Hutchinson-Gilford progeria syndrome." Hypertension **59**(1): 92-97.
Ghosh, S., et al. (2015). "Lamin A Is an Endogenous SIRT6 Activator and Promotes SIRT6-Mediated DNA Repair." Cell Rep **13**(7): 1396-1406.
Gilford, H. (1897). "On a Condition of Mixed Premature and Immature Development." Med Chir Trans **80**: 17-46 25.
Gilford, H. (1904). "Progeria: A form of senilism." Practitioner **73**: 188–217.
Gnanapavan, S., et al. (2002). "The tissue distribution of the mRNA of ghrelin and subtypes of its receptor, GHS-R, in humans." J Clin Endocrinol Metab **87**(6): 2988.
Goldman, R. D., et al. (2004). "Accumulation of mutant lamin A causes progressive changes in nuclear architecture in Hutchinson-Gilford progeria syndrome." Proc Natl Acad Sci U S A **101**(24): 8963-8968.
Gonzalez-Suarez, I. and S. Gonzalo (2010). "Nurturing the genome: A-type lamins preserve genomic stability." Nucleus **1**(2): 129-135.
Gonzalo, S. (2010). "Epigenetic alterations in aging." J Appl Physiol (1985) **109**(2): 586-597.
Gonzalo, S. and J. C. Eissenberg (2016). "Tying up loose ends: telomeres, genomic instability and lamins." Curr Opin Genet Dev **37**: 109-118.
Gonzalo, S. and R. Kreienkamp (2015). "DNA repair defects and genome instability in Hutchinson-Gilford Progeria Syndrome." Curr Opin Cell Biol **34**: 75-83.
Gooley, J. J., et al. (2006). "The dorsomedial hypothalamic nucleus is critical for the expression of food-entrainable circadian rhythms." Nat Neurosci **9**(3): 398-407.
Gordon, L. B., et al. (2016). "Clinical Trial of the Protein Farnesylation Inhibitors Lonafarnib, Pravastatin, and Zoledronic Acid in Children With Hutchinson-Gilford Progeria Syndrome." Circulation **134**(2): 114-125.

Gordon, L. B., et al. (2012). "Clinical trial of a farnesyltransferase inhibitor in children with Hutchinson-Gilford progeria syndrome." Proc Natl Acad Sci U S A **109**(41): 16666-16671.
Gordon, L. B., et al. (2014). "Impact of farnesylation inhibitors on survival in Hutchinson-Gilford progeria syndrome." Circulation **130**(1): 27-34.
Gordon, L. B., et al. (2007). "Disease progression in Hutchinson-Gilford progeria syndrome: impact on growth and development." Pediatrics **120**(4): 824-833.
Green, D. R., et al. (2011). "Mitochondria and the autophagy-inflammation-cell death axis in organismal aging." Science **333**(6046): 1109-1112.
Gruenbaum, Y., et al. (2005). "The nuclear lamina comes of age." Nat Rev Mol Cell Biol **6**(1): 21-31.
Gruenbaum, Y. and O. Medalia (2015). "Lamins: the structure and protein complexes." Curr Opin Cell Biol **32**: 7-12.
Gruenewald, D. A., et al. (1994). "Age-related decrease in neuropeptide-Y gene expression in the arcuate nucleus of the male rat brain is independent of testicular feedback." Endocrinology **134**(6): 2383-2389.
Guan, X. M., et al. (1997). "Distribution of mRNA encoding the growth hormone secretagogue receptor in brain and peripheral tissues." Brain Res Mol Brain Res **48**(1): 23-29.
Gusel'nikova, V. V. and D. E. Korzhevskiy (2015). "NeuN As a Neuronal Nuclear Antigen and Neuron Differentiation Marker." Acta Naturae **7**(2): 42-47.
Gustafsson, J. A., et al. (1987). "Biochemistry, molecular biology, and physiology of the glucocorticoid receptor." Endocr Rev **8**(2): 185-234.
Gutierrez, J. A., et al. (2008). "Ghrelin octanoylation mediated by an orphan lipid transferase." Proc Natl Acad Sci U S A **105**(17): 6320-6325.
Gutman, M. B., et al. (1988). "Effects of plasma angiotensin II and hypernatremia on subfornical organ neurons." Am J Physiol **254**(5 Pt 2): R746-754.
Hahn, T. M., et al. (1998). "Coexpression of Agrp and NPY in fasting-activated hypothalamic neurons." Nat Neurosci **1**(4): 271-272.
Hansson, C., et al. (2011). "Central administration of ghrelin alters emotional responses in rats: behavioural, electrophysiological and molecular evidence." Neuroscience **180**: 201-211.
Harman, D. (1965). "The Free Radical Theory of Aging: Effect of Age on Serum Copper Levels." J Gerontol **20**: 151-153.
Harrison, D. E., et al. (2009). "Rapamycin fed late in life extends lifespan in genetically heterogeneous mice." Nature **460**(7253): 392-395.
Hayflick, L. and P. S. Moorhead (1961). "The serial cultivation of human diploid cell strains." Exp Cell Res **25**: 585-621.
Hekimi, S., et al. (2011). "Taking a "good" look at free radicals in the aging process." Trends Cell Biol **21**(10): 569-576.
Hennekam, R. C. (2006). "Hutchinson-Gilford progeria syndrome: review of the phenotype." Am J Med Genet A **140**(23): 2603-2624.
Heppner, K. M., et al. (2012). "Acylation type determines ghrelin's effects on energy homeostasis in rodents." Endocrinology **153**(10): 4687-4695.
Hernandez, L., et al. (2010). "Functional coupling between the extracellular matrix and nuclear lamina by Wnt signaling in progeria." Dev Cell **19**(3): 413-425.
Heyn, H., et al. (2013). "Aberrant DNA methylation profiles in the premature aging disorders Hutchinson-Gilford Progeria and Werner syndrome." Epigenetics **8**(1): 28-33.
Hill, J. W. (2012). "PVN pathways controlling energy homeostasis." Indian J Endocrinol Metab **16**(Suppl 3): S627-636.
Hilton, B. A., et al. (2017). "Progerin sequestration of PCNA promotes replication fork collapse and mislocalization of XPA in laminopathy-related progeroid syndromes." FASEB J.
Himmerich, H. and A. J. Sheldrick (2010). "TNF-alpha and ghrelin: opposite effects on immune system, metabolism and mental health." Protein Pept Lett **17**(2): 186-196.

Hirasawa, M., et al. (1996). "Neural activity in the VMH associated with suppression of the circulatory system in rats." Physiol Behav **59**(6): 1017-1023.
Hoeijmakers, J. H. (2009). "DNA damage, aging, and cancer." N Engl J Med **361**(15): 1475-1485.
Horvath, T. L., et al. (2001). "Minireview: ghrelin and the regulation of energy balance--a hypothalamic perspective." Endocrinology **142**(10): 4163-4169.
Hosoda, H., et al. (2000). "Ghrelin and des-acyl ghrelin: two major forms of rat ghrelin peptide in gastrointestinal tissue." Biochem Biophys Res Commun **279**(3): 909-913.
Houtkooper, R. H., et al. (2010). "Metabolic networks of longevity." Cell **142**(1): 9-14.
Hozak, P., et al. (1995). "Lamin proteins form an internal nucleoskeleton as well as a peripheral lamina in human cells." J Cell Sci **108 (Pt 2)**: 635-644.
Huang, H. J., et al. (2017). "Ghrelin alleviates anxiety- and depression-like behaviors induced by chronic unpredictable mild stress in rodents." Behav Brain Res **326**: 33-43.
Hutchinson, J. (1886). "Congenital Absence of Hair and Mammary Glands with Atrophic Condition of the Skin and its Appendages, in a Boy whose Mother had been almost wholly Bald from Alopecia Areata from the age of Six." Med Chir Trans **69**: 473-477.
Ibrahim, M. X., et al. (2013). "Targeting isoprenylcysteine methylation ameliorates disease in a mouse model of progeria." Science **340**(6138): 1330-1333.
Ibrahim, N., et al. (2003). "Hypothalamic proopiomelanocortin neurons are glucose responsive and express K(ATP) channels." Endocrinology **144**(4): 1331-1340.
Ishiwata, T., et al. (2001). "The role of preoptic area and anterior hypothalamus and median raphe nucleus on thermoregulatory system in freely moving rats." Neurosci Lett **306**(1-2): 126-128.
Janzen, V., et al. (2006). "Stem-cell ageing modified by the cyclin-dependent kinase inhibitor p16INK4a." Nature **443**(7110): 421-426.
Jeong, H. K., et al. (2013). "Brain inflammation and microglia: facts and misconceptions." Exp Neurobiol **22**(2): 59-67.
Jiang, H., et al. (2006). "Ghrelin amplifies dopamine signaling by cross talk involving formation of growth hormone secretagogue receptor/dopamine receptor subtype 1 heterodimers." Mol Endocrinol **20**(8): 1772-1785.
Johnson, S. C., et al. (2013). "mTOR is a key modulator of ageing and age-related disease." Nature **493**(7432): 338-345.
Kalra, S. P., et al. (1999). "Interacting appetite-regulating pathways in the hypothalamic regulation of body weight." Endocr Rev **20**(1): 68-100.
Katugampola, S. D., et al. (2001). "[125I-His(9)]-ghrelin, a novel radioligand for localizing GHS orphan receptors in human and rat tissue: up-regulation of receptors with athersclerosis." Br J Pharmacol **134**(1): 143-149.
Kaushik, S., et al. (2012). "Loss of autophagy in hypothalamic POMC neurons impairs lipolysis." EMBO Rep **13**(3): 258-265.
Kazak, L., et al. (2012). "Minimizing the damage: repair pathways keep mitochondrial DNA intact." Nat Rev Mol Cell Biol **13**(10): 659-671.
Kermath, B. A., et al. (2014). "Hypothalamic molecular changes underlying natural reproductive senescence in the female rat." Endocrinology **155**(9): 3597-3609.
Kim, J. D., et al. (2014). "Hormonal regulation of the hypothalamic melanocortin system." Front Physiol **5**: 480.
Kim, M. S., et al. (2004). "The mitogenic and antiapoptotic actions of ghrelin in 3T3-L1 adipocytes." Mol Endocrinol **18**(9): 2291-2301.
Kim Sh, S. H., et al. (2002). "Telomeres, aging and cancer: in search of a happy ending." Oncogene **21**(4): 503-511.
Kim, S. W., et al. (2005). "Ghrelin stimulates proliferation and differentiation and inhibits apoptosis in osteoblastic MC3T3-E1 cells." Bone **37**(3): 359-369.
Kim, Y. E., et al. (2013). "Molecular chaperone functions in protein folding and proteostasis." Annu Rev Biochem **82**: 323-355.

Kineman, R. D., et al. (1999). "Growth hormone (GH)-releasing hormone (GHRH) and the GH secretagogue (GHS), L692,585, differentially modulate rat pituitary GHS receptor and GHRH receptor messenger ribonucleic acid levels." Endocrinology **140**(8): 3581-3586.
Kirchner, H., et al. (2009). "GOAT links dietary lipids with the endocrine control of energy balance." Nat Med **15**(7): 741-745.
Kirkwood, T. B. (2005). "Understanding the odd science of aging." Cell **120**(4): 437-447.
Kirschner, M. (1999). "Intracellular proteolysis." Trends Cell Biol **9**(12): M42-45.
Klionsky, D. J., et al. (2016). "Guidelines for the use and interpretation of assays for monitoring autophagy (3rd edition)." Autophagy **12**(1): 1-222.
Koch, C. E., et al. (2017). "Interaction between circadian rhythms and stress." Neurobiol Stress **6**: 57-67.
Koga, H., et al. (2011). "Protein homeostasis and aging: The importance of exquisite quality control." Ageing Res Rev **10**(2): 205-215.
Kohno, D., et al. (2003). "Ghrelin directly interacts with neuropeptide-Y-containing neurons in the rat arcuate nucleus: Ca2+ signaling via protein kinase A and N-type channel-dependent mechanisms and cross-talk with leptin and orexin." Diabetes **52**(4): 948-956.
Kojima, M., et al. (1999). "Ghrelin is a growth-hormone-releasing acylated peptide from stomach." Nature **402**(6762): 656-660.
Kojima, M. and K. Kangawa (2005). "Ghrelin: structure and function." Physiol Rev **85**(2): 495-522.
Kolb, T., et al. (2011). "Lamin A and lamin C form homodimers and coexist in higher complex forms both in the nucleoplasmic fraction and in the lamina of cultured human cells." Nucleus **2**(5): 425-433.
Konner, A. C., et al. (2007). "Insulin action in AgRP-expressing neurons is required for suppression of hepatic glucose production." Cell Metab **5**(6): 438-449.
Korbonits, M., et al. (2001). "Presence of ghrelin in normal and adenomatous human pituitary." Endocrine **14**(1): 101-104.
Kozakowski, J., et al. (2008). "Ghrelin - growth hormone releasing and orexigenic hormone in men declines with age, insulin and with decrease in testosterone concentration." Neuro Endocrinol Lett **29**(1): 100-106.
Krashes, M. J., et al. (2014). "An excitatory paraventricular nucleus to AgRP neuron circuit that drives hunger." Nature **507**(7491): 238-242.
Kristensen, P., et al. (1998). "Hypothalamic CART is a new anorectic peptide regulated by leptin." Nature **393**(6680): 72-76.
Kubben, F. J., et al. (1994). "Proliferating cell nuclear antigen (PCNA): a new marker to study human colonic cell proliferation." Gut **35**(4): 530-535.
Kubben, N., et al. (2016). "Repression of the Antioxidant NRF2 Pathway in Premature Aging." Cell **165**(6): 1361-1374.
Kudlow, B. A., et al. (2008). "Suppression of proliferative defects associated with processing-defective lamin A mutants by hTERT or inactivation of p53." Mol Biol Cell **19**(12): 5238-5248.
Lamming, D. W., et al. (2012). "Rapamycin-induced insulin resistance is mediated by mTORC2 loss and uncoupled from longevity." Science **335**(6076): 1638-1643.
Laplante, M. and D. M. Sabatini (2012). "mTOR signaling in growth control and disease." Cell **149**(2): 274-293.
Larson, K., et al. (2012). "Heterochromatin formation promotes longevity and represses ribosomal RNA synthesis." PLoS Genet **8**(1): e1002473.
Laviano, A., et al. (2012). "The growth hormone secretagogue receptor (Ghs-R)." Curr Pharm Des **18**(31): 4749-4754.
Lavu, S., et al. (2008). "Sirtuins--novel therapeutic targets to treat age-associated diseases." Nat Rev Drug Discov **7**(10): 841-853.

Lee, K., et al. (2005). "Role of neuronal energy status in the regulation of adenosine 5'-monophosphate-activated protein kinase, orexigenic neuropeptides expression, and feeding behavior." Endocrinology **146**(1): 3-10.
Lee, S. J., et al. (2016). "Interruption of progerin-lamin A/C binding ameliorates Hutchinson-Gilford progeria syndrome phenotype." J Clin Invest **126**(10): 3879-3893.
Leung, P. K., et al. (2007). "The truncated ghrelin receptor polypeptide (GHS-R1b) acts as a dominant-negative mutant of the ghrelin receptor." Cell Signal **19**(5): 1011-1022.
Li, E., et al. (2013). "Ghrelin directly stimulates adult hippocampal neurogenesis: implications for learning and memory." Endocr J **60**(6): 781-789.
Li, E., et al. (2014). "Ghrelin stimulates proliferation, migration and differentiation of neural progenitors from the subventricular zone in the adult mice." Exp Neurol **252**: 75-84.
Li, W. G., et al. (2004). "Ghrelin inhibits proinflammatory responses and nuclear factor-kappaB activation in human endothelial cells." Circulation **109**(18): 2221-2226.
Lin, J. S., et al. (1989). "A critical role of the posterior hypothalamus in the mechanisms of wakefulness determined by microinjection of muscimol in freely moving cats." Brain Res **479**(2): 225-240.
Lin, L., et al. (2011). "Ablation of ghrelin receptor reduces adiposity and improves insulin sensitivity during aging by regulating fat metabolism in white and brown adipose tissues." Aging Cell **10**(6): 996-1010.
Linnane, A. W., et al. (1989). "Mitochondrial DNA mutations as an important contributor to ageing and degenerative diseases." Lancet **1**(8639): 642-645.
Liu, B., et al. (2012). "Resveratrol rescues SIRT1-dependent adult stem cell decline and alleviates progeroid features in laminopathy-based progeria." Cell Metab **16**(6): 738-750.
Liu, B., et al. (2005). "Genomic instability in laminopathy-based premature aging." Nat Med **11**(7): 780-785.
Liu, G. H., et al. (2011). "Recapitulation of premature ageing with iPSCs from Hutchinson-Gilford progeria syndrome." Nature **472**(7342): 221-225.
Liu, Y., et al. (2014). "Rapamycin-induced metabolic defects are reversible in both lean and obese mice." Aging (Albany NY) **6**(9): 742-754.
Lopez-Mejia, I. C., et al. (2011). "A conserved splicing mechanism of the LMNA gene controls premature aging." Hum Mol Genet **20**(23): 4540-4555.
Lopez-Otin, C., et al. (2013). "The hallmarks of aging." Cell **153**(6): 1194-1217.
Lu, S., et al. (2002). "Immunocytochemical observation of ghrelin-containing neurons in the rat arcuate nucleus." Neurosci Lett **321**(3): 157-160.
Luque, R. M., et al. (2004). "Homologous and heterologous regulation of pituitary receptors for ghrelin and growth hormone-releasing hormone." Endocrinology **145**(7): 3182-3189.
Lutter, M., et al. (2008). "The orexigenic hormone ghrelin defends against depressive symptoms of chronic stress." Nat Neurosci **11**(7): 752-753.
MacDougald, O. A., et al. (1995). "Regulated expression of the obese gene product (leptin) in white adipose tissue and 3T3-L1 adipocytes." Proc Natl Acad Sci U S A **92**(20): 9034-9037.
Machiels, B. M., et al. (1996). "An alternative splicing product of the lamin A/C gene lacks exon 10." J Biol Chem **271**(16): 9249-9253.
Machluf, Y., et al. (2011). "Development of the zebrafish hypothalamus." Ann N Y Acad Sci **1220**: 93-105.
Mains, R. E., et al. (1977). "Common precursor to corticotropins and endorphins." Proc Natl Acad Sci U S A **74**(7): 3014-3018.
Majdic, G., et al. (2002). "Knockout mice lacking steroidogenic factor 1 are a novel genetic model of hypothalamic obesity." Endocrinology **143**(2): 607-614.
Mano-Otagiri, A., et al. (2006). "Growth hormone-releasing hormone (GHRH) neurons in the arcuate nucleus (Arc) of the hypothalamus are decreased in transgenic rats whose expression of ghrelin receptor is attenuated: Evidence that ghrelin receptor is involved in the up-regulation of GHRH expression in the arc." Endocrinology **147**(9): 4093-4103.

Mao, Y., et al. (2012). "Ghrelin prevents incidence of malignant arrhythmia after acute myocardial infarction through vagal afferent nerves." Endocrinology **153**(7): 3426-3434.
Maraldi, N. M., et al. (2008). "SREBP1 interaction with prelamin A forms: a pathogenic mechanism for lipodystrophic laminopathies." Adv Enzyme Regul **48**: 209-223.
Marino, G., et al. (2010). "Insulin-like growth factor 1 treatment extends longevity in a mouse model of human premature aging by restoring somatotroph axis function." Proc Natl Acad Sci U S A **107**(37): 16268-16273.
Marji, J., et al. (2010). "Defective lamin A-Rb signaling in Hutchinson-Gilford Progeria Syndrome and reversal by farnesyltransferase inhibition." PLoS One **5**(6): e11132.
Markakis, E. A. and L. W. Swanson (1997). "Spatiotemporal patterns of secretomotor neuron generation in the parvicellular neuroendocrine system." Brain Res Brain Res Rev **24**(2-3): 255-291.
Markiewicz, E., et al. (2002). "Lamin A/C binding protein LAP2alpha is required for nuclear anchorage of retinoblastoma protein." Mol Biol Cell **13**(12): 4401-4413.
Marks, J. L., et al. (1992). "Effect of fasting on regional levels of neuropeptide Y mRNA and insulin receptors in the rat hypothalamus: An autoradiographic study." Mol Cell Neurosci **3**(3): 199-205.
Martins, L., et al. (2012). "Hypothalamic mTOR signaling mediates the orexigenic action of ghrelin." PLoS One **7**(10): e46923.
Mateos, J., et al. (2015). "iTRAQ-based analysis of progerin expression reveals mitochondrial dysfunction, reactive oxygen species accumulation and altered proteostasis." Stem Cell Res Ther **6**: 119.
Mattison, J. A., et al. (2012). "Impact of caloric restriction on health and survival in rhesus monkeys from the NIA study." Nature **489**(7415): 318-321.
Maughan, R. J., et al. (1983). "Strength and cross-sectional area of human skeletal muscle." J Physiol **338**: 37-49.
Mazzocchi, G., et al. (2004). "Ghrelin enhances the growth of cultured human adrenal zona glomerulosa cells by exerting MAPK-mediated proliferogenic and antiapoptotic effects." Peptides **25**(8): 1269-1277.
McClellan, K. M., et al. (2006). "Development of the ventromedial nucleus of the hypothalamus." Front Neuroendocrinol **27**(2): 193-209.
McClintock, D., et al. (2007). "The mutant form of lamin A that causes Hutchinson-Gilford progeria is a biomarker of cellular aging in human skin." PLoS One **2**(12): e1269.
McCord, R. P., et al. (2013). "Correlated alterations in genome organization, histone methylation, and DNA-lamin A/C interactions in Hutchinson-Gilford progeria syndrome." Genome Res **23**(2): 260-269.
McKee, K. K., et al. (1997). "Molecular analysis of rat pituitary and hypothalamic growth hormone secretagogue receptors." Mol Endocrinol **11**(4): 415-423.
McKinley, M. J., et al. (2015). "The median preoptic nucleus: front and centre for the regulation of body fluid, sodium, temperature, sleep and cardiovascular homeostasis." Acta Physiol (Oxf) **214**(1): 8-32.
Mebius, R. E. and G. Kraal (2005). "Structure and function of the spleen." Nat Rev Immunol **5**(8): 606-616.
Merideth, M. A., et al. (2008). "Phenotype and course of Hutchinson-Gilford progeria syndrome." N Engl J Med **358**(6): 592-604.
Merino, M. M., et al. (2015). "Elimination of unfit cells maintains tissue health and prolongs lifespan." Cell **160**(3): 461-476.
Miller, R. A., et al. (2014). "Rapamycin-mediated lifespan increase in mice is dose and sex dependent and metabolically distinct from dietary restriction." Aging Cell **13**(3): 468-477.
Min, J. N., et al. (2008). "CHIP deficiency decreases longevity, with accelerated aging phenotypes accompanied by altered protein quality control." Mol Cell Biol **28**(12): 4018-4025.

Minor, R. K., et al. (2009). "Hungry for life: How the arcuate nucleus and neuropeptide Y may play a critical role in mediating the benefits of calorie restriction." Mol Cell Endocrinol **299**(1): 79-88.
Monteleone, P., et al. (2003). "Differential responses of circulating ghrelin to high-fat or high-carbohydrate meal in healthy women." J Clin Endocrinol Metab **88**(11): 5510-5514.
Moon, M., et al. (2009). "Neuroprotective effect of ghrelin in the 1-methyl-4-phenyl-1,2,3,6-tetrahydropyridine mouse model of Parkinson's disease by blocking microglial activation." Neurotox Res **15**(4): 332-347.
Moon, M., et al. (2009). "Ghrelin regulates hippocampal neurogenesis in adult mice." Endocr J **56**(3): 525-531.
Moore, R. Y. (2013). "The suprachiasmatic nucleus and the circadian timing system." Prog Mol Biol Transl Sci **119**: 1-28.
Mori, K., et al. (2000). "Kidney produces a novel acylated peptide, ghrelin." FEBS Lett **486**(3): 213-216.
Moskalev, A. A., et al. (2013). "The role of DNA damage and repair in aging through the prism of Koch-like criteria." Ageing Res Rev **12**(2): 661-684.
Muller, T. D., et al. (2015). "Ghrelin." Mol Metab **4**(6): 437-460.
Murata, M., et al. (2002). "Ghrelin modulates the downstream molecules of insulin signaling in hepatoma cells." J Biol Chem **277**(7): 5667-5674.
Muroi, Y. and T. Ishii (2016). "A novel neuropeptide Y neuronal pathway linking energy state and reproductive behavior." Neuropeptides **59**: 1-8.
Nader, N., et al. (2010). "Interactions of the circadian CLOCK system and the HPA axis." Trends Endocrinol Metab **21**(5): 277-286.
Naetar, N., et al. (2008). "Loss of nucleoplasmic LAP2alpha-lamin A complexes causes erythroid and epidermal progenitor hyperproliferation." Nat Cell Biol **10**(11): 1341-1348.
Nagaya, N. and K. Kangawa (2003). "Ghrelin, a novel growth hormone-releasing peptide, in the treatment of chronic heart failure." Regul Pept **114**(2-3): 71-77.
Nagaya, N., et al. (2001). "Hemodynamic, renal, and hormonal effects of ghrelin infusion in patients with chronic heart failure." J Clin Endocrinol Metab **86**(12): 5854-5859.
Nagaya, N., et al. (2001). "Chronic administration of ghrelin improves left ventricular dysfunction and attenuates development of cardiac cachexia in rats with heart failure." Circulation **104**(12): 1430-1435.
Nakamura, K. and S. F. Morrison (2008). "A thermosensory pathway that controls body temperature." Nat Neurosci **11**(1): 62-71.
Nakamura, K. and S. F. Morrison (2010). "A thermosensory pathway mediating heat-defense responses." Proc Natl Acad Sci U S A **107**(19): 8848-8853.
Nakamura, T. J., et al. (2011). "Age-related decline in circadian output." J Neurosci **31**(28): 10201-10205.
Nakamura, T. J., et al. (2016). "The suprachiasmatic nucleus: age-related decline in biological rhythms." J Physiol Sci **66**(5): 367-374.
Nakazato, M., et al. (2001). "A role for ghrelin in the central regulation of feeding." Nature **409**(6817): 194-198.
Nass, R., et al. (2014). "Age-dependent decline in acyl-ghrelin concentrations and reduced association of acyl-ghrelin and growth hormone in healthy older adults." J Clin Endocrinol Metab **99**(2): 602-608.
Nelson, J. F., et al. (1988). "Age-related changes in proopiomelanocortin messenger ribonucleic acid levels in hypothalamus and pituitary of female C57BL/6J mice." Endocrinology **123**(1): 340-344.
Newton, A. J., et al. (2013). "AgRP innervation onto POMC neurons increases with age and is accelerated with chronic high-fat feeding in male mice." Endocrinology **154**(1): 172-183.
Nishi, Y., et al. (2005). "Ingested medium-chain fatty acids are directly utilized for the acyl modification of ghrelin." Endocrinology **146**(5): 2255-2264.

Nissan, X., et al. (2012). "Unique preservation of neural cells in Hutchinson- Gilford progeria syndrome is due to the expression of the neural-specific miR-9 microRNA." Cell Rep **2**(1): 1-9.
Oberdoerffer, P. and D. A. Sinclair (2007). "The role of nuclear architecture in genomic instability and ageing." Nat Rev Mol Cell Biol **8**(9): 692-702.
Olive, M., et al. (2010). "Cardiovascular pathology in Hutchinson-Gilford progeria: correlation with the vascular pathology of aging." Arterioscler Thromb Vasc Biol **30**(11): 2301-2309.
Organ, J. M., et al. (2016). "Reduced skeletal muscle function is associated with decreased fiber cross-sectional area in the Cy/+ rat model of progressive kidney disease." Nephrol Dial Transplant **31**(2): 223-230.
Osorio, F. G., et al. (2012). "NF-kB in premature aging." Aging (Albany NY) **4**(11): 726-727.
Osorio, F. G., et al. (2011). "Splicing-directed therapy in a new mouse model of human accelerated aging." Sci Transl Med **3**(106): 106ra107.
Pantel, J., et al. (2006). "Loss of constitutive activity of the growth hormone secretagogue receptor in familial short stature." J Clin Invest **116**(3): 760-768.
Park, C. B. and N. G. Larsson (2011). "Mitochondrial DNA mutations in disease and aging." J Cell Biol **193**(5): 809-818.
Pearson, C. A. and M. Placzek (2013). "Development of the medial hypothalamus: forming a functional hypothalamic-neurohypophyseal interface." Curr Top Dev Biol **106**: 49-88.
Peino, R., et al. (2000). "Ghrelin-induced growth hormone secretion in humans." Eur J Endocrinol **143**(6): R11-14.
Pendas, A. M., et al. (2002). "Defective prelamin A processing and muscular and adipocyte alterations in Zmpste24 metalloproteinase-deficient mice." Nat Genet **31**(1): 94-99.
Porporato, P. E., et al. (2013). "Acylated and unacylated ghrelin impair skeletal muscle atrophy in mice." J Clin Invest **123**(2): 611-622.
Powers, E. T., et al. (2009). "Biological and chemical approaches to diseases of proteostasis deficiency." Annu Rev Biochem **78**: 959-991.
Pradhan, G., et al. (2013). "Ghrelin: much more than a hunger hormone." Curr Opin Clin Nutr Metab Care **16**(6): 619-624.
Prokocimer, M., et al. (2013). "Hutchinson-Gilford progeria syndrome through the lens of transcription." Aging Cell **12**(4): 533-543.
Qian, X., et al. (2000). "Timing of CNS cell generation: a programmed sequence of neuron and glial cell production from isolated murine cortical stem cells." Neuron **28**(1): 69-80.
Rando, T. A. and H. Y. Chang (2012). "Aging, rejuvenation, and epigenetic reprogramming: resetting the aging clock." Cell **148**(1-2): 46-57.
Reano, S., et al. (2017). "Unacylated Ghrelin Enhances Satellite Cell Function and Relieves the Dystrophic Phenotype in Duchenne Muscular Dystrophy mdx Model." Stem Cells **35**(7): 1733-1746.
Reddel, C. J. and A. S. Weiss (2004). "Lamin A expression levels are unperturbed at the normal and mutant alleles but display partial splice site selection in Hutchinson-Gilford progeria syndrome." J Med Genet **41**(9): 715-717.
Rediger, A., et al. (2011). "Mutually opposite signal modulation by hypothalamic heterodimerization of ghrelin and melanocortin-3 receptors." J Biol Chem **286**(45): 39623-39631.
Reimer, M. K., et al. (2003). "Dose-dependent inhibition by ghrelin of insulin secretion in the mouse." Endocrinology **144**(3): 916-921.
Reunert, J., et al. (2012). "Neonatal progeria: increased ratio of progerin to lamin A leads to progeria of the newborn." Eur J Hum Genet **20**(9): 933-937.
Revechon, G., et al. (2017). "Rare progerin-expressing preadipocytes and adipocytes contribute to tissue depletion over time." Sci Rep **7**(1): 4405.
Rigamonti, A. E., et al. (2002). "Plasma ghrelin concentrations in elderly subjects: comparison with anorexic and obese patients." J Endocrinol **175**(1): R1-5.

Rivera-Torres, J., et al. (2013). "Identification of mitochondrial dysfunction in Hutchinson-Gilford progeria syndrome through use of stable isotope labeling with amino acids in cell culture." J Proteomics **91**: 466-477.
Roberts, J. L. and E. Herbert (1977). "Characterization of a common precursor to corticotropin and beta-lipotropin: identification of beta-lipotropin peptides and their arrangement relative to corticotropin in the precursor synthesized in a cell-free system." Proc Natl Acad Sci U S A **74**(12): 5300-5304.
Rodier, F. and J. Campisi (2011). "Four faces of cellular senescence." J Cell Biol **192**(4): 547-556.
Roh, E. and M. S. Kim (2016). "Brain Regulation of Energy Metabolism." Endocrinol Metab (Seoul) **31**(4): 519-524.
Romanov, R. A., et al. (2017). "Molecular diversity of corticotropin-releasing hormone mRNA-containing neurons in the hypothalamus." J Endocrinol **232**(3): R161-R172.
Rosengardten, Y., et al. (2011). "Stem cell depletion in Hutchinson-Gilford progeria syndrome." Aging Cell **10**(6): 1011-1020.
Rossi, D. J., et al. (2007). "Deficiencies in DNA damage repair limit the function of haematopoietic stem cells with age." Nature **447**(7145): 725-729.
Rothwell, P. M., et al. (2011). "Effect of daily aspirin on long-term risk of death due to cancer: analysis of individual patient data from randomised trials." Lancet **377**(9759): 31-41.
Rubinsztein, D. C., et al. (2011). "Autophagy and aging." Cell **146**(5): 682-695.
Rufini, A., et al. (2013). "Senescence and aging: the critical roles of p53." Oncogene **32**(43): 5129-5143.
Russell, S. J. and C. R. Kahn (2007). "Endocrine regulation of ageing." Nat Rev Mol Cell Biol **8**(9): 681-691.
Salminen, A., et al. (2012). "Inflammaging: disturbed interplay between autophagy and inflammasomes." Aging (Albany NY) **4**(3): 166-175.
Salmon, A. B. (2015). "About-face on the metabolic side effects of rapamycin." Oncotarget **6**(5): 2585-2586.
Saper, C. B. and D. Levisohn (1983). "Afferent connections of the median preoptic nucleus in the rat: anatomical evidence for a cardiovascular integrative mechanism in the anteroventral third ventricular (AV3V) region." Brain Res **288**(1-2): 21-31.
Saper, C. B., et al. (1976). "The efferent connections of the ventromedial nucleus of the hypothalamus of the rat." J Comp Neurol **169**(4): 409-442.
Sapru, H. N. (2013). "Role of the hypothalamic arcuate nucleus in cardiovascular regulation." Auton Neurosci **175**(1-2): 38-50.
Satoh, A., et al. (2013). "Sirt1 extends life span and delays aging in mice through the regulation of Nk2 homeobox 1 in the DMH and LH." Cell Metab **18**(3): 416-430.
Satoh, A., et al. (2015). "Deficiency of Prdm13, a dorsomedial hypothalamus-enriched gene, mimics age-associated changes in sleep quality and adiposity." Aging Cell **14**(2): 209-218.
Scaffidi, P. and T. Misteli (2005). "Reversal of the cellular phenotype in the premature aging disease Hutchinson-Gilford progeria syndrome." Nat Med **11**(4): 440-445.
Scaffidi, P. and T. Misteli (2006). "Lamin A-dependent nuclear defects in human aging." Science **312**(5776): 1059-1063.
Scaffidi, P. and T. Misteli (2008). "Lamin A-dependent misregulation of adult stem cells associated with accelerated ageing." Nat Cell Biol **10**(4): 452-459.
Schmucker, D. L. (2005). "Age-related changes in liver structure and function: Implications for disease ?" Exp Gerontol **40**(8-9): 650-659.
Schmucker, D. L. and H. Sanchez (2011). "Liver regeneration and aging: a current perspective." Curr Gerontol Geriatr Res **2011**: 526379.
Schumacher, B., et al. (2008). "Delayed and accelerated aging share common longevity assurance mechanisms." PLoS Genet **4**(8): e1000161.
Sebastian, C., et al. (2012). "From sirtuin biology to human diseases: an update." J Biol Chem **287**(51): 42444-42452.

Seim, I., et al. (2007). "Revised genomic structure of the human ghrelin gene and identification of novel exons, alternative splice variants and natural antisense transcripts." BMC Genomics **8**: 298.
Sena, L. A. and N. S. Chandel (2012). "Physiological roles of mitochondrial reactive oxygen species." Mol Cell **48**(2): 158-167.
Senniappan, S., et al. (2013). "The molecular mechanisms, diagnosis and management of congenital hyperinsulinism." Indian J Endocrinol Metab **17**(1): 19-30.
Shah, M., et al. (2010). "AMP-activated protein kinase (AMPK) activation regulates in vitro bone formation and bone mass." Bone **47**(2): 309-319.
Sharpless, N. E. and R. A. DePinho (2007). "How stem cells age and why this makes us grow old." Nat Rev Mol Cell Biol **8**(9): 703-713.
Shekhar, A. and J. A. DiMicco (1987). "Defense reaction elicited by injection of GABA antagonists and synthesis inhibitors into the posterior hypothalamus in rats." Neuropharmacology **26**(5): 407-417.
Shimi, T., et al. (2012). "The functions of the nuclear envelope in mediating the molecular crosstalk between the nucleus and the cytoplasm." Curr Opin Cell Biol **24**(1): 71-78.
Shumaker, D. K., et al. (2006). "Mutant nuclear lamin A leads to progressive alterations of epigenetic control in premature aging." Proc Natl Acad Sci U S A **103**(23): 8703-8708.
Silvera, V. M., et al. (2013). "Imaging characteristics of cerebrovascular arteriopathy and stroke in Hutchinson-Gilford progeria syndrome." AJNR Am J Neuroradiol **34**(5): 1091-1097.
Simerly, R. B. (2004). CHAPTER 14 - Anatomical Substrates of Hypothalamic Integration A2 - Paxinos, George. The Rat Nervous System (THIRD EDITION). Burlington, Academic Press**:** 335-368.
Sinensky, M., et al. (1994). "The processing pathway of prelamin A." J Cell Sci **107 (Pt 1)**: 61-67.
Sofroniew, M. V. and H. V. Vinters (2010). "Astrocytes: biology and pathology." Acta Neuropathol **119**(1): 7-35.
Spencer, S. E., et al. (1990). "L-glutamate mapping of cardioreactive areas in the rat posterior hypothalamus." Brain Res **511**(1): 149-157.
Spencer, S. J., et al. (2012). "Ghrelin regulates the hypothalamic-pituitary-adrenal axis and restricts anxiety after acute stress." Biol Psychiatry **72**(6): 457-465.
Squier, T. C. (2001). "Oxidative stress and protein aggregation during biological aging." Exp Gerontol **36**(9): 1539-1550.
Stephan, F. K. and I. Zucker (1972). "Circadian rhythms in drinking behavior and locomotor activity of rats are eliminated by hypothalamic lesions." Proc Natl Acad Sci U S A **69**(6): 1583-1586.
Sternson, S. M., et al. (2005). "Topographic mapping of VMH --> arcuate nucleus microcircuits and their reorganization by fasting." Nat Neurosci **8**(10): 1356-1363.
Stevanovic, D., et al. (2013). "Ghrelin-induced food intake and adiposity depend on central mTORC1/S6K1 signaling." Mol Cell Endocrinol **381**(1-2): 280-290.
Stotz-Potter, E. H., et al. (1996). "Muscimol acts in dorsomedial but not paraventricular hypothalamic nucleus to suppress cardiovascular effects of stress." J Neurosci **16**(3): 1173-1179.
Strandgren, C., et al. (2015). "Transgene silencing of the Hutchinson-Gilford progeria syndrome mutation results in a reversible bone phenotype, whereas resveratrol treatment does not show overall beneficial effects." FASEB J **29**(8): 3193-3205.
Strong, R., et al. (2008). "Nordihydroguaiaretic acid and aspirin increase lifespan of genetically heterogeneous male mice." Aging Cell **7**(5): 641-650.
Sugiyama, M., et al. (2012). "Ghrelin improves body weight loss and skeletal muscle catabolism associated with angiotensin II-induced cachexia in mice." Regul Pept **178**(1-3): 21-28.
Sullivan, T., et al. (1999). "Loss of A-type lamin expression compromises nuclear envelope integrity leading to muscular dystrophy." J Cell Biol **147**(5): 913-920.

Sun, Y., et al. (2006). "Ablation of ghrelin improves the diabetic but not obese phenotype of ob/ob mice." Cell Metab **3**(5): 379-386.
Swahari, V. and A. Nakamura (2016). "Speeding up the clock: The past, present and future of progeria." Dev Growth Differ **58**(1): 116-130.
Swift, J., et al. (2013). "Nuclear lamin-A scales with tissue stiffness and enhances matrix-directed differentiation." Science **341**(6149): 1240104.
Swindell, W. R., et al. (2009). "Endocrine regulation of heat shock protein mRNA levels in long-lived dwarf mice." Mech Ageing Dev **130**(6): 393-400.
Takaya, K., et al. (2000). "Ghrelin strongly stimulates growth hormone release in humans." J Clin Endocrinol Metab **85**(12): 4908-4911.
Talens, R. P., et al. (2012). "Epigenetic variation during the adult lifespan: cross-sectional and longitudinal data on monozygotic twin pairs." Aging Cell **11**(4): 694-703.
Tannenbaum, G. S., et al. (1998). "Expression of growth hormone secretagogue-receptors by growth hormone-releasing hormone neurons in the mediobasal hypothalamus." Endocrinology **139**(10): 4420-4423.
Taub, D. D., et al. (2010). "Rejuvenation of the aging thymus: growth hormone-mediated and ghrelin-mediated signaling pathways." Curr Opin Pharmacol **10**(4): 408-424.
Theander-Carrillo, C., et al. (2006). "Ghrelin action in the brain controls adipocyte metabolism." J Clin Invest **116**(7): 1983-1993.
Thompson, R. H., et al. (1996). "Organization of projections from the dorsomedial nucleus of the hypothalamus: a PHA-L study in the rat." J Comp Neurol **376**(1): 143-173.
Thompson, R. H. and L. W. Swanson (1998). "Organization of inputs to the dorsomedial nucleus of the hypothalamus: a reexamination with Fluorogold and PHAL in the rat." Brain Res Brain Res Rev **27**(2): 89-118.
Tomaru, U., et al. (2012). "Decreased proteasomal activity causes age-related phenotypes and promotes the development of metabolic abnormalities." Am J Pathol **180**(3): 963-972.
Tomas-Loba, A., et al. (2008). "Telomerase reverse transcriptase delays aging in cancer-resistant mice." Cell **135**(4): 609-622.
Torsello, A., et al. (2003). "Ontogeny and tissue-specific regulation of ghrelin mRNA expression suggest that ghrelin is primarily involved in the control of extraendocrine functions in the rat." Neuroendocrinology **77**(2): 91-99.
Toshinai, K., et al. (2001). "Upregulation of Ghrelin expression in the stomach upon fasting, insulin-induced hypoglycemia, and leptin administration." Biochem Biophys Res Commun **281**(5): 1220-1225.
Toth, J. I., et al. (2005). "Blocking protein farnesyltransferase improves nuclear shape in fibroblasts from humans with progeroid syndromes." Proc Natl Acad Sci U S A **102**(36): 12873-12878.
Tschop, M., et al. (2000). "Ghrelin induces adiposity in rodents." Nature **407**(6806): 908-913.
Ullrich, N. J. and L. B. Gordon (2015). "Hutchinson-Gilford progeria syndrome." Handb Clin Neurol **132**: 249-264.
Ulrich-Lai, Y. M. and J. P. Herman (2009). "Neural regulation of endocrine and autonomic stress responses." Nat Rev Neurosci **10**(6): 397-409.
Van Berlo, J. H., et al. (2005). "A-type lamins are essential for TGF-beta1 induced PP2A to dephosphorylate transcription factors." Hum Mol Genet **14**(19): 2839-2849.
van Deursen, J. M. (2014). "The role of senescent cells in ageing." Nature **509**(7501): 439-446.
Vanhooren, V., et al. (2015). "Protein modification and maintenance systems as biomarkers of ageing." Mech Ageing Dev **151**: 71-84.
Vanni-Mercier, G., et al. (1984). "[Specific neurons for wakefulness in the posterior hypothalamus in the cat]." C R Acad Sci III **298**(7): 195-200.
Varela, I., et al. (2005). "Accelerated ageing in mice deficient in Zmpste24 protease is linked to p53 signalling activation." Nature **437**(7058): 564-568.

Varela, I., et al. (2008). "Combined treatment with statins and aminobisphosphonates extends longevity in a mouse model of human premature aging." Nat Med **14**(7): 767-772.
Varga, R., et al. (2006). "Progressive vascular smooth muscle cell defects in a mouse model of Hutchinson-Gilford progeria syndrome." Proc Natl Acad Sci U S A **103**(9): 3250-3255.
Vautrot, V., et al. (2016). "Enhanced SRSF5 Protein Expression Reinforces Lamin A mRNA Production in HeLa Cells and Fibroblasts of Progeria Patients." Hum Mutat **37**(3): 280-291.
Vertes, R. P., et al. (1995). "Ascending projections of the posterior nucleus of the hypothalamus: PHA-L analysis in the rat." J Comp Neurol **359**(1): 90-116.
Veyrat-Durebex, C., et al. (2013). "Aging and long-term caloric restriction regulate neuropeptide Y receptor subtype densities in the rat brain." Neuropeptides **47**(3): 163-169.
Vidak, S. and R. Foisner (2016). "Molecular insights into the premature aging disease progeria." Histochem Cell Biol **145**(4): 401-417.
Vidak, S., et al. (2015). "Proliferation of progeria cells is enhanced by lamina-associated polypeptide 2alpha (LAP2alpha) through expression of extracellular matrix proteins." Genes Dev **29**(19): 2022-2036.
Volante, M., et al. (2002). "Expression of ghrelin and of the GH secretagogue receptor by pancreatic islet cells and related endocrine tumors." J Clin Endocrinol Metab **87**(3): 1300-1308.
Vujovic, N., et al. (2015). "Projections from the subparaventricular zone define four channels of output from the circadian timing system." J Comp Neurol **523**(18): 2714-2737.
Wang, Q., et al. (2014). "Arcuate AgRP neurons mediate orexigenic and glucoregulatory actions of ghrelin." Mol Metab **3**(1): 64-72.
Wang, Y., et al. (2008). "Epidermal expression of the truncated prelamin A causing Hutchinson-Gilford progeria syndrome: effects on keratinocytes, hair and skin." Hum Mol Genet **17**(15): 2357-2369.
Waseem, T., et al. (2008). "Exogenous ghrelin modulates release of pro-inflammatory and anti-inflammatory cytokines in LPS-stimulated macrophages through distinct signaling pathways." Surgery **143**(3): 334-342.
Weber, K., et al. (1989). "Maturation of nuclear lamin A involves a specific carboxy-terminal trimming, which removes the polyisoprenylation site from the precursor; implications for the structure of the nuclear lamina." FEBS Lett **257**(2): 411-414.
Weidberg, H., et al. (2011). "Biogenesis and cargo selectivity of autophagosomes." Annu Rev Biochem **80**: 125-156.
Wilkinson, J. E., et al. (2012). "Rapamycin slows aging in mice." Aging Cell **11**(4): 675-682.
Willesen, M. G., et al. (1999). "Co-localization of growth hormone secretagogue receptor and NPY mRNA in the arcuate nucleus of the rat." Neuroendocrinology **70**(5): 306-316.
Williams, K. W. and J. K. Elmquist (2012). "From neuroanatomy to behavior: central integration of peripheral signals regulating feeding behavior." Nat Neurosci **15**(10): 1350-1355.
Worman, H. J. and G. Bonne (2007). ""Laminopathies": a wide spectrum of human diseases." Exp Cell Res **313**(10): 2121-2133.
Wright, R. J. and B. M. Frier (2008). "Vascular disease and diabetes: is hypoglycaemia an aggravating factor?" Diabetes Metab Res Rev **24**(5): 353-363.
Wu, D., et al. (2016). "Comparing lamin proteins post-translational relative stability using a 2A peptide-based system reveals elevated resistance of progerin to cellular degradation." Nucleus **7**(6): 585-596.
Wu, J., et al. (2013). "Adaptive thermogenesis in adipocytes: is beige the new brown?" Genes Dev **27**(3): 234-250.
Xia, Q., et al. (2004). "Effects of ghrelin on the proliferation and secretion of splenic T lymphocytes in mice." Regul Pept **122**(3): 173-178.
Yang, J., et al. (2008). "Identification of the acyltransferase that octanoylates ghrelin, an appetite-stimulating peptide hormone." Cell **132**(3): 387-396.
Yang, J., et al. (2008). "Inhibition of ghrelin O-acyltransferase (GOAT) by octanoylated pentapeptides." Proc Natl Acad Sci U S A **105**(31): 10750-10755.

Yang, S. H., et al. (2008). "Progerin elicits disease phenotypes of progeria in mice whether or not it is farnesylated." J Clin Invest **118**(10): 3291-3300.
Yang, S. H., et al. (2005). "Blocking protein farnesyltransferase improves nuclear blebbing in mouse fibroblasts with a targeted Hutchinson-Gilford progeria syndrome mutation." Proc Natl Acad Sci U S A **102**(29): 10291-10296.
Yang, S. H., et al. (2006). "A farnesyltransferase inhibitor improves disease phenotypes in mice with a Hutchinson-Gilford progeria syndrome mutation." J Clin Invest **116**(8): 2115-2121.
Yang, Z. and D. J. Klionsky (2010). "Mammalian autophagy: core molecular machinery and signaling regulation." Curr Opin Cell Biol **22**(2): 124-131.
Yardley, C. P. and S. M. Hilton (1986). "The hypothalamic and brainstem areas from which the cardiovascular and behavioural components of the defence reaction are elicited in the rat." J Auton Nerv Syst **15**(3): 227-244.
Yin, Y., et al. (2014). "The growth hormone secretagogue receptor: its intracellular signaling and regulation." Int J Mol Sci **15**(3): 4837-4855.
Young, J., et al. (2005). "Type A insulin resistance syndrome revealing a novel lamin A mutation." Diabetes **54**(6): 1873-1878.
Young, S. G., et al. (2005). "Prelamin A, Zmpste24, misshapen cell nuclei, and progeria--new evidence suggesting that protein farnesylation could be important for disease pathogenesis." J Lipid Res **46**(12): 2531-2558.
Yu, H., et al. (2013). "The effect of ghrelin on cell proliferation in small intestinal IEC-6 cells." Biomed Pharmacother **67**(3): 235-239.
Yuan, M. J., et al. (2012). "Myocardial angiogenesis after chronic ghrelin treatment in a rat myocardial infarction model." Regul Pept **179**(1-3): 39-42.
Zhang, G., et al. (2013). "Hypothalamic programming of systemic ageing involving IKK-beta, NF-kappaB and GnRH." Nature **497**(7448): 211-216.
Zhang, H., et al. (2013). "Mouse models of laminopathies." Aging Cell **12**(1): 2-10.
Zhang, J., et al. (2011). "A human iPSC model of Hutchinson Gilford Progeria reveals vascular smooth muscle and mesenchymal stem cell defects." Cell Stem Cell **8**(1): 31-45.
Zhang, J. V., et al. (2005). "Obestatin, a peptide encoded by the ghrelin gene, opposes ghrelin's effects on food intake." Science **310**(5750): 996-999.
Zhang, S., et al. (2013). "High mobility group protein N5 (HMGN5) and lamina-associated polypeptide 2alpha (LAP2alpha) interact and reciprocally affect their genome-wide chromatin organization." J Biol Chem **288**(25): 18104-18109.
Zhang, Y., et al. (1994). "Positional cloning of the mouse obese gene and its human homologue." Nature **372**(6505): 425-432.
Zhao, Z., et al. (2014). "Ghrelin administration enhances neurogenesis but impairs spatial learning and memory in adult mice." Neuroscience **257**: 175-185.
Zhu, X., et al. (2006). "On the processing of proghrelin to ghrelin." J Biol Chem **281**(50): 38867-38870.